



HAL
open science

Apport de la spectroscopie à relaxation diélectrique sous pression pour investiguer la mobilité moléculaire dans les polymères thermoplastiques amorphes

Jules Trubert

► **To cite this version:**

Jules Trubert. Apport de la spectroscopie à relaxation diélectrique sous pression pour investiguer la mobilité moléculaire dans les polymères thermoplastiques amorphes. Matériaux. Normandie Université, 2024. Français. NNT : 2024NORMR048 . tel-04807181

HAL Id: tel-04807181

<https://theses.hal.science/tel-04807181v1>

Submitted on 27 Nov 2024

HAL is a multi-disciplinary open access archive for the deposit and dissemination of scientific research documents, whether they are published or not. The documents may come from teaching and research institutions in France or abroad, or from public or private research centers.

L'archive ouverte pluridisciplinaire **HAL**, est destinée au dépôt et à la diffusion de documents scientifiques de niveau recherche, publiés ou non, émanant des établissements d'enseignement et de recherche français ou étrangers, des laboratoires publics ou privés.



Normandie Université



THÈSE

Pour obtenir le diplôme de doctorat

Spécialité **PHYSIQUE**

Préparée au sein de l'**Université de Rouen Normandie**

Apport de la spectroscopie à relaxation diélectrique sous pression pour investiguer la mobilité moléculaire dans les polymères thermoplastiques amorphes

Présentée et soutenue par

JULES TRUBERT

Thèse soutenue le 22/10/2024

devant le jury composé de :

M. LAURENT DELBREILH	Maître de Conférences - Université de Rouen Normandie (URN)	Directeur de thèse
M. FREDERIC AFFOUARD	Professeur des Universités - UNIVERSITE LILLE 1 SCIENCES ET TECHNOLOGIE	Président du jury
MME ALLISSON SAITER-FOURCIN	Professeur des Universités - Université de Rouen Normandie (URN)	Co-directeur de thèse
MME CHRISTIANE ALBA-SIMIONESCO	Directeur de Recherche - UNIVERSITE PARIS-SACLAY	Membre du jury
M. SIMONE NAPOLITANO	Professeur des Universités - Université Libre de Bruxelles	Rapporteur du jury
M. ANATOLI SERGHEI	Directeur de Recherche - Université Claude Bernard - Lyon 1	Rapporteur du jury

Thèse dirigée par **LAURENT DELBREILH** (GROUPE DE PHYSIQUE DES MATERIAUX) et **ALLISSON SAITER-FOURCIN** (Université de Rouen Normandie)



Acknowledgments

Since a few parts of the acknowledgements are intended for some of my close relatives who are not comfortable with English, this section is written in French.

Ce manuscrit ne représente que la partie émergée de l'iceberg qu'ont été mes trois années de thèse. Il ne peut retranscrire la longue route parcourue pour parvenir à sa rédaction, ainsi que les difficultés rencontrées, les hors-pistes effectués ou encore les rencontres survenues. Malgré tout, je profite de ces quelques lignes pour remercier toutes les personnes qui ont pu, de près ou de loin, contribuer au bon déroulement de ma thèse et à la rédaction de ce manuscrit.

Je tiens tout d'abord à remercier les membres de mon jury de thèse. Chacun à votre façon, vous avez laissé une marque importante qui a influencé mon travail, bien avant d'être membre de mon jury. Je remercie mes deux rapporteurs, Simone Simon Napolitano et Anatoli Serghei. Je vous remercie pour vos rapports, qui reflètent l'attention que vous avez portée à mon manuscrit, ainsi que pour les commentaires pertinents et constructifs qui m'ont permis de prendre davantage de recul sur mon travail.

Je tiens plus particulièrement à remercier Simone de m'avoir accueilli dans votre laboratoire. Ce séjour à Bruxelles a été incroyablement enrichissant et a permis d'entrevoir les vastes possibilités offertes à la BDS ainsi que les difficultés qui persistent. Je remercie également Federico, Éric, Florian, Laure, Pascal, Martin, Kai et Chun pour leur accueil chaleureux et bienveillant.

Je remercie également les deux autres membres du jury, Christiane Alba-Simionesco et Frédéric Affouard. Merci Christiane pour les échanges et vos remarques lors de ma soutenance. Grâce à vos précédentes recherches, vous avez inspiré mes travaux, comme en témoignent les nombreuses références de ce manuscrit dont vous êtes autrice. Je remercie également Frédéric d'avoir accepté d'être mon président de jury. Vous avez grandement contribué à la bonne conduite de ma thèse, puisque vous faisiez déjà partie de mon CSI. Merci pour votre accompagnement du début à la fin de ma thèse.

Parmi les membres du jury, il y a deux personnes exceptionnelles à l'origine de cette thèse. Merci à vous, Allison et Laurent. C'est grâce à vous que cette thèse est ce qu'elle est. Tout d'abord, je tiens à vous remercier pour votre patience, votre confiance et votre soutien. Je ne pouvais pas espérer meilleur encadrement. Vous avez été très complémentaires, vous m'avez recadré de manière bienveillante lorsque je me dispersais. Et malgré les difficultés que j'ai pu rencontrer, vous avez toujours cru en ma réussite. Merci à toi, Allison, pour ta rigueur, ta compréhension et ta volonté de

m'impliquer dans des projets collaboratifs. Tu as toujours été d'accord pour les tâches annexes que j'ai souhaité effectuer, tout en me mettant en garde lorsque j'en sollicitais trop. Merci également Laurent pour ton énergie, ta créativité et de m'avoir fait découvrir le monde de la spectroscopie diélectrique. Tu as toujours des idées originales pour étudier un phénomène. Vous avez été de très bons conseils et vous avez consacré beaucoup de temps à me corriger. Pour toutes ces choses, un seul merci ne suffit pas.

J'ai aussi pu réaliser cette thèse grâce au Groupe de Physique des Matériaux, un laboratoire convivial et performant sur le plan scientifique. Je tiens tout d'abord à te remercier, Xavier, pour l'accueil chaleureux que tu m'as réservé dès mon arrivée au GPM. Tu t'es assuré de ma bonne intégration dans le laboratoire et tu as également suivi de près mes travaux en étant membre de mon CSI, malgré les tâches de directeur du laboratoire.

Je remercie également les membres du département Systèmes Désordonnés et Polymères. Merci à Marie-Rose, Éric et Clément pour votre disponibilité sans faille. Vous avez traité chacune de mes requêtes avec soin et ponctualité, même dans l'urgence ! Merci notamment à Éric pour le miel et les parties d'échecs. Merci à Nicolas, Antonella et Éric pour votre regard extérieur, critique et expert sur mes travaux. Les discussions scientifiques ou non ont été un plaisir.

Merci également à l'ensemble des permanents du laboratoire, enseignants-chercheurs, techniciens, ingénieurs, du pôle administratif ou du PoAIR. Je tiens tout particulièrement à remercier Christine, Linda, Caroline et Germain pour votre accompagnement administratif, Marie-Ange pour ton dévouement et ta bonne humeur, ainsi qu'Helena, Étienne, Solène, Bertrand, Sébastien et Jean-Marie pour m'avoir accompagné dans mes missions d'enseignement.

Enfin, je tiens à remercier tous les non-permanents du GPM, qu'ils aient été titularisés, partis dans d'autres laboratoires ou restés au GPM. Ces trois années ont été agréables et sont passées très vite grâce à vous. Merci aux anciens, Christian, Juan, Louis, Grégory, PA, Amandine, Samba, Jeffrey et bien d'autres encore. Je tiens à remercier spécifiquement Blandine et Tasnim de m'avoir accompagné durant vos dernières années en tant que doctorante et pour nous avoir montré la fonction "digitizer" sur Origin ! Merci aux nouveaux (qui ne sont plus si nouveaux que ça maintenant), Sanaa, Arnaud, Alexandre, Yanis, Mehdi, Omar, Alexis, Tom, Marouane, Mohammed, Aissatou, Richel, Florian et tous les autres. Merci à mes collègues de promo, Yuri, JB, Loïc, Sélia et al., ça a été rassurant et motivant d'avancer en même temps que vous, de notre rentrée à nos soutenances, en passant par les journées de doctorants.

Pour finir, merci à Kylian, de m'avoir supporté durant 3 ans, les bons jours comme les mauvais. Toutes nos discussions pour compléter nos lacunes, moi en calo et toi en diélec, pour savoir si une phrase

avait du sens en anglais ou pour résoudre des énigmes, m'ont certainement été d'une très grande utilité ! J'espère que nous arriverons à conclure l'histoire de la bande à Crevé !

J'ai pu réussir ma thèse grâce à un environnement qui m'a permis de m'épanouir. Je tiens donc à remercier chaleureusement tous ceux qui ont rendu mon quotidien agréable et dynamique. Je tiens tout d'abord à remercier Julien de m'avoir accueilli dans notre coloc. Tu as grandement facilité mon installation à Rouen. Je remercie également le GCOB handball et tous les seniors. Je suis convaincu que le dicton "un esprit sain dans un corps sain" est vrai. Vous avez été mon point d'ancrage à Rouen et m'avez permis de me défouler pleinement.

Merci à Julien, tu as été mon plus grand soutien en dehors du laboratoire. Toujours disponible et partant, on ne s'est jamais ennuyé ensemble. Merci de m'avoir fait rencontrer Matthieu, David, Guillaume, Mélody, Louna et Manon. Merci à vous pour nos moments sportifs, festifs et gustatifs. Vous avez su me cerner et me faire voyager, et vous êtes pour moi l'une des meilleures choses qui me soient arrivées à Rouen. Et puis Cécilie, tu m'as été d'une grande aide dans ma préparation de soutenance, et bien plus encore. Merci pour tout.

Toutes mes rencontres à Rennes ont finalement contribué à mon parcours jusqu'à ma thèse. Je remercie Jean-Benoît de m'avoir fait entrer dans le monde de la recherche, ainsi que Adel, Yasser et Adrien, et plus généralement l'Institut Physique de Rennes. Merci également à MPC et compagnie, Clem, Emma, Noémie, Kader, Fiachra, Annaïck, Mathilde, Clara, AE, Malo, Suliac, ainsi qu'aux 4 doigts Thibaut, Mathieu et Grégoire. Vous vous êtes toujours efforcés de comprendre nos sujets de thèse et vous avez été d'un grand soutien à chaque instant, malgré la distance. Je suis très fier de nous, Grégoire, et du parcours que nous avons fait ensemble, de l'IUT jusqu'à nos thèses. Bravo et merci. Merci, enfin à ma famille, Papa, Maman, Léo et Niels, du début à la fin, je vous dois tout.

Table of content

Acknowledgments	I
Table of Content	IV
Introduction	1
Chapter 1. Theoretical Framework	5
I. THE GLASS TRANSITION	6
1) <i>Kinetic point of view</i>	6
2) <i>Dynamic point of view</i>	9
3) <i>Thermodynamic point of view</i>	13
4) <i>Physical aging</i>	16
II. THEORETICAL APPROACHES OF THE GLASS TRANSITION	18
1) <i>Dynamic theories</i>	19
2) <i>The entropic model and cooperativity concept</i>	21
3) <i>Energy landscape</i>	24
4) <i>Dynamic heterogeneity</i>	26
5) <i>Other theories</i>	33
III. PRESSURE INFLUENCE ON THE GLASS TRANSITION	38
1) <i>Experimental observations</i>	38
2) <i>Pressure/volume influence on mobility</i>	43
3) <i>Theoretical model</i>	49
4) <i>Aging under pressure</i>	53
LIST OF ABBREVIATIONS AND SYMBOLS	58
Chapter 2. Materials and Methods	61
I. POLYMERS	62
1) <i>Poly(lactide acid) PLA</i>	64
2) <i>Poly(ethylene terephthalate glycol) PETg</i>	65
3) <i>Poly(vinyl acetate) PVAc</i>	65
4) <i>Poly(ethylene-vinyl acetate) EVA</i>	66
II. CALORIMETRIC EXPERIMENTAL TECHNIQUES.....	67
1) <i>Differential scanning calorimetry DSC</i>	67

2) <i>Modulated temperature differential scanning calorimetry MT-DSC</i>	69
III. DIELECTRIC EXPERIMENTAL TECHNIQUES.....	72
1) <i>Theory of dielectric relaxation</i>	72
2) <i>Broadband dielectric spectroscopy BDS</i>	75
3) <i>Analysis of dielectric spectra</i>	76
4) <i>Broadband dielectric spectroscopy High Pressure HP-BDS</i>	78
IV. DETERMINATION OF EXPERIMENTAL PARAMETERS	79
1) <i>Metrological aspects of HP-BDS</i>	80
2) <i>Cooperativity volume</i>	82
LIST OF ABBREVIATIONS AND SYMBOLS	84
Chapter 3. Volumetric and Thermal Contributions of the Isobaric Fragility	87
I. UNCORRELATION BETWEEN ISOBARIC FRAGILITY AND COOPERATIVITY	88
1) <i>Highlight from various glass formers.</i>	88
2) <i>Interest of pressure</i>	92
II. PRESSURE AND TEMPERATURE DEPENDENCES ON THE SEGMENTAL RELAXATION.....	94
1) <i>Temperature and pressure dependences of relaxation time</i>	94
2) <i>Pressure dependence on glass transition</i>	98
3) <i>Pressure dependence on isochoric fragility</i>	99
III. CORRELATION BETWEEN ACTIVATION VOLUME AND COOPERATIVITY VOLUME.....	100
1) <i>Activation volume</i>	100
2) <i>Cooperativity volume</i>	101
IV. ESTIMATION OF THE CONTRIBUTIONS OF THE ISOBARIC FRAGILITY	104
1) <i>Thermal and volumetric contributions</i>	104
2) <i>Isochoric fragility from Donth definition</i>	106
V. MOLECULAR MOBILITY INFLUENCE OF ISOBARIC FRAGILITY CONTRIBUTIONS	110
1) <i>Contributions of isobaric fragility under pressure</i>	110
2) <i>Interpretation with the intra and intermolecular interactions</i>	113
VI. CONCLUSION	114
LIST OF ABBREVIATIONS AND SYMBOLS	115

Chapter 4. Role of VAc Group on Dielectric Relaxation, Fragility and Cooperativity	119
I. UNCORRELATION BETWEEN FRAGILITY AND GLASS TRANSITION	120
1) <i>The EVA series</i>	120
2) <i>Highlight from various systems</i>	124
II. INTERMOLECULAR INTERACTIONS IN THE PVAc/EVA SERIES	127
1) <i>Dispersion of dielectric relaxation</i>	127
2) <i>Role of dipolar side group in interactions</i>	133
III. INTERMOLECULAR INTERACTION AND COOPERATIVITY	135
1) <i>Isobaric cooperativity</i>	135
2) <i>Cooperativity from pressure fluctuation</i>	136
3) <i>Isothermal cooperativity</i>	138
IV. ROLE OF INTRA AND INTERMOLECULAR INTERACTIONS ON SEGMENTAL RELAXATION	139
1) <i>Segmental mobility of PVAc/EVA series as a function of temperature and pressure</i> 139	
2) <i>Activation volume</i>	141
3) <i>Thermal and volumetric contributions of isobaric fragility in PVAc/EVA series</i>	142
V. CONCLUSION	145
LIST OF ABBREVIATIONS AND SYMBOLS	147
Conclusions and Perspectives.....	149
Appendix	152
References	158

Introduction

Thermoplastic polymers are widely used because of their low density and low processing costs. In some cases, they are used for the unique properties of glass, such as their pellucid property (window, plastic bottle), their biocompatibility (prosthesis, food packaging), their viscoelasticity (gasket, anti-vibration seal) or their dielectric behavior (insulating sheath, capacitor). During their processing and daily use, these materials can undergo viscosity changes as a function of temperature, time, stress, pressure, etc. This can directly change their previously mentioned properties. In this context, understanding how molecular mobility is affected under these conditions has become an intensive field of research. A common feature among glass formers is the viscous slowing down of the structural relaxation dynamics observed around the glass transition temperature T_g (Ediger et al., 1996). Knowledge of viscosity of polymers as a function of temperature has therefore guided research for many years using experimental methods associated with rheology. While there is a vast amount of data on viscosity as a function of temperature, there is only limited information on viscosity or relaxation times of polymers as a function of pressure. Understanding the role of chemical structure on this viscous slowing down, by cooling or by the application of pressure, could help to design specific materials for precise applications, or to optimize manufacturing processes such as extrusion and thermoforming.

Therefore, the relaxation process associated with the glass transition in polymers, known as segmental relaxation, has been extensively studied since the middle of the 20th century (Williams et al., 1955; Bailey and Winey, 2020; Baker et al., 2022). However, the connections between macromolecular chain chemistry, microstructure, and relaxation dynamics remain incompletely understood. Various models and approaches have been proposed to classify the temperature dependence of the dynamic viscosity and the relaxation time. Angell introduced a classification of glass-forming liquids based on relaxation time variations normalized to T_g (Angell, 1985). This classification identifies glass formers as "strong" or "fragile" based on the steepness of their relaxation time temperature dependence near T_g , which is quantified by the isobaric fragility index m_p . Classical theories such as the entropic model of Adam and Gibbs (Adam and Gibbs, 1965) attribute the slowing down dynamics near T_g to the growth of the size of dynamically correlated structural units. This leads to the concept of Cooperative Rearranging Regions (CRR) whose size increases with decreasing temperature, leading to vitrification for a cooperativity volume of approximately 30 nm^3 , regardless of the glass formers (Richert, 1996). Among the studies allowing to estimate the CRR size, the Donth's approach uses the quantification of temperature fluctuations all over the amorphous medium (Donth, 1982).

Such approach has been intensively used by the “Disordered systems and polymers” department from the GPM laboratory. With decades of experience in thermal analysis, the measurement of the volume of cooperativity has been conducted in a multitude of systems, including amorphous (Rijal et al., 2015), crystallized (Lixon et al., 2008), and plasticized polymers (Monnier et al., 2015), multilayer polymer films (Arabeche et al., 2012), and chalcogenide glasses (Saiter et al., 2013). The cooperativity volume has given information on the intermolecular interactions in these systems. Based on the strong assumption that cooperativity volume and activation volume are correlated, several studies of the department have investigated thermal and volumetric contributions of molecular mobility at atmospheric pressure (Bouthegeourd et al., 2013; Delpouve et al., 2014). The intra and intermolecular interactions have been related to the thermal and volumetric contributions, respectively. This has highlighted the impact of changing the chemical structure on the molecular mobility of polymer and therefore, how the structure alters the glass transition and the isobaric fragility (Delpouve et al., 2011; Fosse et al., 2022). It is important to note that the thermal and volumetric contributions of molecular mobility are expressed from isochoric fragility and activation volume, respectively (Hong et al., 2009). These contributions can only be determined experimentally by combining application of controlled pressure with a structural relaxation technique.

High Pressure Broadband Dielectric Spectroscopy (HP-BDS) offers the possibility to follow the relaxation time for frequency from 100 mHz up to 1 MHz and for pressures up to 600 MPa. In this work, the molecular mobility has been investigated on two sets of amorphous thermoplastic polymers, with the goals to confirm assumptions surrounding the relationship between activation volume and cooperativity, and to determine the role of inter and intramolecular interactions on the glass transition and the isobaric fragility. The first set is composed of the poly(lactide acid) PLA, the poly(ethylene terephthalate glycol) PETg and the poly(vinyl acetate) PVAc. These polymers have different backbone rigidity, related to intramolecular interactions. The second set is the PVAc/poly(ethylene-co-vinyl acetate) EVA series. This series has different ratio of lateral group of vinyl acetate (VAc). Thus, the backbone chain remains unchanged, whereas the intermolecular interactions vary with the ratio of VAc. The comparison of thermal and volumetric contributions of molecular mobility in this two sets of polymers reveal how the backbone rigidity and the length of the lateral group influence molecular dynamics.

The manuscript is divided into four chapters. The first chapter is a review of the literature to provide a basic understanding of glass transition and the molecular mobility of glass-forming liquids. Thus, the relaxation time and thermodynamics properties above and below the glass transition temperature are

described. Classical approaches of glass transition theories describing the viscous slowing down are introduced. Moreover, the influence of volume changes on molecular dynamics is developed. The historical experiments of molecular mobility measurement as a function of pressure are presented. Different models allowing the description of relaxation times as a function of the temperature, pressure and volume combination are discussed.

The second chapter describes the polymers selected for this study, including the main features and the thermo-processing conditions. The techniques of calorimetry and dielectric relaxation are described. Details on extraction of physical parameters used in this work are also provided.

The third chapter focuses on the study of the PETg, PLA and PVAc molecular mobility. Their differences of backbone rigidity imply that their molecular mobility behave differently as a function of the temperature and pressure. The use of HP-BDS gives access to activation volume at the glass transition. In parallel, the cooperativity volume can be determined from the extended Donth's approach and can be compared to the activation volume. Moreover, the thermal and volumetric contributions of the isobaric fragility are characterized for providing explanation about the chemical structure role on the polymer molecular dynamics.

The fourth chapter deals with the role of VAc lateral group on molecular mobility in the PVAc/EVA series. The intermolecular interactions are characterized using the dispersion of relaxation time and dielectric strength. The intermolecular interactions are also followed in terms of cooperativity volume in isobaric and isothermal conditions. The thermal and volumetric contributions of the molecular mobility in the PVAc/EVA series are determined and discussed to understand how they justify the steadiness of isobaric fragility regardless the ratio of VAc.

Finally, conclusions presenting the main results and perspectives of this work are provided at the end of the manuscript.

Chapter 1. Theoretical framework

Table of content

CHAPTER 1. THEORETICAL FRAMEWORK	6
I. THE GLASS TRANSITION	6
1) <i>Kinetic point of view</i>	6
2) <i>Dynamic point of view</i>	9
3) <i>Thermodynamic point of view</i>	13
4) <i>Physical aging</i>	16
II. THEORETICAL APPROACHES OF THE GLASS TRANSITION.....	18
1) <i>Dynamic theories</i>	19
2) <i>The entropic model and cooperativity concept</i>	21
3) <i>Energy landscape</i>	24
4) <i>Dynamic heterogeneity</i>	26
5) <i>Other theories</i>	33
III. PRESSURE INFLUENCE ON THE GLASS TRANSITION	38
1) <i>Experimental observations</i>	38
2) <i>Pressure/volume influence on mobility</i>	43
3) <i>Theoretical model</i>	49
4) <i>Aging under pressure</i>	53
LIST OF ABBREVIATIONS AND SYMBOLS	58
REFERENCES	ERREUR ! SIGNET NON DÉFINI.



View of the Surprise Fjord in the southern part of Axel Heiberg Island, Canadian Arctic. Known as piedmont glaciers, they seem to flow while they are made of ice. Taken from (Alean and Hambrey, 2017).

Chapter 1. Theoretical framework

A glass is an amorphous solid material. This quite simple definition is not without meaning. Unlike crystalline solids, which have a highly ordered molecular structure, glasses lack a long-range repeating pattern in its atomic structure arrangement. That is why a glass is called an amorphous material; the atoms or molecules maintain their disordered arrangement in a random manner, such as in the liquid state. Glass is indeed solid material despite its microscopic structure being similar to that of a liquid. The solid nature of glass is established by its high viscosity. Unlike liquids, glass flows too slowly to be considered as such. The transition from liquid to glass begins with sufficiently rapid cooling above the melting temperature to avoid crystallization and remain in a metastable phase. If this cooling is prolonged, the macroscopic properties of this supercooled liquid with rubbery behavior will evolve to become close to those of a solid. The transition from metastable supercooled liquid to glass is known as the glass transition. Although our environment is filled with a multitude of objects in glassy state, the physics behind the glass transition remains one of the century's most significant unresolved mysteries.

I. The glass transition

The glass transition represents a change from solid behavior (glass) to rubbery behavior (or supercooled liquid). Many of the physical properties of the material undergo significant changes in its vicinity (specific volume, enthalpy, entropy, dynamic modulus of elasticity, permittivity, conductivity, specific heat, optical refractive index, etc.).

In rheology, the difference between a solid or fluid material is made using the Deborah number N_D (Reiner, 1964). It is the ratio between the relaxation time τ and the observation time t_0 : $N_D = \tau/t_0$. If $N_D \ll 1$, the material is considered to be fluid. For window glass, it is estimated $\tau = 10^{32}$ years (ten thousand trillion times the age of the universe) at 20 °C. Such a glass can be considered as a solid at 20 °C, even on the scale of the whole of humanity. In contrast, for same temperature, water subjected to extremely rapid stress can be perceived as a solid. In practice, this is nearly impossible, since τ is in the range of picoseconds at room temperature.

1) Kinetic point of view

❖ Viscous slowing down

In glass forming liquid exhibiting a certain level of molecular disorder, the mobility of the relaxing units significantly decelerates as temperature decreases. Assuming no phase transition disrupts or alters this disorder, the relaxation time τ (or viscosity η) progressively lengthens from ten femtoseconds ($\eta =$

10^{-4} Pa. s) to hundreds of seconds ($\eta = 10^{12}$ Pa. s), spanning sixteen orders of magnitude (Zheng and Mauro, 2017). It is conventional to associate the glass transition temperature of the glass formers when a typical experimental duration ($\tau = 100$ s) is reached. At this moment, the supercooled liquid undergoes vitrification during continued cooling. This variation is not proportional to the changes in density induced by temperature. In liquid, at temperatures significantly higher than the glass transition, the dependence of relaxation times follows the Arrhenius law:

$$\tau = \tau_{\infty} \exp \left[\frac{E_A}{k_B T} \right], \quad 1-1$$

where τ_{∞} is a pre-exponential factor corresponding to the theoretical relaxation time at infinite temperature, E_A is the activation energy associated with the relaxation process, and k_B is the Boltzmann constant. According to the Arrhenius law, the activation energy is constant with temperature. Nevertheless, glass forming liquids show a universally viscous slowing down and see their E_A increasing (Debenedetti and Stillinger, 2001). This increase is experimentally observed by a huge increase of relaxation times directly linked with a super-Arrhenius behavior (Hecksher et al., 2008), and it can be described by the Vogel-Fulcher-Tammann-Hesse law (VFTH) (Vogel, 1921; Fulcher, 1925; Tammann and Hesse, 1926):

$$\tau(T) = \tau_{\infty} \exp \left[\frac{DT_0}{T - T_0} \right]. \quad 1-2$$

In this expression, D is the steepness parameter, and T_0 the Vogel temperature associated with an infinitely slow relaxation (also noted T_V).

❖ Fragility

Angell has proposed a useful classification of liquids along a "strong" to "fragile" scale (Angell, 1985). Strong glass forming liquids (with a low isobaric fragility index, m_p close to 16), have almost an Arrhenius behavior, i.e., the activation energy allowing relaxation is practically constant whatever the temperature. At the opposite for fragile liquids such as polymers ($50 < m_p < 200$ (Kunal et al., 2008)), this activation energy increases with cooling. **Figure 1-1** shows the Angell's plot for various liquid viscosities at atmospheric pressure. The logarithm of viscosity is plotted as a function of T_g/T . Isobaric fragility is determined by the steepness of relaxation time (or viscosity) at $T_g/T = 1$. Therefore, the isobaric fragility can be calculated by:

$$m_p = \left(\frac{d \text{Log}_{10}(\tau)}{d \left(\frac{T_g}{T} \right)} \right) \Bigg|_{P, T=T_g}. \quad 1-3$$

The isobaric fragility is the sensitivity of the relaxation time to a temperature variation at the glass transition temperature T_g for a constant pressure. The higher the isobaric fragility, the greater the increase in activation energy from liquid up to the glass.

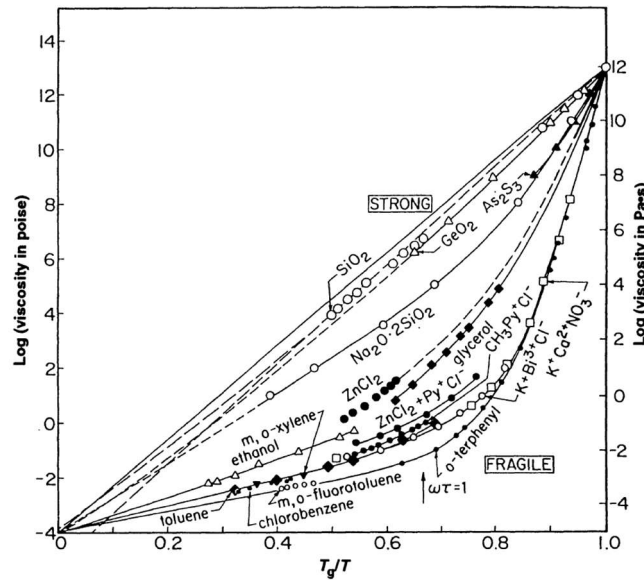


Figure 1-1. Angell's plot of liquid viscosities reveals strong-fragile behaviors. Strong liquids demonstrate near linearity, Arrhenius-like behavior. Fragile liquids display super-Arrhenius behavior, with an activation energy rising as temperature decreases. Adapted from (Angell, 1995).

❖ Crossover temperature

For fragile liquid, such as polymer or molecular glass forming liquid, during the change of trajectory of relaxation times from Arrhenius to super-Arrhenius behaviors, a decoupling of relaxation occurs. The α -relaxation, the main relaxation associated with large amplitude intermolecular movements, deviates from the β -relaxation, secondary relaxation associated with rapid, localized reorientation movements. The decoupling starts when temperature reaches the crossover temperature T^* during cooling as shown in **Figure 1-2**. Other secondary relaxations can occur during cooling before T^* . The secondaries relaxations follow the Arrhenius law with decrease of temperature, thus keep constant activation energy. In the meantime, the α -relaxation slowing down, and see relaxation times drastically increase near T_g . It is conventional to associate the glass transition temperature of the glass formers with a α -relaxation time of the order of 100 s (Delbreilh et al., 2009). Then in the glassy domain, the relaxation times diverges at the Vogel temperature T_V .

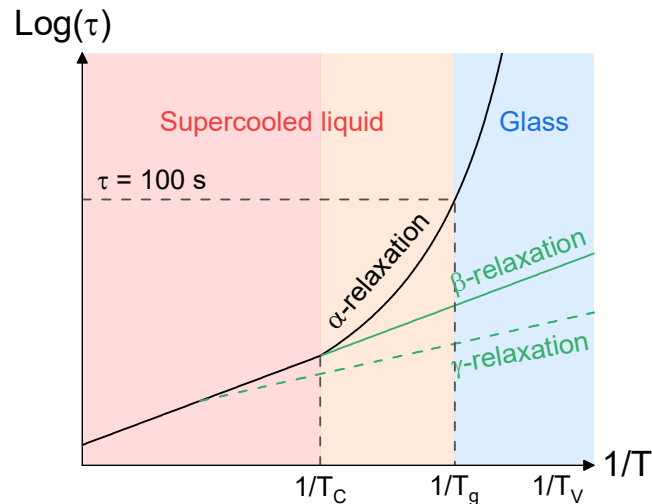


Figure 1-2. Schematic illustration of the temperature dependence of relaxation processes in a forming liquid. The α -relaxation is represented by the black curve, secondary relaxations by green lines. Crossover temperature T^* , glass transition temperature T_g (at $T(\tau = 100 \text{ s})$) and Vogel temperature T_V are indicated by vertical dashed lines.

2) Dynamic point of view

❖ Relaxation function

The experimental measurement of viscous slowing down is usually obtained by solliciting dynamically glass forming liquid. It is exposed to an external perturbation and relaxes over time. The perturbations should be small enough to fulfill the fluctuation-dissipation theorem (FDT)^a, which requires that the magnitude of the perturbation does not exceed the amplitude of the spontaneous fluctuations of the perturbed property. The relaxation function is a measure of its response to the external disturbance as a function of time. Such perturbation can result from an applied electric field, stress or strain, causing polarization, deformation or stress respectively. Relaxation functions can be expressed by the stretched exponential, or Kohlrausch–Williams–Watts (KWW) function (Kohlrausch, 1863; Williams and Watts, 1970):

^a The fluctuation-dissipation theorem (FDT) is a fundamental concept in statistical physics linking the behavior of a system in thermodynamic equilibrium to its response to small perturbations. In other words, it establishes a relationship between the random fluctuations of a system (such as fluctuations in temperature or density) and its response to an external perturbation (such as the application of a force or a weak magnetic field).

$$\Phi(t) = \exp \left[- \left(\frac{t}{\tau_{KWW}} \right)^{\beta_{KWW}} \right]. \quad 1-4$$

The relaxation function, or correlation function, $\Phi(t)$ starts at 1 when t is too short to allow the system to relax, it decreases more or less quickly when $t \approx \tau$, and reaches 0 when the system has entirely relaxed. β_{KWW} is the stretching exponent and it can have values between 0 and 1. The stretching of the relaxation function for glasses reflects a broadening of the peak associated with α -relaxation visible on the response of a relaxation. The relaxation is no longer of the Debye type ($\beta_{KWW} = 1$, characteristic of a single relaxation time, all relaxing units have the same relaxation time) but is characterized by a relaxation time distribution ($0 < \beta_{KWW} < 1$). An example of relaxation function is shown in **Figure 1-3**. It is the normalized polarization of deuterated glycerol after elastic scattering.

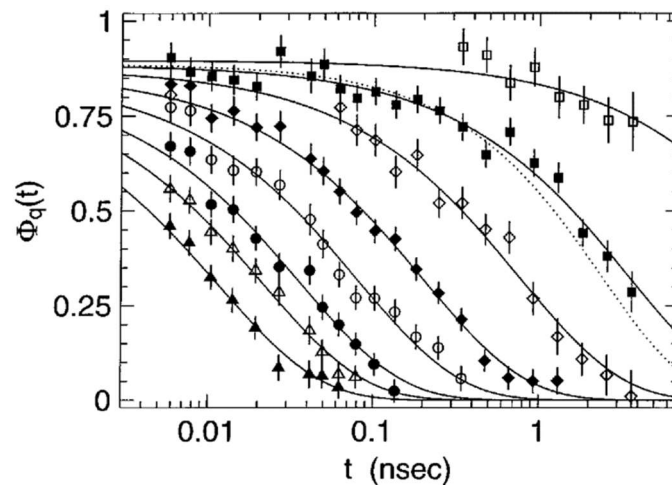


Figure 1-3. Intermediate scattering function of glycerol. Temperatures decrease from 413 K down to 270 K from left to right. The function, represented by solid lines, uses a stretching exponent of 0.7, where the dotted line uses $\beta_{KWW} = 0.82$. Taken from (Wuttke et al., 1996).

❖ Relaxation processes

The glass transition is a time-dependent phenomenon, as is the relaxation function. To consider if a system has a liquid or a glass behavior depends of its observation time. This time dependence meets the concept of Deborah number mentioned earlier. Various experimental techniques rather use the frequency domain to measure the time dependence of α -relaxation. A simple Fourier transform usually links frequency domain and time domain measurements. Such frequency domain measurement can be achieved by dielectric or mechanical spectroscopies. **Figure 1-4** presents schema of two dielectric spectra, illustrating the most common characteristics at different temperatures over a wide range of frequencies (such frequency range is not reachable with only one experimental technique). α -

relaxation is present at lower frequency than the β -relaxation since its relaxation process is slower. In addition, the frequency shift for α -peak between two temperatures is greater than for the β -peak, accordingly to **Figure 1-2**. At higher frequency, a rapid motion corresponds to the fast secondary β -relaxation. The molecule oscillates within the boundaries of its neighboring molecules. In the terahertz frequency range, an additional molecular phenomenon known as the boson peak is observed. Its origin seems to be the result of an excess in the density of vibrational states^b (Buchenau et al., 1992). The impact of these other relaxation processes over the glass transition is unclear and controversial. Some glass forming present a so-called Johari-Goldstein β -relaxation ($JG\beta$) that should be regarded as a precursor for the dynamic glass transition (Johari and Goldstein, 1970). In some glass forming liquids, an excess wing is visible as an excess contribution to the high-frequency flank of the α -peak. Strong evidence suggested that the excess wing is the high-frequency side of a β -peak hidden under the α -peak, whose latter has a higher amplitude (Schneider et al., 2000), however it is still subject under discussion (Guiselin et al., 2022).

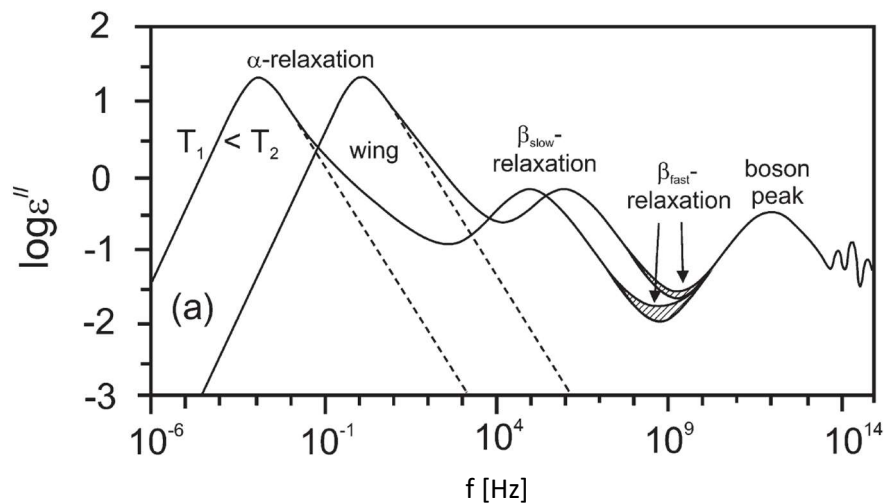


Figure 1-4. Schematic view of dynamics taking place in glass forming liquids. The imaginary part of permittivity is shown as a function of frequency for two temperatures ($T_1 < T_2$). Taken from (Kremer and Schönhals, 2003).

^b In amorphous materials, the density of low-frequency vibrational states shows an anomaly: an excess of states compared with the Debye model, hence the appearance of the so-called boson peak. The exact origin of the boson peak is still a matter of debate, but it is generally attributed to structural disorders and local vibrational modes in amorphous materials (Malinovsky and Sokolov, 1986).

❖ Time Temperature Superposition

The α -relaxation peak can be therefore translated in frequency range with temperature. This phenomenon leads to the principle of time temperature superposition (TTS). It stipulates that isotherm segments of relaxation spectrum can be shifted from reference temperature T^* in frequency with a shift factor $a_T(T)$. **Figure 1-5** shows the TTS of storage modulus of an amorphous copolymer. The shift factor $a_T(T)$ can be determined by the Williams-Landel-Ferry empiric law (WLF) (Williams et al., 1955) as:

$$\text{Log}_{10}(a_T(T)) = \text{Log}_{10}\left(\frac{\tau(T)}{\tau(T^*)}\right) = -\frac{C_1(T - T^*)}{C_2 + T - T^*} \quad 1-5$$

C_1 and C_2 are constants linked to the reference temperature T^* . The principle of TTS is useful for extrapolating relaxation spectra when the physical properties measured are obtained in a short frequency range, like dynamic mechanical analysis (DMA) techniques. As an example, the measure of the α -relaxation for six temperatures over a range of four decades allows to get the master curves over a range of 17 decades (see **Figure 1-5**). By this way the properties at very low frequency are reachable without waiting, in this case, the true measurement of the point at 10^{-15} Hz would have taken at least 32 million of years instead of the dozen hours that were really carried out.

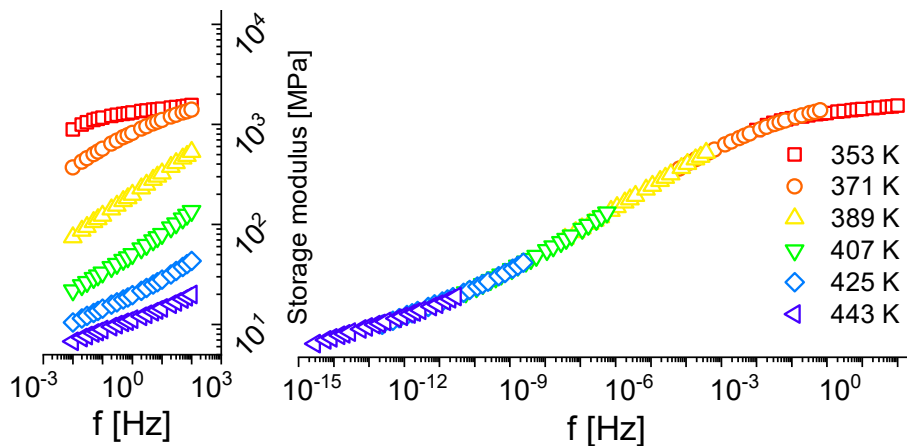


Figure 1-5. The storage modulus of ABS as a function of frequency from 353 K up to 443 K (left panel). TTS master curve of ABS storage modulus by taking 353 K as reference temperature (right panel).

A good TTS is only possible if no other process interferes with the α -relaxation signal, or if the stretching parameters remain constant as a function of temperature.

3) Thermodynamic point of view

❖ Not a first-order phase transition

The mysterious nature of the glass transition resides in its thermodynamic definition. More precisely, in what it is not. It is not a first order phase transition (FOPT). Usually, when a liquid is cooled, a crystal is formed by a FOPT, which induces a sudden change towards much lower values of the first derivatives of Gibbs free energy G , i.e., specific volume V , enthalpy H and entropy S (Dyre, 2006). They are obtained from:

$$V = \left(\frac{\partial G}{\partial P} \right)_T, \quad 1-6a$$

$$H = G - T \left(\frac{\partial G}{\partial T} \right)_P, \quad 1-6b$$

$$S = - \left(\frac{\partial G}{\partial T} \right)_P. \quad 1-6c$$

The formation of glass from liquid phase as function of temperature is shown in **Figure 1-6a**. Unlike the FOPT of liquid-crystal, the change in entropy, enthalpy and specific volume of the glass transition does not undergo a discontinuous jump during cooling and occurs over a wide temperature range (Debenedetti et al., 2001).

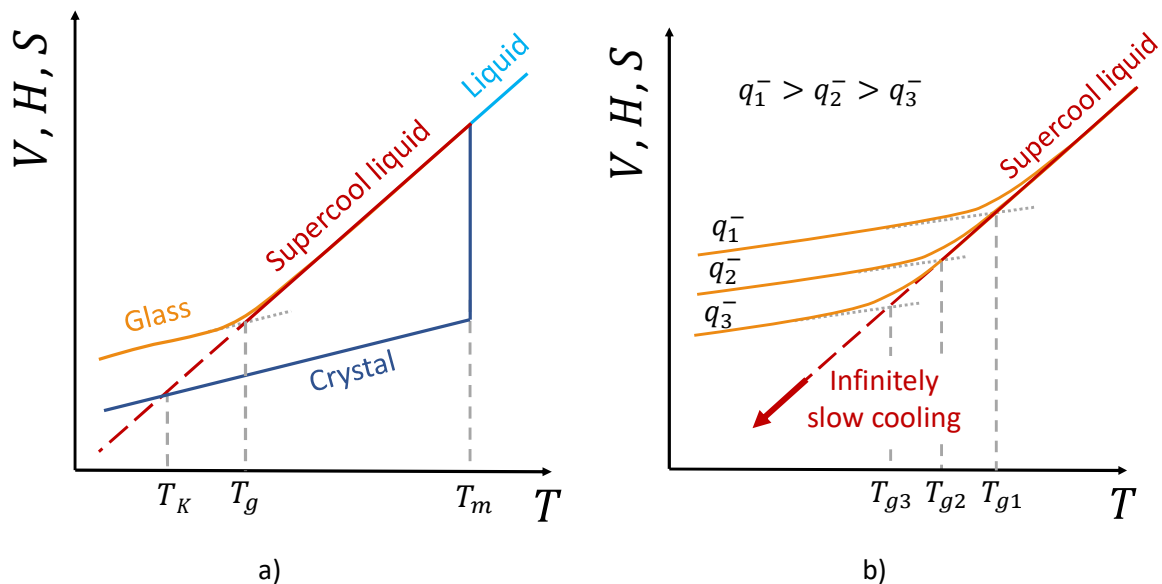


Figure 1-6. Schemas of temperature dependence of the first derivatives of Gibbs free energy (specific volume V , enthalpy H or entropy S) a) during glass transition and FOPT of liquid-crystal type and b) for different cooling rates noted q^- . The Kauzmann temperature T_K , the glass transition temperature T_g and melting the temperature T_m are indicated by vertical dashed lines.

❖ Cooling rate

The fact that cooling rate is fast enough to avoid crystallization is essential to create glass. Moreover, the cooling rate has an influence on the glass transition temperature. The slower the cooling rate, the lower the glass transition temperature as shown in **Figure 1-6b**. Vitrification occurs at T_g , when the relaxation time becomes too large for molecular rearrangements to occur on the time scale allowed by the experiment, the latter being defined by the cooling rate applied (Cangialosi, 2014). Thus, speed of α -relaxations becomes too slow for the system to remain on the liquid equilibrium. Varying the cooling rate allows to dynamically change T_g , and it can be modeled by an adapted VFTH law (Dhotel et al., 2015):

$$\log(q^-) = A - \frac{1}{\ln(10)} \frac{B}{T_g - T_0}, \quad 1-7$$

where q^- is the cooling rate (expressed in $\text{K}\cdot\text{s}^{-1}$), A is a constant and B is a fitting parameter ($= DT_0$ of Equation 1-2). According to this equation, an infinitely slow cooling down should generate a glass with a T_g very close to T_0 . Furthermore, T_g changes by few degree when the cooling rate changes by an order of magnitude (Ediger et al., 1996). Nonetheless, the steepness of the first derivatives of Gibbs free energy in glass is not impacted by the cooling rate.

❖ Almost a second-order phase transition

The glass transition looks like a second order phase transition (SOPT) in the Ehrenfest sense, displaying discontinuous changes in its thermodynamic properties (Goldenfeld, 1999). It maintains continuity in volume and entropy, while having abrupt alterations in their derivatives (the second derivatives of G). **Figure 1-7** illustrates the jump of isobaric thermal expansion α , isobaric specific heat C_p or isothermal compressibility κ in the case of glass transition or FOPT of liquid-crystal. The second derivatives of Gibbs free energy result from:

$$\alpha = \frac{1}{V} \left(\frac{\partial V}{\partial T} \right)_P = \frac{1}{V} \left(\frac{\partial^2 G}{\partial P \partial T} \right), \quad 1-8a$$

$$C_p = \left(\frac{\partial H}{\partial T} \right)_P = -T \left(\frac{\partial^2 G}{\partial T^2} \right)_P, \quad 1-8b$$

$$\kappa = -\frac{1}{V} \left(\frac{\partial V}{\partial P} \right)_T = -\frac{1}{V} \left(\frac{\partial^2 G}{\partial P^2} \right)_T. \quad 1-8c$$

Isothermal compressibility κ corresponds to the inverse of the compression modulus K . Nevertheless, glass transition is neither an Ehrenfest SOPT since it does not fulfil the relation:

$$R = \frac{\Delta\kappa\Delta C_p}{T_g V_g (\Delta\alpha)^2} = 1, \quad 1-9$$

where R is the Prigogine–Defay ratio (Prigogine and Defay, 1986), V_g is the specific volume at T_g , and Δx is the value of the jump of the property x . $R > 1$ for the glass transition (Schmelzer et al. 2011). It reflects that a single order parameter description of the liquid-glass transition is not sufficient according to Goldstein (Goldstein, 1975).

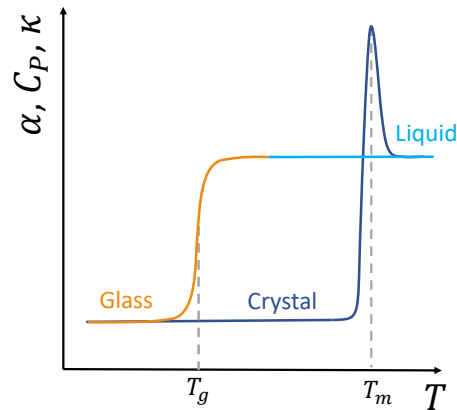


Figure 1-7. Temperature dependence of the second derivatives of the Gibbs free energy (isobaric thermal expansion α , isobaric specific heat C_p or isothermal compressibility κ) during glass transition and FOPT of liquid-crystal type. The glass transition temperature T_g and the melting temperature T_m are indicated by vertical dashed lines.

❖ Kauzmann paradox

Analyzing thermodynamic data across various glass formers, including polymers, Kauzmann has extrapolated a critical point where the first-order thermodynamic properties of the glass matched those of the crystal. This is due to the higher specific heat of supercooled liquids compared to their corresponding crystals (Kauzmann, 1948). Just below the melting point, supercooled liquids exhibit significantly higher entropy than crystals. However, as temperature decreases, the liquid entropy declines more rapidly than that of the crystal (see **Figure 1-6a**). Below a specific temperature, the Kauzmann temperature T_K^c , the liquid entropy becomes lower than that of the crystal, which presents a paradox regarding the disorder of liquids having lower entropy than crystals at the same temperature. The glass transition allows to avoid this issue, leading to the fact that T_K is always

^c Kauzmann temperature T_K is impossible to measure due to the divergence of the relaxation time. A hypothetical phase transition at T_K the basis of some glass transition theories, but has never been observed experimentally.

identified only through extrapolation. Similarities between T_0 and T_K have been reported (Richert and Angell, 1998), however, a direct correlation between both has not been universally proven by experimentation (Tanaka, 2003).

❖ Configurational entropy

The specific heat is typically considered to be the sum of two components: a vibrational aspect that persists in the glass, and a configurational aspect, which becomes null in the glassy state (Goldstein, 1972). Thus, the entropy of liquid comprises these two components. Assuming the vibrational entropy of the liquid closely equal to that of crystal, the configurational entropy S_c can be defined as the entropy excess between the liquid and the crystal: $S_c = S_{\text{liquid}} - S_{\text{crystal}}$. Consequently, S_c becomes null at T_K , which suggests a significant event at this point. On the one hand, this could be interpreted as the occurrence of a phase transition towards a state with zero configurational entropy, which is known as an "ideal glass" (Gibbs and DiMarzio, 1958; Goldstein, 1969). On the other hand, it could imply that the extrapolation is invalid (Stillinger et al., 2001). However, following the metastable supercooled liquid below T_K would lead to a negative S_c and to a violation of the third thermodynamic law (Callen and Callen, 1985). Thus, glasses tend to minimize their configuration entropy over time to reach equilibrium. The evolution of non-equilibrium glasses as a function of time is considered to be the physical aging.

4) Physical aging

During physical aging, the non-equilibrium glass exhibits thermodynamic properties that evolve over time. These properties are in excess and require reduction in order to approach a metastable equilibrium state (Hodge, 1995), which corresponds to the extrapolation of the thermodynamic properties of the supercooled liquid. Physical aging below glass transition can be observed with calorimetry measurement, mainly by differential scanning calorimetry (DSC) analysis. For instance, **Figure 1-8a** illustrates the enthalpy of the glass decreasing along an isotherm (below T_g for a given cooling rate) over time.

Physical aging has been extensively observed since the Tool's experiments on silicate glasses (Tool and Eichlin, 1925), on various glass forming liquids. Ranging from molecular glasses (Sepúlveda et al., 2011; Zhang and Fakhraai, 2017) to metallic glasses (Ketov et al., 2015; Ketkaew et al., 2020), including polymers (Cangialosi, 2024; Mejres et al., 2024), chalcogenide glasses (Evenson et al., 2015; Morvan et al., 2022, 2021), oxide glasses (Mauro et al., 2016; Micoulaut, 2016), amorphous pharmaceuticals (Vyazovkin and Dranca, 2007; Schammé et al., 2016), and colloidal systems (Peng and McKenna, 2016; Bonacci et al., 2020).

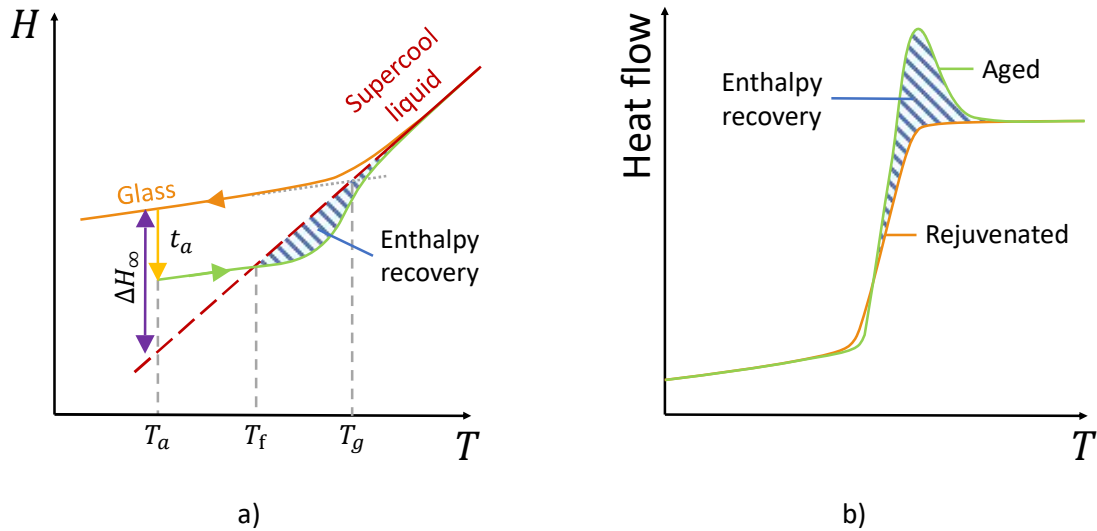


Figure 1-8. a) Schematic diagram of the evolution of the enthalpy of a glass during aging at an aging temperature T_a for a time t_a . The amount of enthalpy recovery is illustrated by the purple double arrow. T_a aging temperature, T_g glass transition temperature and T_f melting temperatures are indicated by vertical dashed lines. b) Heat flow jump associated with the calorimetric glass transition. The endothermic peak associated with structural relaxation of the aged signal (represented in green) is represented by the blue hatched area. The rejuvenated curve is represented in orange.

❖ Enthalpy recovery

The recovery to the supercool liquid of an aged glass is delayed during heating because of the lower energy state reached by itself. This phenomenon manifests by an enthalpy recovery illustrated in **Figure 1-8a**. It leads to an endothermic overshoot on the heat flow signature of the aged material compared to the rejuvenated one, i.e., from glass in the initial configuration (with same cooling rate and which has not undergone physic aging). **Figure 1-8b** shows such overshoot, the longer the aging time t_a , the higher the excess of energy released upon aging. The enthalpy recovery can be estimated from the area between the temperature scan of an aged sample at an aging temperature T_a and an aging time t_a , and rejuvenated sample on the heat flow response with:

$$\Delta H(T_a, t_a) = \int_{T_1}^{T_2} [C_p^a(T) - C_p^r(T)] dT, \quad 1-10$$

where $C_p^a(T)$ and $C_p^r(T)$ are the heat capacity of the aged and the rejuvenated system respectively, T_1 and T_2 are arbitrary temperatures below and above T_g . Based on the assumption that at infinite time the supercooled liquid equilibrium is reached, the expected enthalpy recovery ΔH_∞ at a given aging and glass transition temperatures is deduced from the relation:

$$\Delta H_{\infty} = \Delta C_p(T_g - T_a), \quad 1-11$$

with ΔC_p the heat capacity jump of the material. Furthermore, the physical aging can be studied through the evolution of the fictive temperature T_f . It is defined by the theoretical glass transition temperature of a glass when it reach thermodynamic equilibrium (supercooled liquid) by heating it as shown in **Figure 1-8a** (Tool and Eicitlin, 1931). Indubitably, fictive temperature varies over the time during aging at T_a (Hutchinson, 1995). T_f evolves until the enthalpy and specific volume reach the equilibrium state, at this specific moment, $T_f = T_a$.

❖ Aging scenarios

However, the process by which a glass attains its equilibrium state over extended periods of physical aging remains controversial. Some observations suggest that due to significant steric constraints, polymeric glasses may never reach thermodynamic equilibrium (Gomez Ribelles et al., 1995). Another hypothesis posits that during the glass transition, only a fraction of the glass-forming liquid undergoes vitrification (Hutchinson et al., 2000). Consequently, the theoretical thermodynamic equilibrium may remain elusive due to the coexistence of two distinct relaxation processes: one slow process for the vitrified polymer fraction and another fast process for the non-vitrified fraction. Recent research further reveals rapid equilibration mechanisms within the amorphous phase of polymers, which is associated with a phenomenon of slow liquid dynamics termed the Slow Arrhenius Process (SAP) (Song et al., 2022). slow liquid dynamics. Other investigations propose that while thermodynamic equilibrium may indeed be achievable, it may manifest through the emergence of various intermediate states. The number of these states is influenced by the temperature gap between the glass transition temperature T_g and the aging temperature T_a (Cangialosi et al., 2013). Building upon this notion, it is later proposed that thermodynamic equilibrium is not only attainable, but the transition to a crystalline state may also occur over time, i.e., below the extrapolated supercooled liquid (Androsch et al., 2018).

II. Theoretical approaches of the glass transition

Since the glass transition has been studied, numerous theoretical approaches tried to interpret the experiments which have demonstrated an increase in viscosity and relaxation time. Existing theories describing the viscous slowdown near the glass transition temperature lack consensus, and do not fully explain experimental observations. Despite increasing scientific activity in experimental, theoretical, and numerical approaches to disordered systems, no theory has emerged to comprehensively describe all their properties. The understanding of the glassy state remains a major challenge.

1) Dynamic theories

❖ Free volume model

The earliest approach is probably the free volume theory. The concept was proposed by Eyring and co-workers (Roseveare et al., 1941) and developed by Doolittle (Doolittle, 1951), Cohen and Turnbull (Turnbull and Cohen, 1961). According to the free volume concept, a relaxing unit can kinetically rearrange itself if there is sufficient empty space in its vicinity, i.e., a free volume V_f . The free volume is defined as the difference between the specific volume V and the true volume occupied by atoms or molecules V_0 , which includes the intrinsic volume of molecules and also the volume associated with their vibrational movements. Therefore, $V_f = V - V_0$. Structural units are blocked by a cage formed from their neighbors until they space out by diffusion of free volume due to density fluctuation. The relaxing units can then rearrange when the volume surrounding is superior to a critical volume V^* as shown in **Figure 1-9**. The relaxation phenomenon is therefore driven by a liquid self-diffusion coefficient D :

$$D = D_0 \exp \left[-\frac{\gamma V^*}{V_f} \right], \quad 1-12$$

with $D_0 = ga^*u$, where g is a geometric factor (usually equal to $1/6$), a^* is a molecular diameter and u is the gas kinetic velocity. The parameter γ is an overlap factor between 0.5 and 1. When the probability of having a free space of volume V^* becomes too small, the liquid turns into a glass. According to Cohen and Turnbull, the temperature dependence of the free volume at constant pressure is given by the following equation (Cohen and Turnbull, 1959):

$$V_f = \Delta\alpha \overline{V}_m (T - T_0), \quad 1-13$$

where $\Delta\alpha$ is the coefficient of the thermal expansion, \overline{V}_m is the mean molecular volume, and T_0 is the critical temperature below which the free volume no longer exists. It is worth noting that the combination of **Equations 1-12** and **1-13** with the relation $\tau \propto 1/D$ leads to the VFTH law of **Equation 1-2** for constant pressure.

The free volume theory has a good description of relaxation time (and viscosity) near and above T_g . However, it postulates that liquid turns into a glass from a fix volume depending of V^* , while experiment under pressure has shown that the glass transition can occur at different specific volumes (Goldstein, 1973). Although the theory of free volume has some inconsistencies, it is the basis of many approaches, both past (Williams et al., 1955; Fredrickson and Andersen, 1985; Kivelson et al., 1995) and present (White and Lipson, 2017).

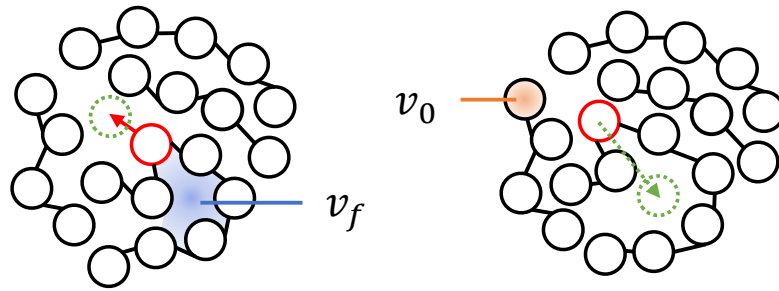


Figure 1-9. Schematic representation of the diffusion of a structural unit during relaxation (left schema). In this configuration, the red structural unit has enough space due to the surrounding volume superior to V^* . The mechanism of free volume diffusion once the structural unit has relaxed is shown by the displacement of the green space (right schema). Example of entities of free volume v_f and occupied volume v_0 are indicated in blue and orange respectively, with $V_f = \sum v_f$ and $V_0 = \sum v_0$.

❖ Mode Coupling Theory (MCT)

Other approaches use the dynamic features for explaining the viscous slowing down, one of the most common used is a theory for the evolution of glassy dynamics in liquids: the mode-coupling theory (MCT) (Götze, 2008). MCT is a mean-field theory firstly proposed by Leutheusser (Leutheusser, 1984), which has been subsequently developed by Bengtzelius, Götze, Sjölander and coworkers (Bengtzelius et al., 1984; Götze and Sjögren, 1996, 1995, 1992). According to the MCT, when a critical temperature T_C (similar to the crossover temperature T^*) is reached, local cages around structural units begin to open up. Beyond this critical temperature, structural units move relatively freely, while below it, the thermal activation of the relaxation process increases. Originally, T^* indicates the transition from Arrhenius to super-Arrhenius behavior. Contrary to this conventional understanding, within MCT framework, activation energies are effectively absent above T_C . Instead, the process to slowing down involves a gradual reduction in unstable relaxing modes. The resulting relaxation time can be understood as arising from an effective energy barrier, which exhibits only a slight increase as temperature decreases (Biroli and Bouchaud, 2012). MCT thus describes two relaxations: a fast relaxation (fast dynamics), which has been identified as corresponding to the first stage of relaxation. This is attributed to movements within the cage, i.e., β -relaxation, while α -relaxation would be linked to the reorganization of cages to allow movement. These two relaxations are separated by the cage effect. **Figure 1-10** presents simulation results of particle motions by plotting the mean-squared displacements over time. A plateau is visible at low temperature due to the cage effect, which separates the fast relaxation (at short time) from the α -relaxation (at longer time).

MCT describes the divergence of relaxation times at T_C , i.e., when the α and β -relaxations decoupled, with (Kob and Andersen, 1994):

$$\tau_\alpha \propto \left(\frac{1}{T - T_C} \right)^\gamma, \quad 1-14$$

where τ_∞ is the relaxation time at infinite temperature γ is a steepness factor. The simplified form of the theory cannot be applied near the experimental glass transition temperature T_g because it forecasts a divergence of relaxation times at a significantly higher temperature.

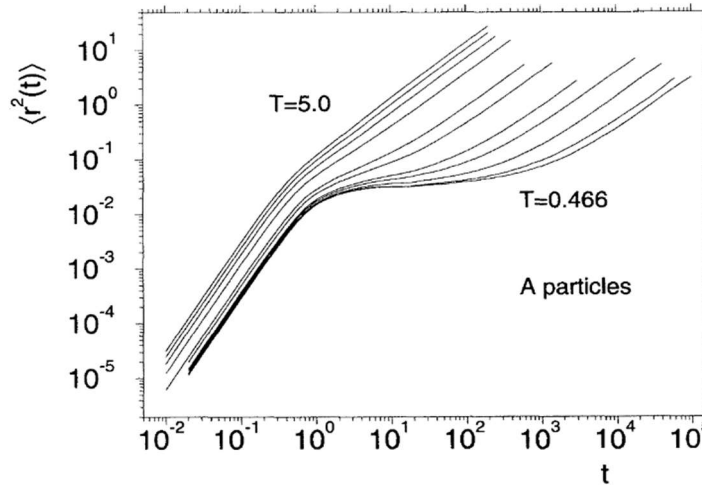


Figure 1-10. Mean-squared displacements of Leonard-Jones (LJ) mixtures^d obtained by molecular dynamics simulations. At shorter times, the β -relaxation is slightly slowed with temperature decrease, while the α -relaxation is drastically slowed down. A plateau between both relaxations occurs at lower temperatures due to the cage effect. Taken from (Kob and Andersen, 1995).

2) The entropic model and cooperativity concept

❖ Adam and Gibbs model

The entropic model of Adam and Gibbs (AG) has been proposed in order to explain the viscous slowing down (Adam and Gibbs, 1965). This theory introduces the concept of cooperative rearranging region (CRR) by the idea that the lower the temperature, the greater the number of structural units N_α that

^d Lennard-Jones mixtures refer to binary or ternary mixtures of particles interacting via Lennard-Jones potentials. The Lennard-Jones potential is a mathematical model commonly used to describe the intermolecular interactions between particles in a system, particularly in molecular dynamics simulations. It consists of two terms: a repulsive term that accounts for short-range repulsion between particles, and an attractive term that represents long-range van der Waals forces. Lennard-Jones mixtures are often studied to understand the behavior of complex systems such as supercooled liquids, glasses, and colloidal systems.

must move cooperatively for allowing the system to relax, as illustrated in **Figure 1-11**. Above the crossover temperature T^* , the structural units are freed from any cooperative movements. Cooling below T^* changes the relaxing nature of glass forming liquid and their behaviors start to be super Arrhenius. It highlights the beginning of cooperative process. The number of structural units increase in CRR as temperature decreases. The CRR is defined as an independent sub-system that can rearrange if a sufficient fluctuation in energy is reached. This is determined by the potential energy hindering the cooperative rearrangement per structural unit $\Delta\mu$. Near the glass transition, the CRR size, hence N_α , suddenly increases drastically, slowing relaxation and energy fluctuation down to the temperature T_0 where N_α should be equal to the number of structural units of the entire glass.

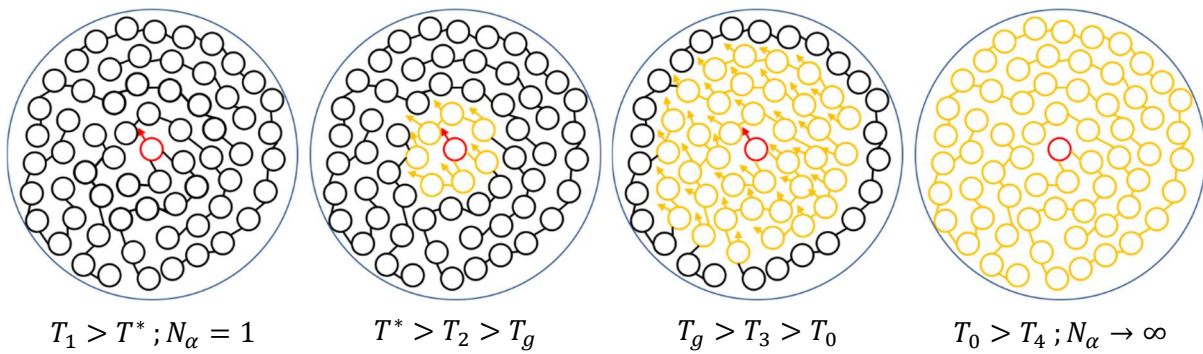


Figure 1-11. Schematic representation of structural units required to cooperatively relax (in orange) in order to allow the rearrangement of the red structural unit. Above T^* , any supplementary structural unit need to move ($N_\alpha = 1$). However, from T_c down to T_0 , the number of structural units that move cooperatively increases until the CRR size being limited by the entire sample ($N_\alpha \rightarrow \infty$).

Adam and Gibbs explained this theoretical phenomenon by a statistic entropic model (Adam and Gibbs, 1965). They defined two sub-systems, those that reside in states which allow a cooperative rearrangement (n sub-systems) and those that do not ($N - n$ sub-systems). They stipulate that the fraction of states allowing rearrangements n/N is proportional to the cooperative transition probability $W(T)$ equal to:

$$W(T) = A \exp \left[-N_\alpha \frac{\Delta\mu}{k_B T} \right], \quad 1-15$$

where A is a temperature independent constant and k_B is the Boltzmann constant. $\Delta\mu$ is assumed to be neither dependent of temperature nor N_α . This probability is associated with the sub-system of N_α relaxing units, independently of the other sub-systems. It is worth mentioning that a structural unit may belong to a CRR at one moment, then the next moment relaxes with another one. The average transition probability $\bar{W}(T)$, is thereby the sum of all possibilities, including the smallest ones. A critical

limit N_α^* is defined as the smallest number of structural units of a sub-system that allows nonnull values of $W(T)$. $\bar{W}(T)$ is then expressed as:

$$\bar{W}(T) = \sum_{N_\alpha=N_\alpha^*}^{\infty} A \exp\left[-N_\alpha \frac{\Delta\mu}{k_B T}\right] \approx \bar{A} \exp\left[-N_\alpha^* \frac{\Delta\mu}{k_B T}\right], \quad 1-16$$

where \bar{A} is a new temperature independent constant. The average transition probability $\bar{W}(T)$ expresses the faculty of CRRs (with an average N_α close to N_α^*) to quickly get enough potential energy to overcome the energy barrier $\Delta\mu$. Thus, \bar{W} is inversely proportional to the relaxation time τ .

On the other hand, the AG model postulates that the size of a CRR is related to the configurational entropy S_C at macroscopic scale as:

$$N_\alpha^* = \frac{N_A s_C^*}{S_C}. \quad 1-17$$

In this expression, N_A is the Avogadro's number and s_C^* is the critical configurational entropy. The latter is defined by $s_C^* = k_B \ln(W_c^{N_\alpha^*/N_A})$ where $W_c^{N_\alpha^*/N_A}$ is a critical average number of configurations available to the subsystem that can perform a rearrangement into another configuration. **Equations 1-16 and 1-17** can be combined for obtaining:

$$\tau = \tau_\infty \exp\left[\frac{s_C^* \Delta\mu}{k_B T S_C}\right] = \tau_\infty \exp\left[\frac{C}{T S_C}\right], \quad 1-18$$

where C is a constant. The AG theory allows to express the relaxation time as a function of configurational entropy, and to link the kinetic and thermodynamic features of viscous slowing down. Moreover, the conceptualization of the number of structural units in a CRR N_α can serve as a potential tool to compare glass forming liquid with each other. The determination of N_α is not an easy task since the configurational entropy cannot be measured experimentally. However, $S_C(T)$ can be evaluated from calorimetry measurements from the entropy variation between any temperatures T_1 and T_2 :

$$S_C(T_1) - S_C(T_2) = \int_{T_1}^{T_2} \left(\frac{\Delta C_P}{T}\right) dT \approx \int_{T_1}^{T_2} \left(\frac{K}{T^2}\right) dT, \quad 1-19$$

by assuming value of the jump between liquid and glass of the specific heat ΔC_P is approximately equal to K/T , where K is a material property that is independent of temperature. Positing $T = T_1$ and $T_K = T_2$ in order to have $S_C(T_K) = 0$, the configurational entropy can therefore be deduced form:

$$S_C(T) = K \left(\frac{1}{T_K} - \frac{1}{T}\right). \quad 1-20$$

These assumptions lead to an equivalence between VFTH law (**Equation 1-2**) and the AG model, and indubitably between T_0 and T_K . The AG model expresses well that the CRR increases with decreasing temperature, causing both a decrease in configurational entropy and an increase in relaxation times. Up to the Kauzmann temperature, where (i) the CRR size is equivalent to the sample dimensions, (ii) S_C vanishes since the entropy of liquid should have reached that of the crystal and (iii) the relaxation time becomes infinitely high, freezing all mobility in glasses. According to the AG theory, the large amplitude motions of α -relaxation are associated with cooperative motion of relaxing units.

3) Energy landscape

Another approach proposed by Angell is to understand why a liquid that has failed to crystallize suddenly becomes super viscous at the glass transition temperature.

❖ A picture of energy landscape

In such a state, it has been postulated that a glass is, in fact, a liquid that has explored its energy landscape until it is kinetically confined to a minimum: a basin. The trapping must occur during cooling, when the relaxation time becomes shorter, allowing the glass to change configuration. This energy landscape, or potential energy hypersurface, can be expressed by theoretical potential energy function of N particles such as $\phi(r_i, \dots, r_N)$, where r_i corresponds to the spatial location of each particle. The energy landscape is therefore convenient to consider the simultaneous interactions with numerous neighbors, making it like a multidimensional surface with $3N + 1$ dimensions.

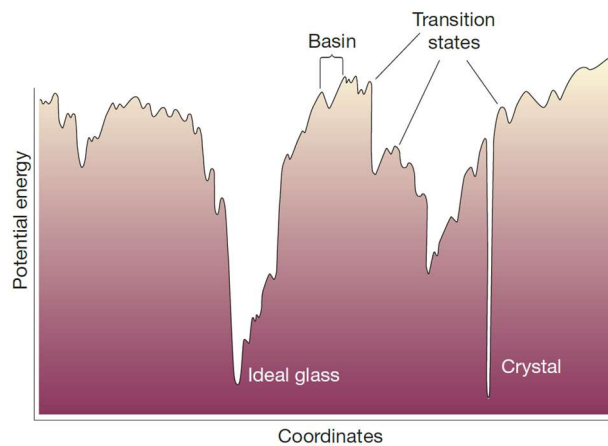


Figure 1-12. Energy landscape of glass forming material. The potential energy is expressed as a function of the possible configuration coordinates of the particles. Taken from (Debenedetti et al., 2001).

Figure 1-12 shows a schematic representation of possible basins as a function of particle coordinates. These basins have a wide distribution of energy minima, corresponding to configurational microstates, with a given number of potential energy minima: the inherent structures. At high temperature, the

inherent structure energy is virtually temperature-independent, because the system has sufficient kinetic energy to explore its entire energy landscape, the system is ergodic. However, as the reduced temperature decreases, the system is unable to overcome the highest energy barrier anymore, and is therefore forced to explore the much rarer deeper basins. The deeper minima usually being associated with higher densities. When this occurs, the kinetics of structural relaxation undergo a shift from exponential to stretched exponential, and the energy activation linked to structural relaxation follows a super-Arrhenius trend, whereby it rises as the temperature decreases. Increasing depth basins is accompanied by a reduction in the number of minima (Angell, 1991).

❖ Strong and fragile energy landscape

Strong glass former has a rather constant activation energy. This steadiness suggests that the process of main relaxation (such as breaking and reforming Si-O bonds for SiO₂ as an example) remains as a function of temperature. For Angell, on the one hand, strong liquids have higher energy barriers to get out from basin of a coordinate configuration than for fragile liquids, they have therefore smaller number of minima. On the other hand, fragile glass former shows a different pattern. Its viscosity doesn't follow Arrhenius behavior, with its activation energy increasing significantly. This indicates a highly varied energy landscape for these systems. At high temperatures, fragile liquids can easily rearrange a few molecules over low barriers, but at $T \approx T_g$, it requires the cooperative rearrangement of many molecules over high barriers. This distinction between strong and fragile behaviors suggests differences in their landscapes. In every fragile glass forming liquids, there should be few minimum energy states that are still higher than the energy of crystal. These states determine the minimum energy that can be achieved over time at a temperature below T_g . The system tends to reach equilibrium at the lowest minima when the temperature approaches the critical temperature T_K , the configurational entropy S_C approaches zero. It has been suggested that such ideal glass could only be obtained at 0 K (Angell and Rao, 1972). A few years ago, Ediger and coworkers have highlighted ultra-stable glasses prepared by physical vapor deposition (Swallen et al., 2007). Such molecular glasses are close to the limits of what is possible for amorphous packing arrangements, with high density and low enthalpy. In addition, vapor-deposited glasses can exhibit greatly enhanced kinetic stability and are described as stable glasses, i.e., close to ideal glass in terms of energy state (Ediger, 2017).

Strong landscapes may have a single large basin, while fragile ones have many separated large basins. The rearrangements in fragile systems are complex and likely involve a series of steps rather than simple transitions. At low temperatures, these rearrangements are rare and persist for an extended period. The multitude of landscape traps and pathways result in a wide range of relaxation times, as

seen in the stretched exponential function (see **Equation 1-4**). This implies that supercooled fragile liquids are dynamically heterogeneous, with mostly non-diffusing molecules and a few mobile regions.

4) Dynamic heterogeneity

This approach states that in a supercooled liquid, some structural unit groups relax over long distances, when others are completely frozen. These sub-ensembles are spatially correlated, leading to correlated movements of these structural units. This heterogeneous dynamic is supported by both experimental (Böhmer et al., 1996; Cicerone and Ediger, 1996) and computational evidences (Donati et al., 1999; Berthier, 2011; Jung et al., 2024). The concept of dynamic heterogeneity can be illustrated by the average relaxation function $\Phi(t)$ of a supercooled liquid, which exhibits a non-exponential relaxation (see **Figure 1-3** and **Equation 1-4**).

❖ Origin of non-exponential relaxation

The notion of dynamic heterogeneity follows from attempts to understand non-exponential relaxation responses. At the molecular scale, this non-exponential nature has two potential explanations. On the one hand, homogeneous dynamics can be suggested. It is proposed that supercooled liquids are intrinsically homogeneous, with each molecule relaxing nearly identically but in a non-exponential manner. In this case, both local and ensemble-averaged dynamics exhibit the same non-exponential behavior. On the other hand, heterogeneous dynamics are posited to govern the relaxation function. In this scenario, different regions of the glass-forming liquid exhibit very different relaxation dynamics. One region may relax much faster than another due to varying local environments. While the relaxation of each region may be locally exponential, the overall relaxation function becomes non-exponential when averaged over these varying timescales. The two explanations, illustrated in **Figure 1-13**, offer distinct interpretations of non-exponential relaxation, with implications for understanding the behavior of supercooled liquids.

The two potential interpretations can be articulated differently. The probable density function $G(\tau)$ is obtained by taking the inverse Laplace transform of the correlation function:

$$\Phi(t) = \int_0^{\infty} G(\tau) \exp\left[-\left(\frac{t}{\tau}\right)\right] d\tau. \quad 1-21$$

The heterogeneous interpretation suggests that $G(\tau)$ reflects a spatial distribution of relaxation times, while the homogeneous interpretation suggests that $G(\tau)$ has no physical interpretation (Ediger, 2000).

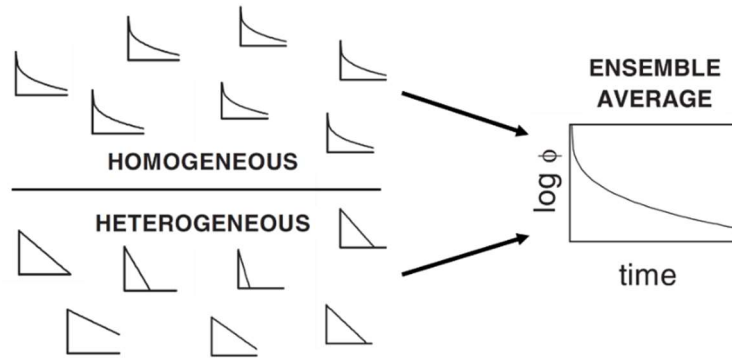


Figure 1-13. Schematic representation of homogenous and heterogeneous scenarios for explaining the non-exponential nature of glass forming liquids. In homogeneous dynamics, all local contributions are identical to the average. In heterogeneous dynamics, the same response is obtained by averaging the heterogeneous relaxation times of individual structural units. Adapted from (Richert, 2002).

Experimental studies have shortened the debate by measuring how long a region remained slow or fast, i.e., the heterogeneity lifetime, using techniques such as nuclear magnetic resonance (NMR) (Schmidt-Rohr and Spiess, 1991) or fluorescence recovery after photobleaching experiments (Cicerone and Ediger, 1993). The NMR and photobleaching experiments, also called dynamic hole-burning experiments, consist in exciting a wide absorption line by a narrow excitation line. If a "hole" appears in the absorption spectrum at the excitation frequency, it shows that the absorption line is not homogeneously broadened, indicating heterogeneous distribution of sub-ensembles in the sample. These experiments have shown that ergodic systems studied fulfill the conditions where time and space averages are equivalent. The characteristic time for a slow sub-ensemble to remain slow has been determined to be comparable to the average relaxation time of the slow sub-ensembles. These experiments have thus established therefore that the dynamics are heterogeneous. Furthermore, they have also measured the lifetime of heterogeneities for a system at a given temperature (Schmidt-Rohr and Spiess, 1991).

❖ Spatiotemporal fluctuations

In the supercooled liquid, dynamics occur across different regions that vary in speed, both in terms of space. Some areas have slow dynamics while others have fast dynamics. Due to the ergodic nature of supercooled liquids, a slow area will eventually change to a fast state, and conversely. The heterogeneity lifetime increases faster than the relaxation time of the system by approaching the glass transition temperature. The range over which particle dynamics are correlated was found to be at most about ten particle sizes, close to the glass transition temperature T_g . **Figure 1-14a** shows a schematic view of spatially heterogeneous dynamics near T_g . This snapshot is therefore likely to appear very

different in the next moment. Ediger provides a brief overview, with experiments indicating that the characteristic size of these regions is approximately 3 nm at T_g , and that the dynamics differ by 1 to 5 orders of magnitude between the fastest and slowest regions near T_g (Ediger, 2000).

The crucial advantage of modern molecular simulations is illustrated in **Figure 1-14b**, which shows a spatial map of displacements of single particles during the simulation. Beyond the reach of most experimental techniques, it reveals that dynamics can vary from one particle to another (Hurley and Harrowell, 1995; Weeks et al., 2000). The presence of spatiotemporal fluctuations in supercooled liquids reflects indubitably dynamic heterogeneity, as evidenced by NMR studies. Furthermore, the existence of spatial correlations between these dynamic fluctuations has been demonstrated. These sub-ensembles spatially correlated lead to correlated movements of structural units, and have been used to follow the characteristic length scale of these sub-ensembles (or dynamic correlation length), noted ξ .

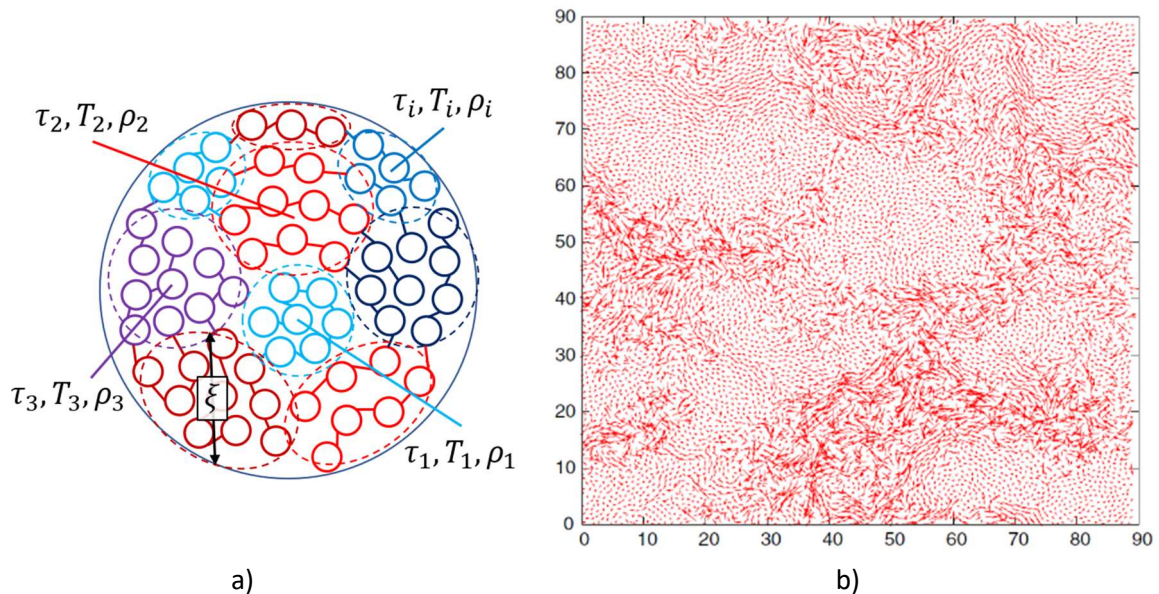


Figure 1-14. a) Schematic representation of a local picture of regions with spatially heterogeneous dynamics near T_g . Regions of particles of the same color are correlated in motion, temperature and density. The regions occupy an average volume $\langle V \rangle$ whose characteristic length scale is ξ (with $\langle V \rangle \approx \xi^3$). b) Spatial map of single-particle displacements in a simulation of a binary mixture of Lennard-Jones particles in two dimensions. The displacement of particles is represented by the trajectory of arrows, while the structural relaxation time is represented by the length of the arrows. Taken from (Berthier, 2011).

❖ Correlated movements

Berthier and coworkers have employed a theoretical approach to estimate the number of dynamically correlated molecules in liquids near the glass transition (Berthier et al., 2007a, 2007b). This approach

is based on the 4-point correlation function $C_4(t)$ ^e. Such correlation function is not experimentally accessible for polymers and molecular glasses. This is why the size of dynamic heterogeneities in glassy systems based on 4-point susceptibility $\chi_4(t)$, which is mathematically linked to $C_4(t)$ (Toninelli et al., 2005), is determined in particular by simulations (Dasgupta et al., 1991; Berthier, 2004; El Masri et al., 2010) or by experiments on colloidal systems (Cipelletti et al., 2002). An example of a Lennard-Jones supercooled liquid is presented in **Figure 1-15**.

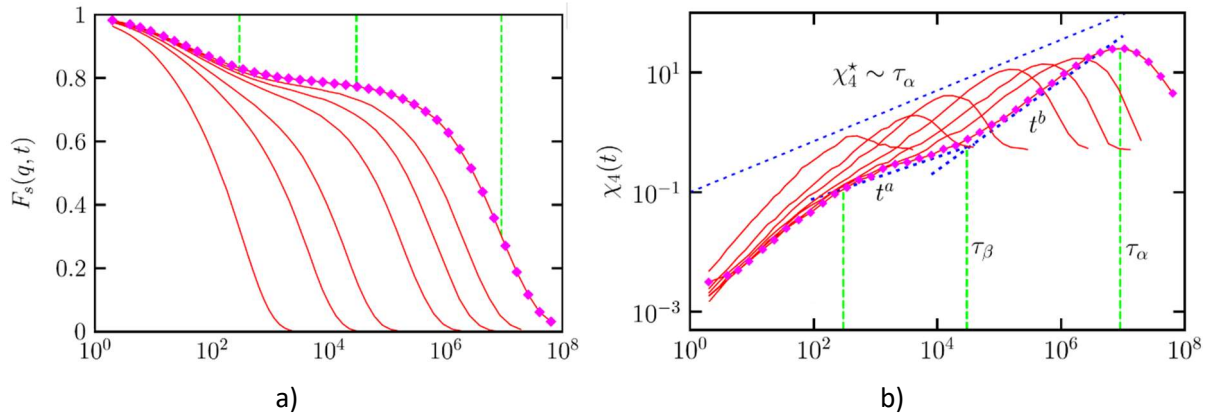


Figure 1-15. a) Self-intermediate scattering function (associated with the relaxation function $\Phi(t)$) and b) the associated 4-point dynamic susceptibility. These graphics are from Monte Carlo simulations of the Lennard-Jones supercooled liquid for different temperatures (represented in red). The temperatures decrease as the relaxation occurs at longer times. At each temperature, a maximum of $\chi_4(t)$ is reached near the relaxation time τ_α . Adapted from (Berthier, 2011).

A relationship between 4-point susceptibility and an accessible 3-point dynamic susceptibility has been found by Berthier et al. (Berthier et al., 2005a). $\chi_4(t)$ is accessible by linking the fluctuation-dissipation theorem to a 3-point susceptibility, which can be experimentally determined using temperature as external perturbation (noted $\chi_T(t)$). $\chi_4(t)$ allows the direct measurement of a correlation volume, representing the number of structural units N_{corr} whose dynamics are correlated over a time scale

^e The 4-point correlation function C_4 uses two space coordinates multiplied by two-time coordinates. C_4 is an estimate of spatiotemporal fluctuations in correlation functions. C_4 contains information on the spatial extension of dynamic heterogeneities, unlike the 2-point correlation function (two-time coordinates). The 2-point correlation function quantifies the change in molecule orientation between a time t_0 and $t_0 + t$. Two-point relaxation functions do not reveal whether the correlation function is intrinsically stretched or not (homogeneous or heterogeneous scenario mentioned in the section “Origin of non-exponential relaxation”).

similar to the mean relaxation time of the system. This quantity corresponds to the maximum value of the 4-point dynamic susceptibility over time, i.e., $N_{corr} = \max(\chi_4(t))$. The number of structural units with correlated dynamics can therefore be followed as a function of temperature, as shown in **Figure 1-15b**. In this system, $N_{corr} (= \chi_4^*)$ is found to increase with temperature and seems to be related to the relaxation time τ_α , as indicated by the blue dashed line.

Dielectric experiments have been used in order to extract the dielectric susceptibility as a function of temperature to measure the increasing number of dynamically correlated structural units (Crauste-Thibierge et al., 2010; Fragiadakis et al., 2011b; Bauer et al., 2013). Using the expression of 3-point susceptibility $\chi_T(t)$ directly, the number of molecules whose dynamics on the time scale of the α -relaxation are correlated with a local enthalpy fluctuation $N_{corr,T}$ can be expressed by (Dalle-Ferrier et al., 2007a):

$$N_{corr,T} = \sqrt{\frac{N_A k_B T^2}{M_0 \Delta C_P}} \max(\chi_T(t)), \quad 1-22$$

which can be simplified as (Fragiadakis et al., 2011a):

$$N_{corr} \approx \frac{N_A k_B}{M_0 \Delta C_P} T^2 \max\left(\frac{\partial \Phi(t)}{\partial T}\right)^2, \quad 1-23$$

where N_A is Avogadro's number, M_0 is the repeat unit molecular weight, k_B is the Boltzmann constant, ΔC_P is the isobaric heat capacity jump at T_g , and $\Phi(t)$ is the correlation function of α -relaxation. Since **Equation 1-4** can describe $\Phi(t)$, the stretching parameter β_{KWW} and the relaxation time τ allow to estimate N_{corr} such as (Capaccioli et al., 2008):

$$N_{corr} = \frac{N_A k_B}{M_0 \Delta C_P} \left(\frac{\beta_{KWW}}{e}\right)^2 \left(\frac{\partial \ln \tau}{\partial \ln T}\right)^2, \quad 1-24$$

where e is the Euler's number. It is worth noting that ΔC_P , β_{KWW} , and τ are considered to be temperature dependent. Dielectric measurements have allowed N_{corr} to be determined for numerous glass former systems (Dalle-Ferrier et al., 2007a; Capaccioli et al., 2008). N_{corr} varies by about 4 decades as the relaxation times change by 6 decades, with the growth of N_{corr} becoming slower as T_g approaches. This suggests that N_{corr} follows a logarithmic law rather than a power law as temperature decreases according to the MCT (Götze, 2008). Dynamics can therefore be expressed by a master curve of two-regime evolution of N_{corr} such as an empirical expression (Dalle-Ferrier et al., 2007a):

$$\tau = A \left(\frac{N_{corr}}{N_0} \right)^Z \exp \left[\left(\frac{N_{corr}}{N_0} \right)^\Psi \right], \quad 1-25$$

where A , N_0 , Z , and Ψ are indicative constants, that serve to have a universal reference of the sample being studied. Glass forming systems are more or less remoted from such master curve. Capaccioli et al. (Capaccioli et al., 2008) proposed a formalism based on the AG theory to have lower dispersion from the logarithm of the number of possible internal states of a CRR, noted $\sigma_{CRR} = N_{corr} S_C / k_B$. However, this scaling assumes that there is a connection between the number of dynamically correlated molecules and the configurational entropy of AG theory.

❖ Donth's approach

Based on the thermal fluctuation approach, Donth develops another method permitting to estimate the volume V_α or the number of structural units N_α of a CRR (Donth, 1982). This approach results from the concept of CRR introduced by the AG theory. CRRs are independent sub-ensembles with their own thermodynamic fluctuations. The i^{th} sub-ensemble has these own relaxation times τ_i , temperatures T_i , and densities ρ_i as already shown in **Figure 1-14a**. By considering a larger portion of the system with multiple CRRs, the internal distributions provide a model with dynamic heterogeneities that fluctuate in space and time. These dynamic heterogeneities lead to a dispersion of relaxation times. Donth proposed a view of the relaxation time surrounded by its dispersion zone, as shown in **Figure 1-16**.

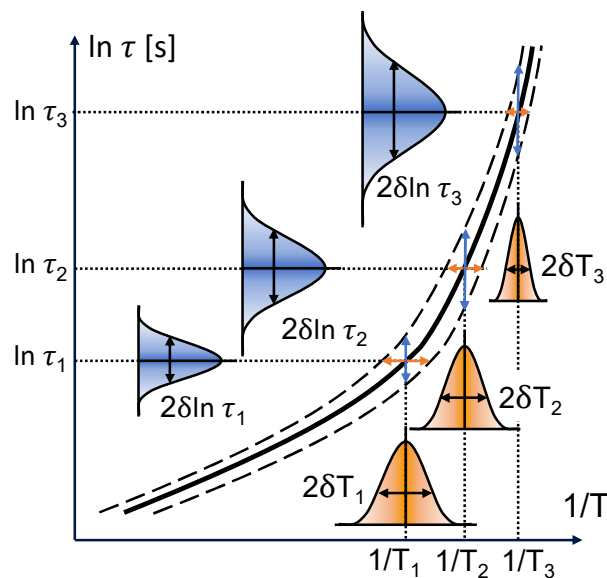


Figure 1-16. Schematic Arrhenius plot of α -relaxation for a glass former. The thick line corresponds to the mean relaxation times as a function of temperature, while the dashed lines are the limits of the α -dispersion zone. The blue and orange Gaussian represent the time and temperature dispersions of the CRR, respectively.

According to the principle of Time Temperature Superposition (TTS) for glass transition, the mean temperature fluctuation of a CRR δT can be expressed as (Donth, 2001):

$$\frac{dT}{d \ln \tau} = \frac{\delta T}{\delta \ln \tau}, \quad 1-26$$

where $\delta \ln \tau$ is the mean fluctuation of $\ln \tau$ per CRR.

This equivalence allows to express the temperature fluctuation from the standard deviation of a Gaussian fit for the isochronal $C_p''(T)$ peak from heat capacity spectroscopy. Moreover, Donth used FDT to connect the spectral density of fluctuations $f(\omega)$ (where $f(\omega)^2 \equiv \delta T^2(\omega)$ for density of temperature fluctuations, with $\omega = 1/\tau$ is the angular pulsation) with the imaginary part of dynamic temperature modulus $K_T''(\omega)$ such as (Schröter, 2006):

$$\delta T^2(\omega) = \frac{k_B T}{\pi \omega} K_T''(\omega). \quad 1-27$$

According to the Wiener-Khinchin's theorem^f and the Kramers-Kronig's relation^g at the pulsation $\omega = 0$, the **Equation 1-27** can be rewritten as (Donth, 1999):

$$\delta T^2(\omega) = k_B T [K_T'(\infty) - K_T'(0)]. \quad 1-28$$

The values ∞ and 0 in the modulus function mean that quantities of the real part of dynamic temperature modulus K_T' are taken far above or below the α -relaxation. The dynamic temperature modulus is the inverse of the corresponding complex compliance $J^*(\omega)$, where it can be linked to the complex heat capacity by $J^*(\omega) = C_p^*(\omega)/T$. It assumes that heat capacity at constant pressure or volume are equivalent (O'Reilly, 1977). Using these relations, the mean squared temperature fluctuation can be expressed by:

$$\delta T^2 \approx k_B T_g^2 \left[\frac{1}{C_{p,glass}} - \frac{1}{C_{p,liquid}} \right], \quad 1-29$$

^f The Wiener-Khinchin's theorem gives the equivalence $\delta T^2 = \int_{-\infty}^{\infty} \delta T(\omega)^2 d\omega < \infty$.

^g The Kramers-Kronig's relation links real $G'(\omega)$ and imaginary $G''(\omega)$ terms of the complex function $G^*(\omega)$ being the Fourier transform of a causal response function. The relation stipulates $G'(\omega) = \frac{1}{\pi} \int_{-\infty}^{\infty} \frac{G''(\omega')}{\omega - \omega'} d\omega' + G'(\infty)$. Such relation can therefore be applied to dielectric susceptibility, dielectric permittivity, complex heat capacity, dynamic elastic modulus, etc.

where C_P is the isobaric heat capacity. The temperature fluctuation can then be linked to cooperativity volume V_α or characteristic cooperative length ξ_α through the specific heat capacity where $c_p = C_P \rho V_\alpha$ where ρ is the density, leading to (Donth, 1982):

$$V_\alpha = (\xi_\alpha)^3 = \frac{\left[\frac{1}{c_{P,liquid}} - \frac{1}{c_{P,glass}} \right]}{\rho(\delta T)^2} k_B T_g^2. \quad 1-30$$

The relationship between V_α and ξ_α as written in **Equation 1-30** is a rough estimate. It is worth noting that a CRR has not universality shape (neither cubic or spherical). According to the observation of Ediger (Ediger, 2000), the Donth's approach used on glass forming polymers finds $\xi_\alpha \approx 3$ nm (Saiter et al., 2010; Rijal et al., 2015). Recently, ξ_α has been measured on polymers from quasi-elastic neutron scattering (QENS) and is consistent with that determined by the thermal fluctuation approach proposed by Donth (Chua et al., 2023).

The number of structural units that rearranges cooperatively can be deduced from the cooperativity volume with:

$$N_\alpha = \frac{\rho V_\alpha N_A}{M_0}, \quad 1-31$$

where N_A is the Avogadro's number and M_0 is the molar mass of the structural units. Rijal et al. have compared N_α from the Donth's approach to the number of structural units dynamically correlated with N_{corr} for polymers (Rijal et al., 2015). In this study, two trends were highlighted: for low M_0 (< 100 g. mol⁻¹) the values of N_{corr} and N_α are similar and, for high M_0 (> 200 g. mol⁻¹) the value of N_{corr}/N_α is close to 10. Furthermore, it evidences that the correlated motions associated with N_{corr} appear on a lower at a time scale than the cooperative motions associated with N_α .

The formalism of the Donth's approach has been applied for various media, including molecular glasses (Błażytko et al., 2024), polymers (Zimny et al., 2023), silicate glasses, metallic glasses, liquid crystals (Hempel et al., 2000), chalcogenide glasses (Saiter et al., 2009), amorphous pharmaceuticals (Vyazovkin and Dranca, 2007; Wojnarowska et al., 2018), and ionic liquids (Grzybowska et al., 2015).

5) Other theories

❖ The random first-order theory (RFOT)

Random First Order Theory (RFOT) is a theoretical approach that aims to describe the mean behavior of complex physical systems by considering random fluctuations and using mean-field techniques to simplify the analysis (Kirkpatrick and Thirumalai, 1987). From the foundation of AG theory and MCT, the RFOT is essentially based on a mechanism where thermodynamics drives the dynamics. This model

is characterized by the presence of a "mosaic" of exponentially numerous sub-ensembles of metastable states at low temperature within the volume V of the system.

The RFOT theory postulates that the rapid increase in the α -relaxation time is primarily due to activated rearrangements of glassy droplets, known as glassites. These small domains are gradually formed in the liquid. Domains in which the molecules are arranged in the configuration of an ideal glass or closely related configurations. Glassites are selected by the amorphous boundary conditions imposed by interactions with molecules just outside them, it corresponds to a temperature dependent interface energy $Y(T)$ (Biroli and Bouchaud, 2012). Thus, the supercooled liquid is a mosaic of small frozen domains that can move relative to each other, but with strongly correlated molecules making movement difficult. As the temperature decreases, the configurational entropy S_C decreases, which means that the average size of each ideal glass domain increases. Glassites grow progressively in size ξ^* , also called point-to-set (Montanari and Semerjian, 2006). This growth is induced by the reduction in configurational entropy. The presence of a glassy length scale ξ^* is expected to manifest itself in the nonlinear rheological properties of supercooled liquids, particularly becoming more pronounced at lower temperatures. The relaxation time can be expressed by (Kirkpatrick et al., 1989):

$$\tau_\alpha = \tau_\infty \exp \left[\frac{\Delta_0 \xi^{*\psi}}{k_B T} \right], \quad 1-32$$

where τ_∞ is the pre-exponential factor, Δ_0 is the activation energy at a temperature above the crossover temperature T_C predicted by the MCT, and ψ is an exponential factor. Physically, this reflects that configurational entropy acts as a limiting factor for the growth of glassites that resist shear. As these regions evolve to facilitate flow, the energy barrier must increase with the glassite size, leading to a correlation with the AG theory. To allow structural relaxation in this mosaic state, not only the molecules but also the entire frozen domains must move. The activation energy barrier depends on the average number of correlated molecules in the frozen domains, since the interfacial energy depends on the glassite size and the configurational entropy with $\xi^{*(d-\theta)} = Y/TS_C(T)$, where d is the dimension of the glassites (basically $d = 3$) and θ is another exponential factor (Bouchaud and Biroli, 2004). **Equation 1-32** can be rewritten as:

$$\tau_\alpha = \tau_\infty \exp \left[c \frac{\Delta_0}{k_B T} \left(\frac{Y}{TS_C(T)} \right)^{\frac{\psi}{d-\theta}} \right], \quad 1-33$$

where c is a numerical constant. In the case of $\psi = \theta = 3/2$, $d = 3$. Considering that $\Delta_0 = Y = \kappa T$ (Goldbart and Goldenfeld, 1989), **Equation 1-33** gives the **Equation 1-18** of the AG theory. The RFOT

theory succeeds in predicting the viscosity divergence law as a function of temperature with the expression of $S_C(T)$ (see **Equation 1-20**), thus satisfying the Kauzmann's paradox. RFOT theory incorporates such a thermodynamic critical point, but universal behavior indicates that supercooled liquids fall out of equilibrium as they approach the presumed T_K . However, two drawbacks are observed in the description of dynamics within RFOT: the stretching of the correlation functions is not explained, and it is indicated by the observation that the dynamic correlation length ξ increases faster than the point-to-set length ξ^* with decreasing temperature (Charbonneau and Tarjus, 2013). Recent successes and ongoing work of the RFOT are reviewed by Biroli and Bouchaud (Biroli and Bouchaud, 2023).

❖ Frustration limited domains (FLD) theory

Kivelson and coworkers developed a theory based on the concept of frustration-limited domains (FLD) (Kivelson et al., 1995). The FLD theory posits fundamental principles:

- Locally Preferred Structures (LPS): Liquids have a local atomic arrangement that differs from the crystalline phase. This arrangement minimizes local free energy.
- Geometric frustration: Due to geometric constraints, the LPS cannot extend infinitely throughout the liquid. This frustration results from the inability of the LPS to fully tile the medium.

To summarize, the FLD are structure favored in terms of free energy, the LPS, which cannot extend indefinitely due to their inefficient space filling. Frustration prevents the LPS from fully ordering, halting a second-order phase transition at a critical point T_C (similar to the crossover temperature), thus preventing the phase transition from occurring over large scales. Without frustration, the liquid would freeze into the LPS at T_C . Frustration leads to cooperative behavior on a mesoscopic scale (Cavagna, 2009). This cooperative behavior results from the growth of the LPS induced by the proximity to an avoided critical point. The FLD theory provides a coherent explanation for the cooperative behavior observed in systems with geometric frustration. It clarifies why systems break into domains and identifies the factors controlling domain growth. The slow relaxation of these frustrated domains leads to slow relaxation in supercooled liquids. If the range of domain sizes is associated with a range of relaxation times, this could provide insights into the experimentally observed spatially heterogeneous dynamics. Considering the FLD theory, the relaxation time can be expressed by (Tarjus et al., 2005):

$$\tau_\alpha = \tau_\infty \exp\left[\frac{E(T)}{k_B T}\right], \quad 1-34$$

with

$$E(T) = \begin{cases} E_{\infty} & \text{for } T > T_C, \\ E_{\infty} + Bk_B T_C \left(\frac{T_C - T}{T_C} \right)^{\psi} & \text{for } T < T_C, \end{cases} \quad 1-35$$

where E_{∞} is the activation energy in the Arrhenius domain, B is a constant and ψ is an exponential factor constant usually taken to be $= 8/3$. Experimental evidence for FDL has been observed in materials showing polyamorphism. It refers to the simultaneous existence of different non-crystalline phases with the same chemical composition, phases that lack clear long-range order. The concept of LPS plays a crucial role in explaining polyamorphism. As mentioned earlier, an LPS can be described as a molecular arrangement that minimizes the local free energy within a specific region of the pressure-temperature phase diagram. Examples of polyamorphic substances have been reported for water (H_2O), silicon dioxide (SiO_2), and germanium dioxide (GeO_2) (Tarjus et al., 2003). Under sufficiently high pressure and low temperature conditions, these substances exhibit the coexistence of multiple amorphous phases. The theory suggests that frustration limited domains may also be present in non-polyamorphic systems, although they may not be detected by standard techniques due to factors such as excessive polydispersivity or unusual symmetry properties. FLD theory provides a comprehensive framework for understanding the effects of geometric frustration on the behavior of liquids, shedding light on phenomena such as domain formation and polyamorphism. Relationships with other theories of the glass transition are reported by Tarjus et al. (Tarjus et al., 2005).

❖ Facilitation and kinetically constrained models (KCM)

Finally, another approach is the dynamic facilitation (Fredrickson and Andersen, 1985). It is based on the free volume theory. Dynamic facilitation stipulates that a relaxed structural unit promotes the relaxation of one of its neighbors, such as a free volume, which can move but disappears at low temperature due to geometric constraints. The theory suggests that mobility defects trigger a feedback mechanism, that clusters mobile and static regions, thus explaining dynamical heterogeneities. At low temperatures, mobility defects become sparse, suppressing the mobility feedback. **Figure 1-17** shows dynamic facilitation and heterogeneities during molecular dynamics at $\tau_{\alpha}/\tau_{\infty} = 10^8$. This approach leads to the development of a class of statistical models called kinetically constrained models (KCM).

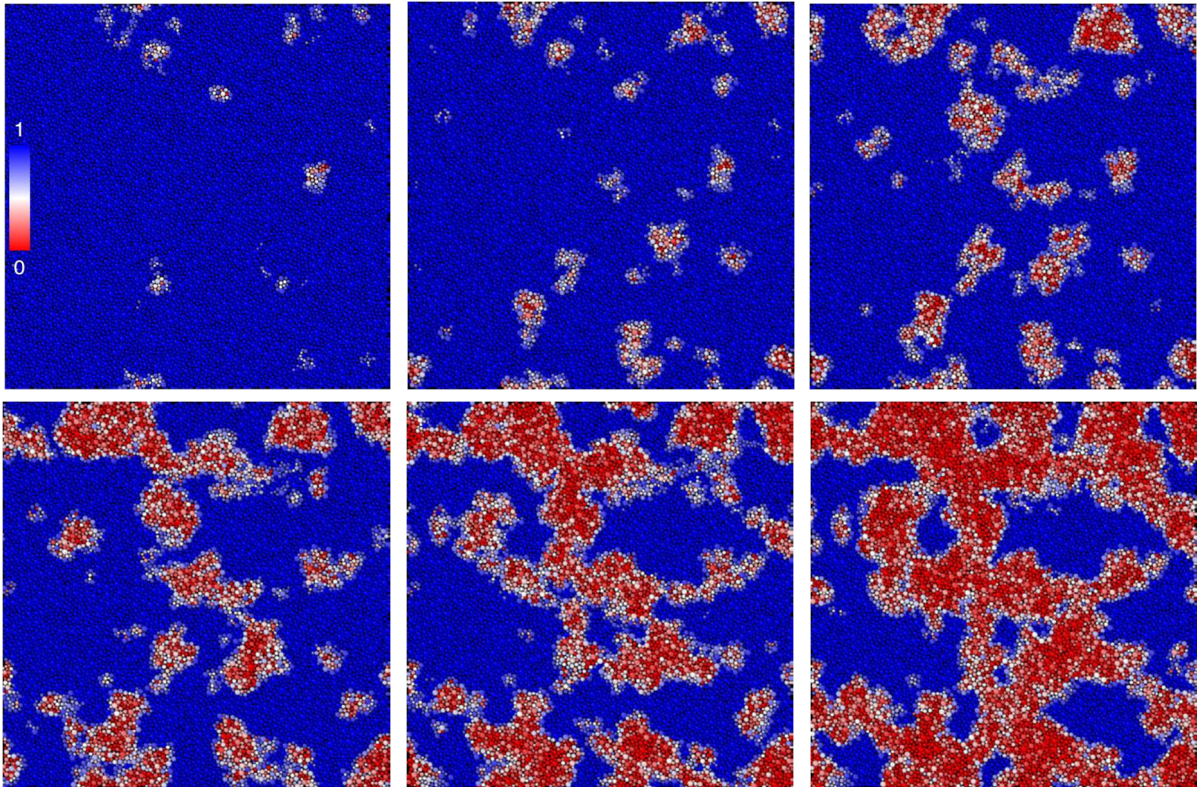


Figure 1-17. Two-dimensional molecular dynamic simulations on 10^4 repulsive spheres. Frames are snapshot logarithmically spaced between $t = 2.10^{-3}\tau_\alpha$ (top left) and $t = 0.6\tau_\alpha$ (bottom right) from left to right and top to bottom. Particle colors are ranging from blue, corresponding to immobile particles, to red, relaxed particles. Taken from (Guiselin et al., 2022).

In KCM, relaxation is accurately described in terms of the movement of sparse defects. In the noncooperative Fredrickson-Andersen's model (Fredrickson and Andersen, 1985), these defects diffuse, while in more complex models, such as the Kob-Andersen's lattice gas (Kob and Andersen, 1993), they can undergo cooperative motions. In the East model (Berthier and Garrahan, 2005), local dynamical rules are defined a manner that precludes the formation of specific arrangements of sites from occurring according to local configurations, leading to complex relaxation dynamics. As the temperature decreases, the density of defects decreases, and their dynamics slow down drastically, leading to a slowing down of the overall relaxation in an activated or possibly super-Arrhenius manner. Furthermore, space-time representations indicate the emergence of large immobility domains with broadly distributed spatial and temporal extent as temperature decreases. To summarize, the system undergoes three distinct phases. At elevated temperatures, the system is characterized by a high density of defects and a fluid dynamic state. At intermediate temperatures, clusters of highly mobile defects coexist with isolated immobile defects. At low temperatures, the defects are typically isolated, and dynamics are constrained. Dynamic facilitation theory posits that dynamical heterogeneities are

the main feature of glassy systems and can be understood at a purely dynamical level without relying on thermodynamic or energy landscape descriptions. Therefore, the dynamic facilitation approach is in strong disagreement with theoretical ideas such as mean field approaches (RFOT, MCT...), AG theory or Kauzmann's transition T_K (Cavagna, 2009). Garrahan et al. provided an overview of the predictions of dynamic heterogeneity with KCMs (Garrahan et al., 2011).

The theoretical approaches presented earlier have been significantly improved by the advent of numerical tools over the last few decades. However, due to the complexity of relaxation, most of simulations based on these theories can only access short scales (in time, space, or by the number of particles), while in the glassy domain, structural relaxation that occurs below the glass transition temperature can take geological times over materials comprising billions of atoms. The theoretical concepts and universal observations of glass show how T_g is impacted by numerous structural factors that affect the capacity of dynamics to evolve with temperature. However, the dynamics are not only thermally activated, the impact of structural factors is, for the most part, a means of increasing or decreasing the free volume that facilitates the movement of macromolecules. Therefore, pressure is also a crucial factor in characterizing and understanding relaxation dynamics.

III. Pressure influence on the glass transition

Studies on the effect of pressure on viscosity began about a century ago (Bridgman, 1925). Since then, numerous techniques have combined pressure vessels with physical measurement techniques to improve understanding of glass-forming liquids.

1) Experimental observations

❖ Thermodynamic observations

PVT data record the specific volume (or density) of a material with pressure and temperature changes. Additional changes can occur due to various factors like phase transitions or degradation reactions. PVT measurements help study these phenomena and provide data crucial for material engineering applications, including compressibility and thermal expansivity. Polymers are particularly sensitive to pressure.

Two dilatometric techniques have been widely practiced for measuring dimensional changes of materials, especially when volume changes are significant and pressure needs to be included as a variable. These techniques are the piston-die and the confining fluid technique (Mark et al., 1986). With the piston-die technique, the material is confined in a rigid die or cylinder, and pressure is applied to the sample using a piston. However, there are fundamental and practical problems with this

method. The main issue is that the state of stress for a solid sample in this setup is not hydrostatic, leading to nonsensical results. Practical complications include sample sticking to the wall, void formation, and leakage around the piston, especially with low-viscosity polymer melts (Lei et al., 1988). The confining fluid technique involves surrounding the material with a confining fluid, such as mercury. The combined volume change of the sample and confining fluid is measured, and the volume of the sample is determined by subtracting the volume change of the confining fluid. This technique has the advantage of maintaining hydrostatic pressure, eliminating the potential friction or leakage problems. Nevertheless, potential interactions between the confining fluid and sample need to be considered. It is possible to achieve a high degree of accuracy by taking into account a number of factors, including as the PVT properties of the confining fluid and appropriate extrapolations when necessary (Zoller et al., 1976). Overall, while both methods have been described in the literature, the confining fluid technique is preferred for generating PVT data due to its hydrostatic pressure conditions and fewer practical complications.

Typically, variations in volume with temperature and pressure are shown in **Figure 1-18**. These PVT data are among those from Zoller and Walsh's book, where a large number of dilatometric measurements of polymers using the confining fluid technique are referenced (Zoller and Walsh, 1995). **Figure 1-18a** and **Figure 1-18b** show the specific volume as a function of temperature in isobar conditions for fully amorphous polystyrene (PS) and semi-crystalline polyvinylidene fluoride (PVDF) respectively. In some cases, glass transition and melt transition can be observed during the same measurement. In **Figure 1-18c**, the poly(ethylene naphthoate) (PEN) the glass transition is marked by a steepness change, then in supercooled liquid crystallization occurs, densifying the polymers up to reach the melting temperature. At this point the steepness of the polymers meets again with the liquid.

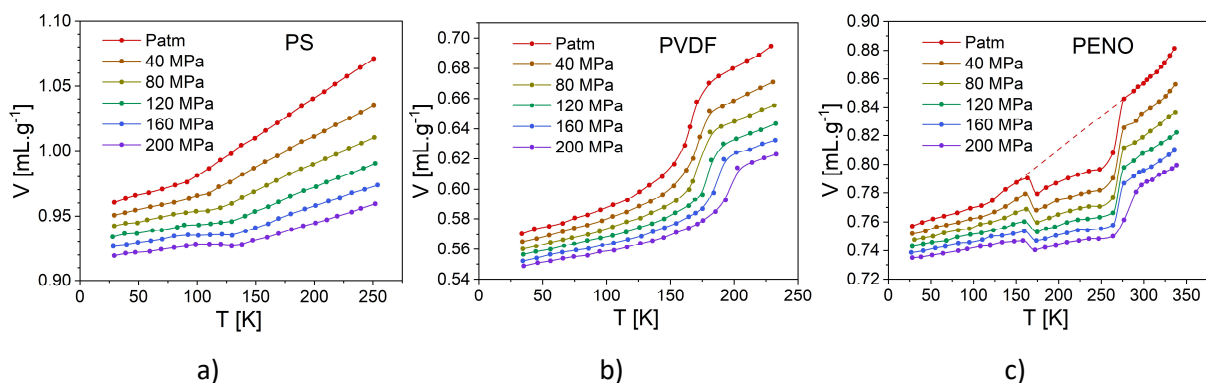


Figure 1-18. Isobars of volume variations during heating for a) PS, b) PVDF and c) PEN. The dashed line represents the supercooled liquid extrapolation of PEN. Data from (Zoller and Walsh, 1995).

In order to facilitate the evaluation of the PVT data for both liquid and glasses, the empirical Tait's equation is particularly suitable for the approximation and extrapolation of non-crystalline polymer volume (Jain and Simha, 1989). Glass or liquid volume can be expressed as a function of temperature and pressure with:

$$V(T, P) = V(T, 0) \left[1 - 0.0894 * \ln \left(1 + \frac{P}{B(T)} \right) \right]. \quad 1-36$$

The volume, in mL.g⁻¹, is expressed with the pressure, in bar. The volume at atmospheric pressure $V(T, 0)$ and a pressure coefficient $B(T)$ are given by:

$$V(T, 0) = A_0 + A_1T + A_2T^2, \quad 1-37a$$

$$B(T) = b_0 \exp(-b_1T), \quad 1-37b$$

where A_0 (in mL.g⁻¹), A_1 (in mL.g⁻¹.K⁻¹), A_2 (in mL.g⁻¹.K⁻²), b_0 (bar) and b_1 (in K⁻¹) are constants. The Tait's equation allows to have smooth values of isobaric thermal expansion $\alpha(T, P)$ and isothermal compressibility $\kappa(T, P)$ (see **Equations 1-8a** and **1-8c**). Orwoll has reported Tait's equation parameters and second derivatives of Gibbs free energy for various polymers (Orwoll, 2007).

In addition to volume measurements, DSC analysis can be extended by performing experiments under pressure. Pressure is applied directly within the calorimeter chamber using gases such as nitrogen, helium, or CO₂. This technique allows researchers to explore the effects of pressure on the thermal properties and phase transitions of materials, providing valuable insight into their behavior under different environmental conditions (Williams and Angell, 1977; Bouthegourd et al., 2014). However, this method has its limitations, as pressure levels are typically restricted to around 20 MPa.

The thermal properties of PVAc, including thermal conductivity λ and specific heat capacity C_p , have been investigated using a transient hot-wire probe technique (Sandberg and Bäckström, 1980). This study involved measuring these properties across a temperature range of 270-470 K under pressures of up to 0.5 GPa as shown in **Figure 1-19**. The results have demonstrated that the C_p baselines and λ increased with pressure, both in the liquid and glassy states of the material. This variation was correlated with that of the thermal expansion coefficient α . Additionally, it was observed that the change in specific heat capacity near the glass-transition (ΔC_p) temperature decreased as pressure increased. This suggests that pressure has a notable influence on the thermal behavior of PVAc, impacting its heat transfer characteristics and thermal stability across different temperature regimes.

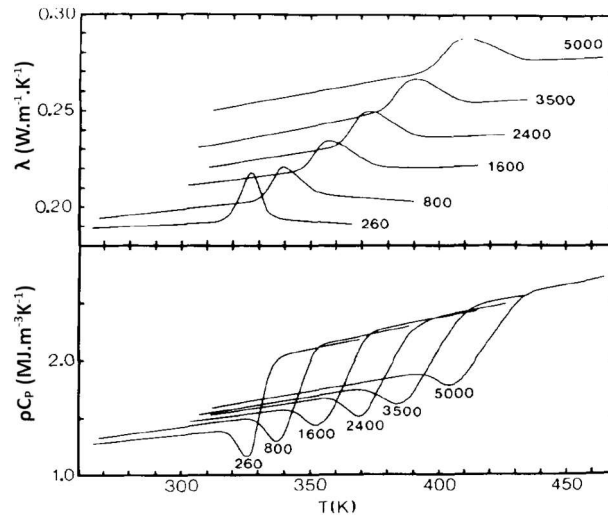


Figure 1-19. Smoothed thermal conductivity λ and heat capacity ρC_p as a function of temperature for PVAc. The pressure for each isobar is given in bars. Taken from (Sandberg and Bäckström, 1980).

❖ Viscosity observation

The viscosity of a liquid, which is a measure of its resistance to flow, increases significantly as it approaches the glass transition temperature, a phenomenon also induced by raising pressure. However, measuring viscosity over broad ranges under high pressure poses experimental challenges, leading to the use of various techniques showing diverse advantages and drawbacks. As shown in **Figure 1-20**, the different techniques show most of the time either high pressure or high viscosity limitations (Cook et al., 1993).

First of all, falling body viscometer made by Bridgman measured viscosities up to 1.2 GPa (Bridgman, 1946). Later, a swinging vane apparatus extended the range up to 3 GPa (Bridgman, 1964). Barnett and Bosco developed capillary-type viscometers measuring up to 6 GPa, albeit with lower precision (Barnett and Bosco, 1969). Piermarini et al. introduced a diamond anvil cell for high-pressure viscosity measurements. Later, work achieving 10% uncertainty with corrections for wall effects (Munro et al., 1979), using a rolling ball technique to enhance precision and the viscosity range was expanded using centrifugal force in a diamond anvil cell (King Jr et al., 1992). Koran and Dealy developed a rheometer for shear-rate dependent viscosity of polymers under shear flow up to 70 MPa (Koran and Dealy, 1999). Quartz-resonator methods measure dynamic viscosity under pressure, but with no control over strain amplitude (Theobald et al., 2001).

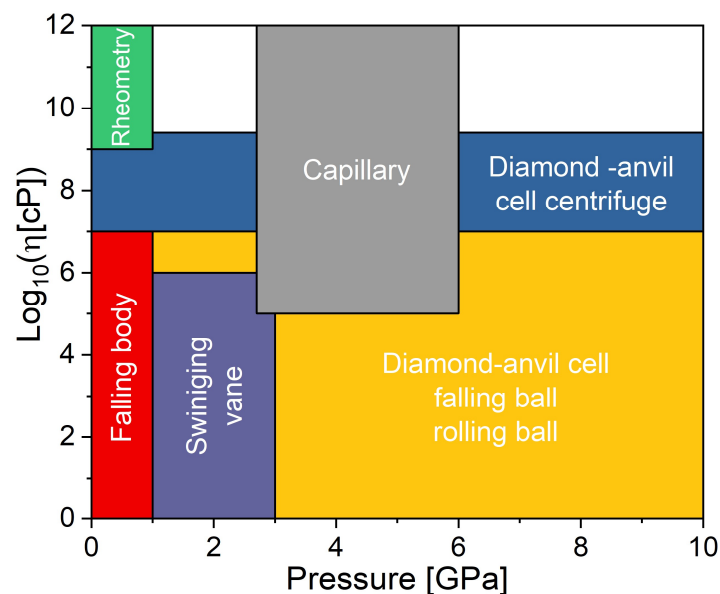


Figure 1-20. The viscosity and pressure ranges of viscometer techniques. Adapted from (Roland et al., 2005).

❖ Dynamic relaxation observation

Various experimental techniques are used to study molecular motions under high pressure. Dielectric spectroscopy allows observation of the movement of ionic species and reorientational motions of dipolar molecules across a wide range of time scales and under different thermodynamic conditions. It allows for monitoring various processes in a single experiment, with spectra covering a wide range of frequencies at ambient pressure. Special high-pressure cells are used to control temperature and pressure during measurements, with pressure exerted either by hydraulic pumps using non-polar liquids or by direct compression with pistons (Urbanowicz et al., 1995). This technique will be deeper detailed in the next chapter. Dynamic light scattering is another experimental technique for the study of molecular motions under high pressure. It is limited to moderate pressures, up to about 200 MPa, with pressure applied by means of gas and membrane compressor (Fytas et al., 1982). To extend light scattering measurements to the GPa range, a diamond anvil cell can be used (Oliver et al., 1991). Numerous techniques are available for investigating dynamic processes within the GHz–THz frequency range. Among these methods, quasielastic neutron scattering (QENS) stands out as particularly skillful and effective. It can be carried out as a function of both temperature and pressure. However, there are few investigations at high pressure due to the difficulty of selecting an appropriate high-pressure vessel and the limitations of neutron spectrometers in terms of frequency range (Frick and Alba-Simionesco, 1999). In addition, NMR offers molecular site specificity due to chemical shift and isotopic labeling. NMR measurements can be conducted at elevated pressures, using either a pressurizing liquid or gas (Hollander and Prins, 2001).

2) Pressure/volume influence on mobility

The structural relaxation time and viscosity of a liquid increase significantly when it is compressed at a constant temperature. This raises the question of which equation is most appropriate to describe the effect of pressure on the structural relaxation time. While temperature decrease and pressure increase are not treated as equivalent thermodynamic variables in traditional thermodynamics, they both have a similar effect from a dynamic point of view: they both lead to a slowing down of molecular rearrangements. Therefore, pressure and temperature can be considered equivalent thermodynamic variables, as $T^{-1} \leftrightarrow P$ (Floudas et al., 2011). According to the free volume concept, the molecular mobility is slowed down with an increase in applied pressure at constant temperature. The free volume ratio should decrease and constrain the mobility. The pressure dependence of the relaxation time for the segmental relaxation can be described by the pressure VFTH law (Paluch et al., 1996) at constant temperature:

$$\tau(P) = \tau_0 \exp \frac{CP}{P_0 - P}, \quad 1-38$$

where τ_0 corresponds to the relaxation time at atmospheric pressure and is determined at P_{atm} , P_0 is the limit pressure where τ diverges, and C is a constant. It is worth mentioning that all these parameters are temperature dependent. This equation is actually equivalent to the **Equation 1-12** of the free volume theory by assuming that local free volume $v_f \propto \kappa(V^* - v_0) \approx (P_0 - P)/P_0$, with κ the isothermal compressibility, V^* the volume for rearranging structural unit and v_0 the occupied volume of a structural unit (Floudas et al., 2011). An example of evolution of relaxation time for PVAc is shown in **Figure 1-21a**.

❖ Glass transition under pressure

When the α -relaxation is slowed down and reaches a time of approximately 100 seconds, the couple pressure/temperature at this point is considered to be the glass transition pressure, designated as P_g and the glass transition temperature T_g . By this way, a supercooled liquid to be transformed into a glass by cooling down the material or by applying a hydrostatic pressure. The structure of the liquid remains frozen due to a lack of configurational entropy, which prevents thermal fluctuations, or a lack of space, which prevents spatial fluctuations. **Figure 1-21b** shows variations in glass transition as a function of pressure for PVAc from relaxation time of **Figure 1-21a**, and **Figure 1-21c** shows similar variations for PS by PVT measurements.

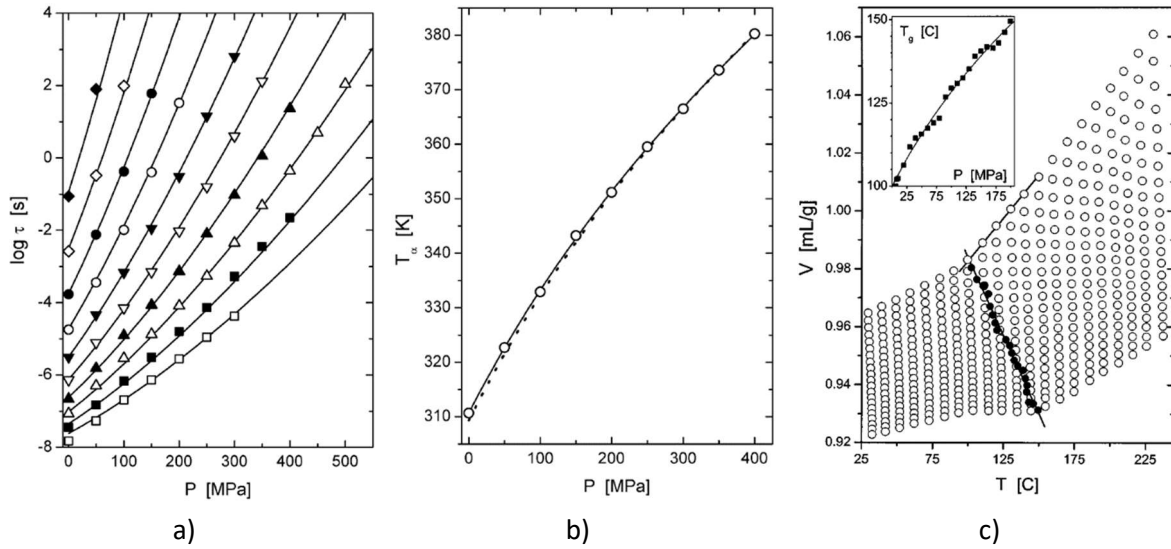


Figure 1-21. a) Dielectric relaxation times of PVAc as a function of pressure for isotherm from 323 K up to 413 K. b) $T_g(\tau = 100s)$ variation with P for PVAc. Lines correspond to Andersson's functions. Taken from (Roland and Casalini, 2003a). c) PVT measurement of PS from P_{atm} up to 200 MPa. The glass transition is highlighted by filled black circles. The inset panel shows the T_g variation with P , with the Andersson's function. Taken from (Roland and Casalini, 2003b).

Overall, the glass transition temperature at $\tau = 100$ s increases with the pressure. However, the higher the pressure, the lower the increase of $T_g(P)$. This nonlinear behavior can be approximated by the Andersson's empirical model through (Andersson and Andersson, 1998):

$$T_g(P) = T_g^0 \left(1 + \frac{P}{\Pi} \right)^{\frac{1}{b}}, \quad 1-39$$

where T_g^0 is the glass transition temperature at atmospheric pressure, Π and b are adjustable parameters. This empirical equation allows to depict the reduction of the T_g variation with the pressure increase. It has been shown that this model is a special case of the Avramov's model when $\tau = 100$ s (Avramov, 2000; Floudas et al., 2011). In this latter model, Π and b are adjustable parameters with physical link expressed by $\Pi = C_p / (\alpha V_m b)$, where C_p is the heat capacity, α is the thermal expansion coefficient and V_m is the molar volume. The parameter b from the Andersson's model is revealing of the T_g steepness variation as a function of pressure. It is also noteworthy that **Equation 1-39** can describe the same trend of parameters $T_0(P)$ of **Equation 1-2** for isobars and $P_0(T)$ of **Equation 1-38** for isotherms (Paluch et al., 2002a). The equivalence between T_g obtained by relaxation time and by PVT measurement has been shown for many class of glass forming liquids (Theobald et al., 2001; Gitsas et al., 2004).

❖ Activation volume

The activation volume, denoted as $\Delta V^\#$, is a significant measure in understanding the dynamics of glass-forming liquids. It represents the difference in volumes occupied by molecules in activated V_A (constant as long as the temperature is unchanged) and non-activated V_{NA} (as the free volume should decrease with pressure increase) states. Therefore, $\Delta V^\#$ increases with pressure at constant temperature since V_{NA} decreases, as illustrated in **Figure 1-22a**. This parameter is influenced by both pressure and temperature, although a linear dependence on pressure is rarely observed in supercooled liquids. The activation volume, analogous to the activation energy, is defined by (Guggenheim, 1937):

$$\Delta V^\# = k_B T \left(\frac{\partial \ln \tau}{\partial P} \right)_T. \quad 1-40$$

Despite its limitations, $\Delta V^\#$ serves as a common metric for the pressure sensitivity of relaxation times τ_α , typically comparable to the size of molecular units. Studies have explored the relationship between apparent activation volume and molecular volume, revealing dependencies on temperature, especially near the glass transition temperature (Casalini et al., 2003). However, such correlation is especially observed for system with strong ability to make hydrogen bonds (Kaminski et al., 2012). The activation volume at the glass transition decreases with increasing pressure, indicating weakened volume effects on relaxation phenomena at higher pressures, as shown in **Figure 1-22b**. The activation volume depends on temperature and remains unaffected by the molecular weight of polymers (Floudas et al., 1999). Expression of relaxation time using the activation volume takes the form of:

$$\tau = \tau_0 \exp \left[\frac{P \Delta V^\#}{k_B T} \right], \quad 1-41$$

with τ_0 the relaxation time at atmospheric pressure equivalent to **Equation 1-38**. In case of secondary relaxation, this equation can use a constant $\Delta V^\#$ (Reiser et al., 2004). Nevertheless, for α -relaxation the increase of $\Delta V^\#$ with pressure does not allow to use this relation for modeling relaxation times, such as the activation energy (Paluch et al., 2001).

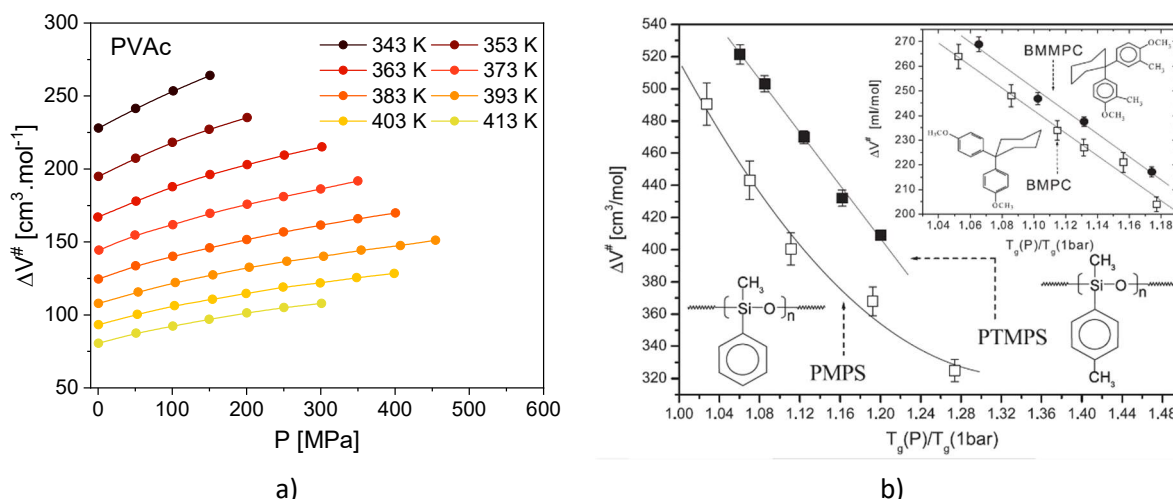


Figure 1-22. a) Activation volume $\Delta V^\#$ as a function of pressure for PVAc isotherms ranging from 343 K up to 413 K. Adapted from (Grzybowski et al., 2013). b) $\Delta V^\#$ at T_g scaled at atmospheric pressure T_g for polymers (poly(methylphenylsiloxane) (PMPS) and poly(methyltolylsiloxane) (PTMPS)) and van der Waals liquids (1,1'-di(4-methoxy-5-methylphenyl)cyclohexane (BMMPC) and 1,1'-bis(*p*-methoxy-phenyl)cyclohexane (BMPC)). Taken from (Paluch et al., 2007).

❖ Fragility under pressure

The isobaric fragility m_p (**Equation 1-3**) of polymers generally decreases with pressure increase, or at worst remains constant (Huang et al., 2002). Some complex behavior of fragility has been reported for small molecules, with strong hydrogen bond, m_p increases with pressure before reaching a plateau (Pawlus et al., 2009). Other H-bonded liquids exhibit a drop in fragility at elevated pressures after have increase at low pressures (Grzybowska et al., 2006).

Isobaric fragility m_p has been correlated with various dynamic properties of the glass or supercooled liquid. These properties include:

- the stretching parameter of the relaxation function (**Equation 1-4**) at the glass transition temperature (Böhmer et al., 1993),
- the relative amplitude of the boson peak at the glass transition temperature (Sokolov et al., 1993),
- the magnitude of the Debye–Waller factor (Roland and Ngai, 1996),
- the temperature dependence of the mean square displacement around T_g (Buchenau and Zorn, 1992),
- the temperature dependence of the configurational entropy (Ito et al., 1999),
- the ratio between elastic and inelastic intensities measured by inelastic X-ray scattering (Scopigno et al., 2003),

- the Poisson ratio (Novikov and Sokolov, 2004),
- the temperature dependence of the high-frequency shear modulus of the liquid and fragility, according to the shoving model (Dyre et al., 2006).

Paluch and coworkers have shown a relation between isobaric fragility m_p and activation volume at the glass transition (Paluch et al., 2001). The activation volume can therefore be determined with:

$$\Delta V^\#(T_g) = m_p k_B \frac{dT_g}{dP} \ln 10. \quad 1-42$$

The ratio dT_g/dP is the steepness of $T_g(P)$, also called the pressure coefficient. This parameter decreases with increasing pressure according to **Equation 1-39**.

Isochoric fragility m_V , analogous to the isobaric fragility m_p , is obtained by taking the derivative at constant specific volume rather than at constant pressure in **Equation 1-3**. By considering constant specific volume for m_V , only temperature variation is considered, without any thermal expansivity. A relation between m_p and m_V has been firstly identified via the chain rule of differentiation leading to (Niss et al., 2007):

$$m_p = m_V \left(1 - \frac{\alpha}{\alpha_\tau} \right), \quad 1-43$$

where α is the isobaric thermal expansivity and α_τ is the isochrone thermal expansivity, i.e., the expansivity along a line of constant α -relaxation time. It is suggested that the value of m_p exceeds that of m_V . It is generally acknowledged that α is positive, then α_τ is lower than 0. The negative value of α_τ is derived from the empirical phenomenon that the volume of the liquid consistently decreases during a heating along an isochrone. Another expression of m_p as a function of m_V has been developed by taking account two contributions: m_p is dependent on its thermal contribution, embodied by m_V , and its volumetric contribution (Hong et al., 2008):

$$m_p = m_V + \frac{\Delta V^\#}{\ln 10} \frac{\alpha}{k_B \kappa'} \quad 1-44$$

where α is the isobaric thermal expansivity and κ is the isothermal compressibility of the supercooled liquid at T_g . The second term on the right-hand side of the equation represents the volume contribution to fragility, also known as $(m_p - m_V)$.

The ratio between m_V and m_p is equivalent to that of activation energy of the relaxation process at constant volume E_V and at constant pressure E_p . This ratio serves as an indicator of the predominance on molecular dynamics between thermal activation process or intermolecular free volume diffusion (Floudas et al., 2006). Floudas and coworkers have linked this ratio to the molar volume for glass

forming liquids, as shown in **Figure 1-23**: the relationship between activation energy ratios E_V/E_P and their repeat unit volume or molecular volume follows a linear dependence.

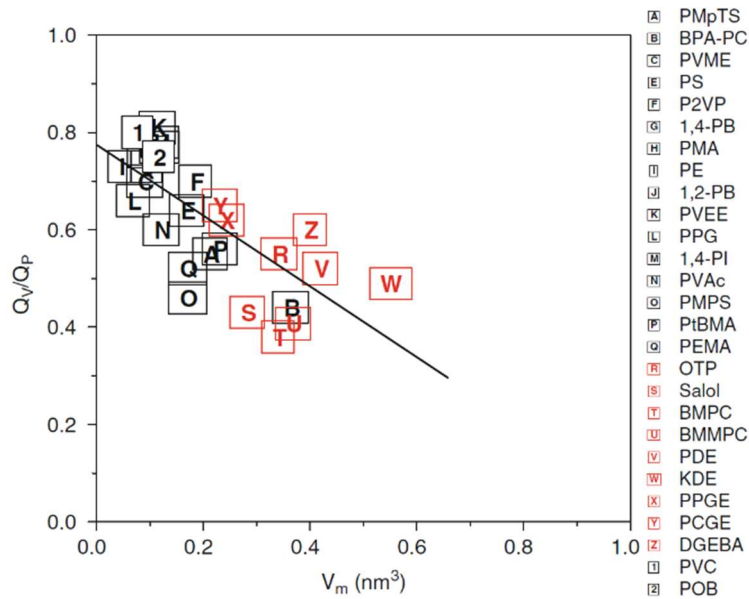


Figure 1-23. The ratio between activation energy at constant volume and at constant pressure E_V/E_P (noted Q_V/Q_P here) plotted against either the volume of the repeat unit (for polymers) or the volume of the molecule (for glass-forming liquids). Taken from (Floudas et al., 2011).

Additionally, the dynamics of these materials are closely linked to static properties such as packing efficiency and repeat unit volume, and this correlation may extend to other variables like the Kuhn length (Floudas et al., 2006).

❖ Cooperativity

According to the AG theory, measurement of characteristic length scale of dynamic heterogeneities ξ has been performed under pressure. Hong et al. have extracted ξ from the ratio between the transversal sound velocity and frequencies of boson peak where an excess density of vibrational states is observed (~ 1 THz) with depolarized light scattering (Hong et al., 2011a). They reported a decrease of ξ at the glass transition temperature with pressure increase, as shown in **Figure 1-24a**. Same behavior has been observed for molecular glasses using dynamic susceptibility (Grzybowski et al., 2012).

Hong et al. also identified a correlation between ξ and the activation volume ΔV^\ddagger . **Figure 1-24b** presents experimental data for ξ and ΔV^\ddagger at the glass transition temperature across various media, including polymers with different molecular weights. Strikingly, the ξ derived from boson peak spectra consistently aligns with the activation volume calculated for structural relaxation at T_g . Furthermore,

the trendline indicates that, on average, $\Delta V^\# \approx 0.03\xi^3$, independently on chemical composition, molecular weight, or external pressure. This suggests that the structural relaxation sensitivity to density is determined by the volume of cooperativity. Notably, materials with hydrogen bonding systems exhibit the smallest characteristic length scale among those examined, potentially explaining their limited structural relaxation sensitivity to pressure, manifested by small $\Delta V^\#$ (Hong et al., 2011b, 2009).

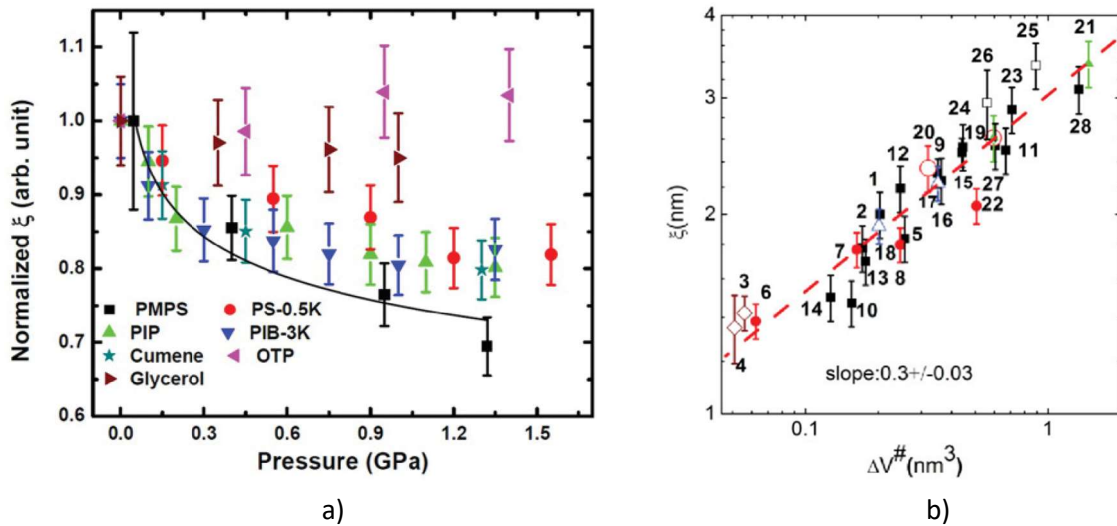


Figure 1-24. a) Variations of normalized characteristic length scale of dynamic heterogeneities ξ with pressure for poly(methyl phenyl siloxane) (PMPS), PS, polyisoprene (PIP), polyisobutylene (PIB), cumene, ortho-terphenyl (OTP) and glycerol. The solid line presents the dependence suggested from simulations. b) ξ as a function of $\Delta V^\#$ in logarithmic scales. Solid squares shown different systems at $T_g(P_{atm})$. Taken from (Hong et al., 2011a).

3) Theoretical model

The models presented earlier, which aim to capture the relaxation time as a function of temperature, frequently neglect the influence of pressure. Since the molecular mobility seems to be governed by both temperature and pressure (or volume), it is fundamental to include their two contributions in the approach for predicting relaxation dynamics.

❖ Thermodynamic scaling

The thermodynamic scaling has been derived from simulations of the glass transition with Leonard-Jones (LJ) potential. These simulations allow to express relaxation times of van der Waals liquids as a function of $T^{-1}V^{-4}$ with a proportionality between the repulsive and attractive parts of LJ particles and the interspecies distance (Tölle, 2001). This relation has been successfully applied to superimposed relaxation times for isotherms of ortho-terphenyl (OTP) measured by dynamic light scattering as a

function of $T^{-1}V^{-4.25}$ (Dreyfus et al., 2003). These observations led to the expression of relaxation times in terms of a function J such as:

$$\tau = J(T^{-1}V^{-\gamma}), \quad 1-45$$

where γ is a scaling exponent. J and γ are material dependent and allow to superimpose isothermal and isobaric relaxation time measurements on a single master curve, as illustrated in **Figure 1-25a**. According to the LJ potential, γ is an indicator of softness of the intermolecular repulsive potential.

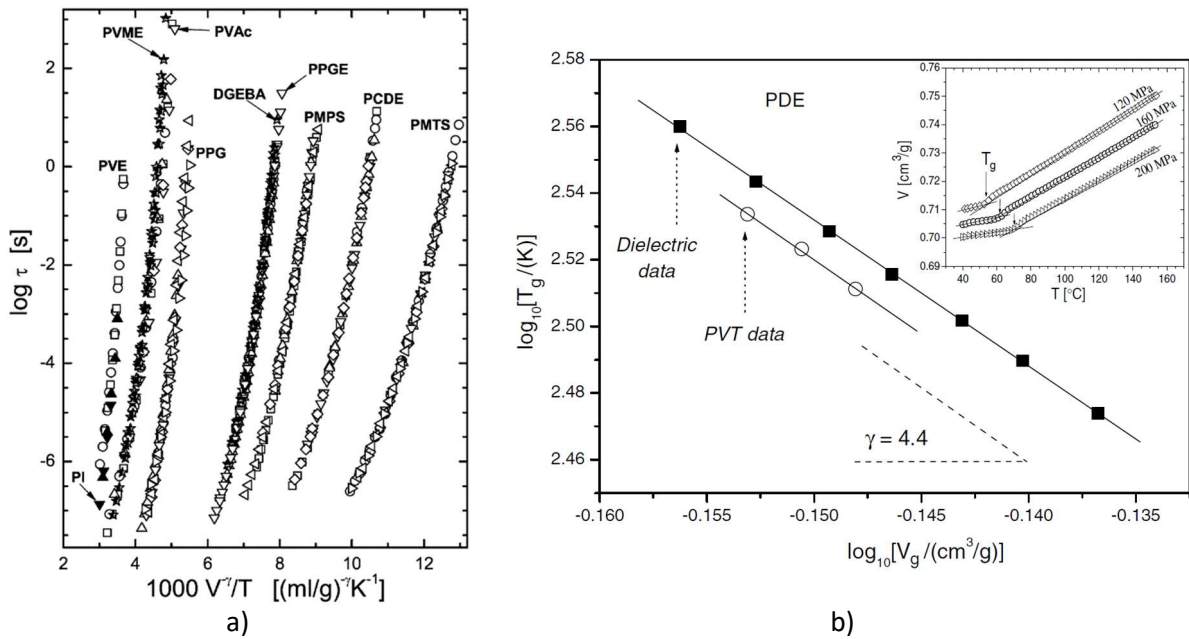


Figure 1-25. a) Dielectric relaxation times as a function of $1000/TV^\gamma$ for polymers. Taken from (Casalini and Roland, 2004a). b) $\log_{10}(T_g)$ as a function of $\log_{10}(V_g)$ for phenylphthalein-dimethylether (PDE) from dielectric (filled squares) and PVT measurement (empty circles). The steepness corresponds to γ . The inset panel is the PVT measurement of PDE. Taken from (Paluch et al., 2007).

Since the $T^{-1}V^{-\gamma}$ scaled the relaxation times, a couple of temperature and pressure at a constant τ leads to $T_\tau^{-1}V_\tau^{-\gamma} = \Gamma_\tau$, where Γ_τ is a constant. Thus, scanning isochrones in temperature and volume allows for the determination of γ from the expression $\log_{10}(T_\tau) = A_\tau - \gamma \log_{10}(V_\tau)$. The scaling exponent γ corresponds to the steepness of this function, such methods is illustrated with **Figure 1-25b**. It is worth mentioning that for $\tau = 100$ s, i.e., at the glass transition, the function takes the form of:

$$\log_{10}(T_g) = \log_{10}(1/\Gamma_g) - \gamma \log_{10}(V_g), \quad 1-46$$

with Γ_g is a constant, equal to $T_g^{-1}V_g^{-\gamma}$. **Figure 1-25b** shows that γ can be obtained through relaxation time and PVT measurements. The scaling exponent γ , which seems to influence the volume dependence of relaxation times, has been linked to the ratio E_V/E_P at the glass transition. The relation at atmospheric pressure is expressed with (Casalini and Roland, 2004b):

$$\frac{E_V}{E_P} = \frac{1}{1 + \alpha T_g \gamma'} \quad 1-47$$

By comparing numerous glass forming liquids, it evidences that the $\alpha T_g = 0.182 \pm 0.009$ at atmospheric pressure (Casalini and Roland, 2004b). **Figure 1-26** shows values for various glass forming liquids whose draw a trend for γ dependence of the ratio E_V/E_P .

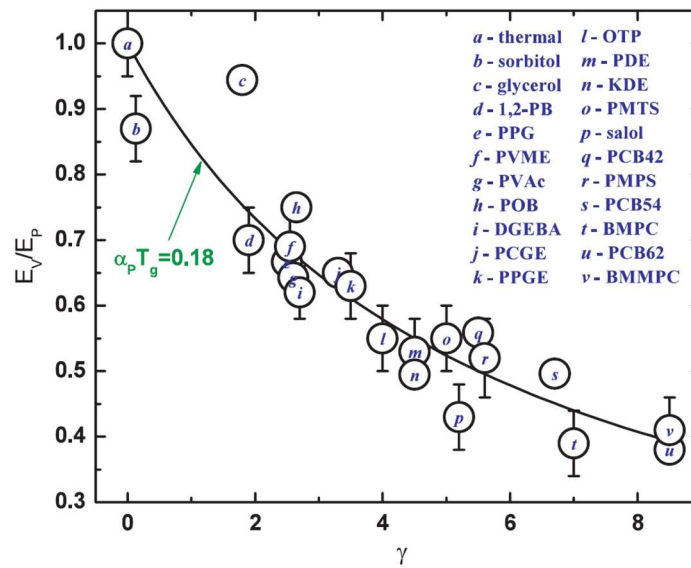


Figure 1-26. The ratio E_V/E_P plotted against the scaling exponent γ for 20 glass forming liquids. Taken from (Roland et al., 2005).

Another approach to use the thermodynamic scaling is to posit that the activation energy $E(T, \rho)$, which is dependent on both temperature and density, can be scaled with density using (Alba-Simionesco and Tarjus, 2006):

$$\tau_\alpha(\rho, T) = \tau_\infty \exp \left[\frac{e(\rho)}{T} F \left(\frac{e(\rho)}{T} \right) \right], \quad 1-48a$$

$$F \left(\frac{e(\rho)}{T} \right) = \frac{E(\rho, T)}{e(\rho)}, \quad 1-48b$$

where τ_∞ is the exponential prefactor, $e(\rho)$ is an effective interaction energy that depends on the density, $F(X)$ is a scaling function and $E(\rho, T)$ an effective activation energy. $e(\rho)$ is assumed to reflect the minimal cooperativity of the molecules with their first neighbors (Niss and Alba-Simionesco, 2006).

By considering that $e(\rho)$ is proportional to ρ^γ , the previous method for scaling can be applied. Another relation, assuming that $e(\rho)$ is proportional to $\rho - \rho^*$ with ρ^* a material constant, has been used for improving some thermodynamic scaling (Alba-Simionesco and Tarjus, 2006). This formalism demonstrates, through experiments on the organic glass-former OTP and the polymer polyvinyl methyl ether (PVME), as well as numerical simulations conducted on a LJ potential, that the activation energy $E(T, \rho)$, can be effectively scaled with density. Moreover, the use of inverse method of the thermodynamic scaling offers to extrapolate relaxation times of supercooled liquids such as the Time Temperature Superposition.

❖ Avramov's model

Avramov proposed an entropic model to describe structural relaxation times as a function of temperature and pressure (Avramov, 2000). This model suggests that the cooperative motion driving structural relaxation is thermally activated, with a derived relationship between relaxation time and system entropy:

$$\tau = \tau_\infty \exp \left[\frac{E_{\max}}{\sigma_r} \exp \left(\frac{-2(S - S_r)}{ZR} \right) \right], \quad 1-49$$

where E_{\max} is the maximum value of the activation energy, σ_r is the dispersion of the reference state having entropy S_r , and Z is the degeneracy of the system, i.e., it indicates the quantity of possible pathways for the localized relaxation of a segment within a polymer, which depends on the short-range order. However, the Avramov's model focuses on the total entropy, whereas the AG model is concerned with configurational entropy (see **Equation 1-18**). Based on thermodynamic considerations, the following connection emerges (Paluch and Roland, 2003):

$$\tau = \tau_\infty \exp \left[30 \left(\frac{T_r}{T} \right)^a \left(1 + \frac{P}{\Pi} \right)^{a/b} \right], \quad 1-50$$

with $a = 2C_p/ZR$ and $b = C_p/(\alpha V_m \Pi)$, where α is the volume expansion coefficient at ambient pressure, C_p the specific heat capacity, V_m the molar volume of structural unit and Π is a constant. The parameters b and Π are identical to those in the Andersson's function (**Equation 1-39**). In addition to the description of both temperature and pressure dependencies simultaneously, the Avramov's model parameters in **Equation 1-50** are linked to measurable thermodynamic properties. Such method is shown in **Figure 1-27**. The experimental data align with the Avramov's model. Casalini and Roland have discussed how the scaling properties can be derived from the temperature and the volume dependences of the entropy. By using the Avramov's model, they derived the expression $\tau =$

$\tau_{\infty} \exp[(A/TV^{\gamma})^{\phi}]$ for relaxation time dependence according to the function J of **Equation 1-45** (Roland et al., 2006).

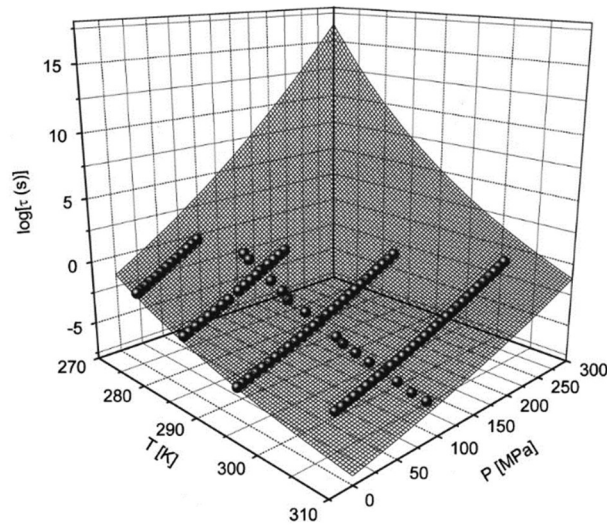


Figure 1-27. Relaxation time as a function of temperature and pressure for poly[(phenyl glycidyl ether)-co-formaldehyde] (PPG). The points are experimental data while the wire surface is the Avramov's model. Taken from (Paluch et al., 2000).

4) Aging under pressure

Recently, the structural relaxation under pressure has been investigated. In these studies, the media are vitrified by the application of pressure, at a constant temperature, before proceeding to the physical aging. These studies use the principle that T_g , which depends on pressure, represents an isomorphous state point, i.e., structure and dynamics in properly reduced units are invariant (Dyre, 2014). Cross T_g to any common state point (with the same T and P) is anticipated to yield same behavior. Consequently, the density and physical aging of an isomorphous material are anticipated to remain unaffected by pressure during the vitrification process.

❖ Densification under pressure

A first approach of physical aging under pressure consists in comparing PVT measurement during heating at low pressure (≈ 10 MPa) after having vitrified the system at low pressure, named conventional glass (CG), or high pressure (up to 200 MPa), called pressure densified glass (PDG). Following pressure release, the glass formed at 200 MPa exhibits a specific volume that is equal to or less than that of the extrapolated liquid, contingent upon temperature. This contrasts with the glass formed under low pressure, which is less dense. Densification under pressure also extends the breadth of the glass transition towards lower temperatures, indicating a more disordered structure (Casalini

and Roland, 2017). At the maximum vitrification pressure, the glass exhibits higher density compared to those formed at the lowest pressure. Upon the release of pressure, the volume expands, yet the material retains a significantly higher density than typical glass, i.e., the relative volume change $\delta > 0$ with (Holt et al., 2019):

$$\delta = \frac{V_L(P_L) - V_H(P_L)}{V_L(P_L) - V_H(P_H)}, \quad 1-51$$

where V_L is the volume in the CG formation, V_H is the volume in the PDG formation, and P_L and P_H are the low and high pressures respectively. Within vitrification pressure range (25-200 MPa), δ can vary by up to 29%, according to the literature on polymers (Weitz and Wunderlich, 1974; Schmidt and Maurer, 2000). The ability of polymers to change density under pressure contradicts their adherence to thermodynamics scaling principles (Casalini and Roland, 2017).

❖ Pressure scanning volumetry

Another approach to aging under pressure has been developed by Sonaglioni et al. (Sonaglioni et al., 2022). When a material is isothermally pressurized, its molten state transitions into glass, and upon depressurization, the formed glass reverts back to a liquid state. This transition exhibits an hysteresis in the thermodynamic jump of $-(dV/dP)_T$ against P , similar to the thermal hysteresis seen in C_p as a function of temperature, as visible in **Figure 1-28a**.

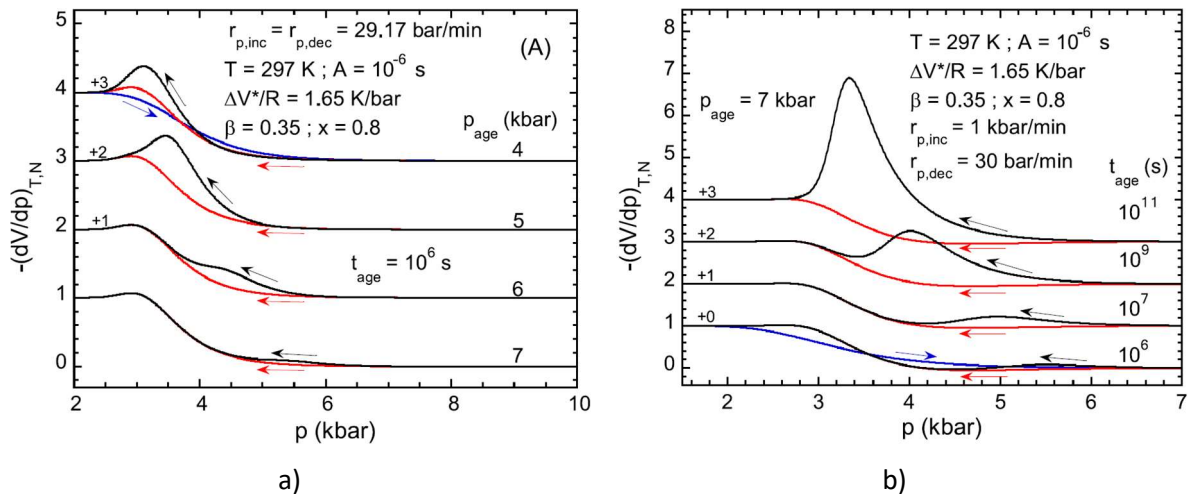


Figure 1-28. Normalized PSV scans simulated for atactic poly(propylene) at constant temperature. The polymer glass samples were formed by pressurizing the melt at $r_{p,inc}$, as shown by the blue line, and the glass was depressurized also at $r_{p,dec}$. The parameters A and $\Delta V^*/R$ used are equivalent to that of **Equation 1-41** with $A = \tau_0$. The parameters β and x are from the TNM. The varied parameters are a) aging pressure P_{age} and b) aging time t_a . Taken from (Sonaglioni et al., 2023).

Named pressure scanning volumetry (PSV) by analogy with DSC, this method employs the Tool-Narayanaswamy-Moynihan (TNM) model (Tool, 1946; Narayanaswamy, 1971; Moynihan et al., 1976) and activation volume for the structural relaxation time ΔV^\ddagger to explore the influence of aging pressure P_{age} , aging time t_a , and pressurizing rate on aging characteristics in PSV scans (Sonaglioni et al., 2023). In PSV, the glass transition pressure P_g and fictive pressure P_f are rather used than their analogous glass transition T_g and fictive temperature T_f (Tool, 1946).

Depressurizing scans show a post- P_g feature emerging for $P_{age} > 40$ MPa, diminishing as P_{age} increases as shown in **Figure 1-28a**. This feature partially overlaps the overshoot peak, distorting it at lower P_{age} and nearly vanishing at higher values. This trend becomes more pronounced as the post- P_g feature shifts to higher pressures and decreases in height. In **Figure 1-28b**, a small post- P_g feature appears at $t_a = 10^6$ s, broadening and increasing in height with increasing P_{age} , overlapping with the overshoot feature as a shoulder on its high-pressure side. As t_a increases from 10^6 up to 10^{11} s, the peak initially shifts towards higher pressures, then towards lower pressures. PSV uncovers a post- P_g feature during depressurization of aged polymers, increasing with longer t_a and lower P_{age} , ultimately merging with the overshoot peak. PSV also reveals that faster depressurization rates push the overshoot peak to higher pressures and shows that decreasing the ratio of depressurization to pressurization rates sharpens and heightens the overshoot peak. Finally, PSV highlights that memory effects in volume and fictive pressure only occur with a distribution of relaxation times.

PSV offers two main benefits. Firstly, simultaneous measurements of isothermal volume changes and $-(dV/dP)_T$ as pressure varies in a single sample run yield direct pressure dependence of volume. In contrast, isobaric change in the heat flow rate is measured in a DSC study, which is then converted into a C_p scan and its integral to obtain the enthalpy as a function of temperature. Secondly, the DSC does not provide insight into volume fluctuations with pressure, which is a key factor for current technologies. DSC measurements require smaller sample sizes and simpler handling than PSV. Furthermore, the enthalpy determination carries a relatively higher error compared to volume determination in PSV (Sonaglioni et al., 2022).

This chapter aimed to expose the main characteristics of the glass transition, as well as the theoretical and experimental approaches that have been used to enhance the understanding of this phenomenon. This chapter sought to elucidate the principal attributes of the glass transition, as well as the theoretical and experimental methodologies that have been employed to augment the comprehension of this phenomenon. Among the various families of glass-forming liquids, amorphous polymers exhibit remarkable characteristics that allow to link their structure to changes in segmental mobility, leading to variations in glass transition temperature according to their chemistry. Finally, pressure is a primary tool for identifying the influence of chemical structure on the volume and molecular mobility of glasses, particularly polymeric glasses. The work presented in the next chapters focuses on the use of pressure through amorphous polymers, which exhibit different molecular interactions due to chemical structure in order to improve the understanding of the glass transition phenomenon.

List of abbreviations and symbols

Symbols			
\bar{A}	Constant (from Adam & Gibbs model)	P_0	Divergent pressure (from pressure VFTH law)
A, B	Constants (from adapted VFTH law)	P_{age}	Aging pressure
$a_T(T)$	Shift factor (from WLF law)	P_f	Fictive pressure
C_1, C_2	Constants (from WLF law)	P_g	Glass transition pressure
$C_4(t)$	4-point correlation function	q^-	Cooling rate
C_p	Isobaric specific heat	R	Prigogine–Defay ratio
$C_p^*(\omega)$	Complex heat capacity	r_i	Spatial location of particle
D	Self-diffusion coefficient	S	Entropy
D	Steepness parameter (from VFTH law)	S_c	Configurational entropy
$e(\rho)$	Effective density dependent interaction energy	s_c^*	Critical configurational entropy
$E(\rho, T)$	Effective activation energy	T	Temperature
E_A	Activation energy	t	Time
E_p	Isobaric activation energy	T^*	Reference temperature (from WLF law)
E_V	Isochoric activation energy	t_0	Observation time
f	Frequency	T_0, T_V	Vogel temperature (from VFTH law)
$F(X)$	Scaling function	T_a	Aging temperature
G	Gibbs free energy	t_a	Aging time
$G(\tau)$	Spatial distribution of relaxation times	T_C	Critical temperature (from MCT)
H	Enthalpy	T^*	Crossover temperature
J	Thermodynamic scaling function	T_f	Fictive temperature
$J^*(\omega)$	Complex compliance	T_g	Glass transition temperature
K	T -independent material property	T_g^0	T_g at atmospheric pressure
K	Compression modulus Specific constant of polymer	T_K	Kauzmann temperature
k_B	Boltzmann constant	V	Specific volume
$K_T(\omega)$	Dynamic temperature modulus	V_0, v_0	Occupied volume of molecules or atoms
M_0	Repeat unit molecular weight	V_∞	Equilibrium specific volume
M_n	Number-average molecular weight	V_f, v_f	Free volume
m_p	Isobaric fragility	V_g	Specific volume at T_g
m_V	Isochoric fragility	\bar{V}_m	Mean molecular volume
N_0	Constant	V_α	Cooperativity volume
N_A	Avogadro's number	$W_c^{N_\alpha^*/N_A}$	Critical average number of configurations
N_{corr}	Number of structural units dynamically correlated	Z	Constant
N_D	Deborah number	Z	Degeneracy of the system
N_α	Number of structural units of a CRR	α	Isobaric thermal expansion
P	Pressure	α_τ	Isochrone thermal expansion

β_{KWW}	Stretching exponent (from KWW function)	FOPT	First Order Phase Transition
γ	Steepness factor (from MCT)	FSC	Fast Scanning Calorimetry
γ	Overlap factor (from free volume theory)	JG β	Johari-Goldstein β -relaxation
	Scaling exponent	KWW	Kohlrausch–Williams–Watts
δ	Specific volume deviation from equilibrium	LJ	Leonard-Jones
Δ_0	Activation energy	MCT	Mode coupling theory
ΔC_p	Isobaric heat capacity jump at T_g	NMR	Nuclear magnetic resonance
ΔH	Enthalpy recovery	PALS	Positron Annihilation Lifetime Spectroscopy
ΔH_∞	Total enthalpy recovery	PDG	Pressure densified glass
δT	Temperature fluctuation	PSV	Pressure scanning volumetry
$\Delta V^\#$	Activation volume	PVT	Pressure-Volume-Temperature
$\Delta\alpha$	Isobaric thermal expansion jump at T_g	QENS	Quasielastic neutron scattering
$\Delta\mu$	Energy barrier (from AG theory)	SAP	Slow Arrhenius Process
η	Viscosity	SOPT	Second Order Phase Transition
θ	Free volume excess	TNM	Tool-Narayanaswamy-Moynihan
κ	Isothermal compressibility	TTS	Time Temperature Superposition
ξ, ξ^*	Characteristic length scale of dynamic heterogeneities	VFTH	Vogel-Fulcher-Tamman-Hesse
ξ_α	Characteristic length scale of CRR	WLF	Williams-Landel-Ferry
Π	Constant (from Andersson's model)		
σ_{CRR}	Number of possible internal states		
τ	Relaxation time		
τ_0	$\tau(T, P_{atm})$		
τ_∞	Pre-exponential factor for $T \rightarrow \infty$		
τ_α	Relaxation time of α -relaxation		
$\Phi(t)$	Relaxation function		
$\chi_4(t)$	4-point susceptibility		
$\chi_T(t)$	3-point susceptibility		
Ψ	Constant		
ψ	Exponential factor		
ω	Angular pulsation ($= 2\pi f$)		

Abbreviations

AG	Adam and Gibbs
CG	Conventional glass
CRR	Cooperative Rearranging Region
DMA	Dynamic Mechanical Analysis
DSC	Differential Scanning Calorimetry
FDT	Fluctuation Dissipation Theorem

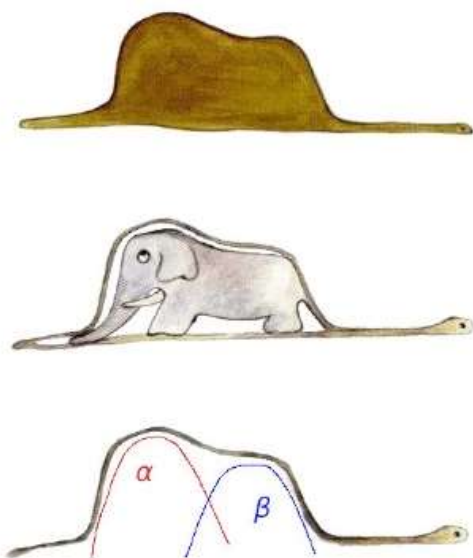
Polymer abbreviations

PAN	Polyacrylonitrile
PB	1,4-polybutadiene
PC	Polycarbonate
PDE	Phenylphthalein-dimethylether
PDMS	Poly(dimethyl siloxane)
PE	Polyethylene
PEEK	Polyetheretherketone
PEF	Poly(ethylene furandicarboxylate)
PENO	Poly(ethylene naphthenoate)
PEO	Poly(ethylene oxide)
PET	Polyethylene terephthalate
PI	1,4-polyisoprene
PIB	Polyisobutylene
PLA	Poly(lactide acid)
PMMA	Atactic poly(methyl methacrylate)
PP	Polypropylene
PS	Atactic polystyrene
PVC	Poly(vinyl chloride)
PVME	Polyvinyl methyl ether

Chapter 2. Materials and methods

Table of content

CHAPTER 2. MATERIALS AND METHODS	62
I. POLYMERS.....	62
1) <i>Poly(lactide acid) PLA</i>	64
2) <i>Poly(ethylene terephthalate glycol) PETg</i>	65
3) <i>Poly(vinyl acetate) PVAc</i>	65
4) <i>Poly(ethylene-vinyl acetate) EVA</i>	66
II. CALORIMETRIC EXPERIMENTAL TECHNIQUES.....	67
1) <i>Differential scanning calorimetry DSC</i>	67
2) <i>Modulated temperature differential scanning calorimetry MT-DSC</i>	69
III. DIELECTRIC EXPERIMENTAL TECHNIQUES.....	72
1) <i>Theory of dielectric relaxation</i>	72
2) <i>Broadband dielectric spectroscopy BDS</i>	75
3) <i>Analysis of dielectric spectra</i>	76
4) <i>Broadband dielectric spectroscopy High Pressure HP-BDS</i>	78
IV. DETERMINATION OF EXPERIMENTAL PARAMETERS	79
1) <i>Metrological aspects of HP-BDS</i>	80
2) <i>Cooperativity volume</i>	82
LIST OF ABBREVIATIONS AND SYMBOLS	84
REFERENCES	ERREUR ! SIGNET NON DÉFINI.



Antoine de Saint-Exupéry once wrote “My drawing was not a picture of a hat (top of the figure). It was a picture of a boa constrictor digesting an elephant. But since the grown-ups were not able to understand it, I made another drawing: I drew the inside of the boa constrictor, so that the grown-ups could see it clearly (middle of the figure). They always need to have things explained.” Personally, I see distinctly two relaxation processes (bottom of the figure). Adapted from (Saint-Exupéry, 1995).

Chapter 2. Materials and methods

The materials section introduces the polymer samples which are studied in this work. This includes details of the sample suppliers, their preparation and their main physical characteristics. The next sections provide a description of the experimental techniques conducted in this study. The experimental set-up, theoretical principles and analytical techniques used for data interpretation are presented together with their specifications and calibration procedures. Furthermore, this chapter outlines the methods and theoretical assumptions used for determining some material parameters. Overall, this chapter serves as a foundation for the other chapters.

I. Polymers

Polymers represent a class of glasses characterized by long chains of repeating units, which exhibit a wide range of properties depending on their molecular architecture. In this context, factors such as chain flexibility, molecular weight, cross-linking, and chemical composition play a significant role in intra and intermolecular interactions that govern the glass transition.

The main chain rigidity influences the segmental mobility of polymers. The first source of polymer backbone chain rigidity is the variation of torsion angles φ_i represented in **Figure 2-1**. Rigid chains tend to remain more aligned and ordered at high temperatures, limiting polymer segmental motions and increasing material viscosity. Rigid chains require more energy to move and rearrange. This leads to a glass transition at higher temperature than those of more flexible chains.

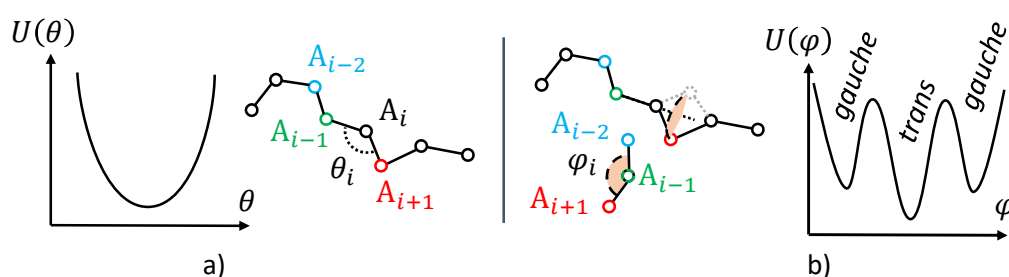


Figure 2-1. Schematic view of few atoms in a backbone chain of polymer. These atoms are linked by covalent bonds between each other. a) The dihedral angle θ_i is defined as the angle between the vectors $\overline{A_{i-1}A_i}$ and $\overline{A_iA_{i+1}}$ in the plan $A_{i-1}A_iA_{i+1}$. The variations of the potential energy as a function of θ show only one minimum. b) The torsion angle φ_i is defined by the rotation of the projection of vectors $\overline{A_iA_{i+1}}$ and $\overline{A_{i-2}A_{i-1}}$ on the plane of the normal vector $\overline{A_{i-1}A_i}$. In the case of $-\text{CH}_2-$ groups, the potential energy of the torsion angle $U(\varphi)$ can have three minima. The lowest minimum corresponds to a *trans* configuration, while the others correspond to *gauche* configurations.

The flexibility of a chain can be estimated using the Kuhn length. This is defined as the ratio between the mean-square end-to-end distance and the contour length $\langle R^2 \rangle$, which is the length of the chain when it is fully extended L , namely the contour length (Hu, 2013).

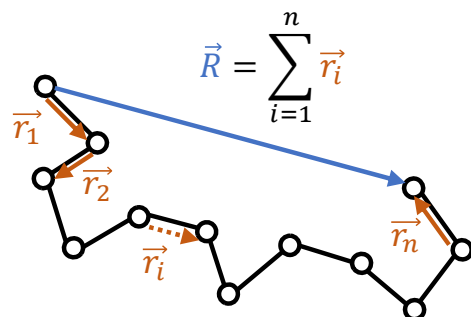


Figure 2-2. Schematic view of few atoms in a backbone chain of polymer where the end-to-end distance R is shown by the blue arrows, and the contour length L is the sum of all segments r . The Kuhn length is equal to $b = \langle R^2 \rangle / L$.

The Kuhn length b is observed to increase with chain rigidity (Fetters et al., 2007). It is generally observed that the higher the chain rigidity of a polymer, and therefore its Kuhn length, the higher the glass transition temperature T_g . **Table 2-1** presents the Kuhn lengths b and T_g for some polymers.

Table 2-1. Kuhn length b and glass transition temperature T_g for usual polymers (Bishop et al., 1985; Rubinstein and Colby, 2003; Everaers et al., 2020).

Polymer	Structure	b [\AA]	T_g [K]
1,4-Polyisoprene (PI)	$-(\text{CH}_2\text{CH}=\text{CHCH}(\text{CH}_3))-$	8.2	200
1,4-Polybutadiene (PB)	$-(\text{CH}_2\text{CH}=\text{CHCH}_2)-$	9.6	200
Poly(oxymethylene) (POM)	$-(\text{CH}_2\text{O})-$	10	180
Polypropylene (PP)	$-(\text{CH}_2\text{CH}_2(\text{CH}_3))-$	11	260
Poly(ethylene oxide) (PEO)	$-(\text{CH}_2\text{CH}_2\text{O})-$	11	220
Poly(dimethyl siloxane) (PDMS)	$-(\text{OSi}(\text{CH}_3)_2)-$	13	120
Polyethylene (PE)	$-(\text{CH}_2\text{CH}_2)-$	14	190
Polyethylene terephthalate (PET)	$-((\text{CH}_2)_2\text{OCOC}_6\text{H}_4\text{COO})-$	15	340
Atactic poly(methyl methacrylate) (PMMA)	$-(\text{CH}_2\text{C}(\text{CH}_3)(\text{COOCH}_3))-$	17	370
Atactic polystyrene (PS)	$-(\text{CH}_2\text{CHC}_6\text{H}_5)-$	18	370
Polyetheretherketone (PEEK)	$-(\text{C}_6\text{H}_4\text{OC}_6\text{H}_4\text{OC}_6\text{H}_4\text{CO})-$	108	410

Increasing chain stiffness through longer rigid units in the backbone or bulky side groups can raise T_g significantly by increasing potential barriers to rotation ($U(\theta)$ and $U(\varphi)$). This also results in an increase in Kuhn length b . Steric barriers to rotation are heightened when additional side groups are

introduced on alternate chain backbone atoms. Introducing phenyl rings into the backbone also increases T_g , as it requires a longer chain segment to undergo molecular displacement. However, b is not directly correlated with the values of T_g . Indeed, other polymer features have influence on the chain mobility.

The presence of side group on the main chain has a huge influence on segmental mobility, through different physical phenomena. The rigidity of side groups can introduce steric hindrance. Larger groups can further hinder the movement of polymer segments, resulting in an increase in T_g . The more rigid the side group, the higher T_g . Polarity can be introduced to polymer chains through side groups, which impacts intermolecular interactions and segmental mobility. The presence of polar side groups can strengthen interactions such as hydrogen bonds, resulting in stronger intermolecular forces and a higher T_g . The intensity of interactions between adjacent polymer chain segments determines the thermal energy required to create holes large enough for a diffusive jump of a chain segment. Thus, higher polymer polarity is associated with a higher T_g , with the perpendicular components of dipole units having the most significant effect. When comparing substituent groups of comparable size, increasing polarity, which enhances intermolecular interactions, tends to raise T_g .

The different materials studied are all amorphous thermoplastic polymers. On the one hand, poly(lactide acid) PLA, poly(ethylene terephthalate glycol) PETg and poly(vinyl acetate) PVAc have been chosen for their relative molecular backbone stiffness which varies gradually, leading to different glass transition temperatures T_g . On the other hand, the poly(ethylene-vinyl acetate) EVA series allows to vary the ratio of polar side groups along the chain. This also induces a variation in T_g . The material sets have been chosen for their controlled differences in intra and intermolecular interactions, and to investigate how the chemical structure influence the molecular mobility, and therefore the glass transition.

1) Poly(lactide acid) PLA

Poly(lactide acid) PLA is a biosourced and biodegradable polyester. For this purpose, it is widely used for packaging or 3D printing. PLA, with a repeating unit shown in **Figure 2-3**, is obtained by transforming lactic acid produced from the fermentation of sugars from corn, beet, tapioca and sugar cane. Lactic acid is a chiral compound with two enantiomers: D and L- lactide. The PLA was purchased from *Nature Works* in the form of pellets grade 4042D composed of 95.7 % of L-lactide and 4.3 % of D-lactide. This isomer ratio allows to avoid fast polymer crystallization. The average molecular weight of PLA is $M_w = 188\,000\text{ g}\cdot\text{mol}^{-1}$ with a molar mass of the repeating unit of $M_0 = 72\text{ g}\cdot\text{mol}^{-1}$. The density of PLA at ambient conditions, i.e., room temperature and atmospheric pressure, is $\rho =$

This is produced by reacting acetic acid with acetylene, or ethylene in the presence of active oxygen. The PVAc powder was acquired from *Aldrich Chemical Company*. The average molecular weight of PVAc is $M_W = 500\,000 \text{ g. mol}^{-1}$ with a molar mass of the repeating unit of $M_0 = 86 \text{ g. mol}^{-1}$. The density of PVAc at ambient conditions is $\rho = 1.19 \text{ g. cm}^{-3}$. The PVAc were dried for 24 hours at $50 \text{ }^\circ\text{C}$ before thermo-processing experiments. The powder was thermo-molded at $120 \text{ }^\circ\text{C}$ under a mass of 1.5 tons during 5 minutes in a manual hydraulic press (from Specac). Templates with thickness ranging from $100 \text{ }\mu\text{m}$ up to $500 \text{ }\mu\text{m}$ were used to form PVAc films. Samples were cooled down at ambient air. Its calorimetric glass transition temperature is found at $T_g = 313 \text{ K}$ at a cooling rate of $q^- = 10 \text{ K. min}^{-1}$ (Rijal et al., 2015).

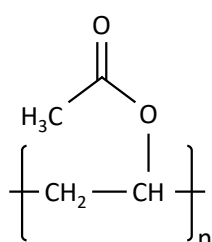


Figure 2-5. Repeating unit of PVAc.

4) Poly(ethylene-vinyl acetate) EVA

Poly(ethylene-co-vinyl acetate) (EVA) are copolymers with different vinyl acetate ratio (VAc), ranging from PVAc (with 100 wt. % VAc) to polyethylene PE (0 wt. % VAc). EVA are used as adhesives or foam rubber. The repeating unit is shown in **Figure 2-6**.

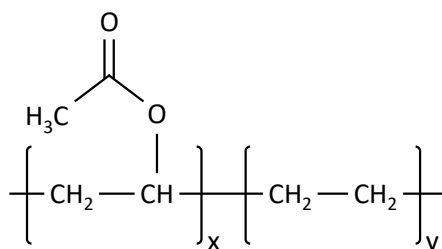


Figure 2-6. Repeating unit of EVA with the ratio x corresponding to wt. % VAc.

EVA with 80 and 60 wt. % VAc are studied in this work, they were provided in the form of pellets. EVA containing 80 wt. % of VAc groups (Levapren® 800) were obtained from *Lanxess Company*. EVA p containing 60 wt. % of VAc groups (Levapren® 600) were obtained from *Bayer Company*. For sake of clarity, EVA80 and EVA60 stand for Levapren® 800 and 600 respectively in the rest of the manuscript. The pellets were dried in an oven at $40 \text{ }^\circ\text{C}$ during 12 hours. The samples were thermo-molded at $80 \text{ }^\circ\text{C}$.

An average thickness of polymer films is 500 μm . The amount of 60 wt. % and 80 wt. % of VAc in EVA60 and EVA80 respectively are sufficient to keep the systems fully amorphous (Kummali et al., 2013). The molar masses M_0 of structural units is calculated by using the molar mass and the molar ratio x of the VAc group ($M_{\text{VAc}} = 86 \text{ g. mol}^{-1}$) and the molar mass of the ethylene group ($m_{\text{Eth}} = 28 \text{ g. mol}^{-1}$) as follows: $M_{0,\text{EVA}x} = M_{\text{VAc}}(x) + M_{\text{Eth}}(1 - x)$. Physical characteristics of EVA80 and EVA60 are presented in **Table 2-2** (Puente et al., 2015).

Table 2-2. Values of average molecular weight M_w , molar mass of the repeating unit M_0 , glass transition temperature T_g and density at ambient conditions ρ of EVA80 and EVA60.

Sample	M_w [g. mol ⁻¹]	M_0 [g. mol ⁻¹]	T_g [K]	ρ [g. cm ⁻³]
EVA80	270 000	60.8	276	1.11
EVA60	250 000	47	248	1.04

II. Calorimetric Experimental techniques

For probing dynamic and thermodynamic properties of the samples, different experimental techniques have been used. They can be distinguished in two classes: calorimetric and dielectric techniques. The functioning of these techniques is described below.

1) Differential scanning calorimetry DSC

Differential scanning calorimetry (DSC) is a thermal analysis technique used to study thermal events such as crystallization, glass transition, melting, or oxidation, as well as physical aging. During these physical transitions, heat is either absorbed (endothermic) or released (exothermic). The fundamental principle of DSC involves quantifying the difference in heat required to increase the temperature of a sample compared to a reference material. The DSC instrument measures the associated heat flow as a function of time and temperature, providing insights into the material behavior. There are two main types of DSC: heat flow and power-compensated DSC. In this work, heat flow DSC has been conducted, which experiments use typically samples weighing few milligrams. For heat flow DSC, a sample and a reference (an empty pan) are placed in the same oven as shown in Figure 2-7, the difference in heat-flow between the sample, the reference and the exterior is analyzed during the same temperature program (maintained under isothermal conditions, or subjected to heating or cooling ramps during which the temperature increases or decreases linearly).

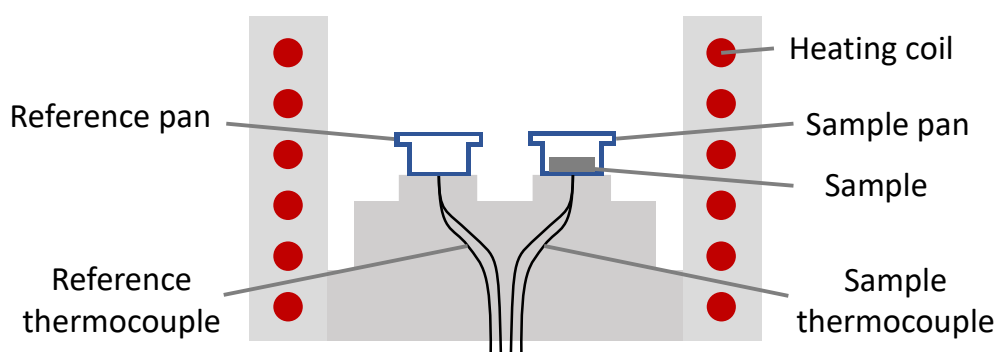


Figure 2-7. Schematic view of a heat flow DSC.

Therefore, a linear temperature ramp applied to the sample and the reference is expressed by $T = T_i + q \cdot t$, in which T is the temperature at the time t , T_i the initial temperature and q the scanning rate. The heat flow Φ resulting in the heat transfer Q is expressed as follow (Schick, 2009):

$$\Phi = \frac{dQ}{dt} = C_p \frac{dT}{dt}, \quad 2-1$$

where C_p is the heat capacity at constant pressure. When the temperature ramp is applied, heat is transferred to the sample Q_S and to the reference Q_R . Thermal events in the sample result in a difference between sample T_S and reference T_R temperatures recorded by the thermocouples. The resulting heat flow can be simplified by a thermal equivalent of the Ohm's law:

$$\Phi = Q_S - Q_R = \frac{\Delta T}{R}, \quad 2-2$$

where $\Delta T = T_S - T_R$ and R is the thermal resistance between the oven and the empty pan. The measurements are performed with the Q100 heat-flow DSC based on *Tzero* technology from *TA Instruments*. Calibration is required, and consists of three steps. A first calibration is made for obtaining the base line with an empty oven. For this purpose, a constant heating ramp is performed without sample and pan. The next step involves mass calibration. A constant heating ramp is conducted using sapphire disks, with different but well-known masses, positioned directly on the sample and reference platforms. The third calibration is the temperature and heat flow calibration, which is performed using a minimum of one standard as Indium, aligning with its known melting temperature $T_m = 156.6 \text{ }^\circ\text{C}$ and its associated enthalpy $\Delta H_m = 28.6 \text{ J} \cdot \text{g}^{-1}$. The indium is positioned in a pan on the sample side, while an empty pan is placed on the reference side. This calibration process needs to be repeated if the scanning rate is modified. To ensure optimal signal-to-noise ratio, sample masses are around 10 mg. A scanning rate of $10 \text{ K} \cdot \text{min}^{-1}$ is selected to enhance the resolution of thermal events under

investigation. All experiments are conducted under a nitrogen atmosphere with a flow rate of 50 mL. min⁻¹.

2) Modulated temperature differential scanning calorimetry MT-DSC

During heating and cooling, the samples are subjected to thermally activated events such as glass transition, melting and crystallization as mentioned earlier. Some of these thermal events occur over partially or completely overlapping temperature ranges. Overlapping events cannot be distinguished by conventional DSC. Heat flow Φ measured from standard DSC can be expressed by (Reading et al., 1993):

$$\Phi = \frac{dQ}{dt} = C_p q + f(t, T), \quad 2-3$$

where $f(t, T)$ denotes the portion of heat-flow associated with kinetic or non-reversing events, referred to as non-reversing heat-flow Φ_{NR} . Conversely, the segment linked to thermodynamic events, known as the reversing heat flow Φ_R , is expressed as the product of the heat capacity and the scanning rate $C_p q$. In modulated temperature differential scanning calorimetry (MT-DSC) experiments, the classical linear temperature ramp is altered by a small perturbation, typically a sinusoidal wave (Reading and Hourston, 2006). A Fourier transform is used to deconvolute the sample response to the perturbation from its response to the original heating ramp. The sinusoidal temperature modulation is added to the underlying linear heating ramp, determining the temperature such as:

$$T = T_i + qt + A \sin(\omega t), \quad 2-4$$

where A is the amplitude of the sinusoidal oscillation, ω is the angular frequency corresponding to a period $p = 2\pi/\omega$. Such sinusoidal heating ramp is shown in **Figure 2-8**.

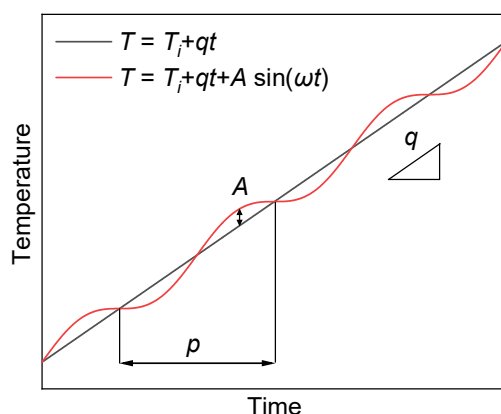


Figure 2-8. Schematic illustration of a temperature ramp with sinusoidal modulation (in red) compared to a classical linear ramp (in black). The parameters defining temperature modulation are shown in this figure.

The modulated heat-flow Φ is then expressed by:

$$\Phi = \frac{dQ}{dt} = C_p^*(q + A\omega \cos(\omega t)), \quad 2-5$$

where C_p^* is the complex heat capacity. Thermodynamic events are related to the rapid vibrational and translational motions of molecules in the sample, which can quickly adjust to small changes in temperature. In contrast, kinetic events cannot follow these temperature changes and do not affect the modulated part of the heat-flow. The reversing heat flow Φ_R and non-reversing heat flow Φ_{NR} can then be estimated with:

$$\Phi_R = C_p^* q, \quad 2-6a$$

$$\Phi_{NR} = \Phi - \Phi_R = C_p^* A\omega \cos(\omega t). \quad 2-6b$$

Furthermore, there is an experimental phase lag φ between the overall response of the calorimeter, which is the total heat flux, and the heating modulation. Considering this phase lag, two components can be distinguished from the complex heat capacity C_p^* : the reversing heat capacity C_p' (in-phase component associated with Φ_R) and the non-reversing heat capacity C_p'' (out-of-phase component associated with Φ_{NR}). These two components are calculated from:

$$C_p' = |C_p^*| \cos(\varphi), \quad 2-7a$$

$$C_p'' = |C_p^*| \sin(\varphi). \quad 2-7b$$

MT-DSC measurements are performed with the Q100 heat flow DSC. Calibration before measurement includes a supplementary step in comparison to a calibration performed for classical DSC measurements. This additional step serves to calibrate the heat capacity. A standard as sapphire is used, since it undergoes no transition in the temperature range swept for sample analysis. Moreover, the heat capacity of sapphire as a function of temperature is stable and well known. Any change in experimental conditions (modulation amplitude, modulation period or scanning rate) requires a new calibration. From the calibration curve, a calibration factor K_{C_p} is calculated by comparing experimental and theoretical values of sapphire heat capacity. The calibration factor is obtained at each temperature, averaged over the temperature range selected for measurement, and used to correct the sample apparent heat capacity. The correction factor can be calculated with:

$$K_{C_p} = \frac{\langle C_{P_{S,th}} \rangle}{\langle C_{P_{S,exp}} \rangle}, \quad 2-8$$

where $\langle C_{P_{S,th}} \rangle$ and $\langle C_{P_{S,exp}} \rangle$ are the average theoretical and experimental sapphire heat capacities respectively.

MT-DSC measurements can be performed with three different temperature modulation modes: heat only ($A\omega < q$), heat-iso (successive isotherms with $q = 0$) and heat cool ($A\omega > q$). **Figure 2-9** shows the temperature and heating rate signals of the different heating modes. It is recommended that the heat only mode be employed to investigate the coupling of different thermal events, such as glass transition and cold-crystallization, or crystallization and melting. The heat-iso mode is recommended for the investigation of melting. The heat cool mode is recommended for the investigation of the glass transition and physical aging.

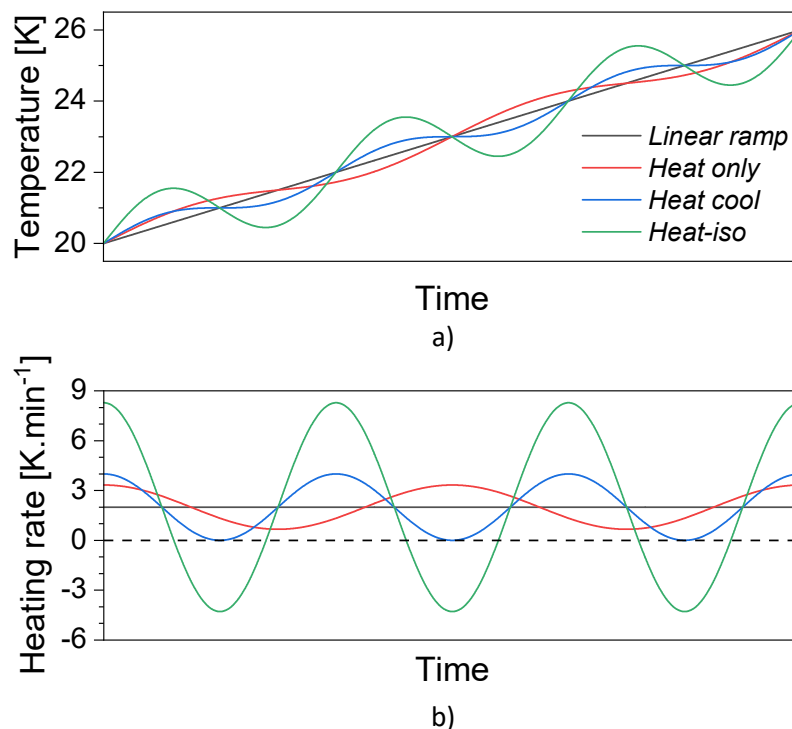


Figure 2-9. Schematic illustration of a) the temperature and b) the heating rate for the different heating ramps achievable in MT-DSC. In this case, the mean heating rate for the different modes is $2 \text{ K} \cdot \text{min}^{-1}$, as shown with the linear ramp in black. The heat only mode (in red) has a modulation amplitude and a period of $A = \pm 0.318 \text{ K}$, $p = 90 \text{ s}$. In this mode, the heating rate is strictly greater than 0. The heat cool mode (in blue) has $A = \pm 1 \text{ K}$ and $p = 60 \text{ s}$. During the measurement, the scanning rate alternates between heating and cooling, even if its mean scanning rate is positive. The heat-iso mode has $A = \pm 0.318 \text{ K}$ and $p = 60 \text{ s}$, and it is characterized by a heating rate that approaches 0 at the lowest point.

Thus, the samples are analyzed using the heat-cool mode with a period of $p = 60$ seconds, an amplitude of $A = \pm 1 \text{ K}$, and with a heating rate $q = 0.5 \text{ K} \cdot \text{min}^{-1}$. Moreover, an additional computational correction is applied to the reversing heat capacity C_p' and the non-reversing heat

capacity C_p'' signals in order to remove the contribution to the phase lag due to the apparatus. This correction is achieved by an homemade software. MT-DSC experiments use a nitrogen atmosphere with a flow rate of $50 \text{ mL} \cdot \text{min}^{-1}$. Furthermore, the samples are placed in *Tzero* pans from *TA Instruments*, which facilitate thermal conduction and ensure more accurate results than those obtained with standard pans. For optimal signal acquisition, sample masses are typically approximately 10 mg.

III. Dielectric experimental techniques

1) Theory of dielectric relaxation

As mentioned earlier, broadband dielectric spectroscopy (BDS) is a highly useful tool for studying molecular mobility in glassy liquids, as it allows the measurement of relaxation times across a wide range of temperatures and frequencies (10^{-5} up to 10^{11} Hz) (Kremer and Schönhal, 2003). During dielectric measurements, an alternating electric current generated by applying controlled voltage U_S is applied to a non-conductive material containing dipoles. This results in a symmetrical distribution of positive and negative charges, known as electric polarization \mathbf{P} . Therefore, dielectric materials such as polymers can be simplified as capacitors. The increase in capacitance is related to the ability of the material to store energy under an external field. From a macroscopic point of view, the polarization of a dielectric material is related to the electric field. The capacitance of such capacitor is given by the relation:

$$C = \varepsilon \frac{\varepsilon_0 S}{e}, \quad 2-9$$

where ε is the relative dielectric permittivity, ε_0 is the dielectric permittivity of vacuum, S and e are the surface and the thickness of the capacitor respectively. It is worth mentioning that $\varepsilon_0 S/e$ corresponds to the equivalent capacitance C_0 of a planar capacitor in vacuum.

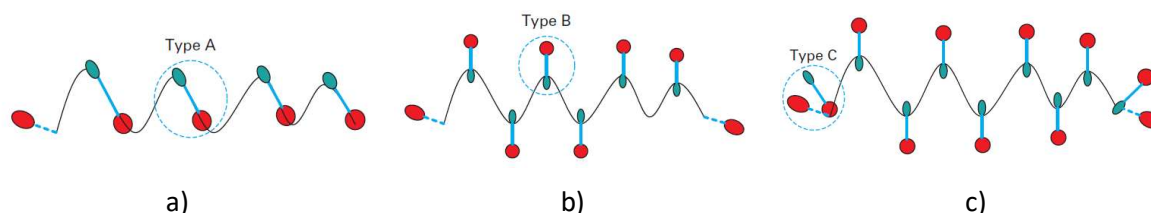


Figure 2-10. Schematic representation of a polymer of type A (dipoles oriented parallel to the backbone chain), type B (dipoles oriented perpendicular to the backbone chain), type C (dipoles localized on flexible side groups or on a flexible molecule at the end of the backbone chain). From (Kahouli, 2016).

Electric polarization \mathbf{P} arises from two main processes, known as induced polarization P_{∞} , and orientational polarization P_{or} (Grzybowska et al., 2016). Induced polarization P_{∞} , involves electronic polarization P_e , and atomic polarization P_a . Orientational polarization P_{or} , is the direct consequence of the rotational movements of permanent dipoles when an external electric field is applied to the sample. Polymers are referenced as three types due to the nature of their permanent dipoles within the molecular chain as shown in **Figure 2-10**.

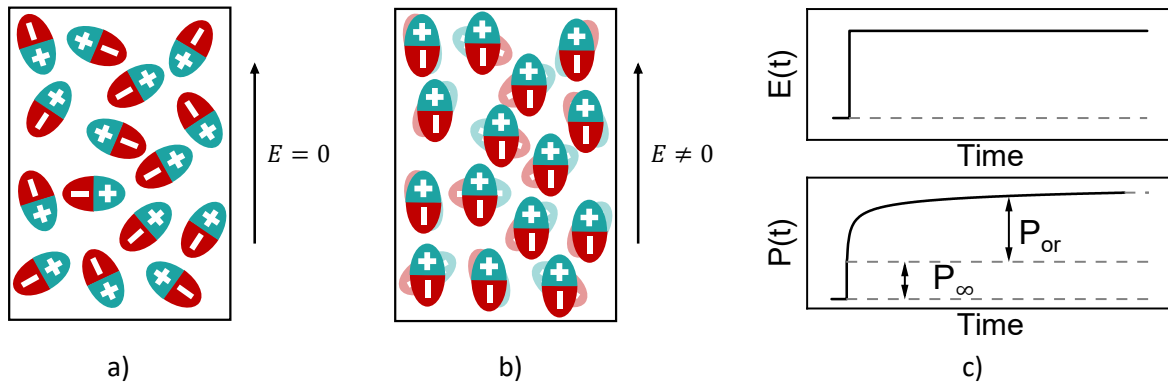


Figure 2-11. Dipole orientations of a dielectric material in absence a) and presence b) of an external electric field E . c) Evolution of electric polarization $\mathbf{P}(t)$ over time due an applied external impulse of the electric field $E(t)$.

In a system of freely floating dipoles, there are no restoring forces tending to impose a preferential direction on dipole vectors. Instead, the random influence of thermal agitation is the only factor influencing the orientation of the dipoles. Consequently, polarization is zero. In the absence of an electric field ($E = 0$), the dipoles are randomly oriented due to the thermal agitation as shown in **Figure 2-11a**. Conversely, when an electric field E is applied to a system where dipoles are initially randomly oriented, a preferential direction is imposed on the dipoles, resulting in induced and oriented polarization as shown in **Figure 2-11b**. Electric polarization \mathbf{P} over time can be calculated from (Kremer and Schönhals, 2003):

$$\mathbf{P}(t) = P_{\infty} + \varepsilon_0 \int_{-\infty}^t \varepsilon(t - t') \frac{dE(t')}{dt'} dt'. \quad 2-10$$

The evolution of polarization $\mathbf{P}(t)$ according to the external electric field $E(t)$ is shown in **Figure 2-11c**. The contribution of the induced polarization P_{∞} is visible at the mean time than the rising edge of $E(t)$, while the orientational polarization $P_{or}(t)$ starting to increase logarithmically until reach a plateau. If a stationary periodic disturbance $E(t, \omega) = E_0 \exp(-i\omega t)$ (where ω is the angular frequency) is applied to the system instead of the pulse shown in **Figure 2-11c**, then polarization is expressed as:

$$\mathbf{P}(t, \omega) = \varepsilon_0(\varepsilon^*(\omega) - 1)\mathbf{E}(t, \omega), \quad 2-11$$

where ε^* is the complex dielectric function. Therefore, dielectric permittivity ε and capacitance C have a complex response if the applied electric field is alternating, given complex permittivity ε^* and complex capacitance C^* respectively. ε^* and C^* are frequency dependent and tend to ε_0 and C_0 at infinite frequencies. The complex dielectric function ε^* includes a real part $\varepsilon'(\omega)$, namely the dielectric storage, proportional to the energy stored reversibly in the system per period, and an imaginary part, the dielectric loss $\varepsilon''(\omega)$, proportional to the energy dissipated per period. Typical dielectric spectra of dielectric storage ε' and loss ε'' for frequency sweep at given temperature and pressure are shown in **Figure 2-12**. If the electric field E is alternated too quickly, i.e., $\omega t \gg \tau_{\max}$, the dipoles don't have time to orient themselves in the direction of E . As a result, no energy is stored or dissipated. The dielectric storage $\varepsilon'(\omega)$ is then equivalent to $\varepsilon_\infty = \lim_{\omega \rightarrow \infty} \varepsilon'(\omega)$. The real permittivity in the high frequency ε_∞ corresponds to its analogous induced polarization P_∞ . If E is alternated too slowly, $\omega t \ll \tau_{\max}$, the dipoles, once oriented, won't store any more energy; they reach their maximal polarization. In this case, the dielectric storage $\varepsilon'(\omega)$ is then equivalent to the static permittivity $\varepsilon_S = \lim_{\omega \rightarrow 0} \varepsilon'(\omega)$.

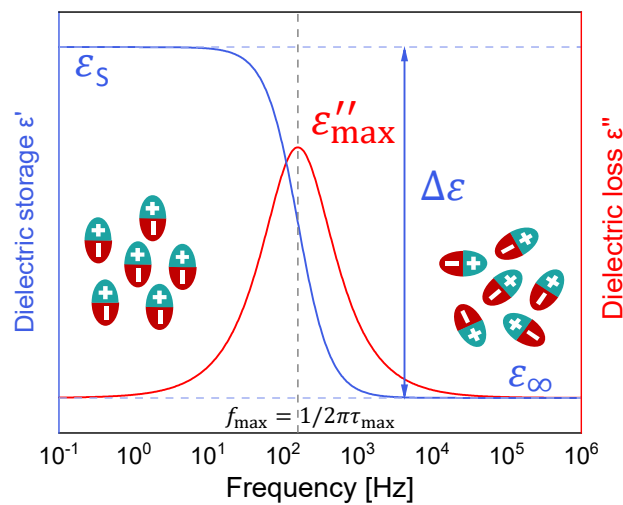


Figure 2-12. Schematic evolution of the real ε' (in blue) and the imaginary ε'' (in red) permittivities as a function of frequency for a Debye relaxation.

Finally, if it is alternated in a way equivalent to the relaxation time τ_{\max} , it is under these conditions that the material have a maximum of energy dissipated in the reorientation of its dipoles. The response of a dielectric material whose relaxation is of the Debye type (i.e. symmetrical and unstretched) can then be expressed as (Debye, 1929):

$$\varepsilon^*(\omega) = \varepsilon'(\omega) - i\varepsilon''(\omega) = \varepsilon_\infty + \frac{\Delta\varepsilon}{1 + i\omega\tau_D}, \quad 2-12$$

where the dielectric strength $\Delta\varepsilon$ is the difference between the dielectric constant measured at low ε_∞ and high ε_S frequencies, and τ_D the relaxation times (for Debye relaxation $\tau_D = \tau_{\max}$). $\Delta\varepsilon$ gives the magnitude of the dielectric loss of the relaxation process. The dielectric strength of a material can be linked to the density of relaxing dipoles through the Onsager-Kirkwood-Fröhlich relation (Onsager, 1936; Kirkwood, 1940; Fröhlich, 1986).

2) Broadband dielectric spectroscopy BDS

In dielectric or impedance measurements, a cell containing the sample is subjected to a voltage U_S of a fixed frequency $f = \omega/2\pi$. This voltage induces a current I_S of the same frequency in the sample cell. There is typically a phase lag between the current and voltage, denoted by the phase angle φ such as:

$$U_S(t) = U_0 \cos(\omega t), \quad 2-13a$$

$$I_S(t) = I_0 \cos(\omega t + \varphi). \quad 2-13b$$

I_S can be measured in output by measuring the voltage U_2 of an analyzer in parallel with a resistor R , as shown in **Figure 2-13a**.

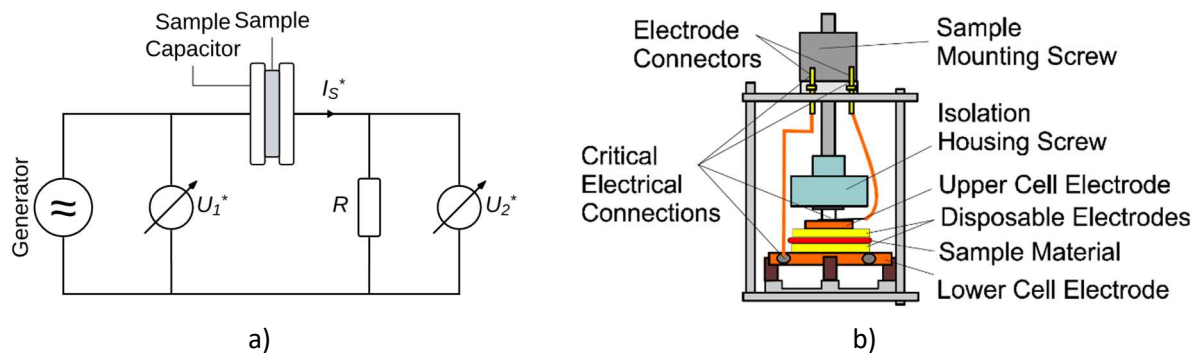


Figure 2-13. a) Scheme of equivalent circuit for the dielectric spectrometer analyzer. Adapted from (Kremer and Schönhals, 2003). b) Assembly of external electrodes in the BDS sample cell. Taken from (Novocontrol Technologies, 2017).

By varying the frequency of the sine wave voltage U_1^* , the complex impedance Z_S^* can be determined by using the voltage divider principle:

$$Z_S^*(\omega) = \frac{U_S^*(\omega)}{I_S^*(\omega)} = R \left(\frac{U_1^*(\omega)}{U_2^*(\omega)} - 1 \right), \quad 2-14$$

where the complex sample current $I_S^*(\omega)$ is given by $I_S^*(\omega) = I'(\omega) + iI''(\omega) = I_0(\cos(\omega t + \varphi) + i \sin(\omega t + \varphi))$, and the complex sample voltage $U_S^*(\omega)$ is only composed of a real part.

The sample can also be considered as a complex sample capacity C^* according to:

$$C^*(\omega) = -\frac{i}{\omega Z_S^*(\omega)}. \quad 2-15$$

Thus, the dielectric function can be derived by measuring the complex impedance $Z_S^*(\omega)$ of the sample with:

$$\varepsilon^*(\omega) = \frac{C^*(\omega)}{C_0} = -\frac{i}{\omega Z_S^*(\omega) C_0}, \quad 2-16$$

where C_0 is the equivalent capacitance of a planar capacitor in vacuum (see **Equation 2-9**). Complex dielectric permittivity is studied using *Novocontrol* broadband dielectric Alpha-A frequency analyzer. The complex dielectric permittivity was measured in the frequency range from 10^{-1} up to 10^6 Hz at atmospheric pressure P_{atm} . Accurate temperature control was implemented using a *Novocontrol* quatro cryosystem that was equipped with a two-electrode circuit as shown in **Figure 2-13b**. Samples are placed between parallel gold-plated electrodes with 30 mm of diameter. Dielectric spectra are collected over a wide temperature range from -150 up to 100 °C with appropriate successive steps and a temperature stability of ± 0.2 °C. The samples are kept in a nitrogen atmosphere.

3) Analysis of dielectric spectra

According to the **Equation 2-12**, dielectric spectra can be approximated using the Debye function. However, this function cannot capture the full complexity of the dielectric loss peak shape. Usually, the half width of loss peaks is up to six decades wider than what can be predicted by **Equation 2-12**, and furthermore, their shapes exhibit asymmetry with a high-frequency tail. This phenomenon is called non-Debye relaxation behavior. A more appropriate model function is the Havriliak-Negami (HN) function (Havriliak and Negami, 1967):

$$\varepsilon^*(\omega) = \varepsilon_\infty + \frac{\Delta\varepsilon}{(1 + (i\omega\tau_{HN})^{\alpha_{HN}})^{\beta_{HN}}}, \quad 2-17$$

where τ_{HN} is the Havriliak-Negami relaxation time and α_{HN} and β_{HN} are the symmetric and the asymmetric broadening parameters ($0 < \alpha_{HN}, \beta_{HN} < 1$), respectively.

The influence of α_{HN} and β_{HN} on the dielectric storage and dielectric loss is shown in **Figure 2-14**. It is worth noting that special cases where $\beta_{HN} = 1$ or $\alpha_{HN} = 1$ correspond to the function Cole-Cole (Cole and Cole, 1941) and Cole-Davidson functions (Davidson and Cole, 1951) respectively. The case of $\alpha_{HN} = \beta_{HN} = 1$ corresponds to the Debye function. **Figure 2-14d** shows clearly that when $\beta_{HN} \neq 1$,

the Havriliak-Negami relaxation time deviates from the τ_{max} . Therefore, the relaxation time corresponding to the position of the maximal loss can be determined with broadening parameters such as:

$$\tau_{max} = \tau_{HN} \left[\sin \frac{\alpha_{HN}\pi}{2 + 2\beta_{HN}} \right]^{-\frac{1}{\alpha_{HN}}} \left[\sin \frac{\alpha_{HN}\beta_{HN}\pi}{2 + 2\beta_{HN}} \right]^{\frac{1}{\alpha_{HN}}}. \quad 2-18$$

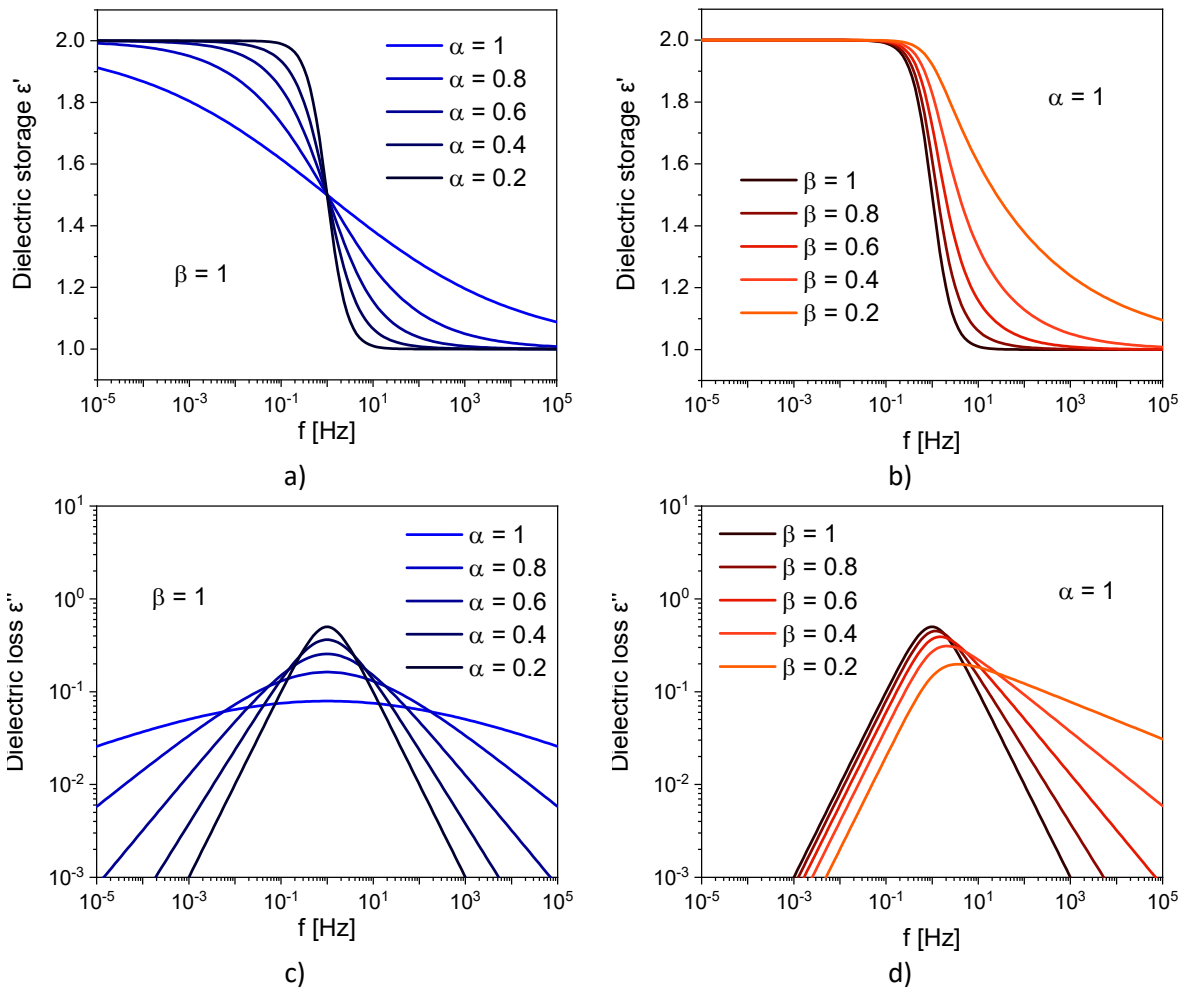


Figure 2-14. Havriliak-Negami function of dielectric storage for fixed a) $\alpha_{HN} = 1$ and b) $\beta_{HN} = 1$ and dielectric loss for fixed c) $\alpha_{HN} = 1$ and d) $\beta_{HN} = 1$. For sake of clarity, $\Delta\varepsilon = 1$, $\varepsilon_{\infty} = 1$ and $\tau_{HN} = 1/2\pi$. Adapted from (Kremer and Schönhals, 2003).

In most of dielectric measurements of polymers, the dielectric loss needs an additional contribution to fit the spectra. Indeed, the fluctuation of mobile charge carriers exhibits a slope decreasing inversely proportional to the frequency such as:

$$\varepsilon'' = \frac{\sigma_0}{\omega\varepsilon_0}, \quad 2-19$$

where σ_0 is the ohmic conduction and ε_0 is the dielectric permittivity of vacuum.

4) Broadband dielectric spectroscopy High Pressure HP-BDS

The High Pressure BDS (HP-BDS), which its setup is shown in **Figure 2-15a**, can provide the opportunity to consider the volumetric effects on the relaxation time changes, independently of temperature variations. The dielectric measurement works similarly as for classical BDS but the sample is immersed in a mixture of octane and silicone oil inside the pressure chamber. For that purpose, a sample cell has been designed for ensure impermeability as shown in **Figure 2-15b**.

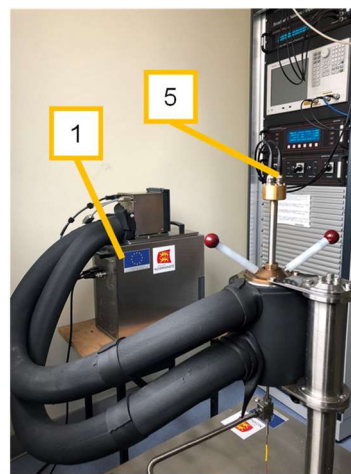
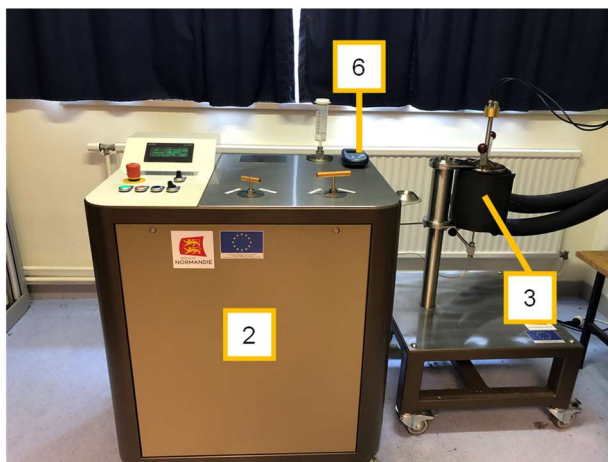
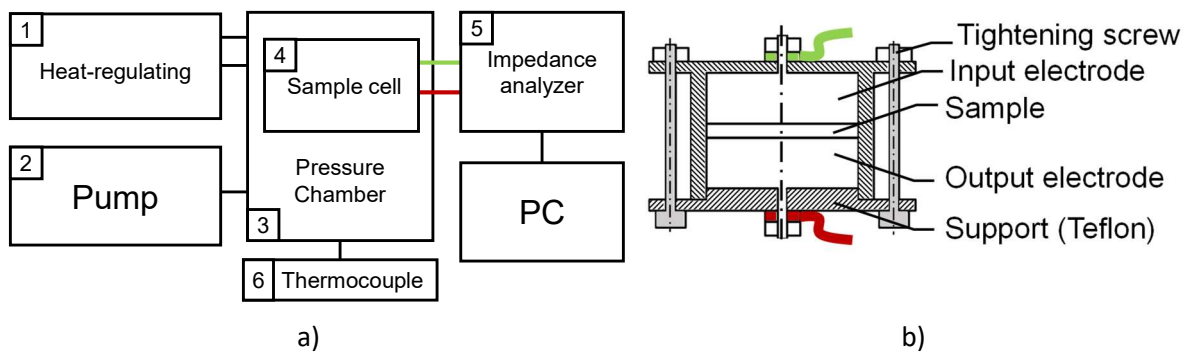


Figure 2-15. a) Experimental setup of the HP-BDS. b) Assembly of external electrodes in the HP-BDS sample cell. c) Photo of the experimental setup with the pump (2), the pressure chamber (3), and the thermocouple (6). d) Photo of the experimental setup with the thermostatic bath (1) and the Alpha-A frequency analyzer (5).

The samples were placed between two circular stainless-steel electrodes with a diameter of 15 mm. The electrodes were placed in a Teflon support, wrapped with a layer of Teflon tape, and sealed with polyisoprene layer. These sealing layers are essential to ensure to have a clean dielectric signal. **Figure**

2-16 depicts the signals from two samples, one of which exhibited a compromised seal and the other a well-sealed condition.

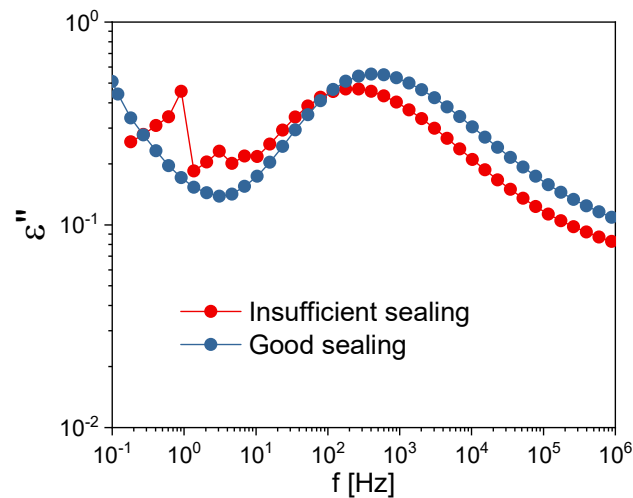


Figure 2-16. Dielectric loss peaks of PLA samples at $T = 535$ K and $P = 25$ MPa. The dielectric response at low frequencies is poor when the sealing is insufficient (in red) while a good sealing provides a order signal (in blue).

The dielectric loss shows clearly a degradation of the signal at low frequencies for the bad sealing while the good seal exhibits a clean response. The pressure is applied to the oil in the chamber by a piston, the pressure is therefore hydrostatic. The high-pressure pump U111 provided by *UNIPRESS EQUIPMENT* is the device for applying pressure up to 600 MPa shown in **Figure 2-15c**. The pressure is measured using a *Nova Swiss* tensiometer with a resolution of ± 0.1 MPa. The temperature is controlled by a thermostatic bath from *Huber* from -10 °C up to 120 °C (see **Figure 2-15d**), and measured by means of a thermocouple with an accuracy of 0.1 °C.

IV. Determination of experimental parameters

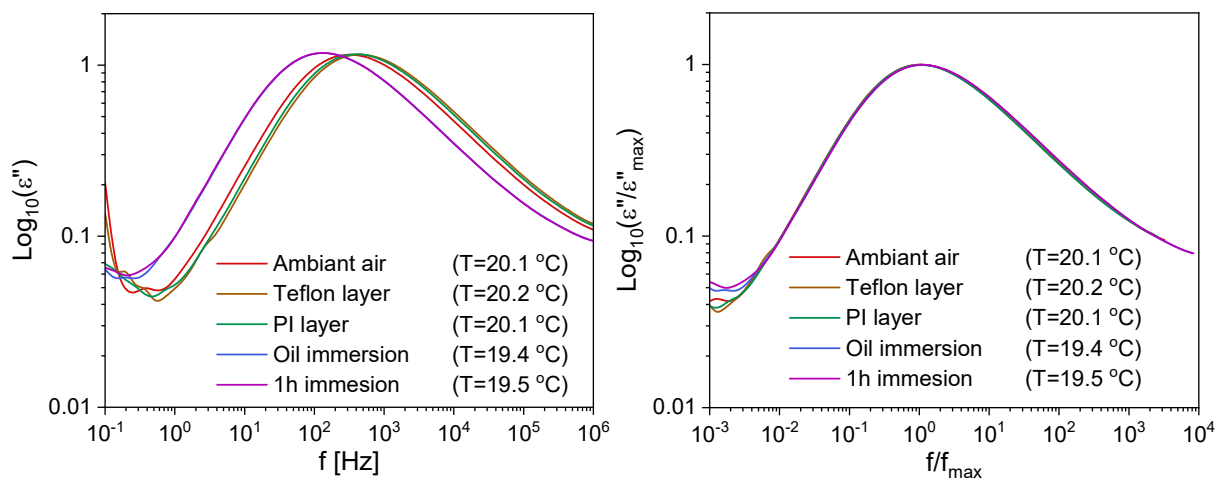
The experimental deviations of the HP-BDS on the HN parameters should be considered through the uncertainties of the parameters. Therefore, a metrological study has been carried out to estimate the influence of the experimental setup. Moreover, in order to extract experimental parameters such as the cooperativity volume, both experimental and computational procedures must be followed. These procedures condition the experimental protocol that must be adopted to obtain the desired physical quantities.

1) Metrological aspects of HP-BDS

The sealing of the sample cell is very important in order to avoid the contamination of the oil. This may occur either due to oil penetration into the sample or due to the parasitic polarity of the oil. A metrological study has been carried out to quantify the uncertainties due to the sealing system on the EVA80 sample. It has been chosen because its α -relaxation peak is in the middle of the BDS frequency range at 20 °C. The average values of the HN parameters of EVA80 are determined at ambient temperature for each successive addition of the sealing assembly layers, namely the Teflon support, the polyisoprene (PI) layer, and immediately and one hour after immersing the sample cell in oil. The uncertainties of HN parameters (see **Equation 2-17**) are shown in **Table 2-3**. Six different samples have been analyzed. The uncertainties are then calculated by comparing the HN parameters in classical BDS and after one hour in oil with the sealing assembly. It is worth mentioning that uncertainty values may be overestimated due to a change in temperature between these two measurements conditions.

Table 2-3. Average values at each successive step and uncertainties (Δx) of HN parameters: the relaxation time τ , the dielectric strength $\Delta\epsilon$, the symmetric and the asymmetric broadening parameters α_{HN} and β_{HN} for EVA80. The temperature corresponds to the ambient conditions during measurements.

Steps	T [°C]	$\text{Log}_{10}(\tau)$ [s]	$\Delta\epsilon$	α_{HN}	β_{HN}
Classical BDS	20.1	-3.3	4.49	0.76	0.52
Teflon layer	20.1	-3.4	4.49	0.77	0.52
PI layer	20.1	-3.4	4.49	0.77	0.52
Oil	19.5	-2.9	4.64	0.78	0.48
1h in Oil	19.5	-2.9	4.64	0.78	0.48
BDS HP Δx	-	± 0.6	± 0.8	± 0.07	± 0.15



a) b)

Figure 2-17. a) Log-log plot of the dielectric loss as a function of frequency and b) the dielectric loss normalized to the peak maximum as a function of the normalized frequency for the different steps of measurements.

To observe the deviation of α -relaxation peaks for different steps from qualitative view, dielectric loss peaks for EVA80 is shown in **Figure 2-17a**. The superposition in **Figure 2-17b** is made by normalizing the frequency and the dielectric loss by the values at the peak maximum. There is a slight shape deviation at low frequency due to the conductivity contribution shifting with temperature in air and oil, otherwise the peaks remain relatively similar regardless of the measurement conditions.

In addition, Fourier-transform infrared (FTIR) spectroscopy has been conducted on samples before and after immersion in the pressure chamber to validate that no oil has penetrated the materials. FTIR spectroscopy provides information on the chemical structure of organic molecules. The vibrational frequencies of different chemical bonds are identified through characteristic absorption peaks. Then, FTIR spectra were collected at room temperature in attenuated total reflectance mode on a Thermo Scientific Nicolet iS10 spectrometer equipped with a diamond crystal. Absorbance spectra were obtained by collecting 16 scans with a resolution of 4 cm^{-1} . Prior to the acquisition of the sample spectrum, a blank scan was recorded in order to correct for the presence of atmospheric CO_2 and H_2O . **Figure 2-18** shows the FTIR spectra of PVAc before and after immersion of PVAc samples in the pressure chamber at 200 MPa during a week. The absence of any additional peaks indicates that the sealing is effective and prevents oil penetration of the samples.

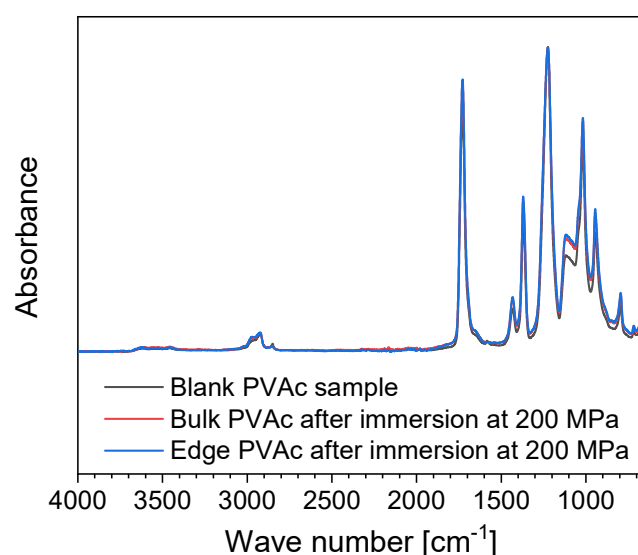


Figure 2-18. FTIR spectra of PVAc before immerge the sample in the HP-BDS (in black), and center (in red) and edge (in blue) of a PVAc sample after being immersed in the pressure chamber at 200 MPa during one week. All the spectra were normalized with respect to the -C-O- bond peak (1225 cm^{-1}).

2) Cooperativity volume

As introduced in the previous chapter, the cooperativity volume, or CRR volume, at the average dynamic glass transition temperature T_α is expressed with (Donth, 1982, 1984):

$$V_\alpha = \frac{\left[\frac{1}{C_{P, \text{glass}}} - \frac{1}{C_{P, \text{liquid}}} \right]}{\rho(\delta T)^2} k_B T_\alpha^2, \quad 2-20$$

where C_P is the specific heat capacity at constant pressure, k_B is the Boltzmann's constant, T_α is the dynamic glass transition temperature, ρ is the density, and δT the mean square temperature fluctuation associated with T_α . The values of δT , T_α and C_P are usually determined from MT-DSC analyses. These parameters are extracted from the reversing heat capacity C_P' and the non-reversing heat capacity C_P'' of the complex heat capacity C_P^* as shown in **Figure 2-19**.

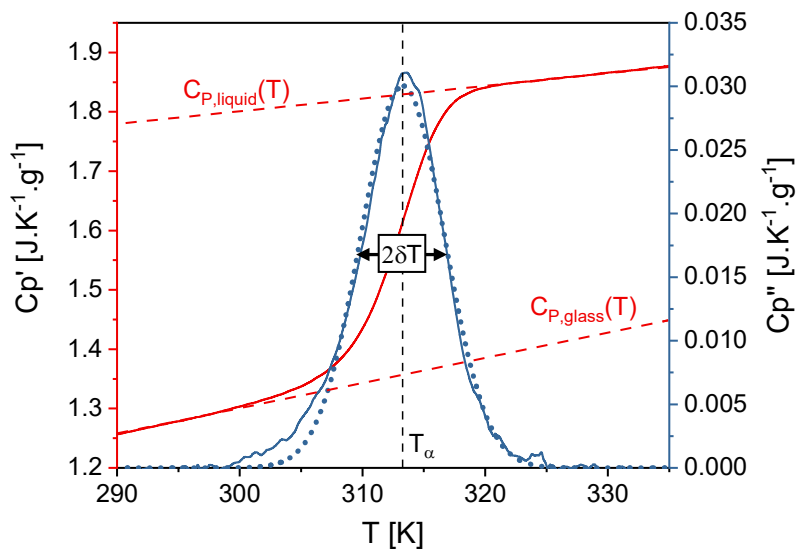


Figure 2-19. The solid lines represent the real part C_P' (in red) and the imaginary part C_P'' (in blue) of the complex heat capacity for PVAc as the function of temperature obtained by MT-DSC. The blue short dot line is the Gaussian fit allowing to determine δT and T_α . The red dashed lines are the extrapolated baselines of the specific heat capacities of the glass and the liquid-like state for PVAc.

δT and T_α are obtained from a Gaussian fit approximating the peak on the non-reversing heat capacity C_P'' signal, expressed by:

$$C_p''(T) = \frac{A}{\sigma_T \sqrt{2\pi}} \exp \left[-\frac{(T - T_\alpha)^2}{2\sigma_T^2} \right], \quad 2-21$$

where A is the Gaussian peak area and σ_T is the standard deviation. It has been shown that the average temperature fluctuation δT corresponds to σ_T . T_α corresponds to the maximum of the Gaussian fit. The specific heat capacities C_p of glass and liquid are obtained by extrapolating the liquid-like and glassy C_p' values at T_α .

In the extended Donth's approach, T_α and δT are determined by approximating the isochronal curves of the dielectric loss ε'' with a Gaussian fit using the same expression as **Equation 2-21** (Saiter et al., 2010). The isochronal curves shown in **Figure 2-20** are deduced from the α -relaxation, without any contribution from the conductivity or from the β -relaxation. The use of MT-DSC measurements presented in **Figure 2-19** allows to extend C_p of glass and liquid. This combined use of BDS and MT-DSC techniques allows to determine cooperativity volume V_α on a wide range of temperature and frequency down to the calorimetric glass transition temperature T_g .

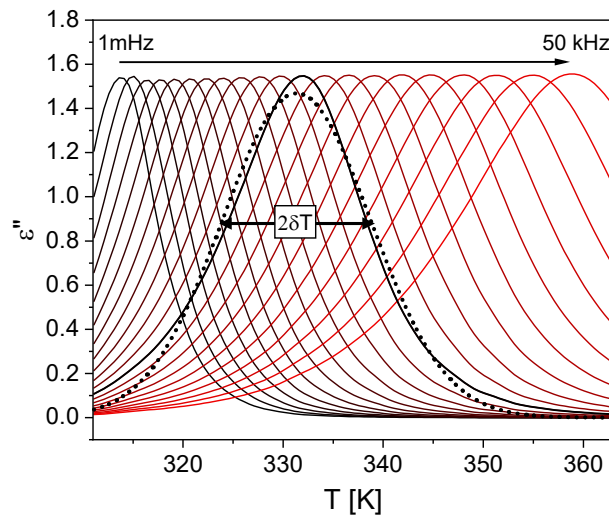


Figure 2-20. Isochronal spectra of the imaginary part of the complex permittivity ε'' as a function of temperature and frequency for PVAc. The black filled curve corresponds to a frequency of 134 Hz. The short dot line is its Gaussian fit to calculate the mean temperature fluctuation δT from the standard deviation.

This chapter introduces the experimental framework used for the investigation of glass transition and molecular mobility in amorphous polymers, which are presented in the next chapters. These chapters aim to expose the results and provide a discussion of the phenomena involved

List of abbreviations and symbols

Symbols			
A	Amplitude of the sinusoidal oscillation of temperature ramp	T_i	Initial temperature during a temperature ramp
	Gaussian peak area	T_m	Melting temperature
C	Capacitance	T_R	Reference temperature
C^*	Complex capacitance	T_S	Sample temperature
C_0	Capacitance of a planar capacitor in vacuum	T_α	Dynamic glass transition temperature
C_p	Isobaric heat capacity	U_S	Voltage applied to the sample
C_p'	Reversing heat capacity	V_α	Cooperativity volume
C_p''	Non-reversing heat capacity	wt. %	Percentage of weight
C_p^*	Complex heat capacity	Z_S^*	Complex impedance
E	Electric field	α_{HN}	Symmetric broadening parameter
e	Sample thickness	β_{HN}	Asymmetric broadening parameter
f	Frequency	ΔH_m	Melting enthalpy
I_S	Induced sample current	δT	Temperature fluctuation
I_S^*	Complex sample current	Δx	Uncertainty of the x parameter
K_{Cp}	Calibration factor	$\Delta \varepsilon$	Dielectric strength
k_B	Boltzmann's constant	ε	relative dielectric permittivity
M_0	Molar mass of the repeating unit	ε'	Dielectric storage
M_W	Average molecular weight	ε''	Dielectric loss
p	Period	ε^*	Complex dielectric function
P	Pressure	ε_0	Dielectric permittivity of vacuum
\mathbf{P}	Electric polarization	ε_∞	Real permittivity in the high frequency
P_∞	Induced polarization	ε_S	Static permittivity
P_a	Atomic polarization	ρ	Density
P_e	Electronic polarization	σ_0	Ohmic conduction
P_{Or}	Orientational polarization	σ_T	Standard deviation
q	Scanning rate	τ_D	Debye relaxation times
Q	Heat transfer	τ_{\max}	Relaxation time
q^-	Cooling rate	φ	Phase shift (calorimetry)
R	Thermal resistance		Phase angle (BDS)
	Ohmic resistance	Φ	Heat flow
S	Sample surface	Φ_{NR}	Non-reversing heat flow
T	Temperature	Φ_R	Reversing heat flow
t	Time	ω	Angular frequency
T_g	Glass transition temperature		

Abbreviations

BDS	Broadband Dielectric Spectroscopy
DSC	Differential Scanning Calorimetry
FTIR	Fourier-transform infrared
HN	Havriliak-Negami
HP-BDS	Broadband Dielectric Spectroscopy High Pressure
MT-DSC	Modulated temperature differential scanning calorimetry

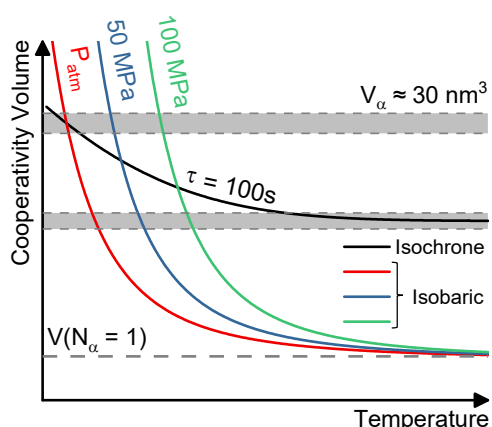
Polymer abbreviations

PB	1,4-Polybutadiene
PMMA	Atactic poly(methyl methacrylate)
PS	Atactic polystyrene
PDMS	Poly(dimethyl siloxane)
PEO	Poly(ethylene oxide)
PETg	Poly(ethylene terephthalate glycol)
EVA	Poly(ethylene-vinyl acetate)
PLA	Poly(lactide acid)
POM	Poly(oxymethylene)
PVAc	Poly(vinyl acetate)
PEEK	Polyetheretherketone
PE	Polyethylene
PET	Polyethylene terephthalate
PI	Polyisoprene
PP	Polypropylene

Chapter 3. Volumetric and thermal contributions of the isobaric fragility

Table of content

CHAPTER 3. VOLUMETRIC AND THERMAL CONTRIBUTIONS OF THE ISOBARIC FRAGILITY	88
I. UNCORRELATION BETWEEN ISOBARIC FRAGILITY AND COOPERATIVITY	88
1) <i>Highlight from various glass formers</i>	88
2) <i>Interest of pressure</i>	92
II. PRESSURE AND TEMPERATURE DEPENDENCE ON THE SEGMENTAL RELAXATION	94
1) <i>Temperature and pressure dependence of relaxation time</i>	94
2) <i>Pressure dependence on glass transition</i>	98
3) <i>Pressure dependence on isochoric fragility</i>	99
III. CORRELATION BETWEEN ACTIVATION VOLUME AND COOPERATIVITY VOLUME.....	100
1) <i>Activation volume</i>	100
2) <i>Cooperativity volume</i>	101
IV. ESTIMATION OF THE CONTRIBUTIONS OF THE ISOBARIC FRAGILITY	104
1) <i>Thermal and volumetric contributions</i>	104
2) <i>Isochoric fragility from Donth definition</i>	106
V. MOLECULAR MOBILITY INFLUENCE OF ISOBARIC FRAGILITY CONTRIBUTIONS.....	110
1) <i>Contributions of isobaric fragility under pressure</i>	110
2) <i>Interpretation with the intra and intermolecular interactions</i>	113
VI. CONCLUSION.....	114
LIST OF ABBREVIATIONS AND SYMBOLS	115
REFERENCES	ERREUR ! SIGNET NON DÉFINI.



The figure represents a schematic view of the evolution of the cooperativity volume of polymers as a function of temperature for the isobars and the isochore that correspond to the glass transition ($\tau = 100$ s).

Part of the work presented in this chapter has been published in the article “Highlighting the interdependence between volumetric contribution of fragility and cooperativity for polymeric segmental relaxation” J. Trubert, L. Matkowska, A. Saiter-Fourcin, L. Delbreilh. *The Journal of Chemical Physics*, 160(4) (2024)

Chapter 3. Volumetric and thermal contributions of the isobaric fragility

The experimental part of the study on the influence of the chemical structure of amorphous polymers on molecular mobility are now presented. As detailed in the material and methods section, the poly(lactide acid) PLA, the poly(ethylene terephthalate glycol) PETg and the poly(vinyl acetate) PVAc have been employed in this work. PETg shows a rigid backbone chain, whereas PVAc has a flexible one. PLA is situated between PETg and PVAc in terms of rigidity. This flexibility difference is reflected proportionally with their glass transition temperature difference, yet PLA shows a high isobaric fragility, approaching that of PETg. As the PVAc has been particularly studied in high pressure BDS (White and Lipson, 2017), it has allowed for the assessment of the results and the extension of the study to PETg and PLA samples.

I. Uncorrelation between isobaric fragility and cooperativity

Although isobaric fragility m_p is an indicator of the molecular mobility at the glass transition temperature T_g , it is not clearly correlated with the glass transition concepts, such as cooperativity and free volume approaches.

1) Highlight from various glass formers.

As presented in Chapter 2, the glass transition temperature T_g and V_α (cooperativity volume at the dynamic glass transition temperature T_α) can be determined from MT-DSC measurements. **Figures 3-1a, 3-1b and 3-1c** represent the reversing heat capacity C_p' and the non-reversing heat capacity C_p'' signals for PETg, PLA and PVAc respectively. Accordingly, Donth's approach (see **Equation 2-20**, p. 82) allows for the calculation of V_α through the use of the Boltzmann's constant k_B , the density ρ , and parameters from MT-DSC analysis, including the specific heat capacity at constant pressure C_p , the dynamic glass transition temperature T_α , and the mean square temperature fluctuation δT associated with the glass transition. The temperature corresponding to the maximum of each peak is identified as T_α . The values of the parameters derived from the MT-DSC analysis and V_α for the three polymers are presented in **Table 3-1**. Simultaneously, the isobaric fragility m_p and the glass transition temperature T_g can be estimated by determining the relaxation time from dielectric measurements. As presented in Chapter 2, BDS allows to extend the measurement of the α -relaxation, which is the dielectric manifestation of the glass transition, in the liquid.

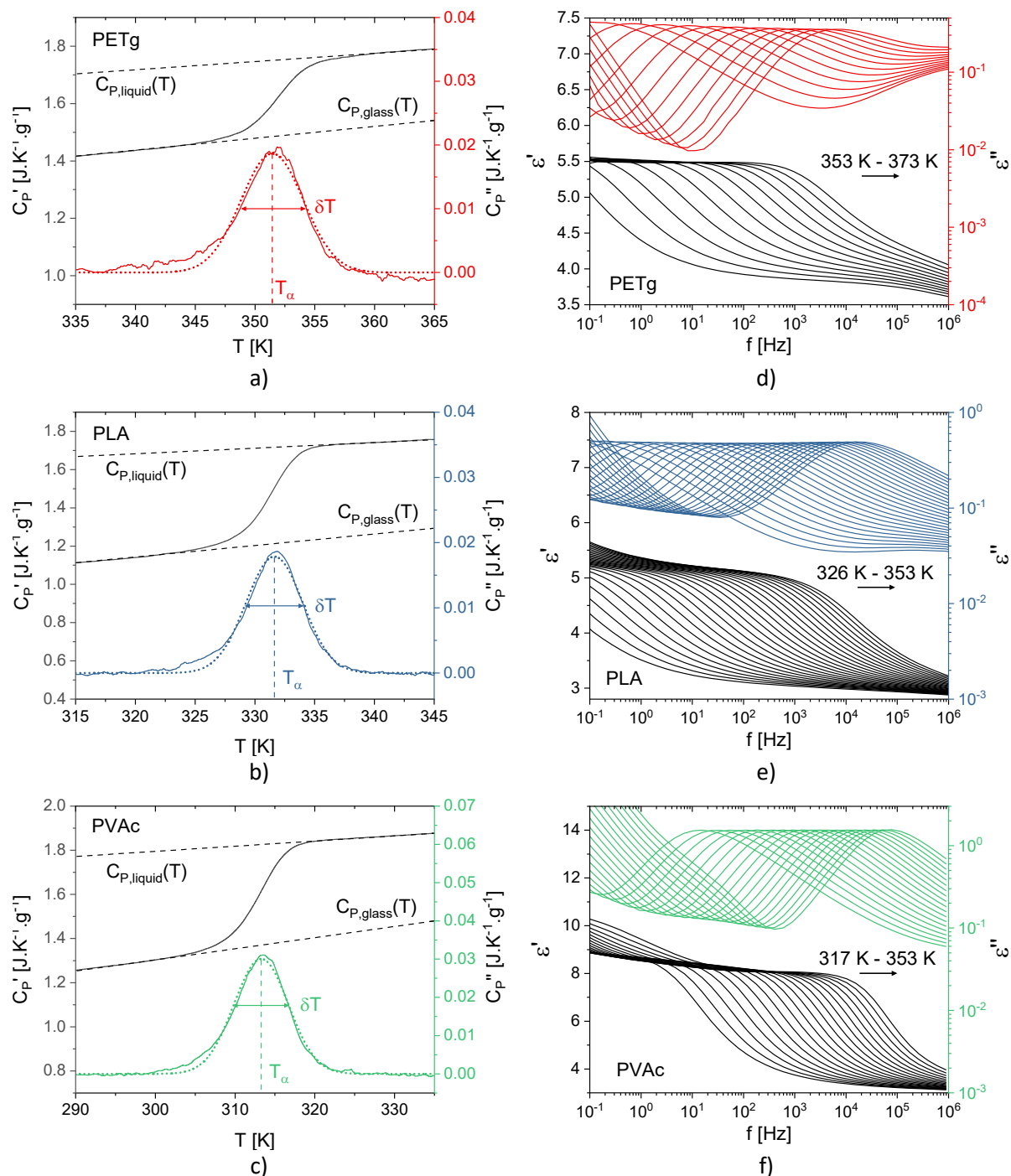


Figure 3-1. Reversing heat capacity C_p' (black line) and the non-reversing heat capacity C_p'' (colored line) signals measured by MT-DSC as a function of temperature in the vicinity of the glass transition for a) PETg, b) PLA, and c) PVAc. The dotted colored lines represent a Gaussian fit of C_p'' . The polymers have been analyzed using the heat-cool mode with a period of $p = 60$ seconds, an amplitude of $A = \pm 1$ K, and with a heating rate $q = 0.5 \text{ K} \cdot \text{min}^{-1}$. The dielectric storage (black lines) and loss (colored lines) have been recorded by BDS as a function of frequency for a) PETg from 353 K up to 373 K, b) PLA from 326 K up to 353 K, and c) PVAc from 317 K up to 353 K.

Thus, **Figures 3-1d, 3-1e** and **3-1f** shows dielectric storage and loss from BDS analysis at atmospheric pressure for PETg, PLA and PVAc respectively. The three polymers exhibit a conductivity contribution at low frequency. Moreover, none of the materials under consideration exhibit an abrupt decline in of the intensity of the dielectric loss peak or in low frequency dielectric storage during the measurements. If such a decrease occurs during heating, it indicates a structural change in the material that hinders dipole orientation, such as cold crystallization. It is reasonable to assume that samples remain amorphous throughout the measurement. As mentioned in Chapter 2, the dielectric signals can be approximated with the Havriliak-Negami function (HN) and a conductivity contribution with:

$$\varepsilon^*(\omega) = \varepsilon'(\omega) + i\varepsilon''(\omega) = -i \frac{\sigma_0}{\omega \varepsilon_0} + \frac{\Delta\varepsilon}{(1 + (i\omega\tau_{HN})^{\alpha_{HN}})^{\beta_{HN}}} + \varepsilon_{\infty}, \quad 3-1$$

where σ_0 is the ohmic conduction, ε_0 is the dielectric permittivity of vacuum, ε_{∞} is the permittivity at high frequency, $\Delta\varepsilon$ is the dielectric strength, τ_{HN} is the relaxation time and α_{HN} and β_{HN} are the symmetric and the asymmetric broadening parameters. Thus, the HN fits allow for the extraction of the relaxation time τ_{max} (see **Equation 2-18**, p. 77) of dielectric spectra for each temperature. **Figure 3-2** presents the evolution of relaxation time τ_{max} as a function of temperature inverse $1000/T$. This representation corresponds to an Arrhenius diagram.

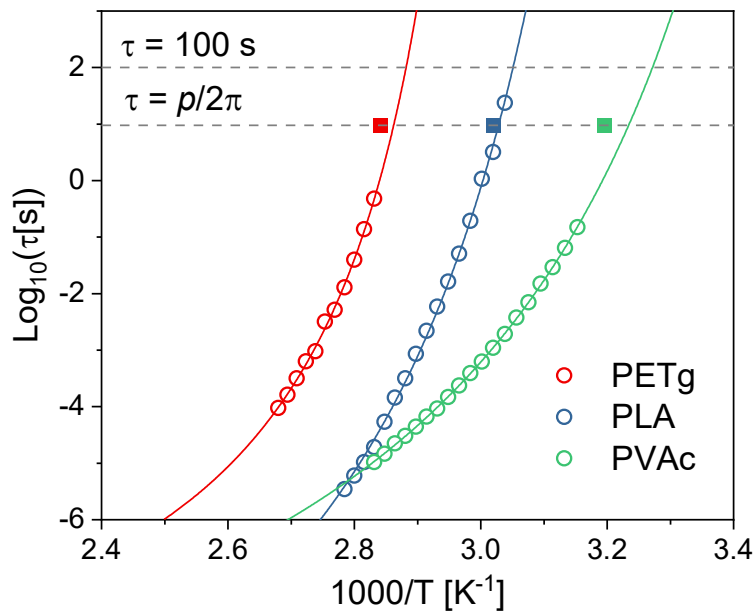


Figure 3-2. Temperature dependence of the α -relaxation time τ for PETg (red circles), PLA (blue circles) and PVAc (green circles) at atmospheric pressure. The squares represent the glass transition temperature determined from MT-DSC analysis for $\tau = p/2\pi$. The lines are VFTH fits, and the dashed gray lines correspond to isochrone for $\tau = 100$ s, i.e., to the glass transition temperature T_g , and for $\tau = p/2\pi$ with $p = 60$ s.

The relaxation times are therefore extrapolated with a VFTH law (see **Equation 1-1**, p. 7). By this way, the temperature associated with a relaxation time of 100 s is deduced from the VFTH law parameters:

$$T_g = T_0 + \frac{DT_0}{\ln\left(\frac{100}{\tau_\infty}\right)}. \quad 3-2$$

This allows to calculate isobaric fragility with:

$$m_p = \log(e) T_g \frac{DT_0}{(T_g - T_0)^2}. \quad 3-3$$

The glass transition temperature T_g and isobaric fragility m_p have been determined using the BDS analysis and are listed in **Table 3-1**. A slight difference is observed between the glass transition temperatures obtained by MT-DSC and BDS measurements. However, both techniques allow for the consistent identification of T_g values in accordance with the backbone flexibility. Additionally, the cooperativity volume V_α of PLA is higher than that of PETg. It is also noteworthy that the isobaric fragility of PLA is closer to that of PETg than to that of PVAc, while the glass transition temperature of PLA is more in the middle of that of PETg and PVAc.

Table 3-1. MT-DSC and BDS results for PETg, PLA and PVAc: the temperature fluctuation δT , the difference between specific heat capacity inverse of the glass and the liquid, density ρ , dynamic glass transition from MT-DSC $T_{\alpha\text{MT-DSC}}$, cooperativity volume V_α , T_g at $\tau = 100$ s from BDS and isobaric fragility m_p .

Polymer	δT [K]	$\Delta(1/C_p)$	ρ [g. mol ⁻¹]	$T_{\alpha\text{MT-DSC}}$ [K]	V_α [nm ³]	$T_{g\text{BDS}}$ [K]	m_p
PETg	2.6	0.156	1.27	351	30.6	345	158
PLA	2.4	0.275	1.25	331	40.6	326	145
PVAc	3.4	0.193	1.19	313	19.5	303	76

Some studies have demonstrated that there is no direct correlation between cooperativity volume and m_p for several glass-forming liquids by glass transition investigation using NMR (Tracht et al., 1998; Qiu and Ediger, 2003), dielectric spectroscopy (Araujo et al., 2018b; Crauste-Thibierge et al., 2010; Puente et al., 2015), Raman and Brillouin scattering (Hong et al., 2009), photon correlation spectroscopy (Dalle-Ferrier et al., 2007b), and molecular dynamic simulations (Berthier et al., 2005b, 2007a). Although there is a rough tendency for the evolution of the isobaric fragility m_p as a function of the glass transition for polymers, no precise correlation has been established. Qin and McKenna have proposed a large correlation zone to capture the trend, as shown in **Figure 3-3** (Qin and McKenna, 2006). It is noteworthy that PETg, PLA, and PVAc fall within the range defined by the zone, despite the fragilities of PETg and PLA appearing to be at the upper limit of the acceptable range.

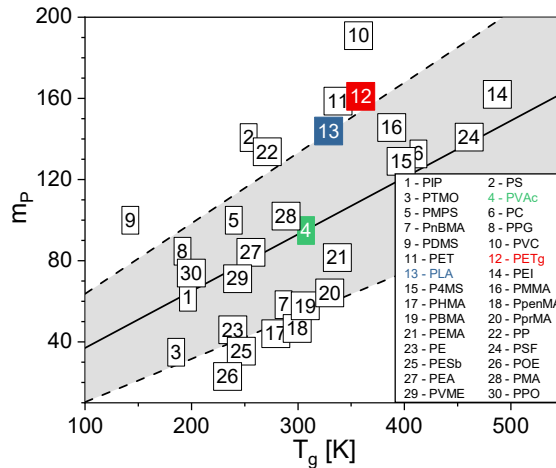


Figure 3-3. The isobaric fragility m_p as a function of the glass transition temperature T_g for different polymers. The values of PETg, PLA and PVAc are indicated in red, blue and green respectively. The line and the gray correlation zone correspond to a linear regression made by Qin and McKenna, which yielded the following equation: $m_p = 0.28(\pm 0.067)T_g + 9(\pm 20)$. Values are taken from Qin and McKenna (2006), Hong et al. (2009) and Rijal et al. (2015).

As explained in Chapter 1, one possible reason of the decorrelation between m_p and the glass transition is associated with the hypothesis of two distinct contributions of the isobaric fragility: the thermal and the volumetric contributions. Hong et al. proposed an expression of m_p by considering both contributions (Hong et al., 2011a):

$$m_p = m_V + \frac{\Delta V^\#}{\ln 10} \frac{\alpha}{k_B \kappa}. \quad 3-4$$

In this equation, the first term represents the thermal contribution (isochoric fragility m_V), while the second term denotes the volumetric contribution, also noted $(m_p - m_V)$. $\Delta V^\#$ is the activation volume, k_B is the Boltzmann's constant, α is the thermal volume expansivity and κ is the compressibility. These two contributions have been determined in previous studies as factors influencing m_p variations in relation to the chemical structure of polymers (Delpouve et al., 2014; Araujo et al., 2018a, 2018b, 2019).

2) Interest of pressure

Most of time, studies using the two contributions of the isobaric fragility have estimated them at atmospheric pressure, discussing the structural dependence of the contributions. The thermal contribution is associated with intramolecular interactions, while the volumetric one is linked to intermolecular interactions, which are in turn associated with the CRR size (Hempel et al., 2000; Bauer et al., 2013; Puente et al., 2015).

Since the density changes during a cooling at constant pressure, these contributions require the study of glass forming liquids in isobaric or isochoric conditions (Casalini and Roland, 2005; Niss and Alba-Simionesco, 2006). The use of the BDS under controlled atmosphere enables the application of a complementary pressure control to the classical thermal control (Paluch et al., 1999; Capaccioli et al., 2004). This approach allows for the modification of pressure at a constant temperature, reducing the available space for structural unit movements, and thus hindering relaxation. In particular, it enables the calculation of activation volume and isochoric fragility m_V (Roland et al., 2005; Niss et al., 2007). Activation volume is defined by:

$$\Delta V^\# = k_B T \left(\frac{\partial \ln \tau}{\partial P} \right)_T, \quad 3-5$$

while the isochoric fragility m_V is obtained by counterbalancing the thermal expansion by compressing the system in order to maintain a constant volume.

Figure 3-4 shows the different ways for calculating the isochoric fragility m_V and activation volume $\Delta V^\#$ from isobaric, isothermal or isochoric measurements. The activation volume is typically derived through the application of **Equation 3-5** to the isothermal measurements of relaxation time.

However, as presented in **Equation 1-42** (p. 47), $\Delta V^\#$ can be calculated from isobaric fragility and pressure dependence of glass transition temperature. Both can be derived from isobaric measurements of relaxation times.

Isochoric fragility m_V is defined by the relaxation times variation with temperature at T_g for constant volume. Thus, this value can be deduced by knowing the specific volume variation as a function of temperature and pressure, which is given by the Tait's equation (**Equation 1-36** p. 40), and the relaxation times variation as a function of temperature and pressure.

Otherwise, m_V (or thermal contribution of m_P) can be estimated by subtracting the volumetric contribution to m_P . Volumetric contribution ($m_P - m_V$) is determined by considering the ratio α/κ at the glass transition temperature in a range from 1 up to 2 MPa/K for polymers (Hong et al., 2011a). The HP-BDS enables the experimental determination of the thermal (m_V) and the volumetric ($m_P - m_V$) contributions to the isobaric fragility m_P .

Moreover, the cooperativity volume can also be determined through the extended Donth's approach applied to dielectric spectra and compared with the activation volume as proposed by the hypothesis that the volumetric contribution ($m_P - m_V$) is related to cooperative interactions.

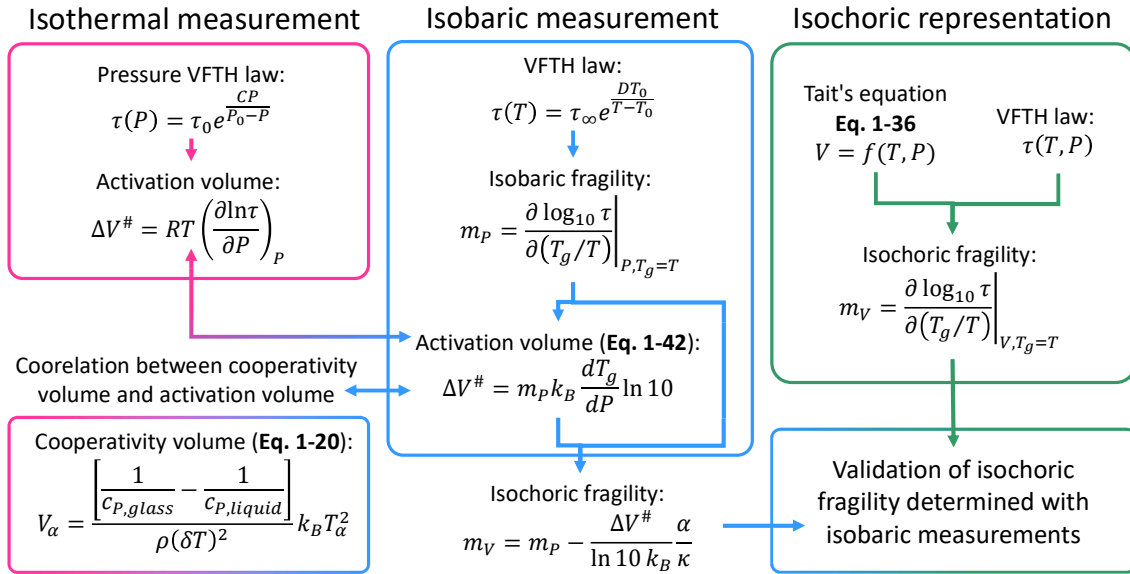


Figure 3-4. Schematic representation of different approaches for calculating the activation volume $\Delta V^\#$ and the isochoric fragility m_V .

A notable difference in isobaric fragility is observed for PETg, PLA and PETg, which does not appear to be directly correlated to glass transition temperature or V_α . The experimental determination of thermal and volumetric contributions of the isobaric fragility may provide insight into this difference.

II. Pressure and temperature dependences on the segmental relaxation

The study examines the effects of temperature and pressure on relaxation time variations, in order to follow the different paths of **Figure 3-4**.

1) Temperature and pressure dependences of relaxation time

As mentioned in the Chapter 2, the segmental relaxation time is extracted from the dielectric storage and loss spectra. The typical dielectric spectra are shown in **Figure 3-5**. The dielectric storage and loss are plotted as a function of frequency and pressure for an isotherm. The higher the pressure, the more the dielectric relaxation spectra shift to lower frequencies.

The dielectric spectra can be fitted with the HN function to extract the relaxation. It should be noted that measurements at temperatures around and above 370 K for PETg and 350 K for PLA must be recorded quickly before isothermal crystallization of the sample can occur. In these temperature ranges, the pressure steps are then increased in order to accelerate the measurements.

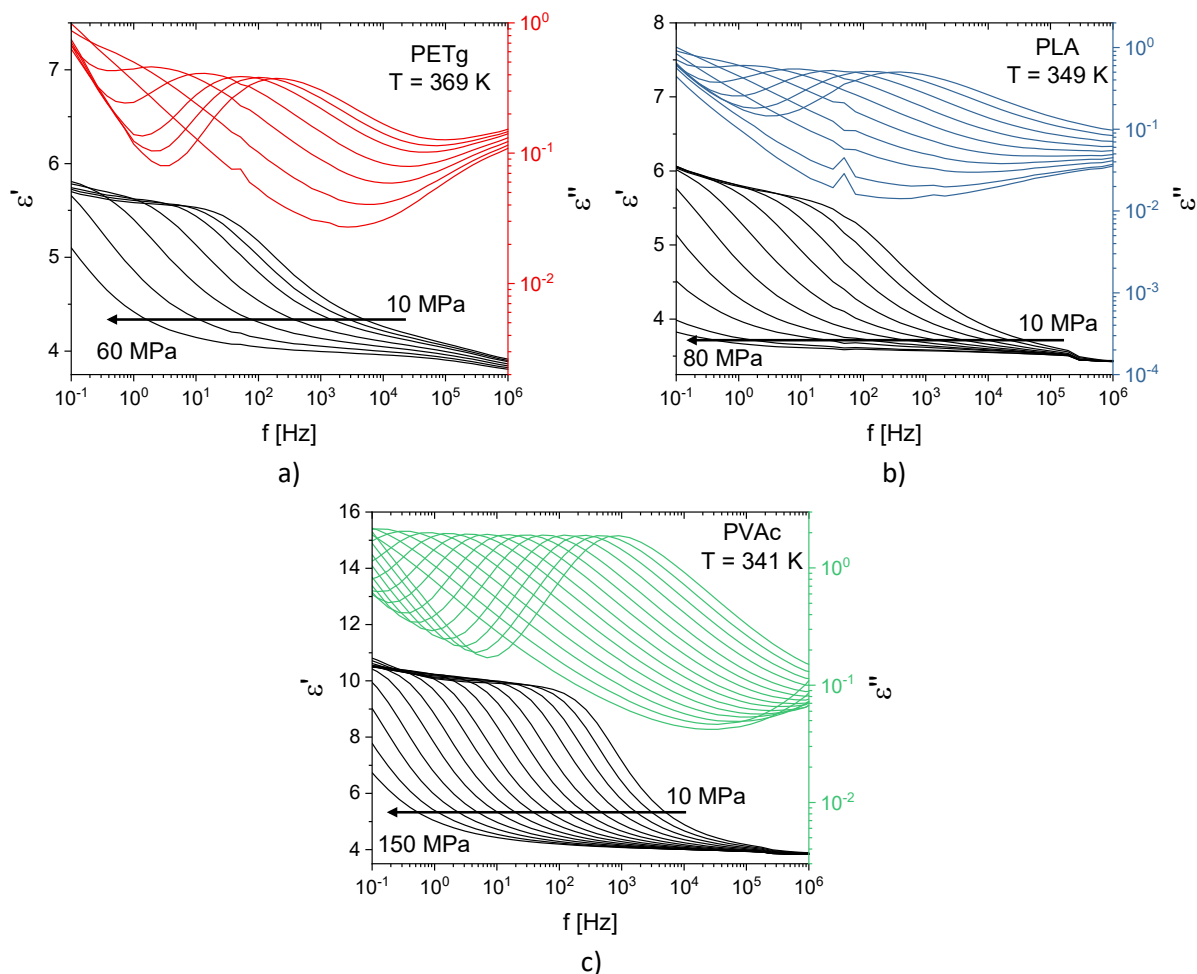


Figure 3-5. Dielectric storage (black lines) and loss (colored lines) for a) PETg, b) PLA, and c) PVAc samples as a function of the frequency and the pressure at $T = 369$ K, $T = 349$ K and $T = 341$ K, respectively. The dielectric spectra show isobaric measurements from 10 MPa up to 60 MPa, 80 MPa and 150 MPa for PETg, PLA and PVAc respectively.

The segmental relaxation time as a function of the pressure is plotted for PETg (**Figure 3-6a**), PLA (**Figure 3-6b**) and PVAc (**Figure 3-6c**) under isothermal conditions. Each point corresponds to the relaxation times τ_{HN} found by HN fitting of the complex permittivity.

The higher the temperature, the more the segmental relaxation is seen over a wide pressure range. According to the free volume concept, the molecular mobility slows down with increasing the applied pressure at constant temperature. The free volume ratio should decrease and limit the mobility.

The pressure dependence of the relaxation time for the segmental relaxation can be described by the pressure VFTH law (Corezzi et al., 1999; Johari, 1973; Paluch et al., 1996) at constant temperature (see **Equation 1-38**, p. 43). The parameters of the pressure VFTH law for isothermal measurements are given in **Table A-1** in **Appendix**. For the three polymers, the pressure VFTH fits show a nonlinear

pressure dependence of the segmental relaxation time (Casalini et al., 2004; Paluch et al., 1998).

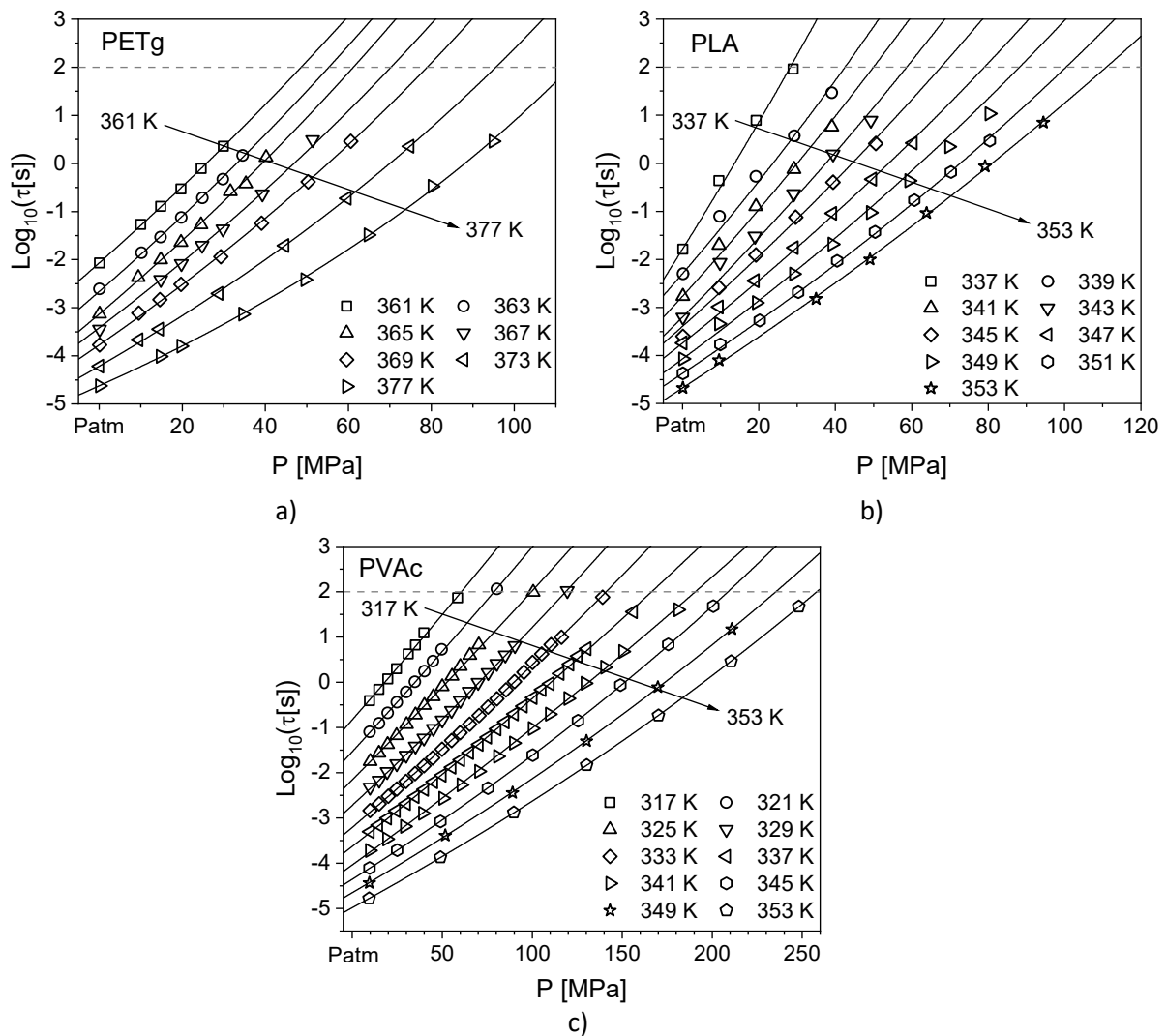


Figure 3-6. Pressure dependence of the isothermal α -relaxation time for a) PETg, b) PLA and c) PVAc. The black lines are the pressure VFTH fits for each isotherm. The dashed gray lines correspond to the isochrone $\tau = 100$ s, i.e., the glass transition pressure P_g , analogous to the glass transition temperature T_g .

From the classical VFTH law, the temperature dependence of the segmental relaxation times at constant pressure can be derived. **Figure 3-7** shows the isobaric evolution of the relaxation time extrapolated from the pressure VFTH law (the law parameters are given in **Table A-2** in **Appendix**). The isobaric curves range from P_{atm} up to 70 MPa for PETg (**Figure 3-7a**), up to 100 MPa for PLA (**Figure 3-7b**) and up to 130 MPa for PVAc (**Figure 3-7c**). For the three polymers, the super-Arrhenius behavior of the segmental relaxation is well observed for each isobaric measurement.

The decrease in temperature and the increase in pressure have similar effects on the molecular mobility. In both cases the relaxation time is slowed down. When this slowing process reaches the α -relaxation time of 100 s, the pressure/temperature couple at this point is considered as the glass transition pressure P_g and the glass transition temperature T_g . In this way, a supercooled liquid can be transformed into a glass by cooling down the material or by applying a hydrostatic pressure. The structure of the liquid remains "frozen", either because the system does not have enough configurational entropy to undergo thermal fluctuations, or because it does not have enough space to undergo spatial fluctuations.

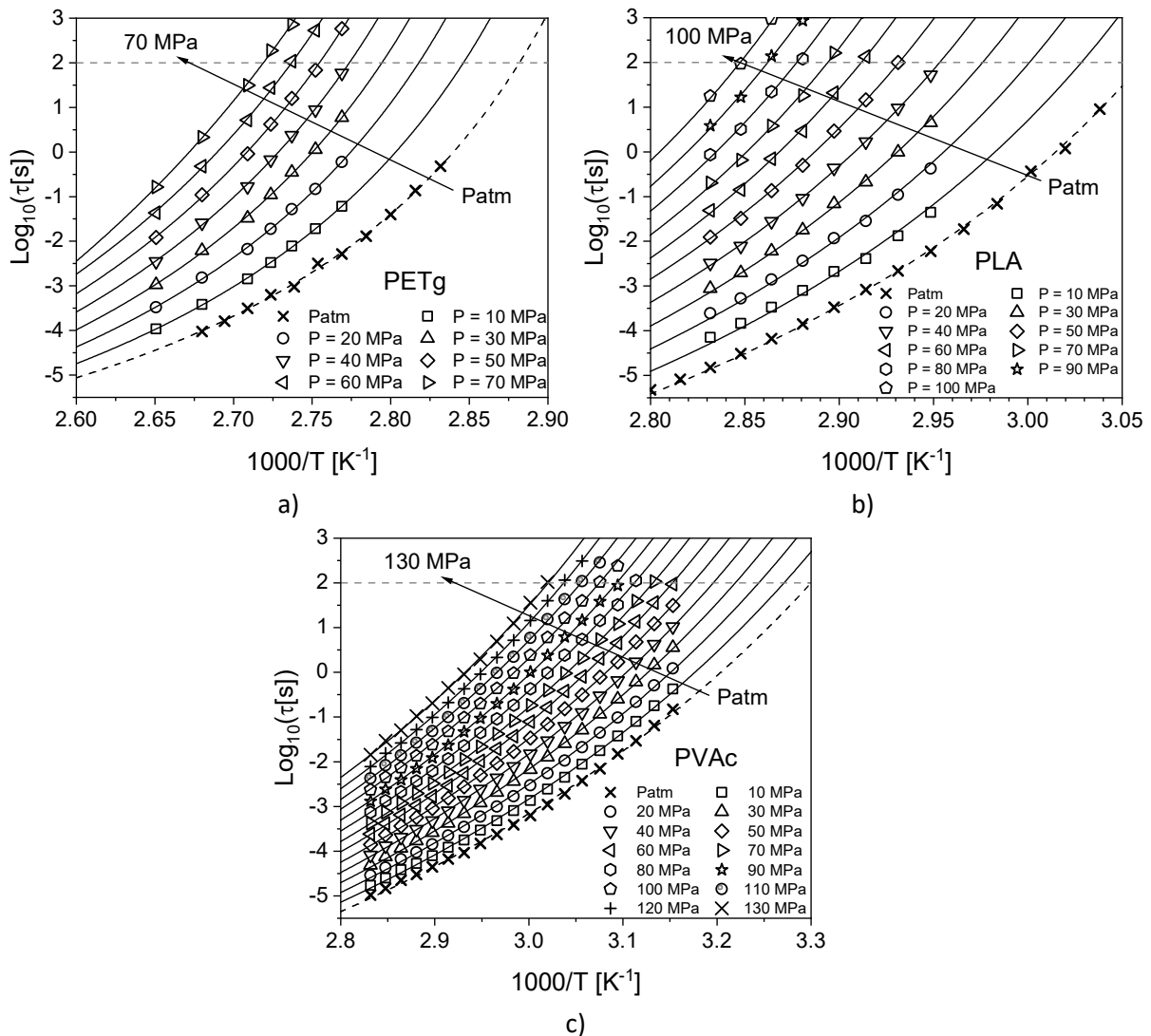


Figure 3-7. Temperature dependence of the isobaric α -relaxation time τ for a) PETg, b) PLA and c) PVAc. Black lines are VFTH fits of each isobar. The dashed black lines correspond to the VFTH fit at P_{atm} . The dashed gray lines correspond to the isochrone $\tau = 100$ s, i.e., the glass transition temperature T_g .

2) Pressure dependence on glass transition

In **Figure 3-8**, the glass transition temperatures T_g of the three polymers determined by BDS analysis are plotted as a function of pressure. Overall, the glass transition temperature at $\tau = 100$ s increases with pressure. This corresponds to the equivalent glass transition determined by MT-DSC measurements (Puente et al., 2015). The T_g values are in agreement with the literature (Roland et al., 2005), where dT_g/dP is found between 0.1 and 0.4 K. MPa⁻¹. However, the higher the pressure, the smaller the increase in $T_g(P)$.

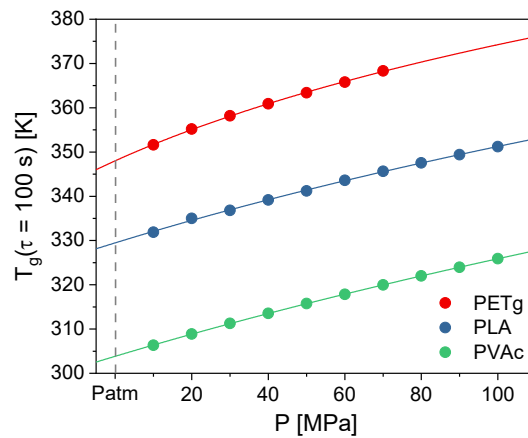


Figure 3-8. Glass transition temperature as a function of pressure for PETg in red, PLA in blue and PVAc in green. The lines correspond to the approximation of the experimental data with the Andersson's fit function.

This nonlinear behavior can be approximated by the Andersson's empirical model through the **Equation 3-6** (Andersson and Andersson, 1998):

$$T_g(P) = T_g^0 \left(1 + \frac{P}{\Pi} \right)^{\frac{1}{b}} \quad 3-6$$

Here T_g^0 is the glass transition temperature at atmospheric pressure, Π and b are adjustable parameters. They are given in **Table 3-2**. This empirical equation allows to describe the reduction of the variation of T_g with the increase of the pressure. It has been shown that this model is a special case of the Avramov's model when $\tau = 100$ s (Avramov, 2000; Floudas et al., 2011). In the latter model, Π and b are adjustable parameters with physical connection expressed by $\Pi = C_p / (\alpha_T V_m b)$, where C_p is the heat capacity, α_T is the thermal volume expansivity and V_m is the molar volume. The parameter b from the Andersson's model is informative about the variation of T_g slope as a function of pressure. It indicates that for PETg ($b = 11.2$), the value of dT_g/dP decreases more than for PLA ($b = 7$), and PVAc ($b = 5.5$), as the pressure increases.

Table 3-2. Fit parameters (T_g^0 , b , Π), their uncertainties and the R-squared of the Andersson's model (Equation 3-6) for PETg, PLA and PVAc.

Polymer	T_g^0	ΔT_g^0	b	Δb	Π	$\Delta \Pi$	R^2
PETg	348	0.29	11.2	1.5	80	4.7	0.99943
PLA	330	0.28	7.0	1.4	177	9.9	0.99898
PVAc	304	0.04	5.5	0.2	213	1.8	0.99997

3) Pressure dependence on isochoric fragility

Figure 3-9a shows the effect of pressure on the isobaric fragility m_p (see Equation 1-3, p. 7). On one hand, PETg and PLA show a high fragility at P_{atm} , which then decreases as the pressure increases. This behavior was expected from previous studies (Paluch et al., 2007; Roland and Casalini, 2005). On other hand, PVAc has a relatively low isobaric fragility for a polymer and the influence of pressure on m_p seems to be very low. Most of the time, it has been shown that the isobaric fragility of polymers decreases with pressure, however poly(ethyl acrylate) PEA, poly(butadiene) PBD and PVAc have $dm_p/dP = 0$ (Huang et al., 2002). It is noteworthy that these three polymers have low m_p and T_g values at atmospheric pressure (PEA and PBD have isobaric fragilities of 83 and 67 and glass transition temperature of 252 K and 208 K, respectively) and quite flexible backbone chain. Such behavior seems to be difficult to relate directly to the chemical structure of the repeating unit (see Chapter 2) because PLA has a very high isobaric fragility, close to that of PETg, despite a backbone stiffness intermediate between those of PETg and PVAc and a glass transition temperature lower than that of PETg.

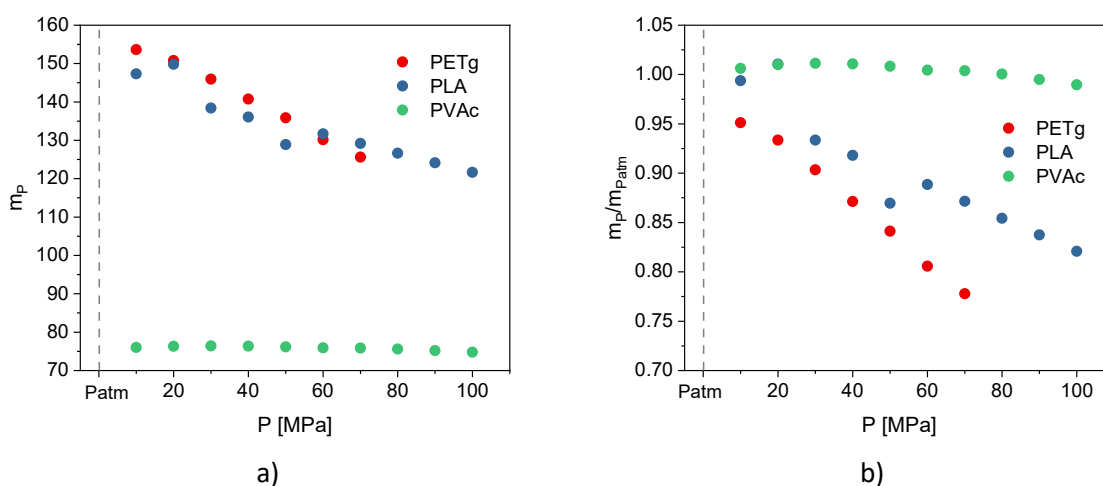


Figure 3-9. a) Isobaric fragility m_p as a function of the pressure. b) Isobaric fragility normalized to the isobaric fragility at P_{atm} as a function of the pressure (PETg in red, PLA in blue and PVAc in green).

Figure 3-9b shows the isobaric fragility m_p normalized to the value at P_{atm} . It clearly shows that the isobaric fragility decrease of PLA and PETg is significant compared to the m_p stability of PVAc. This plot allows to observe that the PLA isobaric fragility seems to be less affected by the pressure increase than the PETg isobaric fragility. In the case of PVAc, the stability of the isobaric fragility with increasing glass transition temperature indicates that the isobaric activation energy of the segmental relaxation process also increases with pressure. Again, isobaric fragility and glass transition are not correlated as a function of pressure. Investigation of the volumetric contribution of the isobaric fragility, and more specifically the activation volume, may explain this uncorrelation.

III. Correlation between activation volume and cooperativity volume

As introduced in Chapter 1, Sokolov and coworkers (Hong et al., 2009, 2011a) identified an empirical correlation between the activation volume $\Delta V^\#$ and the cooperativity volume V_α . Considering that $\Delta V^\#$ is the main parameter influencing the volumetric contribution ($m_p - m_V$) of the isobaric fragility m_p , this could be the reason for the uncorrelation between m_p and V_α .

1) Activation volume

❖ Activation volume from isotherms

On the one hand, in the classical definition of the activation volume (see **Equation 3-5**), $\Delta V^\#$ must be calculated from the VFTH pressure parameters of the isothermal measurements (see **Figure 3-6**) with:

$$\Delta V^\# = k_B T \frac{C}{P_0 - P_g} \quad 3-7$$

❖ Activation volume from isobars

On the other hand, the activation volume $\Delta V^\#$ at T_g can be determined from **Equation 1-42** (p. 47). In this equation, the glass transition temperature dependence of pressure is obtained by using the parameters of the Andersson's model such as:

$$\frac{dT_g}{dP} = \frac{T_g}{\Pi b \left(1 + \frac{P}{\Pi}\right)}, \quad 3-8$$

where Π and b are adjustable parameters. $\Delta V^\#$ calculated from **Equation 1-42** is obtained from the isobaric measurements of **Figure 3-7**. Activation volume determined this manner is noted $\Delta V^\#(P, T_g)$.

❖ Comparison between activation volume from isobars and isotherms

Figure 3-10 guarantees that both manners for calculating $\Delta V^\#$ are consistent with each other. The variations of the activation volumes at T_g are similar to those reported by Roland and Casalini for

PVAc, with activation volumes ranging from 0.217 up to 0.333 nm³ for temperatures from 390 down to 340 K (Roland and Casalini, 2003a).

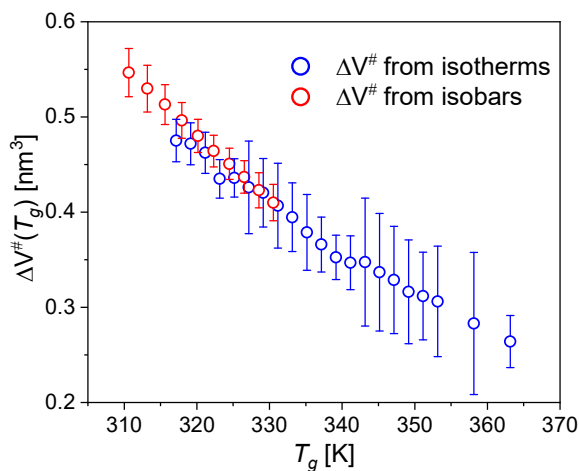


Figure 3-10. Activation volume $\Delta V^\#$ at the glass transition temperature T_g calculated from isothermal measurements and classical definition of $\Delta V^\#$ (Equations 3-5 et 3-7) in empty blue circles, and from isobaric measurements and Equation 1-42 (p. 47) in empty red circles for PVAc.

2) Cooperativity volume

The higher the pressure, the smaller the free and activation volumes. Thus, the distance between macromolecules is distorted. Thereby, the parameter $(m_p - m_V)$ has been directly related to the intermolecular interactions (Araujo et al., 2018b). In literature, cooperativity has been related to the intermolecular interactions (Ngai and Roland, 1993a; Nakanishi and Nozaki, 2011; Grigoras and Grigoras, 2011; Monnier et al., 2015). Then, it seems interesting to follow the cooperativity as a function of pressure and to connect it to the activation volume included in the expression of $(m_p - m_V)$ (see Equation 3-4) in order to better understand the influence of interactions on the molecular mobility under pressure. Some studies have already suggested such relationship (Berthier, 2004; Zhang and Douglas, 2013), and defined an empirical relation of $\Delta V^\# \approx (2 - 5\%)V_\alpha$ for polymers (Hong et al., 2011a; Araujo et al., 2018b). By combining MT-DSC and BDS, the extended Donth's approach proposed by Saiter et al. (Saiter et al., 2013, 2010) allows the determination of the cooperativity volume V_α . The specific heat capacity is obtained from the MT-DSC analysis (see Figure 3-1), by extrapolating the liquid and glassy heat capacities at T_α . These values obtained from heat capacity measurements at atmospheric pressure can be used on a wide range of pressures, as observed in the literature (Sandberg and Bäckström, 1980).

❖ Two methods for determined activation volume

Figure 3-11 shows the temperature dependence of the activation volume calculated by two methods. In this figure, the first method gives the empty squares. The activation volumes at the glass transition are determined from isobaric measurements of relaxation time and **Equation 1-42** (p. 47) mentioned earlier, namely $\Delta V^\#(P, T_g)$.

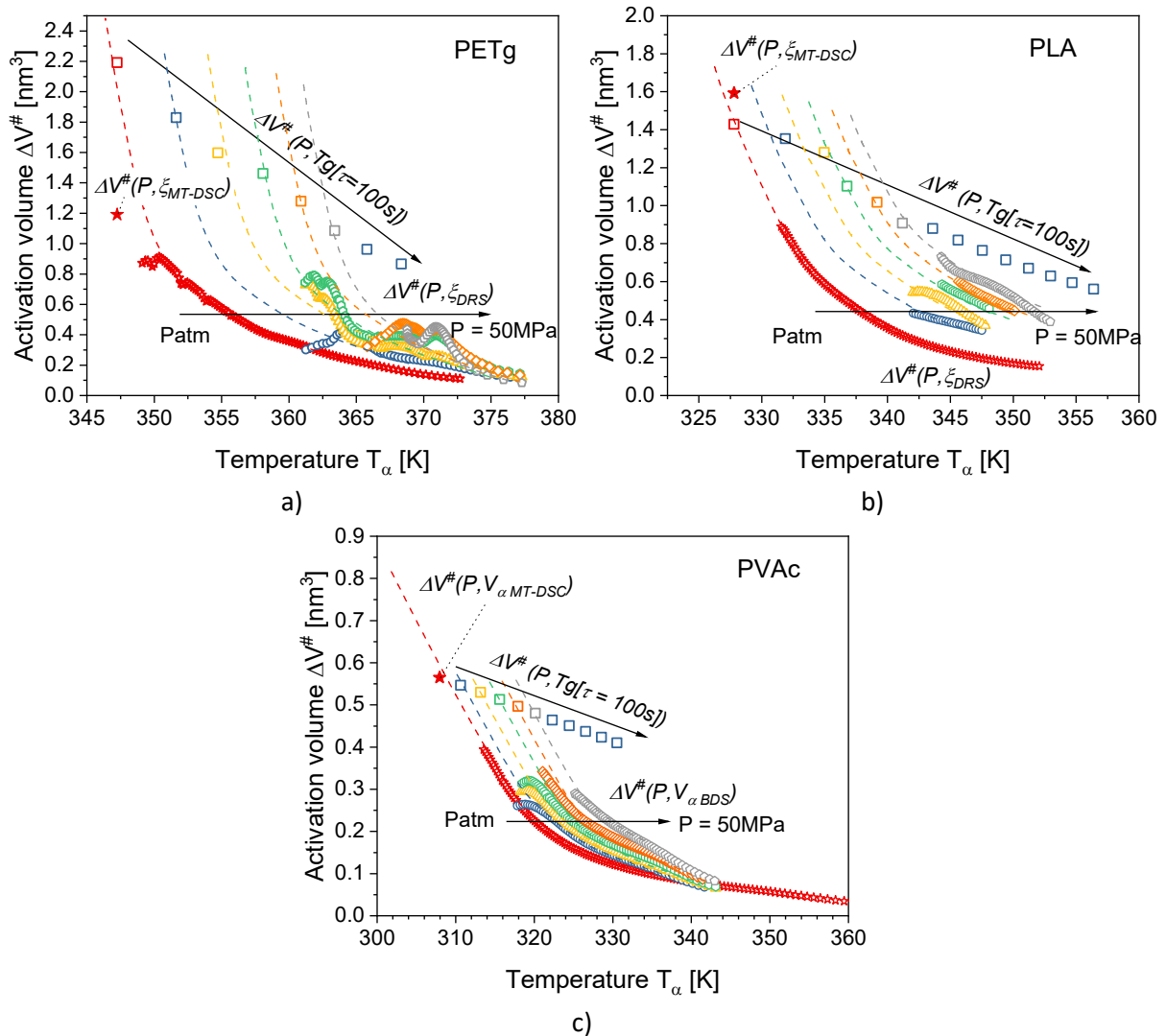


Figure 3-11. Activation volume $\Delta V^\#$ as a function of the temperature T_α for a) PETg, b) PLA and c) PVAc. The colored squares (\square) are the activation volumes $\Delta V^\#(P, T_g)$ calculated from the **Equation 1-42** (p. 47) and isobaric measurements at $\tau = 100$ s. The red filled star (\star) corresponds to $\Delta V^\# \approx 0,04 \times V_\alpha$ from MT-DSC measurements at P_{atm} . The empty symbols are associated with $\Delta V^\# \approx 0,04 \times V_\alpha$ determined from BDS analyses at P_{atm} (red empty stars), 10 MPa (blue circles), 20 MPa (yellow triangles), 30 MPa (green hexagons), 40 MPa (orange diamonds) and 50 MPa (gray pentagons). The dashed lines represent the extrapolation of $\Delta V^\#$ by this latter method at P_{atm} , transposed for the high pressure.

The second method uses $\Delta V^\# \approx (0.04 \pm 0.01) \times V_\alpha$ (see **Equation 2-20**, p. 82 for V_α calculation). This activation volume can be written as $\Delta V^\#(P, V_\alpha)$. On the one hand, $\Delta V^\#(P, V_\alpha)$ is derived from cooperativity volume from MT-DSC measurements at P_{atm} . This value is in **Table 3-3** and is shown as red filled star in **Figure 3-11**. On the other hand, $\Delta V^\#(P, V_\alpha)$ can be determined from the extended Donth's approach. $\Delta V^\#(P, V_\alpha)$ are determined for pressure range from the atmospheric pressure up to 50 MPa and plotted in **Figure 3-11** as empty symbols.

❖ Comparison of activation volume and cooperativity at P_{atm}

An extrapolation of these data seems to reach relatively the true activation volume at the conventional glass transition $\Delta V^\#(P, T_g)$. At higher temperatures, the cooperativity volume should converge at the crossover temperature T^* to a value close to the volume of a relaxing unit, i.e., the case where the number N_α of structural units in the cooperativity volume is about 1. These values are listed in **Table 3-3**. It also lists the values of activation volumes at atmospheric pressure obtained by HP-BDS measurements or in the relation to the cooperativity volume calculated by MT-DSC analysis.

Table 3-3. Values of activation volume and cooperativity volume calculation: activation volume $V_\alpha(T^*)$ and cooperativity volume $\Delta V^\#(T^*)$ when the temperature tends to the crossover temperature T^* , activation volume $\Delta V_{P_{atm} HP-BD}^\#$ calculated from the relaxation time variations with the pressure measured by HP-BDS, activation volume $\Delta V_{P_{atm} MT-DSC}^\#$ from the relationship between $\Delta V^\#$ and V_α , where $V_{\alpha P_{atm} MT-DSC}$ is calculated by the Donth's approach with MT-DSC measurements, and the number N_α of structural units in V_α .

Polymer	$V_\alpha(T^*)$ [nm ³]	$\Delta V^\#(T^*)$ [nm ³]	$\Delta V^\#(P, T_g)$ [nm ³]	$\Delta V_{P_{atm} MT-DSC}^\#$ [nm ³]	$V_{\alpha P_{atm} MT-DSC}$ [nm ³]	N_α [–]
PETg	0.28	8.6×10^{-3}	2.19	1.19	30.6	104
PLA	0.10	2.9×10^{-3}	1.43	1.57	40.6	414
PVAc	0.12	4.8×10^{-3}	0.57	0.57	19.5	167

The activation volume values at P_{atm} calculated from MT-DSC analyses are in perfect agreement with those obtained from BDS measurements for PVAc. Nevertheless, the values calculated by the two approaches for PLA and PETg are significantly different, although both values could have been obtained by extrapolating the activation volume associated with $\Delta V^\# \approx 0,04 \times V_\alpha$ determined from BDS analyses at P_{atm} .

❖ Comparison of activation volume and cooperativity volume with other polymers

In **Figure 3-12**, PETg, PLA and PVAc are with other polymers in the correlation between activation volume $\Delta V^\#$ and cooperativity volume V_α . It is worth mentioning that the gray area fits well for other families of glass formers, including covalent and ionic glasses, molecular glasses and hydrogen bonding glasses (Hong et al., 2011b).

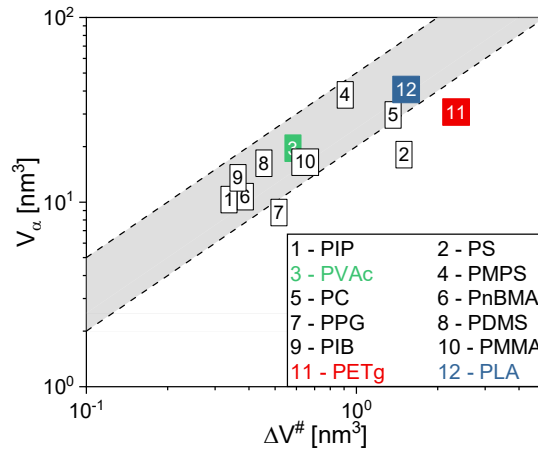


Figure 3-12. Cooperativity volume V_α as a function of the activation volume $\Delta V^\#$ for different polymers. Values for PETg, PLA and PVAc are shown in red, blue and green respectively. The gray area corresponds to the acceptable range of the empirical relationship $\Delta V^\# = [0.02\sim 0.05] \times V_\alpha$. Values are taken from Hong et al. (2011a).

Having observed the relationship between $\Delta V^\#$ and V_α , this comforts their respective interconnectivity with intramolecular interactions. Thus, the volumetric contribution ($m_p - m_v$) of the isobaric fragility, which depends mainly on $\Delta V^\#$, could provide explanation on the relationship between isobaric fragility and cooperativity.

IV. Estimation of the contributions of the isobaric fragility

1) Thermal and volumetric contributions

The separated contributions of isobaric fragility can therefore be calculated from **Equation 3-4**. The ratio α/κ is assumed to be around 1.5 MPa/K for polymers (Hong et al., 2011a). The thermal contribution is then derived from the difference between the isobaric fragility and its volumetric contribution. The isobaric fragility and its two contributions are plotted as a function of pressure for PETg, PVAc and PLA (see **Figure 3-13**). Since the decrease in ($m_p - m_v$) is steeper than the increase in m_v , it causes a decrease in m_p for PETg and PLA, while these two contributions cancel each other for PVAc, leading to the invariance of m_p with pressure. By rising the pressure, the two contributions

of the isobaric fragility have two different behaviors. This difference between the volumetric ($m_p - m_v$) and thermal m_v contributions is expected for polymers (Huang et al., 2002) since the activation volume at the glass transition decreases when the pressure rises. The volumetric contribution ($m_p - m_v$) does not favor the structural units to relax as the pressure increases. On the other hand, in order to have a molecular mobility that allows relaxation fast enough to reach the glass transition, there must be an energy gain to compensate for the deficit of activation volume at T_g . It can be assumed that the thermal contribution of m_p increases with pressure to provide sufficient energy. Nevertheless, the isochoric fragility seems to converge to an asymptotic value at high pressure. This effect can be directly related to the asymptotic behavior of the glass transition at high temperature (Paluch et al., 2003; Roland et al., 2005; Roland and Casalini, 2003a).

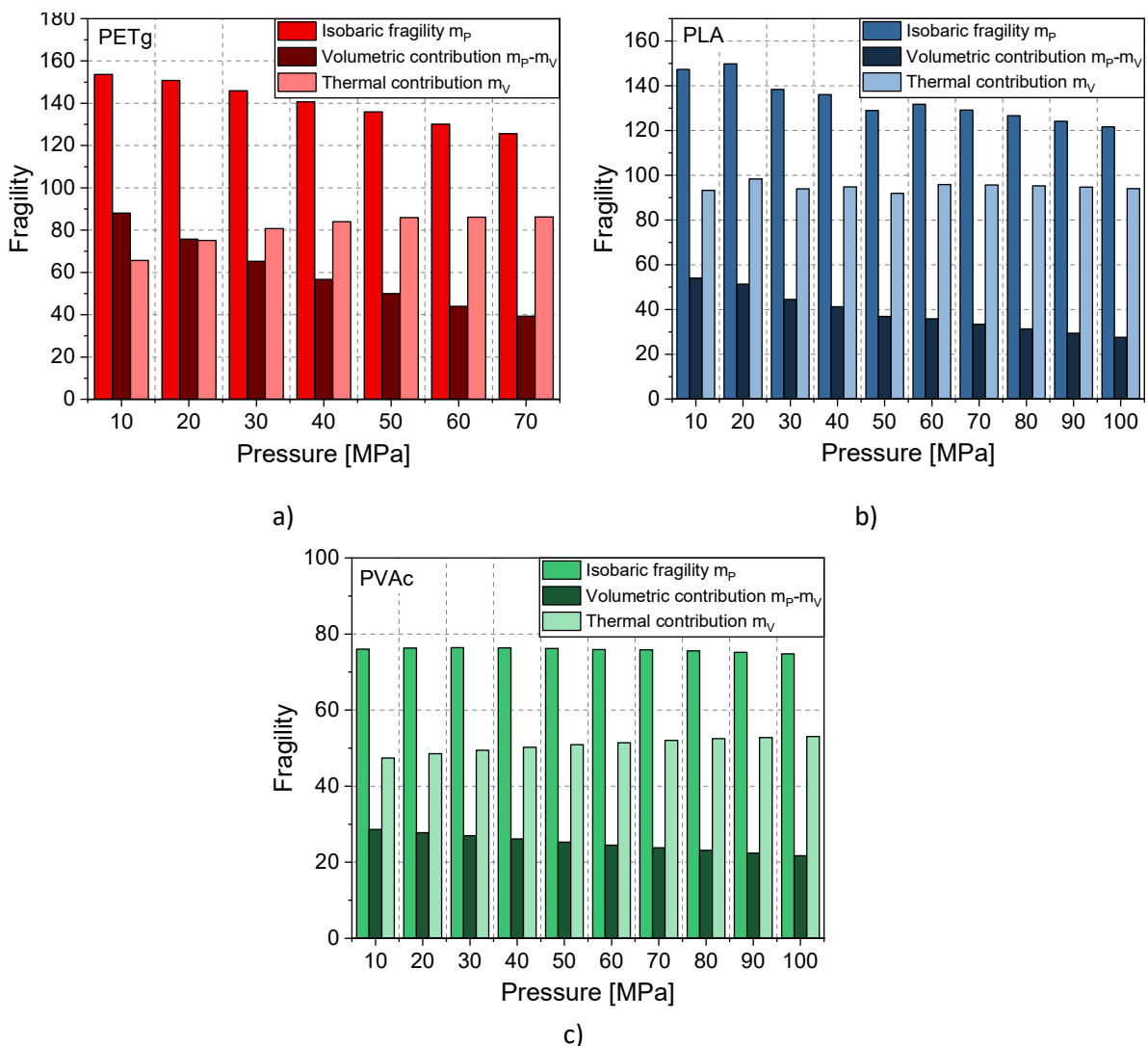


Figure 3-13. Isobaric fragility m_p , its volumetric ($m_p - m_v$) and thermal m_v contributions as a function of pressure for a) PETg, b) PLA, and c) PVAc.

2) Isochoric fragility from Donth definition

In the method based on **Equation 3-4**, the thermal contribution is derived from the difference between the isobaric fragility m_p and its volumetric contribution. Another way to determine the thermal contribution m_V is to use the Angell's definition of fragility. The variation of relaxation time in isochoric conditions as a function of temperature is then required for the experimental calculation of m_V .

❖ Pressure and temperature dependence on the specific volume

During pressure or temperature scans, the specific volume variation can be measured by PVT apparatus as shown in **Figure 3-14** (Zoller et al., 1976). As explained in the Chapter 1, the temperature or pressure dependence of the volume undergoes a change in steepness at the glass transition. The pressure dependence of the glass transition temperature, as determined by HP-BDS for PVAc, appears to be consistent with the change in volume steepness observed in PVT measurements. Only PVAc is presented here because it is the only one that does not undergo structural changes such as crystallization during the PVT measurement, which would have affected the observation of the change of volume steepness at T_g . Since the BDS measurement measures the relaxation time above the glass transition temperature, only the specific volume of the supercooled liquid is considered when determining the parameters of the Tait's equation, i.e., volume at higher temperature and pressure than the red line in **Figure 3-14**. The PVT data for PLA and PVAc are obtained from the literature (McKinney and Simha, 1974; Zoller and Walsh, 1995).

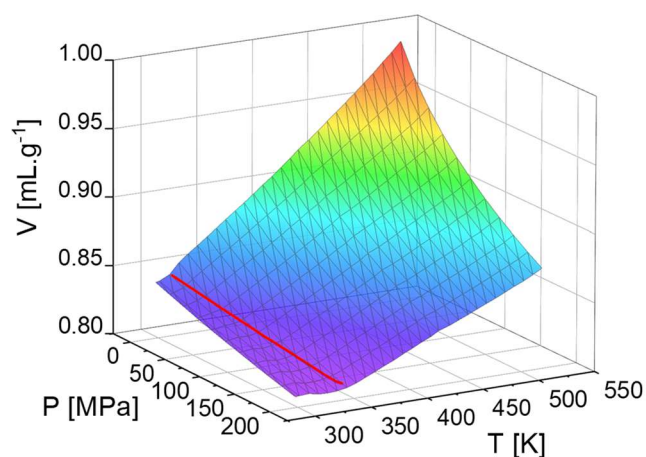


Figure 3-14. Specific volume as a function of temperature and pressure for PVAc. The red line corresponds to the glass transition temperature variation from the Andersson's model. Data are taken from (Zoller and Walsh, 1995).

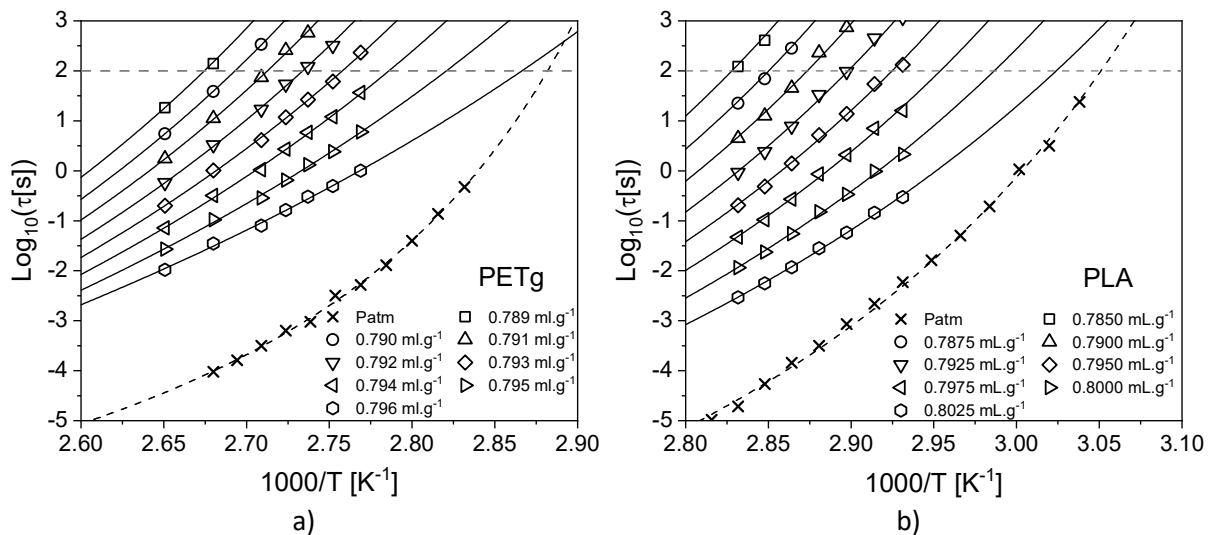
❖ Tait's equation parameters

The volume of the supercooled liquid can then be expressed as a function of pressure and temperature. For this purpose, the empirical Tait's equation (**Equation 1-36**, p. 40) allows the approximation of the PVT data and the definition of the volume above T_g independent of pressure and temperature (Jain and Simha, 1989). The Tait's equation for PETg has been derived from the density at ambient temperature and the second derivatives of the free energy, i.e., the thermal volume expansivity α and the compressibility κ . The parameters of the Tait's equation are given in **Table 3-4**.

Table 3-4. Parameters of the Tait's equation (**Equation 1-36**, p. 40) for PETg, PLA and PVAc.

Polymer	A_0 [mL. g ⁻¹]	A_1 [mL. g ⁻¹ . K ⁻¹]	A_2 [mL. g ⁻¹ . K ⁻²]	b_0 [bar]	b_1 [K ⁻¹]
PETg	7.86×10^{-1}	6.80×10^{-5}	9.39×10^{-7}	9.00×10^3	6.00×10^{-3}
PLA	7.94×10^{-1}	1.15×10^{-4}	1.36×10^{-6}	4.12×10^3	5.90×10^{-3}
PVAc	8.28×10^{-1}	5.31×10^{-4}	5.17×10^{-7}	2.43×10^4	4.94×10^{-3}

From the VFTH pressure fits (see **Figure 3-6**) and the PVT data given by Tait's equation, the relaxation time for constant volume is defined and approximated by the VFTH law as shown in **Figure 3-15**. A striking difference between the isochores and the measurement at atmospheric pressure is the difference in steepness, although the relaxation time still exhibits a super-Arrhenius behavior.



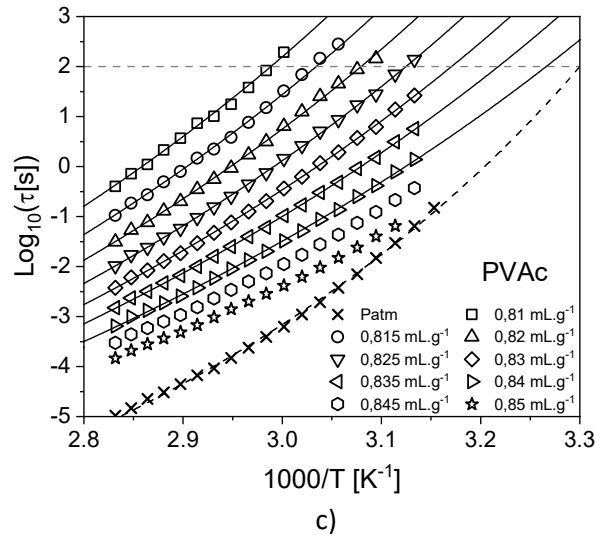


Figure 3-15. Temperature dependence of the isochoric α -relaxation time τ for a) PETg, b) PLA and c) PVAc. Black lines are VFTH fits of each isobar. The dashed black lines correspond to the VFTH fit at P_{atm} . The dashed gray lines correspond to isochrone $\tau = 100$ s.

❖ Thermodynamic scaling

From the PVT data and the evolution of the relaxation time with temperature and pressure, it is also possible to proceed to a thermodynamic scaling (Alba-Simionesco et al., 2004; Casalini and Roland, 2004a, 2004b, 2005). It consists in expressing the relaxation time as a function of $T^{-1}V^{-\gamma}$, where γ is the scaling exponent corresponding to a material constant. γ is obtained from the expression: $\log(T_g) = A - \gamma \log(V_g)$ (Paluch et al., 2007).

The thermodynamic scaling for PETg, PVAc and PLA is shown in **Figure 3-16**. It can be observed that the consistency of the scaling is much better for PVAc than for PLA and PETg. Paluch et al. have already shown that such scaling does not work for some H-bonded liquids such as dipropylene glycol (DPG) (Paluch et al., 2007). They explain this by a strong influence of thermodynamic conditions over the degree of H-bonding. Here, it can be hypothesized that for PLA and PETg, the difficulty in achieving good scaling can be due to the large decrease in the isobaric fragility with pressure, as shown in **Figure 3-9**. The scaling exponent can be used to express m_p as a function of m_V according to $m_p = m_V(1 + \alpha T_g \gamma)$ where α is the thermal volume expansivity (Casalini and Roland, 2004b).

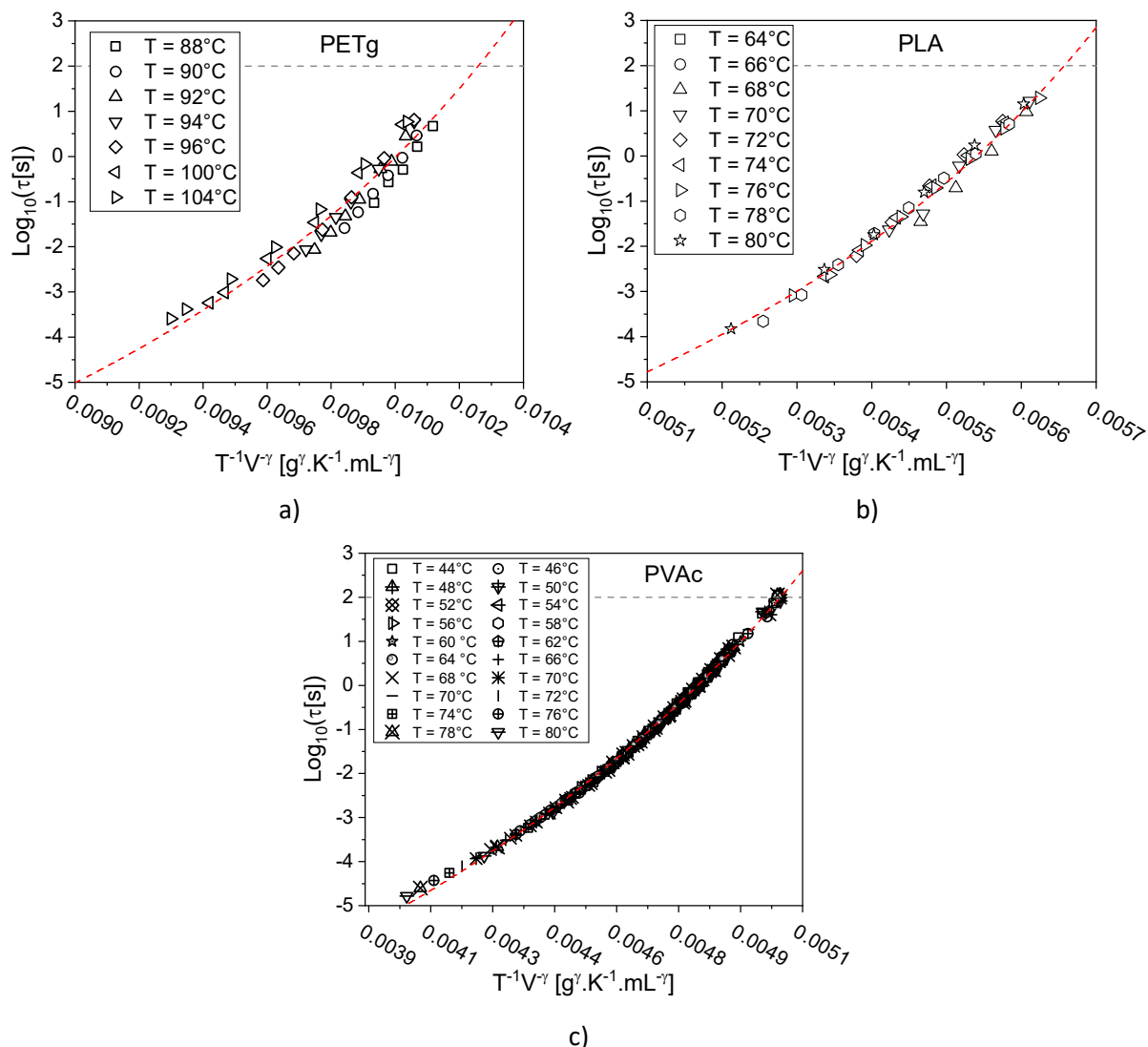


Figure 3-16. Relaxation times of the isothermal measurements as a function of inverse product of temperature and specific volume to the power of the scaling exponent γ for a) PETg (where $\gamma = 5.975$; $\Delta\gamma = 0.178$), b) PLA (where $\gamma = 2.737$; $\Delta\gamma = 0.042$) and c) PVAc (where $\gamma = 2.477$; $\Delta\gamma = 0.029$). Red dashed lines are only guides for the eyes. The dashed gray lines correspond to the isochrone $\tau = 100$ s.

❖ Comparison of the two methods

The isochoric fragilities m_V derived from the isochoric expression of the relaxation times are plotted in **Figure 3-17** as an empty circle as a function of the density at the glass transition normalized to the density at ambient temperature and atmospheric pressure. m_V values from Angell's definition of the isochoric fragility are also plotted in **Figure 3-17** as filled circles. The isochoric fragility values obtained with the two methods agree well, the same increase in m_V is observed.

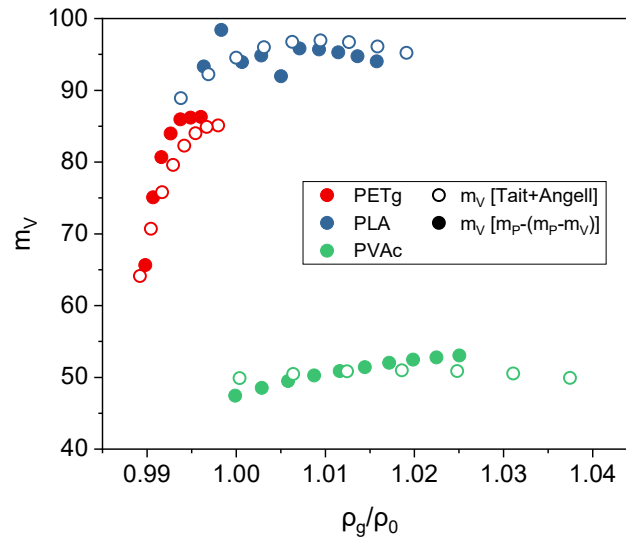


Figure 3-17. Isochoric fragility as a function of the density at the glass transition normalized to the density at atmospheric pressure and ambient temperature. The fragility of PETg (red), PLA (blue) and PVAc (green) is calculated both according to the Angell's definition applied to the isochoric relaxation times deduced by Tait's equation (empty circles) and from the difference between the isobaric fragility and the volumetric contribution (filled circles).

V. Molecular mobility influence of isobaric fragility contributions

Therefore, the activation volume ΔV^\ddagger is related to the intensity of cooperative interactions. It also allows the determination of the volumetric contribution to the isobaric fragility. By comparing the values of ΔV^\ddagger with the volumetric contributions for different polymers, it is possible to identify the relative contribution to these quantities of molecular mobility in polymeric glass formers.

1) Contributions of isobaric fragility under pressure

❖ Intermolecular interactions

Figure 3-18a shows the variations of ΔV^\ddagger as a function of the pressure. Since this study has emphasized the direct correlation between activation volume and cooperativity size, PETg is the most cooperative at P_{atm} ($\Delta V^\ddagger = 2.18 \text{ nm}^3$), then PLA has intermediate cooperativity ($\Delta V^\ddagger = 1.44 \text{ nm}^3$), and PVAc has the lowest cooperativity ($\Delta V^\ddagger = 0.64 \text{ nm}^3$). These values are of the same order of magnitude as those obtained by Rijal et al. (2015). The slope of the activation volume seems to decrease at high pressure. The fit of the one-phase exponential decay function, which allows to extrapolate the activation volume at high pressure, is expressed by:

$$\Delta V^\ddagger = \Delta V_\infty^\ddagger + A \cdot e^{-\frac{P}{P\%}}, \quad 3-9$$

where $\Delta V_{\infty}^{\#}$ is the asymptotic value of the activation volume at very high pressure, A is the amplitude from $\Delta V^{\#}(P = 0)$ up to $\Delta V_{\infty}^{\#}$. Thus $\Delta V_{(P=0)}^{\#} = A - \Delta V_{\infty}^{\#}$ and $P_{\%}$ is a pressure at which the activation volume $\Delta V^{\#}(P)$ has reached 63% of the amplitude from $\Delta V_{(P=0)}^{\#}$ down to $\Delta V_{\infty}^{\#}$. The fit parameters are given in **Table 2-3**. For pressures around $5 \times P_{\%}$, they correspond to pressures at which the activation volumes $\Delta V^{\#}(P)$ have reached 99% of the amplitude. It can be assumed that the values of $\Delta V_{\infty}^{\#}$ for the three polymers are almost reached at this point. In the worst case, PVAc has the highest values of $P_{\%}$, then it can be considered that at $P = 5 \times P_{\%PVAc} = 530$ MPa, the activation volume $\Delta V^{\#}$ should have converged down to $\Delta V_{\infty}^{\#}$.

Table 3-5. Fit parameters ($\Delta V_{\infty}^{\#}$, A , $P_{\%}$), their uncertainties and the R-squared of the one-phase exponential decay function (**Equation 3-9**) for PETg, PLA and PVAc.

Polymer	$\Delta V_{\infty}^{\#}$ [nm ³]	$\pm \Delta V_{\infty}^{\#}$ [nm ³]	A [nm ³]	$\pm A$ [nm ³]	$P_{\%}$ [MPa]	$\pm P_{\%}$ [MPa]	R^2
PETg	0.36	0.013	1.824	0.009	52	0.8	0.99997
PLA	0.35	0.069	1.090	0.025	81	2.8	0.98892
PVAc	0.36	0.052	0.280	0.004	106	3.1	0.99298

Therefore, regardless of the sample, the variations of $\Delta V^{\#}$ show an asymptotic behavior at high pressure, toward a value of 0.35 nm³, corresponding to a cooperativity volume of about 7~17.5 nm³ from the relation $\Delta V^{\#} \approx (2 - 5\%)V_{\alpha}$. **Figure 3-18b** plots the activation volume at T_g ($\Delta V^{\#}$) normalized to that at P_{atm} ($\Delta V_{P_{atm}}^{\#}$) as a function of the pressure. PETg, which has the highest cooperativity, seems to be the most sensitive to the pressure. Conversely, PVAc is the one with the lowest variation as a function of pressure. **Figure 3-18c** shows the evolution of the volumetric contribution ($m_p - m_V$) with pressure, and **Figure 3-18d** shows this contribution normalized to $(m_p - m_V)_{P_{atm}}$. As with $\Delta V^{\#}$, the more cooperative the polymer, the stronger the decrease in $(m_p - m_V)$.

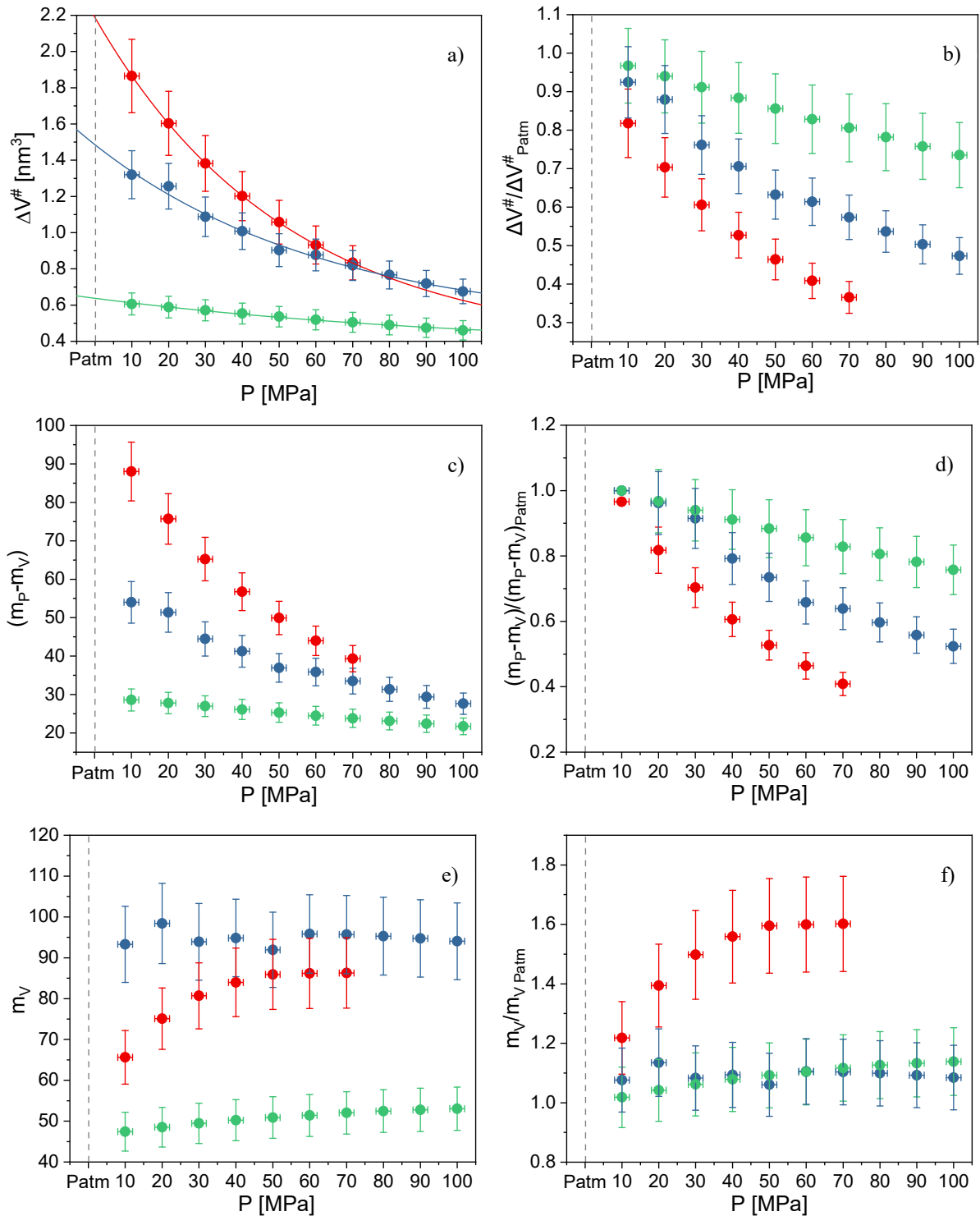


Figure 3-18. a) Activation volume ΔV^\ddagger at $T_g(P)$ (the lines correspond to the one-phase exponential decay function), b) ΔV^\ddagger normalized to its value at P_{atm} , c) volumetric contribution $(m_P - m_V)$, d) $(m_P - m_V)$ normalized to its value at P_{atm} , e) thermal contribution m_V and f) m_V normalized to its value at P_{atm} as a function of pressure for PETg in red, PLA in blue and PVAc in green. The vertical dashed line represents the atmospheric pressure.

❖ Intramolecular interactions

Figures 3-18e and **3-18f** show the thermal contribution m_V and this contribution normalized to $m_V P_{\text{atm}}$ as a function of pressure, respectively. PLA shows a high isochoric fragility at P_{atm} and does not seem to vary much with pressure. In contrast, m_V increases drastically before reaching a plateau for PETg, and m_V seems to increase slightly for PVAc, with values two times smaller than in the case of PLA.

2) Interpretation with the intra and intermolecular interactions

Thus, **Figure 3-18** shows that the higher the volumetric contribution ($m_p - m_V$), the activation volume and thus cooperativity, the stronger the decrease as a function of pressure. Since cooperativity is related to intermolecular interactions (Nakanishi and Nozaki, 2011; Ngai and Roland, 1993a), the volumetric contribution is an indicator of the intensity of these interactions. As the pressure increases, these intermolecular interactions are reduced, and then the cooperativity decreases (Araujo et al., 2019, 2018a; Hong et al., 2011a; Puente et al., 2015). However, Dudowicz et al. and Kunal et al. suggest that the thermal contribution associated with the isochoric fragility m_V is related to the backbone flexibility and thus to intramolecular interactions (Dudowicz et al., 2005a, 2006; Kunal et al., 2008). The question raised earlier about the high m_p value at atmospheric pressure for PLA, seems to find part of the answer thanks to the calculation of the thermal contribution. Its isochoric fragility at P_{atm} is 86. In contrast, PETg and PVAc have values of 54 and 41, respectively. The value of thermal contribution m_V of the isobaric fragility at P_{atm} does not seem to be related only to the backbone flexibility for PLA. This contribution may rather be related to the packing efficiency of the polymers (Kunal et al., 2008; Dudowicz et al., 2005b).

As shown previously in **Figure 3-13**, the thermal contribution increases with the pressure up to a certain pressure. It can be suggested that the convergence of this contribution to a maximum could be explained by a minimum activation volume, where an increase in pressure is no longer sufficient to modify the volume. At this point, the thermal contribution, which allows molecular mobility, provides sufficient energy above the glass transition to allow rearrangements to proceed, and should not increase further.

Some studies have shown an increase in the isobaric fragility with pressure in non-polymeric glass forming liquids (Pawlus et al., 2009; Hu et al., 2017; Phan et al., 2020; Assouli et al., 2023). In metallic glasses, the structural network has metallic bonds that have a very different interatomic interactions (Rouxel et al., 2008). Nevertheless, Roland et al. found that for normal liquids without a strong H-bond, the isobaric fragility should decrease with increasing pressure (Casalini and Roland, 2005; Roland et al., 2005). As shown previously in **Figure 3-11**, the activation volume at low temperature appears to

decrease more rapidly with increasing pressure. The red filled star corresponding to the activation volume at T_g and P_{atm} corresponds to $N_\alpha = 167$. Since the activation volume at $T_g(P)$ decreases with pressure, the cooperativity volume should, in the worst case, reach the value of a volume equivalent to $N_\alpha = 1$. In other words, at extremely high pressure, the volumetric contribution ($m_p - m_V$) can decrease until it reaches the same volumetric contribution as a relaxing unit. In this case, the isochoric fragility should be nearly equal to the isobaric fragility. At this point, m_p should reach a value around 60~90 (Ding et al., 2004).

VI. Conclusion

The segmental relaxation has been studied for PETg, PLA and PVAc. The relaxation time has been expressed as a function of temperature, pressure and also specific volumes, using BDS under pressure. Then, the molecular mobility at T_g and in the liquid of three thermoplastic polymers has been explored by separating the isobaric fragility m_p into its thermal m_V and volumetric ($m_p - m_V$) contributions. The activation volume ΔV^\ddagger is the critical parameter allowing to calculate the volumetric contribution ($m_p - m_V$). The connection between the cooperativity volume V_α defined by the Donth's Model, and ΔV^\ddagger calculated from the isobaric measurement, is validated and lengthened above the glass transition thanks to the extended Donth's approach. The cooperativity seems to correlate better with the volumetric contribution of m_p , than with the isobaric fragility itself. Moreover, although the similarity of PLA and PETg at atmospheric pressure in terms of m_p , this study has shown that PLA and PETg isochoric fragilities m_V present variations drastically different with pressure. Furthermore, this work allows to correlate the fragility values at atmospheric pressure with the evolution of the thermal and volumetric contributions. Thus, the high isobaric fragility values for PLA at atmospheric pressure can be related to the magnitude of the thermal contribution, which is related to the stiffness of the backbone and the packing efficiency. Nevertheless, the volumetric contribution ($m_p - m_V$) associated with the interchain interactions decreases significantly with increasing pressure for PLA, PETg and PVAc. Isobaric fragility m_p seems to converge to values 60~90. It can be postulated that at high pressure, the glass transition temperature is of such importance that the volume contributions reach a universal value, independent of the chemical structure of the polymers.

List of abbreviations and symbols

Symbols

A	Amplitude
b, Π	Constants (from Andersson's model)
C_p	Isobaric heat capacity
C'_p	Reversing heat capacity
C''_p	Non-reversing heat capacity
D	Steepness parameter
f	Frequency
k_B	Boltzmann's constant
M_0	Molar mass of the repeating unit
M_W	Average molecular weight
m_p	Isobaric fragility
$m_p - m_v$	Volumetric contribution of m_p
m_v	Isochoric fragility Thermal contribution of m_p
P	Pressure
P_{atm}	Atmospheric pressure
P_g	Glass transition pressure
T	Temperature
T_g	Glass transition temperature
T_g^0	T_g at atmospheric pressure
T_0	Vogel temperature
T_α	Dynamic glass transition temperature
V_α	Cooperativity volume
α	Isobaric thermal expansion
α_{HN}	Symmetric broadening parameter
β_{HN}	Asymmetric broadening parameter
γ	Scaling exponent
δT	Temperature fluctuation
Δx	Uncertainty of the x parameter
$\Delta \epsilon$	Dielectric strength
ϵ	relative dielectric permittivity
ϵ'	Dielectric storage
ϵ''	Dielectric loss
ϵ^*	Complex dielectric function
ϵ_0	Dielectric permittivity of vacuum
ρ	Density

κ	Isothermal compressibility
σ_0	Ohmic conduction
ξ_α	Characteristic length scale of CRR
τ_{\max}	Relaxation time
τ_∞	Pre-exponential factor for $T \rightarrow \infty$
τ_0	$\tau(T, P_{\text{atm}})$
ω	Angular frequency

Abbreviations

BDS	Broadband Dielectric Spectroscopy
CRR	Cooperative Rearranging Region
HP-BDS	Broadband Dielectric Spectroscopy High Pressure
DSC	Differential Scanning Calorimetry
NMR	Nuclear magnetic resonance
MT-DSC	Modulated temperature differential scanning calorimetry
HN	Havriliak-Negami
VFTH	Vogel-Fulcher-Tamman-Hesse

Polymer abbreviations

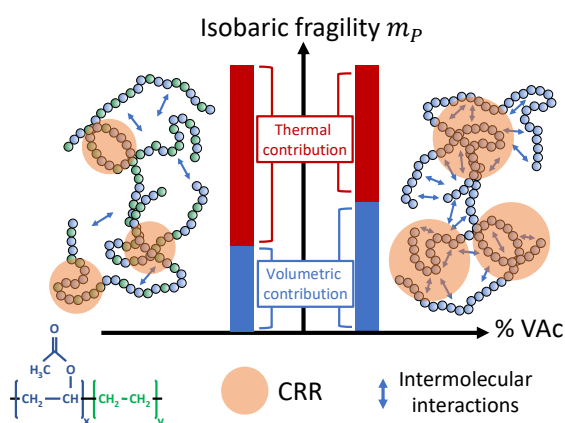
PBMA	Poly(n-butyl methacrylate)
PC	Polycarbonate
PDMS	Poly(dimethyl siloxane)
PE	Polyethylene
PEA	Poly(ethyl acrylate)
PEMA	Poly(ethyl methacrylate)
PESb	Poly(ethylene sebacate)
PET	Polyethylene terephthalate
PETg	Poly(ethylene terephthalate glycol)
PHMA	Poly(hexyl methacrylate)
PI	1,4-cis-polyisoprene
PIB	Polyisobutylene
PLA	Poly(lactide acid)
PMA	Poly(methyl acrylate)
PMMA	Poly(methyl methacrylate)
PMPS	Poly(methyl phenylsiloxane)
POE	Poly(oxyethylene)
PP	Polypropylene
PpenMA	Poly(n-pentyl methacrylate)
PPG	Poly(propyleneglycol)

PPO	Polypropylene oxide
PprMA	Poly(n-propyl methacrylate)
PS	Polystyrene
PSF	Polysulfone
PTMO	Polytetramethylene oxide
PVAc	Poly(vinyl acetate)
PVC	Poly(vinyl chloride)
PVME	Poly(vinyl methyl ether)

Chapter 4. Role of VAc group on dielectric relaxation, fragility and cooperativity

Table of content

CHAPTER 4. ROLE OF VAc GROUP ON DIELECTRIC RELAXATION, FRAGILITY AND COOPERATIVITY	120
I. UNCORRELATION BETWEEN FRAGILITY AND GLASS TRANSITION	120
1) <i>The EVA series</i>	120
2) <i>Highlight from various systems</i>	124
II. INTERMOLECULAR INTERACTIONS IN THE PVAc/EVA SERIES.....	127
1) <i>Dispersion of dielectric relaxation</i>	127
2) <i>Role of dipolar side group in interactions</i>	133
III. INTERMOLECULAR INTERACTION AND COOPERATIVITY.....	135
1) <i>Isobaric cooperativity</i>	135
2) <i>Cooperativity from pressure fluctuation</i>	136
3) <i>Isothermal cooperativity</i>	138
IV. ROLE OF INTRA AND INTERMOLECULAR INTERACTIONS ON SEGMENTAL RELAXATION	139
1) <i>Segmental mobility of PVAc/EVA series as a function of temperature and pressure</i>	139
2) <i>Activation volume</i>	141
3) <i>Thermal and volumetric contribution of isobaric fragility in PVAc/EVA series</i>	142
V. CONCLUSION.....	145
LIST OF ABBREVIATIONS AND SYMBOLS	147
REFERENCES	ERREUR ! SIGNET NON DÉFINI.



The figure represents a schematic view of the evolution of the thermal and volumetric contribution of isobaric fragility, intermolecular interactions and cooperativity volume as a function of the VAc ratio.

Part of the work presented in this chapter is currently being published in article "Study of PVAc/EVA Polymer Series: Influence of the Inter/Intra -molecular Interaction Ratio on the Molecular Mobility at the Glass Transition" J. Trubert, L. Matkowska, A. Saiter-Fourcin, L. Delbreilh.

Chapter 4. Role of VAc group on dielectric relaxation, fragility and cooperativity

Polymers have relatively different chemical structures, making difficult to accurately interpret the separated roles of backbone stiffness, lateral side groups, polarity or molecular weight. In this chapter, the molecular mobility at the glass transition of poly(vinyl acetate) (PVAc) and poly(ethylene-co-vinyl acetate) (EVA) amorphous sample series has been investigated. As introduced in chapter 2, in this series, the ratio of VAc side group varies from 100 wt. % for PVAc down to 60 wt. % for EVA60. In this way, the backbone chain remains same in the whole series while density of polar side group varies. The temperature and pressure dependencies of the intermolecular interactions are investigated through time-temperature-pressure superpositions, and from the relaxation time dispersion of the segmental relaxation. The difference in the intermolecular interactions due to the lateral group ratio of vinyl acetate (VAc), was then estimated from the activation volume and related to the cooperative behavior. The method presented in Chapter 3 for determining the volumetric and thermal contributions to the isobaric fragility is applied to the PVAc/EVA series.

I. Uncorrelation between fragility and glass transition

1) The EVA series

Molecular mobility is primarily analyzed by variation of relaxation time variations with temperature. Therefore, dielectric measurements have been performed on the EVA80 and EVA60 as shown in **Figure 3-1**.

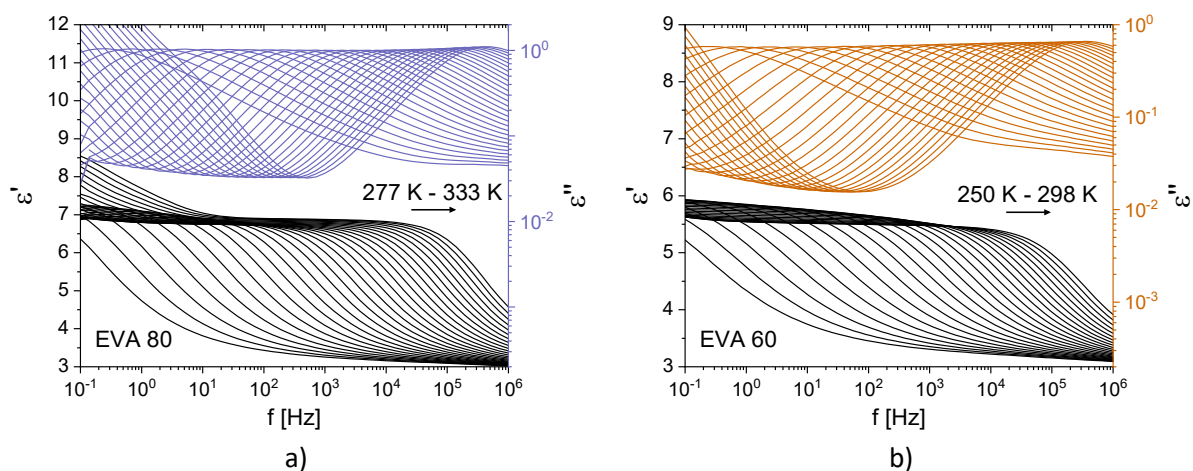


Figure 4-1. The dielectric storage (black lines) and loss (colored lines) have been recorded by BDS as a function of frequency for a) EVA80 from 277 K up to 333 K and b) EVA60 from 250 K up to 298 K.

The spectra are dielectric storage and loss from BDS analysis at atmospheric pressure. PVAc measurements are presented in Chapter 3. The samples show a clear segmental relaxation with a peak shape that is not obscured by the conductivity. The spectra can be fitted with the Havriliak-Negami function (HN), as shown in **Figure 4-2**. Examples of the contribution of conductivity, α and β -relaxations are given for the dielectric loss of EVA80 and EVA60 at 291 K and 262 K, respectively.

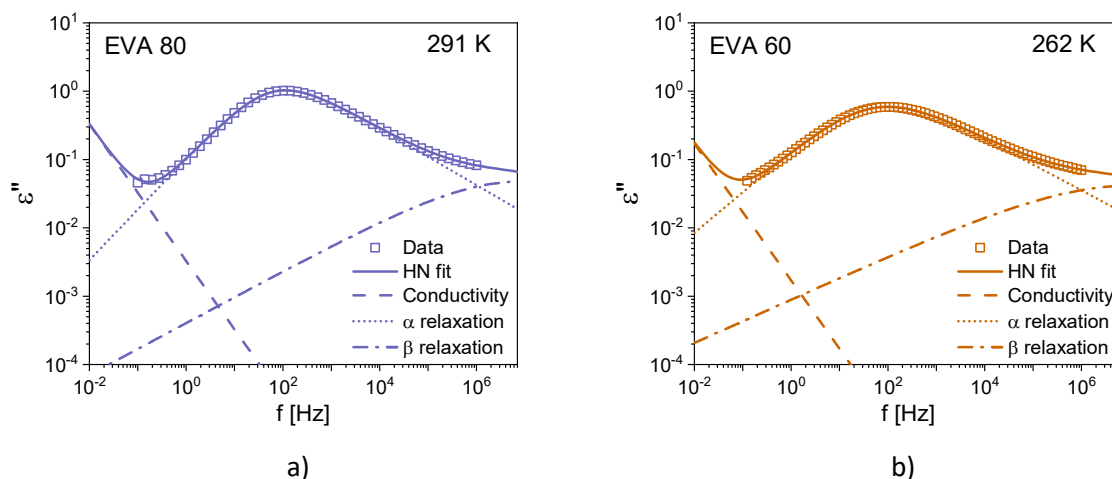


Figure 4-2. The contribution of conductivity (dashed lines), α -relaxation (dotted lines), and β -relaxation (dash-dotted lines) to the dielectric loss for a) EVA80 and b) EVA60 at 291 K and 262 K, respectively. Filled lines correspond to the Havriliak-Negami fits of the data shown by empty squares.

Thus, the relaxation time of the polymer segmental relaxation can be approximated by the VFTH. Relaxation time is taken as τ_{max} (see **Equation 2-18**, p. 77). The temperature dependence of the relaxation time of the samples is shown in **Figure 3-3a** with the corresponding VFTH laws. The glass transition temperature T_g can be obtained by extrapolating the law to a relaxation time of 100 s (Delbreilh et al., 2009). Both T_g and m_p values are plotted as the function of the VAc ratio in **Figure 3-3b**. The values are also presented in **Table 3-1**. As previously observed by Puente et al., the glass transition decreases whereas the isobaric fragility remains fairly constant. The invariance of m_p has been attributed to the constant backbone stiffness present in EVA regardless of the VAc ratio (Puente et al., 2015), while the variation of the glass transition is explained by the role of steric hindrance and the polarity of the side group (Kummali et al., 2013). In addition, Puente et al. observed that the cooperativity at the glass transition increases with the VAc ratio (Puente et al., 2015).

As presented in Chapter 2, the number of structural units per CRR, N_α , and the CRR volume V_α can be determined either by MT-DSC measurement using the Donth's approach or by BDS measurement using an extended Donth's approach proposed by Saiter et al. (see **Equations 2-20** and **2-21**, p. 82).

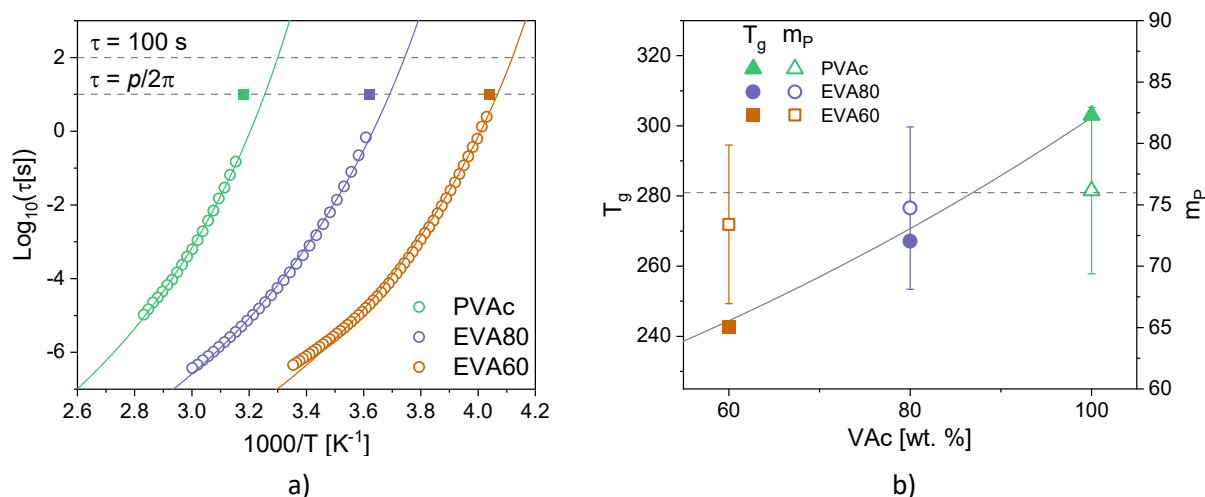


Figure 4-3. a) Temperature dependence of the relaxation time for PVAc (green), EVA80 (blue) and EVA60 (brown). The lines represent the VFTH fits. The filled squares correspond to T_g determined by MT-DSC analysis with a period of modulation of $p = 60$ s. The dashed lines correspond to the isochrone $\tau = 100$ s, i.e., to the glass transition temperature T_g , and $\tau = p/2\pi$. b) T_g and m_p as a function of the VAc ratio at atmospheric pressure. Straight and dashed lines correspond to the glass transition temperature and isobaric fragility variations as a function of VAc ratio, respectively, according to Kummalı et al. (2013) and Puente et al. (2015).

Some values have been extracted from MT-DSC measurements and are shown in **Figure 4-4**, which represents the reversing heat capacity C_p' and the non-reversing heat capacity C_p'' signals for EVA80 and EVA60. The values of V_α and N_α obtained this way are given in **Table 3-1**.

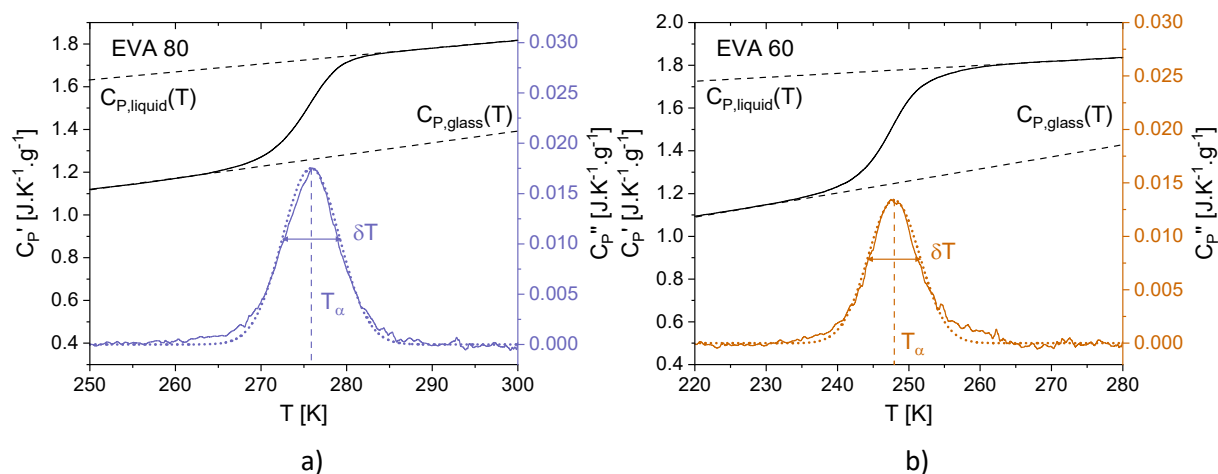


Figure 4-4. Reversing heat capacity C_p' (black line) and the non-reversing heat capacity C_p'' (colored line) signals measured by MT-DSC as a function of temperature for a) EVA80 and b) EVA60. The dotted colored lines represent a Gaussian fit of C_p'' . The polymers have been analyzed in the heat-cool-T mode with a period of $p = 60$ seconds, an amplitude of $A = \pm 1$ K, and with a heating rate of $q = 0.5 \text{ K} \cdot \text{min}^{-1}$.

Using the extended Donth's approach, T_α and δT are determined from BDS measurements, which are presented in **Figure 3-1**. The specific heat capacities in glassy and liquid states are determined by extrapolating the baselines of the liquid and the glass at T_α . **Figure 4-5** shows the variations of N_α as the function of the inverse of temperature normalized to T_g ($\tau = 100$ s).

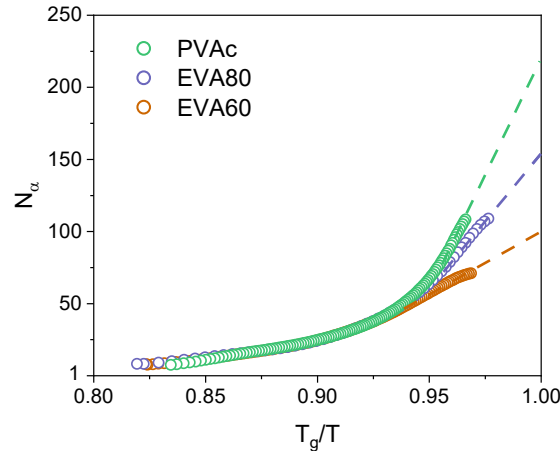


Figure 4-5. N_α as a function of T_g/T , where $T_g = T(\tau = 100$ s). The dashed lines represent the linear extrapolation of the data to visualize N_α at $T = T_g$.

N_α at the glass transition temperature can be extrapolated from its temperature dependence (represented by the dashed lines in **Figure 4-5**). The values are given in **Table 3-1**. The cooperativity at the glass transition temperature seems to be correlated with the ratio of polar groups in the macromolecular chain, since EVA60 has fewer relaxing units in a CRR than EVA80 and PVAc. Similar results on cooperativity have been reported when intermolecular interactions are reduced through temperature increase (Saiter et al., 2010).

Table 4-1. MT-DSC and BDS results for PVAc, EVA80 and EVA60: the temperature fluctuation δT , the difference between the inverse of specific heat capacity of the glass and the liquid, the dynamic glass transition $T_{\alpha\text{MT-DSC}}$ and the number of relaxing structural units per CRR $N_{\alpha\text{MT-DSC}}$ from MT-DSC, the cooperativity volume V_α , T_g at $\tau = 100$ s and $N_{\alpha\text{BDS}}$ from BDS and the isobaric fragility m_P .

Polymer	δT [K]	$\Delta(1/C_P)$ [K.g.J ⁻¹]	$T_{\alpha\text{MT-DSC}}$ [K]	V_α [nm ³]	$N_{\alpha\text{MT-DSC}}$ at T_g	$N_{\alpha\text{BDS}}$ at T_g	$T_{g\text{BDS}}$ [K]	m_P
PVAc	3.4	0.193	313	19.5	167	218	303	76
EVA80	3.3	0.275	276	21.0	230	152	267	74
EVA60	3.6	0.241	248	14.8	197	99	243	73

The T_g obtained by MT-DSC and BDS for the PVAc/EVA series are consistent with the ratio of VAc and appear to be relatively equivalent. However, the values of V_α and N_α obtained by MT-DSC do not agree with that determined by BDS. V_α and N_α obtained by BDS are more consistent with those from literature, i.e., the higher the VAc ratio, the higher the V_α and N_α (Rijal et al., 2016). Furthermore, the uncorrelation between m_p and T_g is observed. A method for verifying the assumptions surrounding the different roles of chemical structure on m_p , T_g and V_α , uses the pressure as a tool to isolate intermolecular interactions related to steric hindrance and side group polarity from intramolecular interactions more related to the backbone stiffness.

2) Highlight from various systems

Uncorrelation between T_g , m_p and V_α is already reported in literature. Similar studies focus on varying only one structural parameter to analyze the variations in glass transition temperature T_g and isobaric fragility m_p . **Figure 4-6** shows some observations from these studies. **Figure 4-6a** clearly shows that variations of glass transition T_g do not correlate with variations of m_p and V_α , while the initial polymer system is relatively within the acceptable range defined by Qin and McKenna as shown in **Figure 4-6b** (the correlation zone is defined from the trend of m_p and T_g variations for several glass formers, as mentioned in Chapter 3).

Among the systems in **Figure 4-6a**, three PLA series are shown, i.e., series in which one structural parameter is varied. One of them is PLA series with different plasticizer ratio as shown by blue filled circles. In this series, glass transition and isobaric fragility decrease as the plasticizer ratio increases. Plasticizers can facilitate molecular motions by increasing the free volume in the polymer. The addition of plasticizer to polymers affects the intermolecular interactions while the intramolecular interactions related to the backbone stiffness remain fairly constant (Araujo et al., 2019).

Another series shown in **Figure 4-6a** by blue filled triangles is the crystallized PLA series (Delpouve et al., 2011). A large decrease in isobaric fragility is observed while the glass transition increases by a few degrees. Semi-crystalline polymers are composed of a crystalline phase, an amorphous phase, and tie molecules in both phases (also called the rigid amorphous fraction RAF). The presence of crystalline regions limits the mobility of polymer chains in the amorphous regions, especially in RAF. As a result, the glass transition temperature of semi-crystalline polymers tends to be higher than that of fully amorphous polymers (Bourdet et al., 2023).

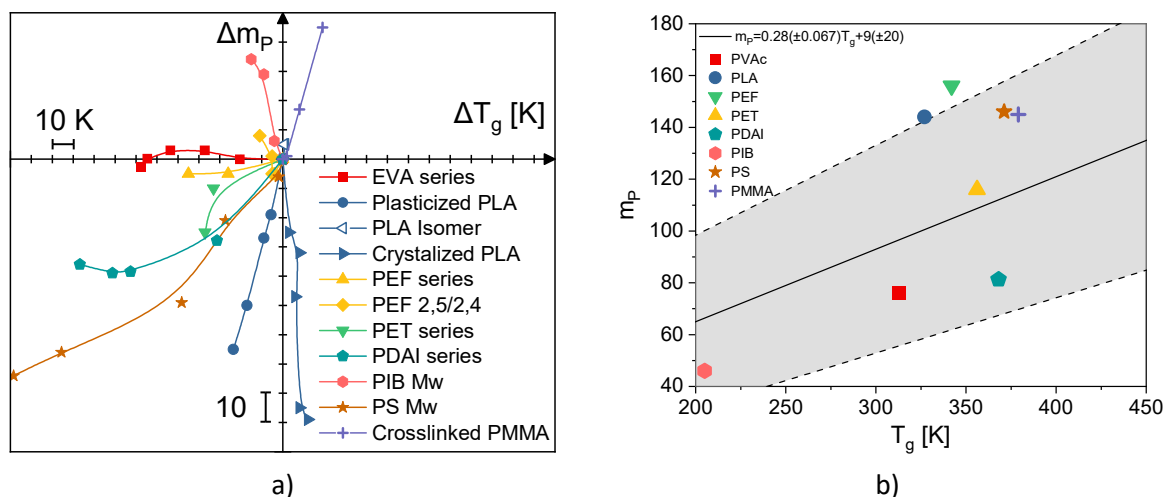


Figure 4-6. a) The isobaric fragility variation Δm_p as a function of the glass transition temperature difference ΔT_g for various polymers whose structural changes imply m_p and T_g value variations. The axes intersect at the origin and are graduated in units of 10. The EVA series have a variation in the ratio of side groups. Three PLA series have variations in the ratio of plasticizers, isomerism, and the manner of sample crystallization. The PEF, PET and PDAI series have a variation in the number of methylene units in their backbone chain, and PIB and PS series have a variation in molecular weight. The PMMA series have a variation crosslinking ratio. b) Isobaric fragility m_p as a function of T_g for polymers whose structure is unchanged. The line and grey area correspond to the linear regression presented in Chapter 3. Details of the values shown and references are given in **Table A-3** in **Appendix**.

Two different isomeric effects are shown in **Figure 4-6a**: the PLA series, where the ratio of D and L isomers is varied, (empty blue triangles) (Varol et al., 2020) and the poly(ethylene furandicarboxylate) PEF 2,5/2,4 series (filled yellow diamonds) (Bourdet et al., 2018). Both have isobaric fragility variation by varying isomerism, but the PLA series keeps T_g constant while that of PEF 2,5/2,4 changes. Isomerism can also alter the glass transition, but in different manners, depending on the type of the isomerism involved: stereochemical or constitutional. Polymers with isomeric variation can exhibit differences in chain flexibility, polarity or steric hindrance (Ngai and Roland, 1993b). In general, the influence of isomerism on the glass transition temperature depends on the ability of the structure to facilitate molecular mobility. Stereochemical variations in tacticity have a measurable effect on the T_g . This discrepancy can be attributed to additional steric repulsion during rotation caused by asymmetric double side groups on alternate chain backbone atoms. Consequently, extended planar zig-zag arrangements of the chains are not feasible, resulting in distinct helical shapes with varying stiffness (Chat et al., 2021). The class of constitutional isomerism can be divided into positional isomerism, skeletal isomerism and functional isomerism. An example of positional isomerism is the PEF 2,5/2,4 series. A comparison between poly(ethylene 2,5-furandicarboxylate) (2,5-PEF) and poly(ethylene 2,4-

furandicarboxylate) (2,4-PEF) suggests that the properties of PEF series can be significantly influenced by the location of the carbonyl group on the furan ring. 2,5-PEF exhibits a greater polarity, resulting in a higher T_g compared to 2,4-PEF (Bourdet et al., 2018).

In **Figure 4-6a**, the PIB (Dalle-Ferrier et al., 2010) and PS series (Santangelo and Roland, 1998) are plotted by pink hexagons and brown stars, respectively. In these series, the molecular weight is reduced. Both series show a decrease in glass transition temperature as the molecular weight decreases, while they have opposite variations in isobaric fragility. In fact, when the polymer chains are long enough, they form stable entanglements that restrict flow. The critical molecular weight required for stable entanglement depends on chain flexibility. Thus, low molecular weight polymers are less entangled and see their T_g decrease as a function of temperature according to the empirical Fox-Flory equation (Fox and Flory, 1954) $T_g(M_n) = T_g(\infty) - K/M_n$.

Crosslinking has the opposite effect on the glass transition temperature as molecular weight reduction, as shown by the PMMA series (purple cross) in **Figure 4-6a**. By increasing the number of crosslinking nodes in the network, the mobility of the chains is hindered and the glass transition and isobaric fragility are increased (Alves et al., 2004).

Finally, the PET (green triangles), PEF (yellow triangles) (Fosse et al., 2022) and poly(di-*n*-alkylitaconate) (PDAI) (turquoise pentagons) (Genix and Lauprêtre, 2005) series shown in **Figure 4-6a** contain different methylene units in their backbone. They all exhibit a decrease in glass transition temperature and isobaric fragility as the number of methylene units increases. As introduced in Chapter 2, the stiffness of the backbone chain can influence T_g and m_p . In the case of PET, PEF and PDAI series, the lower the number of methylene units in the backbone, the more flexible the backbone chain. T_g and m_p can also be influenced by the length and relative rigidities of the side groups. Polymers with a flexible backbone have a T_g that generally increases monotonically with side group length, with greater growth observed for species containing stiffer side groups (Dudowicz et al., 2005a). Kunal et al. proposed to compare the isobaric fragility of polymers by their relative flexibility between the backbone chain and side groups (Kunal et al., 2008). Polymers with flexible backbones tend to be less fragile. Polymers with rigid backbones containing aromatic rings tend to be fragile due to inefficient chain packing. The term packing efficiency describes the order in which chains are grouped within the polymer (Dudowicz et al., 2005b). The relative flexibility of backbone and side group units, rather than individual flexibility, controls polymer fragility. Fragility increases when either the side groups or the backbone become relatively stiffer.

This study aims to understand why the isobaric fragility remains unchanged as a function of wt% VAc, while the glass transition and V_{α} vary significantly. To this purpose, pressure can be used as a tool to understand this uncorrelation. Segmental relaxation can therefore be observed under different conditions, including isothermal, isobaric, and isochronal conditions. Analysis of the segmental relaxation spectra in these configurations can provide insight into the dispersion of the characteristic relaxation times.

II. Intermolecular interactions in the PVAc/EVA series

1) Dispersion of dielectric relaxation

The dispersion is directly related to the dielectric spectrum shape of the segmental relaxation (Ngai, 2000). In the literature, wide or narrow dispersion of relaxation times is associated with dipole mobility within due to intermolecular interactions. For example, variation of the dispersion is reported for changes in steric constraints related to rigid or flexible side groups (Ngai and Roland, 1993b), for variations in hydrogen bond concentration (Ngai et al., 2005), or for changes in the supramolecular organization of molecules (Heczko et al., 2021).

The dielectric spectrum can be analyzed with HN function (**Equation 2-17**, p. 76). The symmetric α_{HN} and asymmetric β_{HN} broadening parameters are determined from 0.1 MPa up to 200 MPa. The α_{HN} and β_{HN} parameters are plotted in **Figures 4-7a**, **4-7b** and **4-7c**, for PVAc, EVA80 and EVA60, respectively. The α_{HN} values increase slowly as the temperature increases, and increase strongly with the VAc ratio indicating that the segmental relaxation becomes narrower in both cases. Moreover, the symmetrical broadening parameters appear to remain constant as the dipole ratio increases. Equivalence between broadening parameters with HN function from frequency domain, and dispersion of segmental relaxation of Kohlrausch–Williams–Watts (KWW) function (**Equation 1-4**, p. 10) from time domain has been found, leading to the following approximation (Alegria et al., 1995; Alvarez et al., 1991):

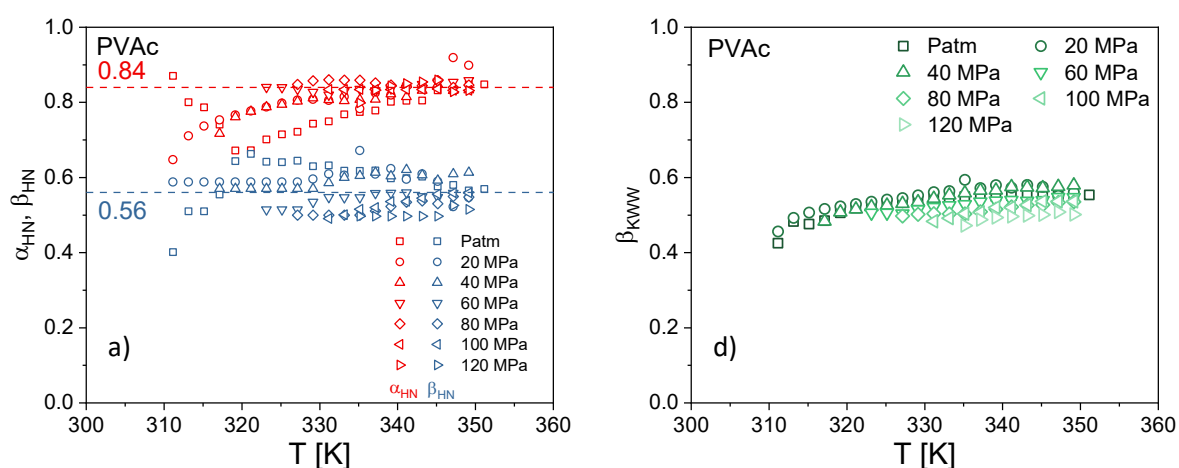
$$\beta_{KWW} = (\alpha_{HN}\beta_{HN})^{0.813}. \quad 4-1$$

The stretching parameter β_{KWW} , linked to the dispersion of the relaxation times, is reported to be related to intermolecular interactions through dielectric strength and steric hindrance provoked by side groups in polymers (Ngai and Roland, 1993b; Paluch et al., 2016). Despite differences in models using distribution of relaxation times for prediction of dynamic heterogeneities, there is a shared understanding that the dispersion does not fully govern structural relaxation dynamics (Ngai et al.,

2005; Roland et al., 2003; Romanini et al., 2017). It is often treated independently, whether in time or frequency. The dispersion and the structural relaxation time are determined separately, with β_{KWW} possibly remaining constant for different temperature and pressure combinations due to compensating effects on molecular mobility. However, the dispersion may vary as it depends on factors like specific volume, configurational entropy, and static structure factor (Ngai et al., 2005). The heterogeneous dynamics suggest that relaxation processes involve multiple independent relaxations, while the growing heterogeneity length scale is the cause of the drastic relaxation time increase with the system cooling. Therefore, a change in the heterogeneity characteristic length scale would typically alter the spectral shape of relaxation, and independent relaxation modes could deviate from time-temperature-pressure superposition (Niss and Hecksher, 2018).

As mentioned in Chapter 1, the stretching parameter β_{KWW} is present in approaches to predict the relaxation dynamics. It has been used for explaining the super-Arrhenius behaviors of relaxation time in the coupling model (Ngai, 2023). Moreover, β_{KWW} can be used as the contribution of the correlation function in the experimental calculation of the number of dynamically correlated units N_{corr} according to the dynamical heterogeneities (Berthier et al., 2005a; Capaccioli et al., 2008; Dalle-Ferrier et al., 2007a).

Figures 4-7d, 4-7e and 4-7f show the variations of β_{KWW} from 0.1 MPa up to 200 MPa as a function of the temperature for PVAc, EVA80 and EVA60, respectively. The stretching parameter β_{KWW} increases with temperature, and the temperature dependence of β_{KWW} seems to be shifted to higher temperature when pressure increases. This reflects the fact that polymer structure needs to be further compressed during heating to keep same dispersion of relaxation times.



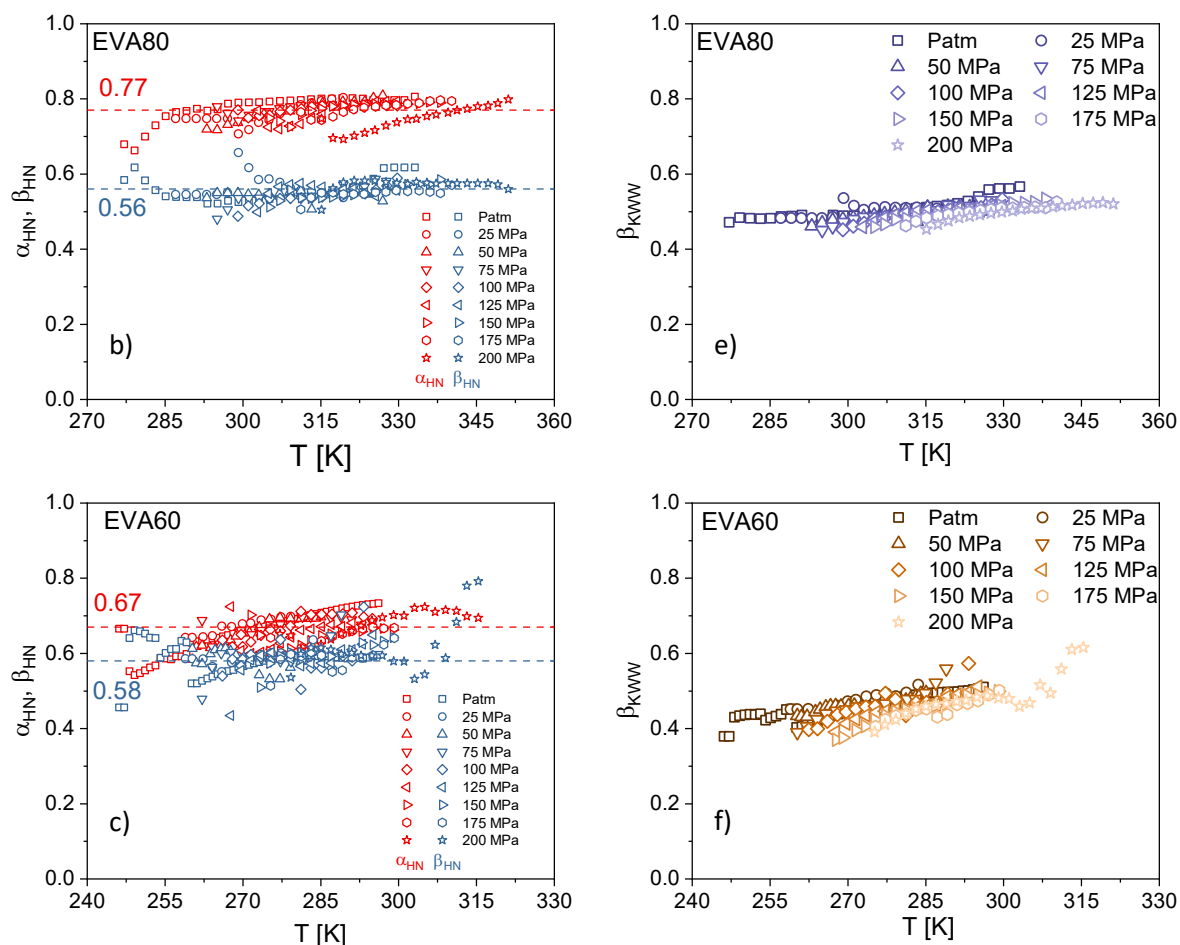


Figure 4-7. Isobaric temperature variations of the symmetric α_{HN} (blue symbols) and asymmetric β_{HN} (red symbols) broadening parameters from the segmental relaxation for a) PVAc, b) EVA80 and c) EVA60, and the stretching parameter β_{KWW} for d) PVAc, e) EVA80 and f) EVA60 in the same conditions. Blue and red dashed lines correspond to mean values of α_{HN} and β_{HN} values, respectively. Symbols for β_{KWW} values are differently colored for each pressure.

Studying the role of intermolecular interactions can be biased by multiple contributions due to pressure, temperature or volume. The dispersion of relaxation time can be interpreted following isovalues, i.e., isotherms, isobars, isochores and isochrones. The latter correspond to a constant average relaxation time. **Figure 3-5** illustrates the evolution of these configurations as a function of temperature and pressure.

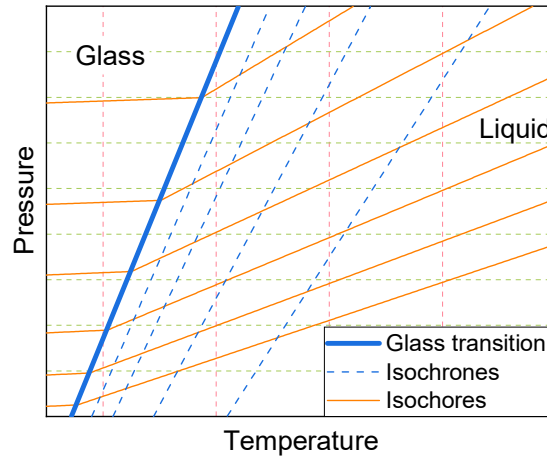
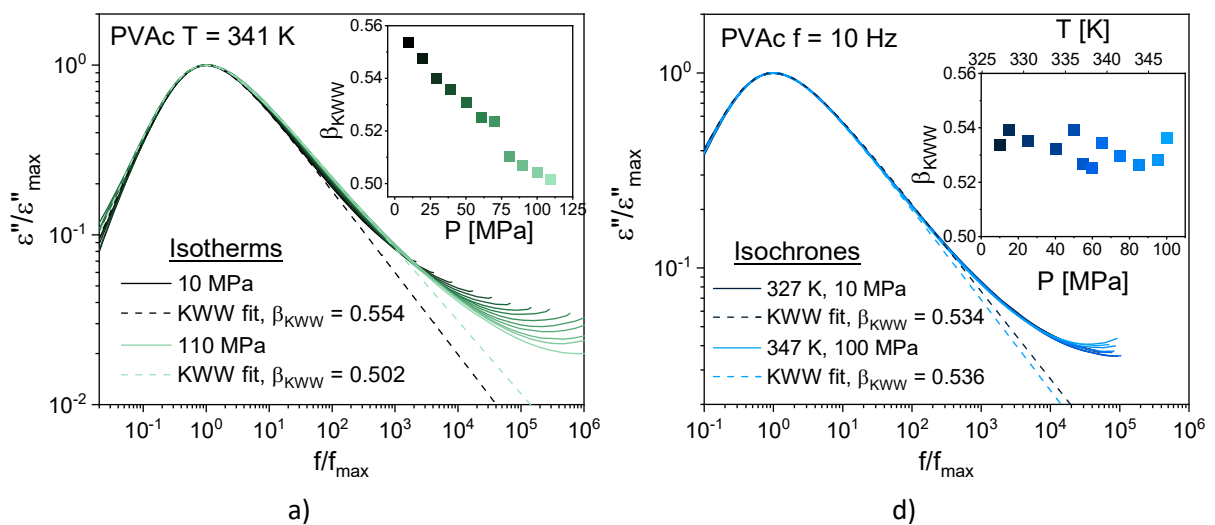


Figure 4-8. Schema of the temperature/pressure dependence of isochrones (blue dashed lines) and isochores (orange lines). The blue thicker line corresponds to the glass transition for a given cooling rate. The glassy state is at higher pressure or lower temperature from this line, the liquid state is at the opposite side. Vertical and horizontal dashed lines correspond to isotherms and isobars respectively. Adapted from (Niss and Hecksher, 2018).

As shown in **Figure 4-9**, the superposition of dielectric spectra offers a clear overview of the dispersion variations through isovalues. It consists of superimposing spectra by scaling to the maximum of dielectric loss (ϵ''_{max}) and its associated frequency ($f_{max} = 1/2\pi\tau$) of segmental relaxation peak. By this way, a master curve of the segmental relaxation is created, centered at $f/f_{max} = 1$ with an amplitude of $\epsilon''/\epsilon''_{max} = 1$. The dispersion is associated to β_{KWW} values. The numerical Fourier transforms of the KWW function for the lowest and highest values of temperature and/or pressure are superimposed in the master curves. β_{KWW} variations are also plotted as a function of temperature and/or pressure depending on the isovalues.



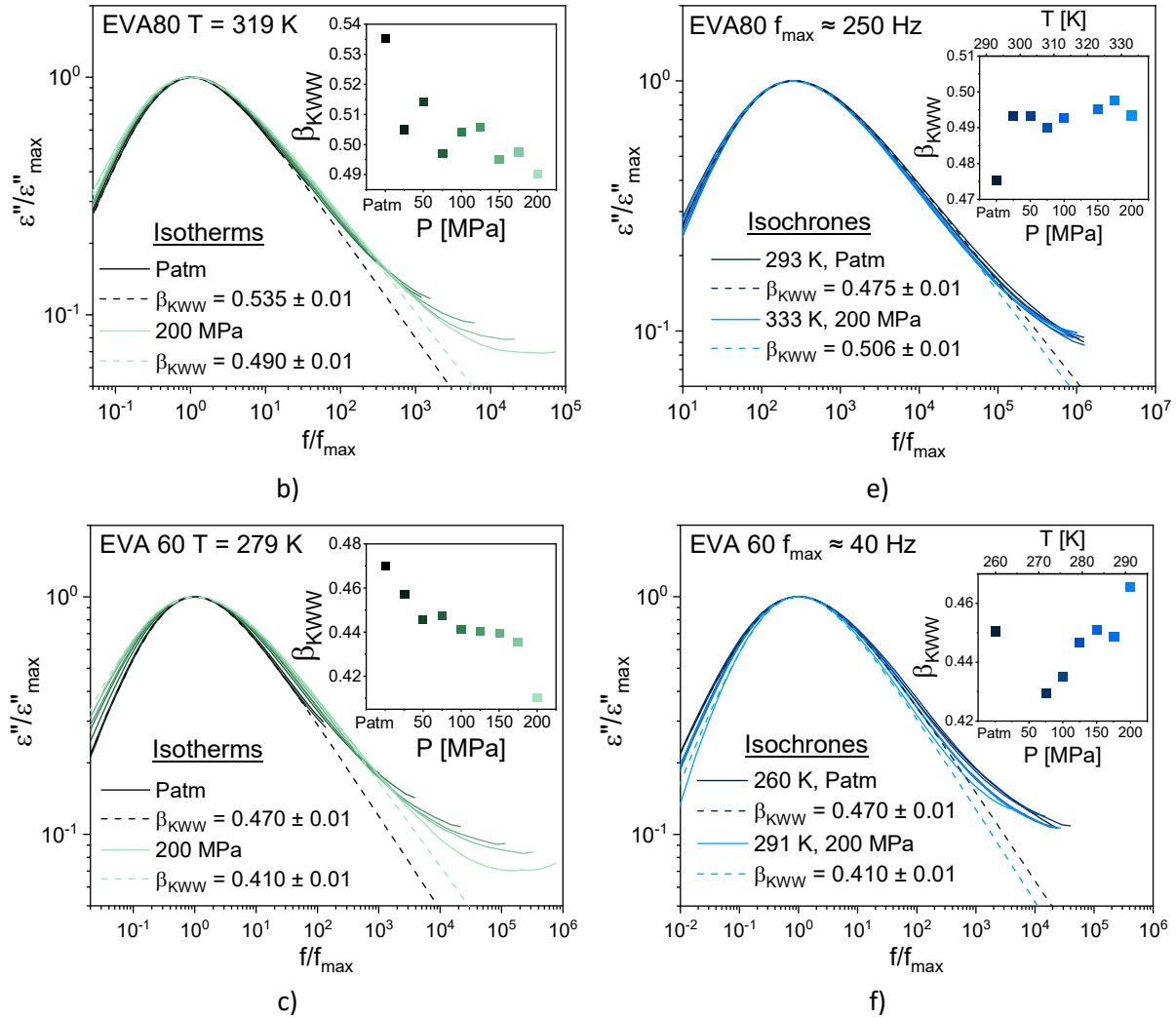


Figure 4-9. Log-log plot of the dielectric loss normalized to the peak maximum as a function of the normalized frequency for PVAc a) in isothermal conditions (341 K) from 0.1 MPa up to 110 MPa and b) in isochronal conditions (10 Hz), for EVA80 c) in isothermal conditions (319 K) from 0.1 MPa up to 200 MPa and d) in isochronal conditions (250 Hz), and for EVA60 a) in isothermal conditions (279 K) from 0.1 MPa up to 200 MPa, b) in isochronal conditions (40 Hz). The conductivity contribution has been removed from the spectra. The corresponding β_{KWW} values are plotted as a function of pressure, temperature or both in the insets.

Figures 4-9a, 4-9b and **4-9c** present the pressure superposition of dielectric loss spectra for PVAc, EVA80 and EVA60, respectively. As mentioned earlier, pressure increases the relaxation time dispersion since β_{KWW} values decrease (see inset in **Figures 4-9a, 4-9b** and **4-9c**). In the case of isochronal superposition, temperature and pressure vary by keeping τ constant. According to the literature (Hensel-Bielowka et al., 2004; Niss and Hecksher, 2018; Tölle et al., 1998), isochronal superposition does not exhibit any dispersion variations with pressure and temperature. It is a common feature of glass forming liquids when any secondary relaxations and excess wings occurred

close to the segmental relaxation. **Figures 4-9d, 4-9e** and **4-9f** show the isochronal superposition of dielectric spectra with f_{max} close to 10 Hz for PVAc, 250 Hz for EVA80 and 40 Hz for EVA60, respectively. The frequency is chosen for clearly observing the α -peak. As shown in the inset in **Figure 4-9d**, the superposition shows a stability of β_{KWW} with pressure and temperature when the data are compared under isochronal conditions. As already observed in literature (Ngai et al., 2005), invariance of the α -peak shape is noticed for PVAc. Such behavior is observed for EVA80 and EVA60 in the in **Figures 4-9e** and **4-9f**.

In a similar way than pressure superposition, for temperature superposition, the isobaric spectra are measured at different temperatures. **Figure 4-10a** shows the temperature superposition of dielectric loss spectra at 100 MPa. Temperature has an opposite effect on dispersion than pressure, i.e., β_{KWW} values increase with temperature, as shown in the inset in **Figure 4-10a**. Finally, the last isovalue is the isochore, which can be obtained by using different temperature and pressure combinations for a same specific volume. From PVT data of PVAc (taking from (Zoller and Walsh, 1995)), the evolution of dispersion under constant specific volume is achievable.

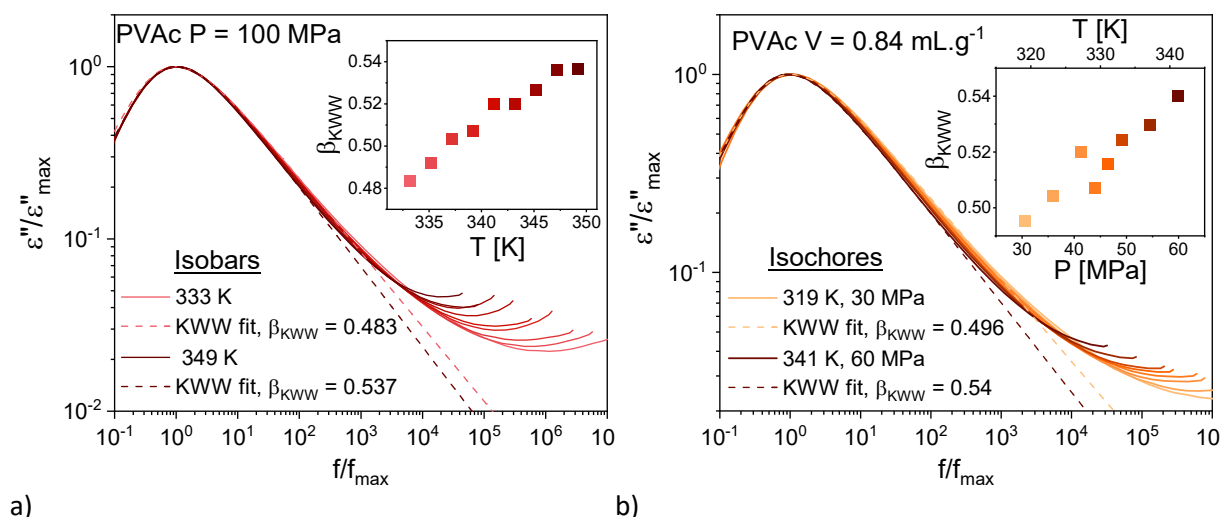


Figure 4-10. Log-log plot of the dielectric loss normalized to the peak maximum as a function of the normalized frequency for PVAc. a) Isobaric conditions (100 MPa) from 333 K up to 349 K. The corresponding β_{KWW} values are plotted as a function of temperature in the inset. b) Isochoric conditions (0.84 mL.g^{-1}). β_{KWW} values are given as a function of temperature and pressure in the inset. The conductivity contribution has been removed from the spectra.

As illustrated in **Figure 4-10b**, the specific volume superposition has been achieved for a $V = 0.84 \text{ g.mol}^{-1}$, for pressure varying from 30 MPa up to 60 MPa and coupled temperature varying from 319 K up to 341 K. The inset in **Figure 4-10b** shows that a larger dispersion of relaxation times at high

pressure/temperature is observed for the same specific volume. The influence of temperature on β_{KWW} predominates over that of pressure in isochoric conditions.

As mentioned earlier, a dispersion variation of segmental relaxation is attributed to a change of intermolecular interactions, which are related to cooperativity. The decrease in β_{KWW} with decreasing temperature or increasing pressure is qualitatively consistent with an increase in cooperativity with increasing relaxation time. Then, a stability of β_{KWW} in isochronal condition should lead to a constant cooperativity volume whatever the pressure and temperature for a given relaxation time.

2) Role of dipolar side group in interactions

The isobaric master curves at 100 MPa for PVAc, EVA80, EVA60 are presented in **Figure 4-11a**. Only 100 MPa isobar is presented for sake of clarity. The numerical Fourier transforms of the KWW used to fit the master curves are shown as dashed lines for each sample. Deviations from the KWW function are observed at high and low frequency ranges of the segmental relaxation. The low frequency deviations are due to the ohmic conduction related to the mobile charge carriers. The high frequency deviations arise from the involvement of non-cooperative and localized molecular mobility corresponding to the β -relaxation (Ngai and Paluch, 2004). **Figure 4-11b** shows the variations of β_{KWW} at various temperatures for PVAc, EVA80, EVA60 at 100 MPa calculated from **Equation 3-4**.

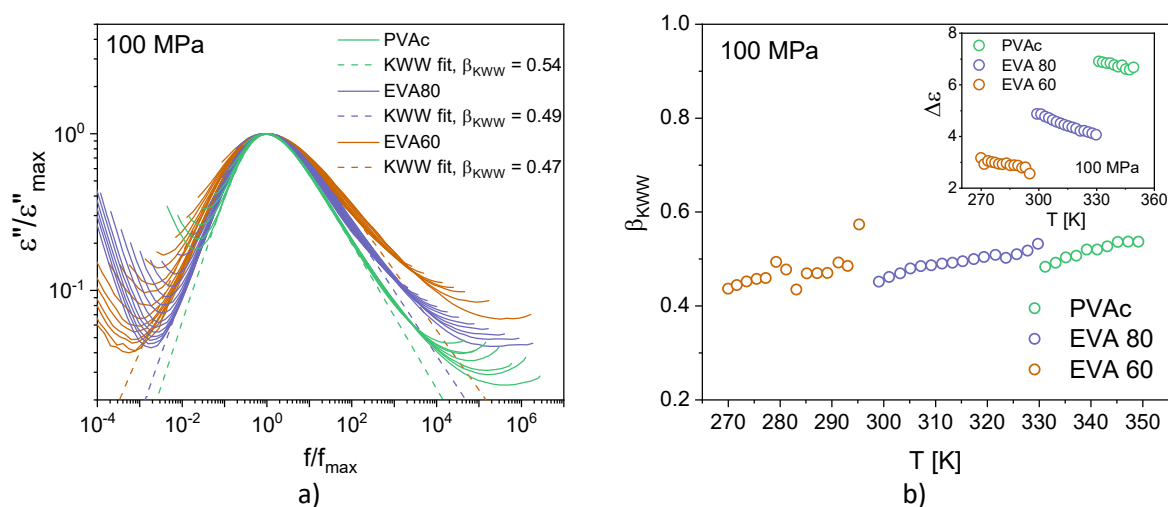


Figure 4-11. a) Log-log plot of the dielectric loss normalized to the peak maximum as a function of the normalized frequency at various temperatures for PVAc, EVA80, EVA60 at 100 MPa. An average β_{KWW} is given for each sample with uncertainty of ± 0.01 . b) Variations of the stretching parameter β_{KWW} at various temperatures for PVAc, EVA80, EVA60 at 100 MPa. The dielectric strength $\Delta\epsilon$ to the HN fit is plotted in the inset.

The β_{KWW} value shifts to higher values with temperature and VAc ratio increases, from 0.47 for EVA60 up to 0.54 for PVAc. The difference between these two β_{KWW} values is significant. Indeed, in the case

of a polymer whose chemical structure is modified for increasing intermolecular interactions, same β_{KWW} variations have been reported (Ngai and Roland, 1993a). Such an increase can be explained by a lower dispersion of the relaxation time due to an increase in the ratio of dipoles (Richert, 2002). These observations are consistent with those showing that intermolecular interactions, and therefore cooperativity, become more important with increasing VAc content (Puenta et al., 2015).

Previous studies have noticed coupled effects of intermolecular interaction decrease and dispersion increase. As an example, the addition of plasticizer, which increases the free volume, reduces the intermolecular interactions, while the β_{KWW} stretching parameters decreases (Araujo et al., 2018b). In the case of semi-crystalline polymers, the crystalline phase hinders the amorphous phase, increasing dispersion while cooperativity decreases (Ngai and Roland, 1993b; Delpouve et al., 2011; Hamonic et al., 2014; Esposito et al., 2016). Nevertheless, some glass forming liquids show opposite behavior, such as colloidal suspension of soft spherical particles (Mattsson et al., 2009; Ngai, 2011). The dielectric strength $\Delta\varepsilon$ is rather an indicator of such interactions according to the Debye theory of dielectric relaxation generalized by Kirkwood and Fröhlich (Kirkwood, 1940). Thus, $\Delta\varepsilon$ of the α -relaxation process depends on parameters that influence interactions: the mean dipole moment μ , the dipole density N/V of the process, and the Kirkwood correlation factor g_K . This factor considers short range intermolecular interactions related to the static correlation between the dipoles. Dielectric strength is therefore expressed with the following equation:

$$\Delta\varepsilon = \frac{1}{3\varepsilon_0} g_K \frac{\mu^2 N}{k_B T V}, \quad 4-2$$

where ε_0 is the dielectric permittivity of vacuum. As expressed in **Equation 4-2** and shown in the inset in **Figure 4-11b**, the dielectric strength is inversely proportional to the temperature. The $\Delta\varepsilon$ variations and the β_{KWW} increase are attributed to the reduction of intermolecular interactions due to the temperature (Nozaki and Mashimo, 1987; Yin et al., 2012; Déjardin et al., 2022). Schönhals has associated the increase of intermolecular interactions between dipoles with temperature decrease, to the cooperative character of the molecular motion, i.e., the lower the temperature, the stronger the cooperative interactions (Schönhals, 2001).

However, increase of intermolecular interactions is associated with increase of β_{KWW} values for structural hindrances, as already mentioned. Therefore, variations of the intermolecular interactions due to structural changes have an opposite influence on the stretching parameter than variations due to temperature change. In the case of EVA/PVAc, β_{KWW} increases as a function of VAc ratio, as well as intermolecular interactions. Paluch et al. have shown a correlation between $\Delta\varepsilon$ and β_{KWW} for

molecular glass formers (Paluch et al., 2016). This correlation is attributed to the nature of intermolecular interactions through dipole-dipole interactions. As mentioned by Paluch et al., since these interactions should be more harmonic when $\Delta\varepsilon$ is stronger, the dispersion of the relaxation times is narrower (Paluch et al., 2016). This observation is in agreement with the effect of intermolecular interactions on the dispersion of relaxation times (Reinsberg et al., 2002; Ngai, 2007) and cooperativity mentioned in literature (Bauer et al., 2013; Hempel et al., 2000).

III. Intermolecular interaction and cooperativity

1) Isobaric cooperativity

Using the extended Donth's approach, cooperativity volume is determined in isobaric conditions from **Equation 2-20** (p. 82) used in Chapter 3. **Figure 3-6** shows the evolution of cooperativity volume V_α as a function of the relaxation time for pressure from P_{atm} up to 50 MPa. Relaxation time seems to govern the evolution of the cooperativity for a given chemical structure, varying with pressure and temperature along a master curve. This observation meets the steadiness of β_{KWW} in isochronal conditions, i.e., the dispersion is unchanged at constant relaxation time whatever the temperature and pressure in supercooled liquids for PVAc (Ngai et al., 2005).

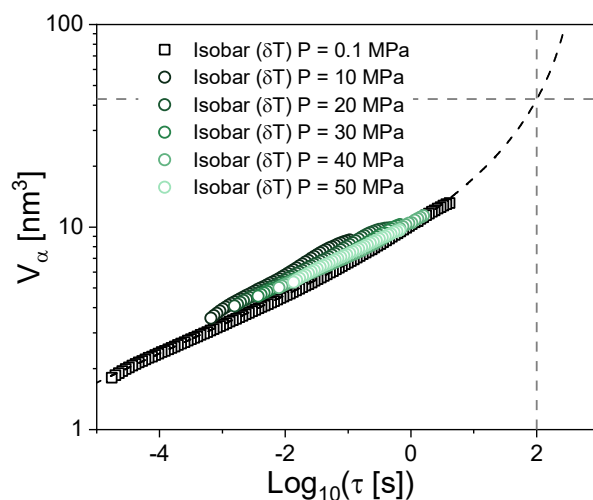


Figure 4-12. Cooperativity volume as a function of the relaxation time for isobaric measurements, from P_{atm} up to 50 MPa. The black dashed line corresponds to the extrapolated function of cooperativity volume from the extrapolation of parameters of **Equation 2-20** (p. 82). Dashed grey lines corresponds to relaxation time of 100 s and cooperativity volume of $42,9 \text{ nm}^3$.

The extrapolation of cooperativity volume leads to an approximated cooperativity volume of 40 nm^3 at $\tau = 100 \text{ s}$. This value agrees with the characteristic heterogeneity length of $\xi_\alpha = \sqrt[3]{V_\alpha} \approx 3 \text{ nm}$ at the glass transition temperature (Saiter et al., 2010).

The extended Donth's approach have limits in pressure with the HP-BDS setup. Since the temperature cannot heat at temperature higher than 393 K, the higher the pressure, the fewer the temperature range between the glass transition and the maximal temperature reachable by the HP-BDS.

2) Cooperativity from pressure fluctuation

Conversely, when the temperature of isothermal measurement rises, the pressure range for performing dielectric measurement becomes larger. Determining the cooperativity volume from isothermal measurements could solve the limitation encounters with isobaric measurements. Donth also proposed a formula for determining the CRR volume V_α from pressure fluctuations such as (Donth, 2001):

$$V_\alpha = \frac{\left[\frac{1}{\kappa_{T, \text{glass}}} - \frac{1}{\kappa_{T, \text{liquid}}} \right]}{(\delta P)^2} k_B T, \quad 4-3$$

where $\kappa_{T, \text{glass}}$ and $\kappa_{T, \text{liquid}}$ are the isothermal compressibilities of glass and liquid, δP is the pressure fluctuation, k_B is the Boltzmann's constant and T is the temperature. In the original equation, Donth uses the adiabatic compressibility, i.e., at constant entropy. Here, it is assumed that this quantity is almost equal to the isothermal compressibility. Pressure fluctuations δP are determined by approximating the isochronal curves of dielectric loss ε'' by a Gaussian fit (**Equation 2-21**, p. 83). For this purpose, the isobaric measurements used in Chapter 3 (see **Figure 3-5c**, p. 95) for a unique temperature are expressed in isochronal manner. **Figure 4-13a** represents the isochronal curves of dielectric loss ε'' normalized to the peak maximum for PVAc ranging from 100 mHz up to 300 Hz. As the method based on thermal fluctuations, the pressure fluctuation corresponds to the standard deviation of the Gaussian fit.

Figure 4-13b shows evolution of pressure fluctuations for several isotherms. The pressure fluctuations decrease with a rise in pressure. Analogically to the thermal fluctuation, when the relaxation time dispersions are supposed to become extremely larger approaching the glass transition, pressure and thermal fluctuations decrease drastically. It is noteworthy that the pressure reachable at 345 K is getting close to 200 MPa.

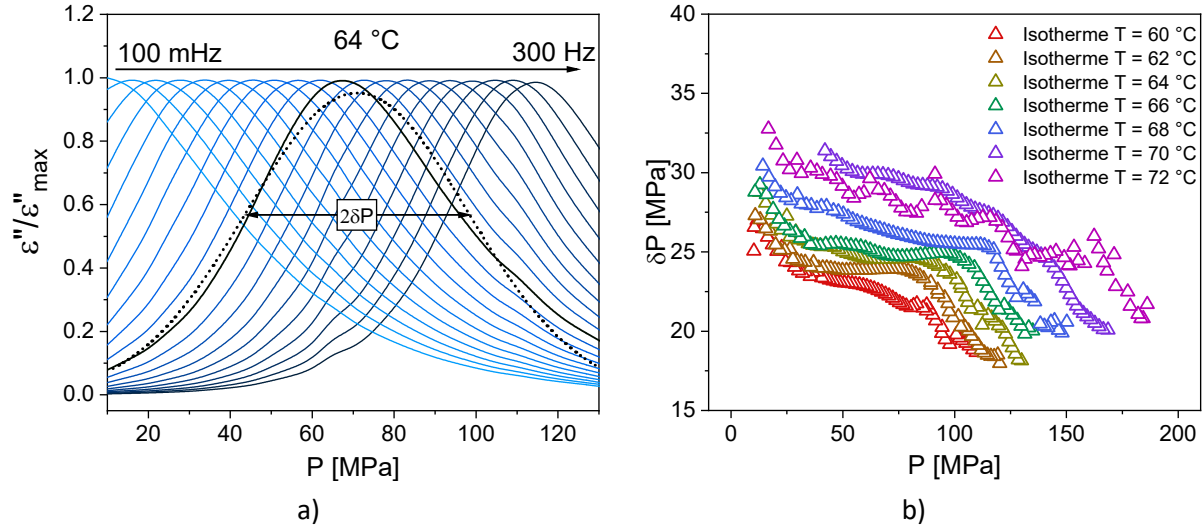


Figure 4-13. a) Isochronal spectra of the imaginary part of the complex permittivity ε'' normalized to the peak maximum as a function of pressure and frequency for PVAc. The black filled curve corresponds to a frequency of 4 Hz. The short dot line is its Gaussian fit to calculate the mean pressure fluctuation δP from the standard deviation. b) Mean pressure fluctuation δP as a function of pressure. Pressure fluctuation δP are determined for isothermal measurement from 333 K up to 345 K.

The isothermal compressibility κ_T is determined from the extrapolation of PVT measurements of PVAc, according to the expression:

$$\kappa_T = -\frac{1}{V} \left(\frac{\partial V}{\partial P} \right)_T. \quad 4-4$$

The volumes of glass and liquid must be extrapolated for large temperature and pressure. The Tait's equation allows such extrapolation, by using the PVT data shown in **Figure 3-14** (p. 106). Parameters of the Tait's equation for PVAc liquid and glass are referenced in **Table 3-4**. Since PVT data of EVA80 and EVA60 have not yet been measured in the literature, their volume variations are not estimated. Therefore, only the cooperativity volume determined with pressure variation of PVAc is presented here.

Table 4-2. Parameters of the Tait's equation (**Equation 1-36**, p. 40) for PVAc glass and liquid.

Polymer	A_0 [mL. g ⁻¹]	A_1 [mL. g ⁻¹ . K ⁻¹]	A_2 [mL. g ⁻¹ . K ⁻²]	b_0 [bar]	b_1 [K ⁻¹]
PVAc glass	8.30×10^{-1}	2.46×10^{-5}	5.10×10^{-7}	3.14×10^4	2.64×10^{-3}
PVAc liquid	8.28×10^{-1}	5.31×10^{-4}	5.17×10^{-7}	2.43×10^4	4.94×10^{-3}

Figure 4-14a shows the surface of extrapolated volume of glass and liquid for PVAc. According to the thermodynamics, the liquid volume shows a steeper variation as a function of temperature and pressure than the glass volume.

Therefore, the difference of isothermal compressibility inverses of glass and liquid, expressed as:

$$\Delta\left(\frac{1}{\kappa_T}\right) = \frac{1}{\kappa_{T, \text{glass}}} - \frac{1}{\kappa_{T, \text{liquid}}}, \quad 4-5$$

can be obtained, as shown in **Figure 4-14b**. $\Delta(1/\kappa_T)$ seems to be relatively linear at high pressure, but it seems to have a null steepness approaching the atmospheric pressure.

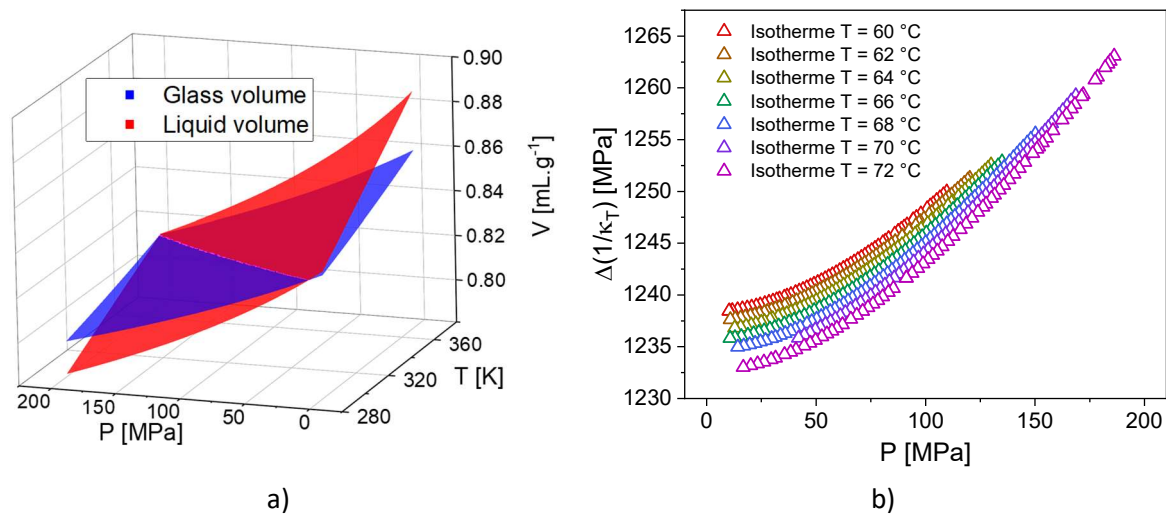


Figure 4-14. a) Extrapolated glass (blue) and liquid (red) volumes of PVAc. The surfaces are determined from the Tait's equation parameters of the **Table 3-4**. b) Variation of the difference of isothermal compressibility inverse of glass and liquid $\Delta(1/\kappa_T)$ as a function of pressure for isotherms.

3) Isothermal cooperativity

All the parameters of the **Equation 4-3** have been calculated, then the cooperativity volume in isothermal conditions can be derived. **Figure 4-15a** shows the evolution of V_α as a function of pressure. The cooperativity volume is quite stable at low pressure and increases approaching the glass transition pressure P_g . It is noteworthy that the values of V_α at low pressure seems high compared to the values obtained from thermal fluctuation atmospheric pressure. Thus, the V_α from isothermal measurements can be expressed as a function of the relaxation time, as shown in **Figure 4-15b**. For relaxation time inferior to ~ 0.1 s, the cooperativity volume from isothermal measurements are higher than the cooperativity volume from isobaric measurements at P_{atm} . Donth has already remarked that cooperativity volumes from **Equation 4-3** are larger than that obtained from **Equation 2-20** (p. 82)

(Donth, 2001). However, approaching the glass transition, values of cooperativity volume seem to overlap.

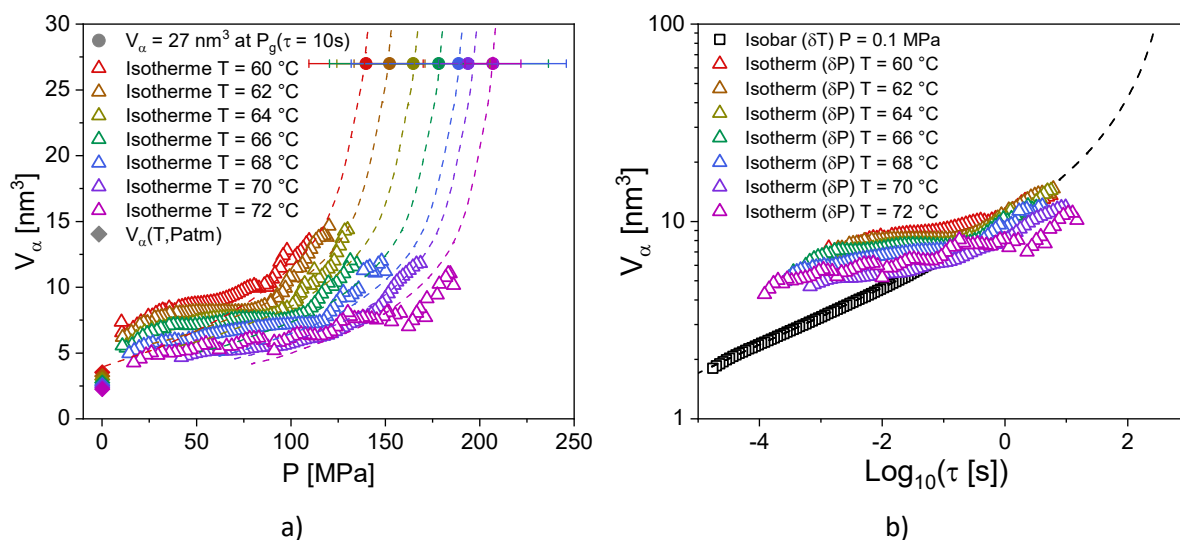


Figure 4-15. Cooperativity volume as a function of the pressure for isobaric measurements (empty up triangles), from 333 K up to 345 K. The filled circles correspond to a cooperativity volume of 27 nm^3 at the glass transition pressure P_g defined when the relaxation time $\tau = 100 \text{ s}$. The filled diamonds represent the values of cooperativity from the thermal fluctuations at P_{atm} . The dashed lines correspond to a guide for the eyes, going from $V_\alpha(T, P_{atm})$ up to $V_\alpha(T, P_g)$. b) Cooperativity volume as a function of the relaxation time for isothermal measurements. The black dashed line corresponds to the extrapolated function of cooperativity volume derived from thermal fluctuation at P_{atm} , which are represented by the black empty squares.

The overlap of cooperativity volume from the isothermal measurements is consistent with the overlap of cooperativity volume from the isobaric measurements and the steadiness of β_{KWW} in isochronal conditions. Therefore, intermolecular interactions, which are followed with the dispersion of relaxation times, provide as qualitative information as the variation of cooperativity volume.

IV. Role of intra and intermolecular interactions on segmental relaxation

Another approach for evaluating the intermolecular interactions is achievable with the determination of the activation volume ΔV^\ddagger (Drozd-Rzoska, 2019; Grzybowski et al., 2017). This value is defined from the isothermal relaxation times but can be also obtained from isobaric measurements (Paluch et al., 2001).

1) Segmental mobility of PVAc/EVA series as a function of temperature and pressure

For all the samples, the temperature dependence of the relaxation time with pressure is plotted in the Arrhenius representation (**Figure 3-7**). Relaxation time is taken at the maximum of the α -relaxation

peak, namely τ_{max} . The curves are well fitted by the VFTH law (see **Equation 1-1**, p. 7). The fit parameters are reported in **Table A-4** of **Appendix**. The temperature decrease and the pressure increase have comparable effects on the molecular mobility, resulting in an increase of both scenarios.

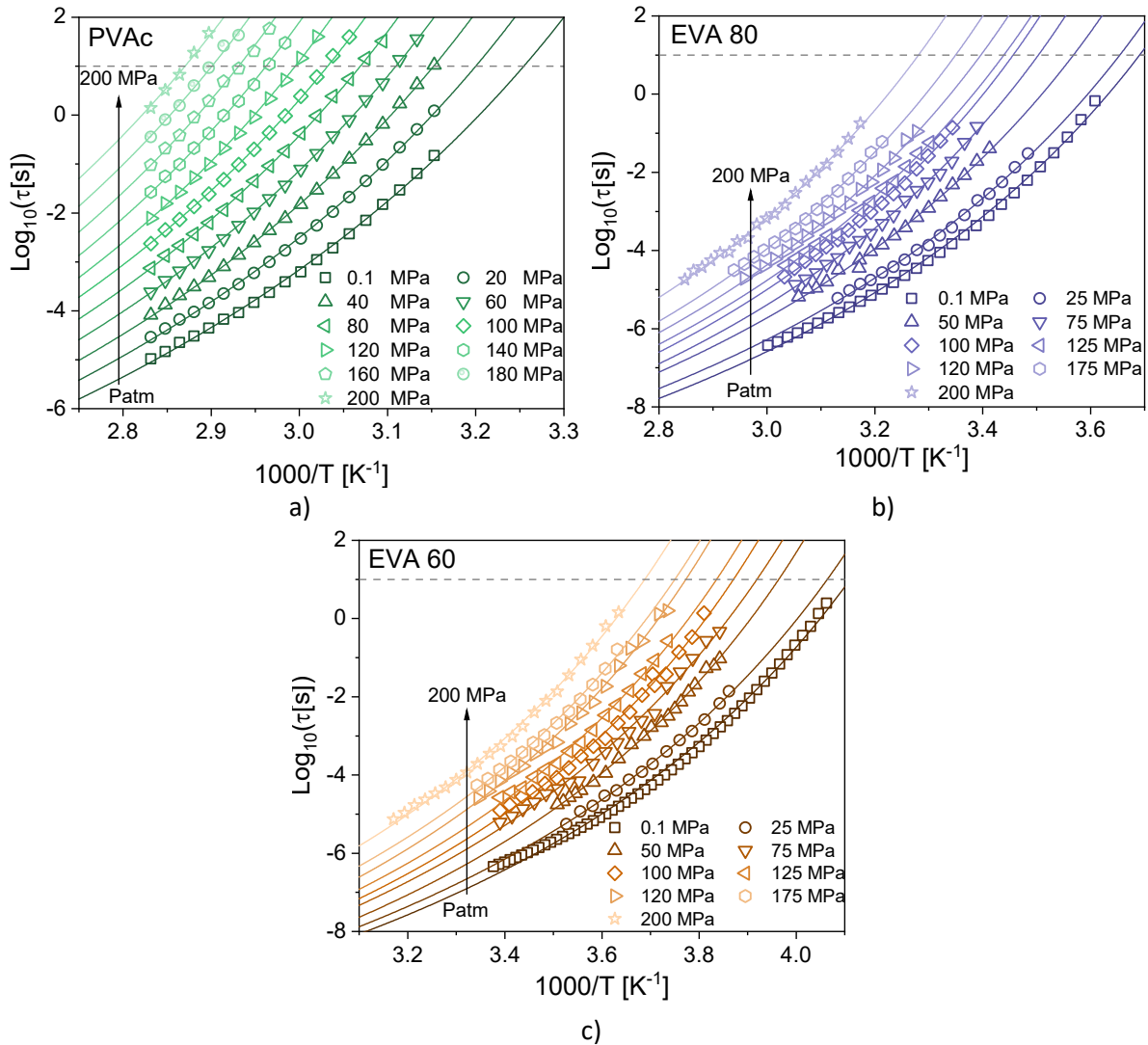


Figure 4-16. Logarithm of the dielectric relaxation time as a function of the inverse temperature for a) PVAc, b) EVA80 and c) EVA60 under pressure. Solid lines represent the VFTH fits with colors for each pressure. The dashed grey lines correspond to $\tau = 100$ s, i.e., to the calorimetric glass transition temperature T_g .

The glass transition temperature T_g was taken at $\tau = 100$ s. According to the data obtained from VFTH fits, the pressure influence on T_g can be analyzed for the PVAc/EVA series as shown in **Figure 3-8**. The glass transition temperature increases nonlinearly with the pressure. Thus, the experimental data can be fitted by an Andersson-Andersson model (**Equation 1-39**, p. 44).

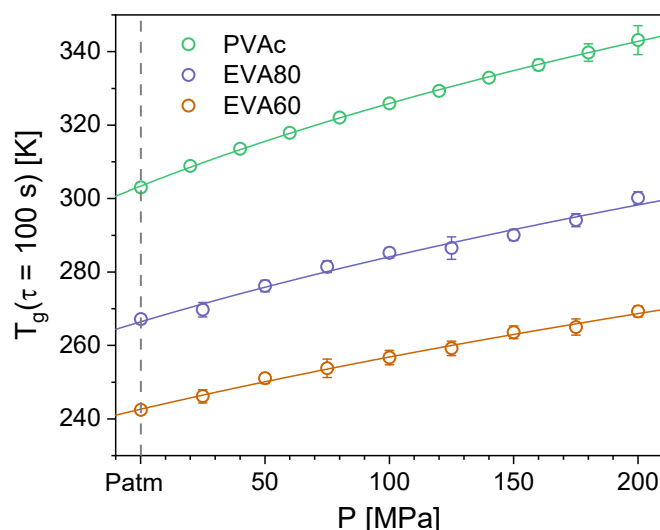


Figure 4-17. Pressure dependence of the glass transition temperature (from the extrapolation of VFTH fit to $\tau = 100$ s) for EVA60, EVA80 and PVAc. Solid lines indicate an experimental data fit to the Andersson–Andersson model.

The T_g differences observed in **Figure 3-3b** and depending on the VAc ratio, are also maintained in **Figure 3-8** as pressure increase, while the T_g increases with pressure. The Andersson’s model parameters are listed in **Table 3-2**.

Table 4-3. Fit parameters (T_g^0 , b , Π), their uncertainties and the R-squared of the Andersson’s model (**Equation 1-39**, p. 44) for EVA60, EVA80 and PVAc.

Polymer	T_g^0	ΔT_g^0	b	Δb	Π	$\Delta \Pi$	R^2
EVA60	348	0.29	11.2	1.5	80	4.8	0.99943
EVA80	330	0.28	7.0	1.4	177	9.9	0.99898
PVAc	304	0.04	5.5	0.2	212	1.8	0.99997

2) Activation volume

From the glass transition and the isobaric fragility variations as a function of the pressure, the activation volume at the glass transition is calculated from (Paluch et al., 2001):

$$\Delta V^\# = m_p k_B \frac{dT_g}{dP} \ln 10. \quad 4-6$$

Classically, the higher the pressure at constant temperature, the higher the activation volume. As introduced in Chapter1, $\Delta V^\#(P, T)$ expresses the difference between, an activated volume $V_A(T)$ and a non-activated volume $V_{NA}(P, T)$ (Floudas, 2004). The activated volume $V_A(T)$ is the volume allowing

the relaxation of a structural unit. It decreases with the rise in temperature, and it is pressure independent. V_{NA} expresses a volume which does not allow relaxation. As the free volume, V_{NA} should decrease with pressure increase at constant temperature. **Figure 4-18** presents the evolution of $\Delta V^\#$ at the glass transition temperature as a function of the pressure. PVAc shows the highest value at atmospheric pressure. Whatever the sample, $\Delta V^\#$ decreases with a rise in pressure, a behavior which has been reported in many glass forming liquids (Paluch et al., 2002b; Casalini et al., 2003; Mpoukouvalas et al., 2009). During the pressure increase, V_{NA} decreases due to free volume compression. In the meantime, $V_A(T_g)$ decreases with pressure due to T_g increase. The fact that $\Delta V^\#$ at T_g diminishes with a rise in pressure indicates that $V_{NA}(P, T_g)$ contraction is weaker than $V_A(T_g)$. Since $\Delta V^\#$ has been related to CRR volume V_α (Hong et al., 2011a; Błażytko et al., 2024), the activation volume $\Delta V^\#$ values are correlated to the intensity of the intermolecular interactions in the PVAc/EVA copolymers.

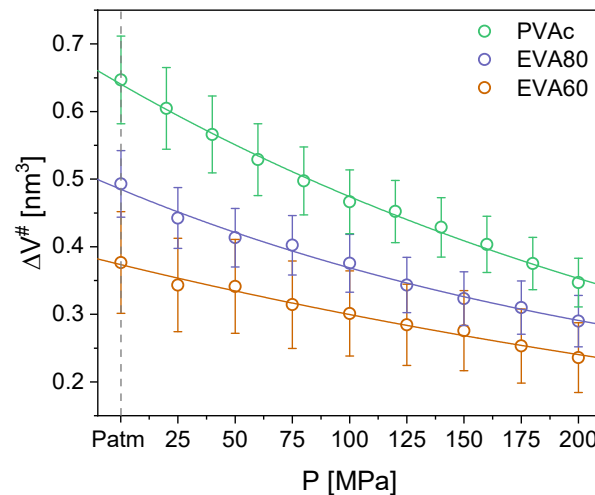


Figure 4-18. Activation volume $\Delta V^\#$ at $T_g(P)$ as a function of the pressure. The lines correspond to a one-phase exponential decay function, it serves as a guide for the eyes. The vertical dashed line corresponds to the atmospheric pressure.

3) Thermal and volumetric contributions of isobaric fragility in PVAc/EVA series

According to the equation separating the volumetric and thermal contributions of the isobaric fragility m_p :

$$m_V = m_p - \frac{\Delta V^\#}{\ln 10} \frac{\alpha}{k_B \kappa}, \quad 4-7$$

the volumetric contribution can be deduced from the activation volume $\Delta V^\#$ by assuming that the ratio of thermal expansion to compressibility α/κ is equal to $\approx 1.5 \text{ MPa} \cdot \text{K}^{-1}$. The effect of pressure

on the isobaric fragility m_p , volumetric $m_p - m_v$ and thermal m_v contributions for the PVAc/EVA series are presented at T_g in **Figure 4-19**.

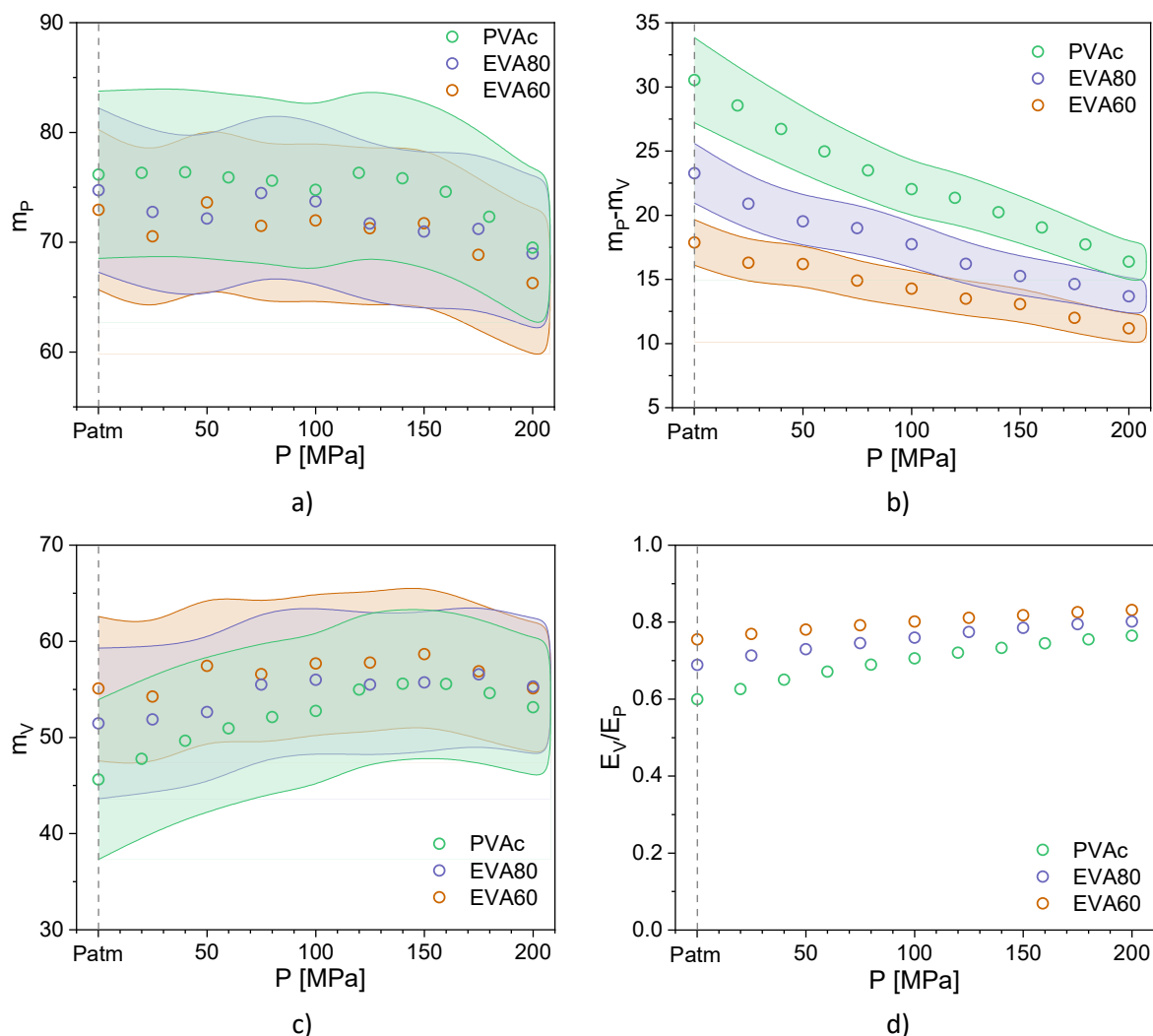


Figure 4-19. a) . a) Isobaric fragility m_p , b) volumetric contribution ($m_p - m_v$) and c) thermal contribution m_v as the function of the pressure for PVAc in green, EVA80 in blue and EVA60 in brown. The colored areas are the uncertainty zones of the values. d) Ratio E_v/E_p as a function of pressure. The vertical dashed lines correspond to the atmospheric pressure.

As shown in **Figure 4-19b**, a decrease of the volumetric contribution is observed with the pressure increase whatever the sample. Supported by preliminary results at atmospheric pressure, the m_p values appear to be weakly sensitive to pressure variations, and to the different ratios of vinyl acetate groups. According to the literature, the volumetric contribution is mainly related to the intermolecular interactions and the free volume ratio in the liquid-like state (Araujo et al., 2018a), which may depend on the amount of lateral groups causing the steric hindrance (Ngai and Roland, 1993a). The volumetric contribution values in the PVAc/EVA series are consistent with the density of intermolecular

interactions due to the VAc ratio. Thus, the reduction of these interactions at the glass transition due to the pressure agrees with the reduction of the free volume in the samples. Previous works supported the idea that such increases in intermolecular interactions due to the VAc ratio are correlated with the evolution of the cooperativity volume (Puentes et al., 2015).

As shown in **Figure 4-19c**, the thermal contribution shows a slight increase for PVAc values with the pressure, while it remains fairly stable for EVA60. In the literature, m_V is characterized as a purely energetic factor, influenced by the types of intermolecular and intramolecular bonds, as well as the internal degrees of freedom within the molecules (Hong et al., 2011a). Thus, some studies have suggested that the thermal contribution may be impacted by the backbone stiffness (Kunal et al., 2008; Dudowicz et al., 2005b). Although m_V values are in the uncertainty range, the PVAc/EVA series should not have such variations, since the main carbon chain remains the same in the whole series. At high pressure, the impact of the pendant group on the thermal contribution m_V is reduced, and therefore, values for PVAc and EVA80 seem to reach the steadiness of EVA60. Such behavior leads to the assumption that the backbone stiffness is not the only feature affecting the thermal contribution.

It can be assumed that the side groups have an impact on the thermal contribution, which could be provoked by the packing efficiency. Also called chain packing, it describes the order in which chains are grouped together within the amorphous polymer (Dudowicz et al., 2005a). It is influenced by the flexibility of the chain backbone and side groups, as well as by the processing and cooling conditions of polymers (Kunal et al., 2008; Mapesa et al., 2020). High packing efficiency means that polymer chains are tightly and uniformly arranged. This results in a reduction in free volume and an increase in local density (Pan et al., 2007). Variations in packing efficiency directly influence the polymer mechanical properties, such as brittleness and fracture resistance (Huang et al., 2015; Zhang et al., 2024). In general, an increase in packing efficiency is associated with an increase in brittleness, whereas a decrease in packing efficiency is associated with higher chain mobility and ductility. For polymer blends of poly(lactic acid) and EVA with VAc ranging from 50 wt. % up to 80 wt. %, the higher the VAc ratio, the more brittle the sample (Ma et al., 2012). Stukalin et al. demonstrated that the packing efficiency of macromolecules can be enhanced when the flexibility of chain side groups is increased (Stukalin et al., 2009). Studies have shown that a change in packing efficiency could be correlated with a reduction of m_V without changing the polymer chemical structure (Delpouve et al., 2014; Zhang et al., 2024). They have observed an increase of the thermal contribution m_V due to an increase in the degrees of freedom in the mobile amorphous fraction of semi-crystalline polymers. That degrees of freedom are associated to the packing efficiency of the amorphous chain (Delpouve et al., 2014).

As presented in Chapter 1, another approach for comparing the thermal and volumetric contributions is presented in the literature (Floudas et al., 2006; Roland et al., 2005). It consists in calculating the ratio between the constant-volume activation energy E_V and the constant-pressure activation energy E_P at the glass transition. This ratio at T_g is equal to the ratio between isochoric and isobaric fragilities m_V/m_P (Casalini and Roland, 2004b). **Figure 4-19d** shows an increase of the ratio E_V/E_P with pressure whatever the sample. Supported by the literature (Floudas et al., 2006; Rams-Baron et al., 2024), it indicates that the pressure increases the thermal contribution rate despite the volumetric contribution rate. This observation is consistent with the variations of the volumetric and thermal contributions in **Figures 4-19b** and **4-19c** respectively. Moreover, the lower the VAc ratio, the more the thermal activation process dominates the relaxation process. The value for EVA60 at P_{atm} ($E_V/E_P \approx 0.75$) is reached for EVA80 and PVAc at pressures of 100 MPa and 200 MPa, respectively.

The invariance of the isobaric fragility at atmospheric pressure in the PVAc/EVA series can be explained by the thermal and volumetric contributions, which offset each other with the VAc ratio. On the one hand, the volumetric contribution increases with the VAc ratio due to intermolecular interactions, and thus the associated cooperativity also increases. On the other hand, the thermal contribution decreases with VAc ratio. Such variation could be explained by the change in packing efficiency with the density of the dipolar side group in the PVAc/EVA series. The VAc ratio in this series has a combined effect on the isobaric fragility m_P , which keeps its value constant at atmospheric pressure, while the thermal contribution predominates over the volumetric contribution toward high pressure.

V. Conclusion

The analysis of the segmental relaxation spectra allows getting an idea of the dispersion of the characteristic relaxation time distributions, and evaluating the intermolecular interactions through the dielectric strength. Isothermal, isobaric, isochoric and isochronal configurations are investigated to quantify these interactions for PVAc/EVA series. The opposite effects of temperature and pressure are confronted, showing that increasing both at constant volume implies a dispersion decrease, while at constant average relaxation time, the dispersion remains constant. The activation volume values $\Delta V^\#$ at the glass transition, are consistent with the amount of intermolecular interactions related to the VAc ratio. From the activation volume $\Delta V^\#$, the volumetric ($m_P - m_V$) and thermal (m_V) contributions of the isobaric fragility m_P are deduced. The VAc ratio increase in the chain structure seems clearly correlated with an increase of ($m_P - m_V$), this volumetric contribution diminishing with a rise in pressure, and the thermal one converging towards the same value at high pressure. Thus, only

the backbone stiffness seems to influence the thermal contribution at high pressure. Nonetheless, PVAc has the lowest m_V value at atmospheric pressure, such behavior being counter-intuitive since the backbone flexibility is the same than for EVA60 and EVA80. Therefore, the notion of packing efficiency seems to be another way for explaining such thermal contribution differences. Indeed, the VAc groups seem facilitate the packing efficiency, thereby lowering m_V . Thus, the question of the steadiness of the isobaric fragility whatever the VAc ratio seems to find answer in its volumetric and thermal contributions. The sum of the two contributions justifies why the PVAc/EVA series keeps the same isobaric fragility separately from the rate of dipole in the macromolecular chain.

List of abbreviations and symbols

Symbols		ω	Angular frequency
C'_p	Reversing heat capacity		
C''_p	Non-reversing heat capacity	Abbreviations	
E_p	Isobaric activation energy	BDS	Broadband Dielectric Spectroscopy
E_V	Isochoric activation energy	CRR	Cooperative Rearranging Region
f	Frequency	HP-BDS	Broadband Dielectric Spectroscopy High Pressure
k_B	Boltzmann's constant	KWW	Kohlrausch–Williams–Watts
M_n	Average molecular mass	MT-DSC	Modulated temperature differential scanning calorimetry
m_p	Isobaric fragility	NMR	Nuclear magnetic resonance
$m_p - m_V$	Volumetric contribution of m_p	HN	Havriliak-Negami
m_V	Isochoric fragility Thermal contribution of m_p	TTS	Time Temperature Superposition
N_α	Number of structural units of a CRR	VFTH	Vogel-Fulcher-Tamman-Hesse
P	Pressure		
P_{atm}	Atmospheric pressure	Polymer abbreviations	
P_g	Glass transition pressure	EVA	Poly(ethylene-vinyl acetate)
T	Temperature	PDAI	Poly(di- <i>n</i> -alkylitaconate)
T_g	Glass transition temperature	PEF	Poly(ethylene furandicarboxylate)
T_g^0	T_g at atmospheric pressure	PET	Polyethylene terephthalate
T_α	Dynamic glass transition temperature	PIB	Polyisobutylene
V_α	Cooperativity volume	PLA	Poly(lactide acid)
α_{HN}	Symmetric broadening parameter	PMMA	Poly(methyl methacrylate)
β_{HN}	Asymmetric broadening parameter	PS	Polystyrene
β_{KWW}	Stretching exponent	PVAc	Poly(vinyl acetate)
δT	Temperature fluctuation	VAc	Vinyl acetate
Δx	Uncertainty of the x parameter		
$\Delta \varepsilon$	Dielectric strength		
κ_T	Isothermal compressibility		
ε	relative dielectric permittivity		
ε'	Dielectric storage		
ε''	Dielectric loss		
ε^*	Complex dielectric function		
ε_0	Dielectric permittivity of vacuum		
ρ	Density		
ξ_α	Characteristic length scale of CRR		
σ_0	Ohmic conduction		
τ_{max}	Relaxation time		

Conclusions and Perspectives

In this work, the influence of the chemical structure on the molecular mobility at the glass transition is studied in amorphous thermoplastic polymers. The study focuses on the role of backbone chain stiffness using a series of polymers including the poly(lactide acid) PLA, the poly(ethylene terephthalate glycol) PETg and the poly(vinyl acetate) PVAc, and on the role of dipolar side group using the PVAc and poly(ethylene-co-vinyl acetate) (EVA) series. For this purpose, the molecular dynamics of these thermoplastic polymers are studied by separating the isobaric fragility m_p into its thermal (m_V) and volumetric ($m_p - m_V$) contributions. Using HP-BDS, the relaxation time is therefore analyzed as a function of temperature, pressure and specific volume.

In Chapter 1, the segmental relaxation behavior of PETg, PLA, and PVAc is studied. The critical parameter for calculating the volumetric contribution is the activation volume ΔV^\ddagger . The relationship between the cooperativity volume V_α defined from the Donth's approach and the activation volume ΔV^\ddagger calculated from isobaric measurements is validated and extended above the glass transition using the extended Donth's approach. It has been found that cooperativity correlates better with the volumetric contribution of m_p than with the isobaric fragility itself. Despite the similarity of PLA and PETg in terms of m_p at atmospheric pressure, this study reveals that the thermal contribution m_V of PLA and PETg show significantly different variations with pressure. Furthermore, the fragility values at atmospheric pressure are correlated with the evolution of the thermal and volumetric contributions. In particular, the high isobaric fragility values for PLA at atmospheric pressure are related to the magnitude of the thermal contribution, which is related to the stiffness of the polymer backbone and the packing efficiency. The volumetric contribution $m_p - m_V$ associated with interchain interactions decreases significantly with increasing pressure for PLA, PETg, and PVAc. The isobaric fragility seems to converge to values of around 60-90 at high pressure. This suggests that at high pressure, the glass transition temperature becomes so significant that the volumetric contributions reach a universal value, independent of the chemical structure of the polymers.

In Chapter 2, the molecular mobility of the PVAc/EVA series is studied. The segmental relaxation spectra provide insights into a qualitative correlation between the dispersion of the characteristic relaxation time and intermolecular interactions through cooperativity volume. The study shows that increasing both temperature and pressure at constant volume reduces the dispersion, while at constant average relaxation time, the dispersion remains constant. This behavior is supported by the determination of cooperativity volume in both isobaric and isothermal conditions. The cooperativity volume is found to scale a master curve when it is expressed as function of relaxation times. The

activation volume at the glass transition is consistent with the level of intermolecular interactions associated with the VAc ratio. As the VAc ratio in the polymer chain increases, the volumetric contribution $m_p - m_V$ also increases while decreasing with higher pressure. Meanwhile, the thermal contribution approaches a common value at elevated pressures. Therefore, at high pressure, only the stiffness of the polymer backbone seems to affect the thermal contribution. Notably, PVAc show the lowest m_V value at atmospheric pressure, which is surprising given its comparable backbone flexibility to EVA60 and EVA80. This suggests that packing efficiency is a significant contributor to the differences in thermal contribution. Increasing the ratio of VAc groups improves the effect of the packing efficiency, thereby reducing m_V . The study concludes that the invariance of isobaric fragility, regardless of the VAc ratio, can be attributed to its volumetric and thermal contributions. The combination of these contributions explains why the PVAc/EVA series exhibits stable isobaric fragility regardless of the dipole rate within the macromolecular chain.

The use of HP-BDS offers the possibility of quantifying the thermal and volumetric contributions to molecular mobility at the glass transition and in polymer liquids more accurately than is possible with thermal analysis techniques at atmospheric pressure. Such a formalism could be applied to many polymeric systems where the origin of a molecular mobility changes remains unclear. Thus, the series of PLA and its oligomers could be studied. The reduction in molecular weight involves an increase of the ratio of the end chain interactions in the polymers. Such interactions are expected to increase the volumetric contributions, but the isobaric fragility has been found to decrease in PLA oligomers. Moreover, in the global case of polymers, the chain entanglement hinders the molecular mobility. Following the thermal and volumetric contributions for polymers whose molecular weight has been reduced to escape the entanglement phenomenon, such as in PLA oligomers, could clarify its role in the molecular mobility of polymers.

Another aspect that could be interesting to explore is the physical aging under pressure, the physical aging is usually studied by calorimetric techniques but is also visible by dielectric relaxation spectroscopy. Such a study can provide useful information for industrial polymers, and understanding which properties related to molecular mobility can be affected under pressure. Aging under pressure could also be used to study the different aging scenarios. Indeed, investigations of structural relaxation of well-chosen polymers should allow studying the different aging scenarios, i.e. does pressure facilitate intermediate aging steps? Does pressure influence the Slow Arrhenius Process (SAP)? Can polymers reach equilibrium and even crystalline state during aging under pressure?

As a matter of fact, crystallization can also be a field of research. Since the driving force of crystallization and the molecular dynamics are pressure dependent, the nucleation and crystal growth in polymers should also be affected by pressure. The formation of different crystals could affect the amorphous phase and bind molecules to both phases. The methods for determining the volumetric and thermal contributions of molecular mobility can therefore be applied to analyze how the crystalline phase affects the amorphous fractions. Such semi-crystalline polymers processed under pressure could have properties useful for industrial applications.

Appendix

Table A-1. Fit parameters ($\log(\tau_0)$, C , P_0), the uncertainties of C and P_0 , glass transition pressure P_g and the R-squared of the pressure VFTH law of isotherms (**Equation 1-38**, p. 43) for PETg, PLA and PVAc.

PETg							
T [K]	$\log(\tau_0[s])$	C	ΔC	P_0 [MPa]	ΔP_0 [MPa]	P_g [MPa]	R^2
361.15	-2.21	90.08	2.86	413.63	12.43	40.22	0.93770
363.35	-2.61	90.05	1.50	463.86	7.29	48.90	0.98465
365.35	-2.94	100.91	1.23	556.71	6.44	56.38	0.99255
367.15	-3.21	168.59	2.09	994.48	5.82	66.11	0.99815
369.15	-3.50	105.82	2.13	708.11	7.86	75.67	0.99500
373.15	-4.01	177.54	5.20	1301.45	22.97	94.10	0.99013
377.25	-4.44	72.98	1.21	671.05	5.99	113.36	0.99651

PLA							
T [K]	$\log(\tau_0[s])$	C	ΔC	P_0 [MPa]	ΔP_0 [MPa]	P_g [MPa]	R^2
337.15	-1.06	92.19	3.95	377.13	5.82	26.74	0.99662
339.15	-1.70	88.34	2.08	454.23	6.39	39.94	0.99154
341.15	-2.15	82.18	0.62	484.50	2.45	50.45	0.99954
343.15	-2.46	89.00	3.89	545.15	11.82	56.37	0.98565
345.15	-2.83	83.35	1.99	539.92	6.50	63.60	0.99433
347.15	-3.28	82.52	1.02	585.30	3.90	75.15	0.99850
349.15	-3.80	84.14	1.11	638.00	5.72	87.37	0.99613
351.15	-4.09	70.51	1.16	580.81	4.74	96.40	0.99744
353.15	-4.37	78.38	0.75	667.82	3.03	105.25	0.99912

PVAc							
T [K]	$\log(\tau_0[s])$	C	ΔC	P_0 [MPa]	ΔP_0 [MPa]	P_g [MPa]	R^2
317.15	-0.83	250.00	—	2363.78	692.46	60.03	0.99661
319.15	-1.20	250.00	—	2403.02	585.11	68.70	0.99755
321.15	-1.54	250.00	—	2475.62	567.45	78.07	0.99920
323.15	-1.83	250.00	—	2654.72	450.55	90.46	0.99769
325.15	-2.16	250.00	—	2672.78	323.50	98.58	0.99868
327.15	-2.43	106.24	12.27	1234.39	130.58	108.12	0.99986
329.15	-2.72	138.89	23.88	1618.79	259.47	117.49	0.99978
331.15	-2.96	110.12	7.86	1365.98	88.94	128.37	0.99993
333.15	-3.21	129.77	21.65	1652.48	254.27	139.79	0.99971

335.15	-3.41	113.84	10.93	1542.99	135.31	152.23	0.99987
337.15	-3.63	148.35	27.85	2051.50	358.64	164.83	0.99966
339.15	-3.83	174.15	42.88	2491.52	575.89	178.37	0.99963
341.15	-4.04	142.88	33.27	2129.73	456.75	188.88	0.99956
343.15	-4.18	66.33	4.43	1098.22	63.32	193.90	0.99992
345.15	-4.36	69.31	4.23	1187.77	60.35	207.05	0.99994
347.15	-4.52	73.39	6.02	1288.73	88.30	218.85	0.99993
349.15	-4.65	72.85	4.41	1343.77	68.53	233.42	0.99996
351.15	-4.84	83.14	4.94	1537.34	76.61	244.70	0.99996
353.15	-4.98	67.03	1.32	1323.41	21.12	256.07	0.99999

Table A-2. Fit parameters ($\log(\tau_\infty)$, D , T_0), the uncertainties of D and T_0 , glass transition temperature T_g , isobaric fragility m_P and the R-squared of the VFTH law of isobars (**Equation 1-1**, p. 7) for PETg, PLA and PVAc.

PETg								
P [MPa]	$\log(\tau_\infty[s])$	D	ΔD	T_0 [K]	ΔT_0 [K]	T_g	m_P	R^2
P_{atm}	-9.76	2.13	0.46	321.97	3.73	347.25	161.53	0.99743
10	-10.47	2.54	0.38	323.08	2.98	351.63	153.64	0.99506
20	-10.73	2.70	0.57	325.19	3.98	355.18	150.79	0.99777
30	-11.12	2.98	0.69	325.99	4.25	358.18	145.92	0.99796
40	-11.60	3.35	0.76	326.02	4.20	360.88	140.73	0.99815
50	-12.18	3.80	0.84	325.48	4.13	363.41	135.87	0.99836
60	-13.04	4.52	0.07	323.52	0.62	365.79	130.16	0.99858
70	-17.08	7.87	5.37	312.38	17.44	368.34	125.63	0.99881
PLA								
P [MPa]	$\log(\tau_\infty[s])$	D	ΔD	T_0 [K]	ΔT_0 [K]	T_g	m_P	R^2
P_{atm}	-14	4.60	0.06	291.37	0.48	327.76	144.12	0.99839
10	-14	4.49	0.09	295.84	0.80	331.89	147.30	0.99747
20	-14	4.41	0.15	299.19	0.80	334.98	149.79	0.99243
30	-14	4.82	0.09	297.85	0.73	336.79	138.39	0.99810
40	-14	4.91	0.11	299.30	0.86	339.18	136.07	0.99716
50	-14	5.22	0.13	298.83	1.01	341.18	128.90	0.99691
60	-14	5.09	0.09	301.86	0.66	343.60	131.70	0.99881
70	-14	5.21	0.10	302.81	0.70	345.62	129.17	0.99858
80	-14	5.33	0.11	303.64	0.74	347.55	126.64	0.99836
90	-14	5.45	0.12	304.38	0.77	349.42	124.14	0.99815
100	-14	5.58	0.12	305.04	0.80	351.22	121.67	0.99796

PVAc								
P [MPa]	$\log(\tau_\infty[s])$	D	ΔD	T_0 [K]	ΔT_0 [K]	T_g	m_p	R^2
P_{atm}	-14	9.80	0.12	239.36	0.83	307.27	67.76	0.99847
10	-14	9.82	0.06	241.87	0.39	310.63	68.01	0.99900
20	-14	9.77	0.05	244.11	0.30	313.19	68.10	0.99937
30	-14	9.76	0.04	246.09	0.24	315.61	68.06	0.99961
40	-14	9.76	0.04	247.86	0.24	317.93	67.90	0.99976
50	-14	9.79	0.04	249.43	0.24	320.16	67.64	0.99983
60	-14	9.84	0.05	250.83	0.32	322.31	67.60	0.99983
70	-14	9.85	0.07	252.47	0.45	324.47	67.37	0.99983
80	-14	9.89	0.09	253.84	0.53	326.54	67.01	0.99973
90	-14	9.96	0.06	255.01	0.39	328.56	66.66	0.99950
100	-14	10.03	0.05	256.16	0.30	330.55	67.76	0.99928

Table A-3. Values of T_g and m_p variations as a function of structural parameter shown in **Figure 4-6**. The EVA series have a variation in the ratio of side groups. Three PLA series have variations in the ratio of plasticizers, isomerism, and the manner of sample crystallization. The PEF, PET and PDAI series have a variation in the number of methylene units in their backbone chain, and PIB and PS series have a variation in molecular weight. The PMMA series have a variation crosslinking ratio.

EVA series (Puente et al., 2015)			PLA with plasticizers (Araujo et al., 2019)		
wt. % VAc	ΔT_g [K]	Δm_p	% plasticizers	ΔT_g [K]	Δm_p
100	0	0	0	0	0
90	-21	0	2.5	-6	-19
80	-37	3.0	5	-9	-27
70	-54	3.0	9	-17	-50
60	-65	0.1	13	-24	-65
50	-68	-2.8			

PEF series (Fosse et al., 2022)			PET series (Puente et al., 2015)		
methylene units number	ΔT_g [K]	Δm_p	methylene units number	ΔT_g [K]	Δm_p
2	0	3	2	0	0
3	-26	4	3	-33	-10
4	-45	-5	4	-37	-25

PDAI series (Genix and Lauprêtre, 2005)			PLA isomer series (Varol et al., 2020)		
methylene units number	ΔT_g [K]	Δm_p	isomerism	ΔT_g [K]	Δm_p
1	0	0	DL	0	0
3	-31	-28	L	1.3	5
6	-73	-38	D	0.6	5
8	-81	-39			
10	-97	-36			

PEF 2,4/2,5 (Bourdet et al., 2018)			Crystallized PLA series (Delpouve et al., 2011)		
% 2,5-FDCA	ΔT_g	Δm_p	Process of crystallization	ΔT_g	Δm_p
100	0	3	A	0	0
90	-4	4	SB2	3	-25
85	-5	-5	SEQ	8	-32
50	-5	1	UCW	6	-47
0	-11	8	SB3	8	-85
			SB4	12	-89

PIB series (Dalle-Ferrier et al., 2010)			PS series (Santangelo and Roland, 1998)		
M_w [kg. mol ⁻¹]	ΔT_g [K]	Δm_p	M_w [kg. mol ⁻¹]	ΔT_g [K]	Δm_p
500	0	0	3840	0	0
3.58	-4	6.18053	90	-1.8	-6
1.19	-9	28.95823	3.68	-27.3	-21
0.68	-15	34.13183	2.36	-48.2	-49
Crosslinked PMMA (Alves et al., 2004)			0.76	-105.6	-66
			0.59	-128.4	-74
Crosslinking %	ΔT_g [K]	Δm_p			
0.5	0	0			
1	2	1			
5	8	17			
9	19	45			

Table A-4. Fit parameters ($\log(\tau_\infty)$, D , T_0), the uncertainties of D and T_0 , glass transition temperature T_g , isobaric fragility m_p and the R-squared of the VFTH law of isobars (**Equation 1-1**, p. 7) for PVAc, EVA80 and EVA60.

PVAc								
P [MPa]	$\log(\tau_\infty [s])$	D	ΔD	T_0 [K]	ΔT_0 [K]	T_g	m_p	R^2
P_{atm}	-14	9.8	0.12	239	0.8	307	68	0.99847
20	-14	9.8	0.08	244	0.7	309	76	0.99937
40	-14	9.8	0.05	248	0.3	314	76	0.99976
60	-14	9.8	0.04	251	0.2	318	76	0.99983
80	-14	9.9	0.05	254	0.3	322	76	0.99973
100	-14	10.0	0.09	256	0.5	326	75	0.99928
120	-14	9.8	0.06	260	0.4	329	76	0.99971
140	-14	9.9	0.09	263	0.5	333	76	0.99937
160	-14	10.1	0.15	264	0.9	336	75	0.99689
180	-14	10.5	0.23	265	1.3	340	72	0.99305
200	-14	11.0	0.39	264	2.1	343	70	0.99847

EVA80								
P [MPa]	$\log(\tau_\infty [s])$	D	ΔD	T_0 [K]	ΔT_0 [K]	T_g	m_p	R^2
P_{atm}	-14	10	0.13	210	0.8	267	75	0.99773
25	-14	10.4	0.22	210	1.3	270	73	0.9964
50	-14	10.5	0.23	215	1.4	276	72	0.99599
75	-14	10.1	0.16	221	1.0	281	74	0.99784

100	-14	10.2	0.16	223	1.0	285	74	0.99817
125	-14	10.6	0.27	223	1.6	287	72	0.99604
150	-14	10.7	0.18	225	1.1	290	71	0.99774
175	-14	10.7	0.21	228	1.3	294	71	0.99735
200	-14	11.1	0.19	231	1.2	300	69	0.99734

EVA60

P [MPa]	$\log(\tau_\infty[\text{s}])$	D	ΔD	T_0 [K]	ΔT_0 [K]	T_g	m_p	R^2
P_{atm}	-14	9.4	0.11	191	0.6	240	70	0.99654
25	-14	9.4	0.15	193	0.9	243	70	0.99817
50	-14	8.9	0.13	200	0.7	249	73	0.99797
75	-14	9.3	0.24	201	1.4	252	71	0.99318
100	-14	9.1	0.23	205	1.3	255	72	0.99356
125	-14	9.3	0.22	205	1.2	257	71	0.99575
150	-14	9.2	0.19	209	1.1	262	71	0.99613
175	-14	9.7	0.24	208	1.4	263	68	0.99591
200	-14	10.2	0.17	209	0.9	267	66	0.99722

References

- Adam, G., Gibbs, J.H., 1965. On the Temperature Dependence of Cooperative Relaxation Properties in Glass-Forming Liquids. *The Journal of Chemical Physics* 43, 139–146. <https://doi.org/10.1063/1.1696442>
- Alba-Simionesco, C., Cailliaux, A., Alegría, A., Tarjus, G., 2004. Scaling out the density dependence of the α relaxation in glass-forming polymers. *Europhys. Lett.* 68, 58–64. <https://doi.org/10.1209/epl/i2004-10214-6>
- Alba-Simionesco, C., Tarjus, G., 2006. Temperature versus density effects in glassforming liquids and polymers: A scaling hypothesis and its consequences. *Journal of Non-Crystalline Solids* 352, 4888–4894. <https://doi.org/10.1016/j.jnoncrysol.2006.05.037>
- Alean, J., Hambrey, M., 2017. *Glaciers of the World* [WWW Document]. SwissEduc. URL https://swisseduc.ch/glaciers/earth_icy_planet/glaciers02-en.html?id=9
- Alegría, A., Guerrica-Echevarria, E., Goitiandia, L., Telleria, I., Colmenero, J., 1995. α -Relaxation in the Glass Transition Range of Amorphous Polymers. 1. Temperature Behavior across the Glass transition. *Macromolecules* 28, 1516–1527. <https://doi.org/10.1021/ma00109a025>
- Alvarez, F., Alegria, A., Colmenero, J., 1991. Relationship between the time-domain Kohlrausch-Williams-Watts and frequency-domain Havriliak-Negami relaxation functions. *Phys. Rev. B* 44, 7306–7312. <https://doi.org/10.1103/PhysRevB.44.7306>
- Alves, N.M., Gómez Ribelles, J.L., Gómez Tejedor, J.A., Mano, J.F., 2004. Viscoelastic Behavior of Poly(methyl methacrylate) Networks with Different Cross-Linking Degrees. *Macromolecules* 37, 3735–3744. <https://doi.org/10.1021/ma035626z>
- Andersson, S.P., Andersson, O., 1998. Relaxation Studies of Poly(propylene glycol) under High Pressure. *Macromolecules* 31, 2999–3006. <https://doi.org/10.1021/ma971282z>
- Androsch, R., Zhuravlev, E., Schmelzer, J.W.P., Schick, C., 2018. Relaxation and crystal nucleation in polymer glasses. *European Polymer Journal* 102, 195–208. <https://doi.org/10.1016/j.eurpolymj.2018.03.026>
- Angell, C.A., 1995. Formation of Glasses from Liquids and Biopolymers. *Science* 267, 1924–1935. <https://doi.org/10.1126/science.267.5206.1924>
- Angell, C.A., 1991. Relaxation in liquids, polymers and plastic crystals — strong/fragile patterns and problems. *Journal of Non-Crystalline Solids* 131–133, 13–31. [https://doi.org/10.1016/0022-3093\(91\)90266-9](https://doi.org/10.1016/0022-3093(91)90266-9)
- Angell, C.A., 1985. Spectroscopy simulation and scattering, and the medium range order problem in glass. *Journal of Non-Crystalline Solids* 73, 1–17. [https://doi.org/10.1016/0022-3093\(85\)90334-5](https://doi.org/10.1016/0022-3093(85)90334-5)
- Angell, C.A., Rao, K.J., 1972. Configurational Excitations in Condensed Matter, and the “Bond Lattice” Model for the Liquid-Glass Transition. *The Journal of chemical physics* 57, 470–481.
- Arabeche, K., Delbreilh, L., Adhikari, R., Michler, G.H., Hiltner, A., Baer, E., Saiter, J.-M., 2012. Study of the cooperativity at the glass transition temperature in PC/PMMA multilayered films: Influence of thickness reduction from macro- to nanoscale. *Polymer* 53, 1355–1361. <https://doi.org/10.1016/j.polymer.2012.01.045>
- Araujo, S., Batteux, F., Li, W., Butterfield, L., Delpouve, N., Esposito, A., Tan, L., Saiter, J.-M., Negahban, M., 2018a. A Structural Interpretation of the Two Components Governing the Kinetic Fragility from the Example of Interpenetrated Polymer Networks. *J. Polym. Sci. Part B: Polym. Phys.* 56, 1393–1403. <https://doi.org/10.1002/polb.24722>
- Araujo, S., Delpouve, N., Dhotel, A., Domenek, S., Guinault, A., Delbreilh, L., Dargent, E., 2018b. Reducing the Gap between the Activation Energy Measured in the Liquid and the Glassy States

- by Adding a Plasticizer to Polylactide. *ACS Omega* 3, 17092–17099. <https://doi.org/10.1021/acsomega.8b02474>
- Araujo, S., Delpouve, N., Domenek, S., Guinault, A., Golovchak, R., Szatanik, R., Ingram, A., Fauchard, C., Delbreilh, L., Dargent, E., 2019. Cooperativity Scaling and Free Volume in Plasticized Polylactide. *Macromolecules* 52, 6107–6115. <https://doi.org/10.1021/acs.macromol.9b00464>
- Assouli, S., Jabraoui, H., El hafi, T., Bajjou, O., Kotri, A., Mazroui, M., Lachtioui, Y., 2023. Exploring the impact of cooling rates and pressure on fragility and structural transformations in iron monatomic metallic glasses: Insights from molecular dynamics simulations. *Journal of Non-Crystalline Solids* 621, 122623. <https://doi.org/10.1016/j.jnoncrysol.2023.122623>
- Avramov, I., 2000. Pressure dependence of viscosity of glassforming melts. *Journal of Non-Crystalline Solids* 262, 258–263. [https://doi.org/10.1016/S0022-3093\(99\)00712-7](https://doi.org/10.1016/S0022-3093(99)00712-7)
- Bailey, E.J., Winey, K.I., 2020. Dynamics of polymer segments, polymer chains, and nanoparticles in polymer nanocomposite melts: A review. *Progress in Polymer Science* 105, 101242. <https://doi.org/10.1016/j.progpolymsci.2020.101242>
- Baker, D.L., Reynolds, M., Masurel, R., Olmsted, P.D., Mattsson, J., 2022. Cooperative Intramolecular Dynamics Control the Chain-Length-Dependent Glass Transition in Polymers. *Phys. Rev. X* 12, 021047. <https://doi.org/10.1103/PhysRevX.12.021047>
- Barnett, J.D., Bosco, C.D., 1969. Viscosity measurements on liquids to pressures of 60 kbar. *Journal of Applied Physics* 40, 3144–3150.
- Bauer, Th., Lunkenheimer, P., Loidl, A., 2013. Cooperativity and the Freezing of Molecular Motion at the Glass Transition. *Phys. Rev. Lett.* 111, 225702. <https://doi.org/10.1103/PhysRevLett.111.225702>
- Bengtzelius, U., Götze, W., Sjölander, A., 1984. Dynamics of supercooled liquids and the glass transition. *Journal of Physics C: solid state Physics* 17, 5915.
- Berthier, L., 2011. Dynamic Heterogeneity in Amorphous Materials. *Physics* 4, 42. <https://doi.org/10.1103/Physics.4.42>
- Berthier, L., 2004. Time and length scales in supercooled liquids. *Phys. Rev. E* 69, 020201. <https://doi.org/10.1103/PhysRevE.69.020201>
- Berthier, L., Biroli, G., Bouchaud, J.-P., Cipelletti, L., Masri, D.E., L'Hôte, D., Ladieu, F., Pierno, M., 2005a. Direct Experimental Evidence of a Growing Length Scale Accompanying the Glass Transition. *Science* 310, 1797–1800. <https://doi.org/10.1126/science.1120714>
- Berthier, L., Biroli, G., Bouchaud, J.-P., Cipelletti, L., Masri, D.E., L'Hôte, D., Ladieu, F., Pierno, M., 2005b. Direct Experimental Evidence of a Growing Length Scale Accompanying the Glass Transition. *Science* 310, 1797–1800. <https://doi.org/10.1126/science.1120714>
- Berthier, L., Biroli, G., Bouchaud, J.-P., Kob, W., Miyazaki, K., Reichman, D.R., 2007a. Spontaneous and induced dynamic correlations in glass formers. II. Model calculations and comparison to numerical simulations. *The Journal of Chemical Physics* 126, 184504. <https://doi.org/10.1063/1.2721555>
- Berthier, L., Biroli, G., Bouchaud, J.-P., Kob, W., Miyazaki, K., Reichman, D.R., 2007b. Spontaneous and induced dynamic fluctuations in glass formers. I. General results and dependence on ensemble and dynamics. *The Journal of Chemical Physics* 126, 184503. <https://doi.org/10.1063/1.2721554>
- Berthier, L., Garrahan, J.P., 2005. Numerical Study of a Fragile Three-Dimensional Kinetically Constrained Model. *J. Phys. Chem. B* 109, 6916–6916. <https://doi.org/10.1021/jp058079n>
- Biroli, G., Bouchaud, J., 2012. The Random First-Order Transition Theory of Glasses: A Critical Assessment, in: Wolynes, P.G., Lubchenko, V. (Eds.), *Structural Glasses and Supercooled Liquids*. Wiley, pp. 31–113. <https://doi.org/10.1002/9781118202470.ch2>
- Biroli, G., Bouchaud, J.-P., 2023. The RFOT theory of glasses: Recent progress and open issues. *Comptes Rendus. Physique* 24, 1–15.

- Bishop, M.T., Karasz, F.E., Russo, P.S., Langley, K.H., 1985. Solubility and properties of a poly(aryl ether ketone) in strong acids. *Macromolecules* 18, 86–93. <https://doi.org/10.1021/ma00143a014>
- Błażytko, A., Rams-Baron, M., Paluch, M., 2024. The influence of molecular shape on reorientation dynamics of sizable glass-forming isomers at ambient and elevated pressure. *Sci Rep* 14, 887. <https://doi.org/10.1038/s41598-023-50894-8>
- Böhmer, R., Hinze, G., Diezemann, G., Geil, B., Sillescu, H., 1996. Dynamic heterogeneity in supercooled ortho-terphenyl studied by multidimensional deuteron NMR. *Europhysics Letters* 36, 55.
- Böhmer, R., Ngai, K.L., Angell, C.A., Plazek, D.J., 1993. Nonexponential relaxations in strong and fragile glass formers. *The Journal of Chemical Physics* 99, 4201–4209. <https://doi.org/10.1063/1.466117>
- Bonacci, F., Chateau, X., Furst, E.M., Fusier, J., Goyon, J., Lemaître, A., 2020. Contact and macroscopic ageing in colloidal suspensions. *Nature Materials* 19, 775–780.
- Bouchaud, J.-P., Biroli, G., 2004. On the Adam-Gibbs-Kirkpatrick-Thirumalai-Wolynes scenario for the viscosity increase in glasses. *The Journal of Chemical Physics* 121, 7347–7354. <https://doi.org/10.1063/1.1796231>
- Bourdet, A., Esposito, A., Thiyagarajan, S., Delbreilh, L., Affouard, F., Knoop, R.J.I., Dargent, E., 2018. Molecular Mobility in Amorphous Biobased Poly(ethylene 2,5-furandicarboxylate) and Poly(ethylene 2,4-furandicarboxylate). *Macromolecules* 51, 1937–1945. <https://doi.org/10.1021/acs.macromol.8b00108>
- Bourdet, A., Fosse, C., Garda, M.-R., Thiyagarajan, S., Delbreilh, L., Esposito, A., Dargent, E., 2023. Microstructural consequences of isothermal crystallization in homo-and co-polyesters based on 2, 5-and 2, 4-furandicarboxylic acid. *Polymer* 272, 125835.
- Bouthegourd, E., Esposito, A., Lourdin, D., Saiter, A., Saiter, J.M., 2013. Size of the cooperative rearranging regions vs. fragility in complex glassy systems: Influence of the structure and the molecular interactions. *Physica B: Condensed Matter* 425, 83–89. <https://doi.org/10.1016/j.physb.2013.05.029>
- Bouthegourd, E., Esposito, A., Saiter, A., 2014. Effect of Mechanical Compression and Hydrostatic Pressure on the Molecular Mobility of Poly(lactic acid). *Macromolecular Symposia* 341, 26–33. <https://doi.org/10.1002/masy.201300154>
- Bridgman, P.W., 1964. *Collected Experimental Papers, Volume VI*. Harvard University Press. <https://doi.org/10.4159/harvard.9780674287839>
- Bridgman, P.W., 1946. Recent Work in the Field of High Pressures. *Rev. Mod. Phys.* 18, 1–93. <https://doi.org/10.1103/RevModPhys.18.1>
- Bridgman, P.W., 1925. The Viscosity of Liquids under Pressure. *Proceedings of the National Academy of Sciences* 11, 603–606. <https://doi.org/10.1073/pnas.11.10.603>
- Buchenau, U., Galperin, Yu.M., Gurevich, V.L., Parshin, D.A., Ramos, M.A., Schober, H.R., 1992. Interaction of soft modes and sound waves in glasses. *Phys. Rev. B* 46, 2798–2808. <https://doi.org/10.1103/PhysRevB.46.2798>
- Buchenau, U., Zorn, R., 1992. A relation between fast and slow motions in glassy and liquid selenium. *Europhysics Letters* 18, 523.
- Callen, H.B., Callen, H.B., 1985. *Thermodynamics and an introduction to thermostatistics*, 2. ed. ed. Wiley, New York, NY.
- Cangialosi, D., 2024. Physical aging and vitrification in polymers and other glasses: Complex behavior and size effects. *Journal of Polymer Science* pol.20230850. <https://doi.org/10.1002/pol.20230850>
- Cangialosi, D., 2014. Dynamics and thermodynamics of polymer glasses. *J. Phys.: Condens. Matter* 26, 153101. <https://doi.org/10.1088/0953-8984/26/15/153101>

- Cangialosi, D., Boucher, V.M., Alegría, A., Colmenero, J., 2013. Direct Evidence of Two Equilibration Mechanisms in Glassy Polymers. *Phys. Rev. Lett.* 111, 095701. <https://doi.org/10.1103/PhysRevLett.111.095701>
- Capaccioli, S., Lucchesi, M., Prevosto, D., Casalini, R., Rolla, P., 2004. Effect of the isobaric and isothermal reductions in excess and configurational entropies on glass-forming dynamics. *Philosophical Magazine* 84, 1513–1519. <https://doi.org/10.1080/14786430310001644288>
- Capaccioli, S., Ruocco, G., Zamponi, F., 2008. Dynamically Correlated Regions and Configurational Entropy in Supercooled Liquids. *J. Phys. Chem. B* 112, 10652–10658. <https://doi.org/10.1021/jp802097u>
- Casalini, R., Paluch, M., Psurek, T., Roland, C.M., 2004. Temperature and pressure dependences of the structural dynamics: an interpretation of Vogel–Fulcher behavior in terms of the Adam–Gibbs model. *Journal of Molecular Liquids* 111, 53–60. [https://doi.org/10.1016/S0167-7322\(03\)00260-5](https://doi.org/10.1016/S0167-7322(03)00260-5)
- Casalini, R., Paluch, M., Roland, C.M., 2003. Influence of molecular structure on the dynamics of supercooled van der Waals liquids. *Phys. Rev. E* 67, 031505. <https://doi.org/10.1103/PhysRevE.67.031505>
- Casalini, R., Roland, C.M., 2017. Communication: Effect of density on the physical aging of pressure-densified polymethylmethacrylate. *The Journal of Chemical Physics* 147, 091104. <https://doi.org/10.1063/1.4995567>
- Casalini, R., Roland, C.M., 2005. Scaling of the supercooled dynamics and its relation to the pressure dependences of the dynamic crossover and the fragility of glass formers. *Phys. Rev. B* 71, 014210. <https://doi.org/10.1103/PhysRevB.71.014210>
- Casalini, R., Roland, C.M., 2004a. Scaling of the segmental relaxation times of polymers and its relation to the thermal expansivity. *Colloid Polym Sci* 283, 107–110. <https://doi.org/10.1007/s00396-004-1156-6>
- Casalini, R., Roland, C.M., 2004b. Thermodynamical scaling of the glass transition dynamics. *Phys. Rev. E* 69, 062501. <https://doi.org/10.1103/PhysRevE.69.062501>
- Cavagna, A., 2009. Supercooled liquids for pedestrians. *Physics Reports* 476, 51–124. <https://doi.org/10.1016/j.physrep.2009.03.003>
- Charbonneau, P., Tarjus, G., 2013. Decorrelation of the static and dynamic length scales in hard-sphere glass formers. *Phys. Rev. E* 87, 042305. <https://doi.org/10.1103/PhysRevE.87.042305>
- Chat, K., Tu, W., Beena Unni, A., Adrjanowicz, K., 2021. Influence of Tacticity on the Glass-Transition Dynamics of Poly(methyl methacrylate) (PMMA) under Elevated Pressure and Geometrical Nanoconfinement. *Macromolecules* 54, 8526–8537. <https://doi.org/10.1021/acs.macromol.1c01341>
- Chua, Y.Z., Zorn, R., Schmelzer, J.W.P., Schick, C., Holderer, O., Zamponi, M., 2023. Determination of Cooperativity Length in a Glass-Forming Polymer. *ACS Phys. Chem Au* 3, 172–180. <https://doi.org/10.1021/acspchemau.2c00057>
- Cicerone, M.T., Ediger, M.D., 1996. Enhanced translation of probe molecules in supercooled o-terphenyl: Signature of spatially heterogeneous dynamics? *The Journal of chemical physics* 104, 7210–7218.
- Cicerone, M.T., Ediger, M.D., 1993. Photobleaching technique for measuring ultraslow reorientation near and below the glass transition: tetracene in o-terphenyl. *J. Phys. Chem.* 97, 10489–10497. <https://doi.org/10.1021/j100142a037>
- Cipelletti, L., Bissig, H., Trappe, V., Ballesta, P., Mazoyer, S., 2002. Time-resolved correlation: a new tool for studying temporally heterogeneous dynamics. *Journal of Physics: Condensed Matter* 15, S257.
- Cohen, M.H., Turnbull, D., 1959. Molecular Transport in Liquids and Glasses. *The Journal of Chemical Physics* 31, 1164–1169. <https://doi.org/10.1063/1.1730566>

- Cole, K.S., Cole, R.H., 1941. Dispersion and Absorption in Dielectrics I. Alternating Current Characteristics. *The Journal of Chemical Physics* 9, 341–351. <https://doi.org/10.1063/1.1750906>
- Cook, R.L., Herbst, C.A., King, H.E., 1993. High-pressure viscosity of glass-forming liquids measured by the centrifugal force diamond anvil cell viscometer. *J. Phys. Chem.* 97, 2355–2361. <https://doi.org/10.1021/j100112a041>
- Corezzi, S., Rolla, P.A., Paluch, M., Ziolo, J., Fioretto, D., 1999. Influence of temperature and pressure on dielectric relaxation in a supercooled epoxy resin. *Phys. Rev. E* 60, 4444–4452. <https://doi.org/10.1103/PhysRevE.60.4444>
- Crauste-Thibierge, C., Brun, C., Ladieu, F., L'Hôte, D., Biroli, G., Bouchaud, J.-P., 2010. Evidence of Growing Spatial Correlations at the Glass Transition from Nonlinear Response Experiments. *Phys. Rev. Lett.* 104, 165703. <https://doi.org/10.1103/PhysRevLett.104.165703>
- Dalle-Ferrier, C., Niss, K., Sokolov, A.P., Frick, B., Serrano, J., Alba-Simionesco, C., 2010. The Role of Chain Length in Nonergodicity Factor and Fragility of Polymers. *Macromolecules* 43, 8977–8984. <https://doi.org/10.1021/ma101622f>
- Dalle-Ferrier, C., Thibierge, C., Alba-Simionesco, C., Berthier, L., Biroli, G., Bouchaud, J.-P., Ladieu, F., L'Hôte, D., Tarjus, G., 2007a. Spatial correlations in the dynamics of glassforming liquids: Experimental determination of their temperature dependence. *Phys. Rev. E* 76, 041510. <https://doi.org/10.1103/PhysRevE.76.041510>
- Dalle-Ferrier, C., Thibierge, C., Alba-Simionesco, C., Berthier, L., Biroli, G., Bouchaud, J.-P., Ladieu, F., L'Hôte, D., Tarjus, G., 2007b. Spatial correlations in the dynamics of glassforming liquids: Experimental determination of their temperature dependence. *Phys. Rev. E* 76, 041510. <https://doi.org/10.1103/PhysRevE.76.041510>
- Dasgupta, C., Indrani, A.V., Ramaswamy, S., Phani, M.K., 1991. Is There a Growing Correlation Length near the Glass Transition? *EPL* 15, 307. <https://doi.org/10.1209/0295-5075/15/3/013>
- Davidson, D.W., Cole, R.H., 1951. Dielectric relaxation in glycerol, propylene glycol, and n-propanol. *The Journal of Chemical Physics* 19, 1484–1490.
- Debenedetti, P.G., Stillinger, F.H., 2001. Supercooled liquids and the glass transition. *Nature* 410, 259–267. <https://doi.org/10.1038/35065704>
- Debenedetti, P.G., Truskett, T.M., Lewis, C.P., Stillinger, F.H., 2001. Theory of supercooled liquids and glasses: Energy landscape and statistical geometry perspectives, in: *Advances in Chemical Engineering*. Elsevier, pp. 21–79. [https://doi.org/10.1016/S0065-2377\(01\)28003-X](https://doi.org/10.1016/S0065-2377(01)28003-X)
- Debye, P.J.W., 1929. *Polar molecules*. Dover publications.
- Déjardin, P.-M., Pabst, F., Cornaton, Y., Helbling, A., Blochowicz, T., 2022. Temperature dependence of the Kirkwood correlation factor and linear dielectric constant of simple isotropic polar fluids. *Phys. Rev. E* 105, 024108. <https://doi.org/10.1103/PhysRevE.105.024108>
- Delbreilh, L., Negahban, M., Benzohra, M., Lacabanne, C., Saiter, J.M., 2009. Glass transition investigated by a combined protocol using thermostimulated depolarization currents and differential scanning calorimetry. *J Therm Anal Calorim* 96, 865–871. <https://doi.org/10.1007/s10973-009-0060-1>
- Delpouve, N., Delbreilh, L., Stoclet, G., Saiter, A., Dargent, E., 2014. Structural Dependence of the Molecular Mobility in the Amorphous Fractions of Polylactide. *Macromolecules* 47, 5186–5197. <https://doi.org/10.1021/ma500839p>
- Delpouve, N., Saiter, A., Dargent, E., 2011. Cooperativity length evolution during crystallization of poly (lactic acid). *European polymer journal* 47, 2414–2423.
- Dhotel, A., Rijal, B., Delbreilh, L., Dargent, E., Saiter, A., 2015. Combining Flash DSC, DSC and broadband dielectric spectroscopy to determine fragility. *J Therm Anal Calorim* 121, 453–461. <https://doi.org/10.1007/s10973-015-4650-9>

- Ding, Y., Novikov, V.N., Sokolov, A.P., A. Cailliaux, Dalle-Ferrier, C., Alba-Simionesco, C., Frick, B., 2004. Influence of Molecular Weight on Fast Dynamics and Fragility of Polymers. *Macromolecules* 37, 9264–9272. <https://doi.org/10.1021/ma0492420>
- Donati, C., Glotzer, S.C., Poole, P.H., Kob, W., Plimpton, S.J., 1999. Spatial correlations of mobility and immobility in a glass-forming Lennard-Jones liquid. *Phys. Rev. E* 60, 3107–3119. <https://doi.org/10.1103/PhysRevE.60.3107>
- Donth, E., 1999. Phenomenological treatment of dynamic glass transition heterogeneity. *Acta Polymerica* 50, 240–251. [https://doi.org/10.1002/\(SICI\)1521-4044\(19990701\)50:7<240::AID-APOL240>3.0.CO;2-H](https://doi.org/10.1002/(SICI)1521-4044(19990701)50:7<240::AID-APOL240>3.0.CO;2-H)
- Donth, E., 1984. The size of cooperatively rearranging regions in polystyrene and styrene-dimethylsiloxane diblock copolymers at the glass transition temperature. *Acta Polymerica* 35, 120–123. <https://doi.org/10.1002/actp.1984.010350202>
- Donth, E., 1982. The size of cooperatively rearranging regions at the glass transition. *Journal of Non-Crystalline Solids* 53, 325–330. [https://doi.org/10.1016/0022-3093\(82\)90089-8](https://doi.org/10.1016/0022-3093(82)90089-8)
- Donth, E.-J., 2001. *The Glass Transition: Relaxation Dynamics in Liquids and Disordered Materials*, Springer Series in MATERIALS SCIENCE. Springer Berlin Heidelberg, Berlin, Heidelberg. <https://doi.org/10.1007/978-3-662-04365-3>
- Doolittle, A.K., 1951. Studies in Newtonian Flow. I. The Dependence of the Viscosity of Liquids on Temperature. *Journal of Applied Physics* 22, 1031–1035. <https://doi.org/10.1063/1.1700096>
- Dreyfus, C., Aouadi, A., Gapinski, J., Matos-Lopes, M., Steffen, W., Patkowski, A., Pick, R.M., 2003. Temperature and pressure study of Brillouin transverse modes in the organic glass-forming liquid orthoterphenyl. *Phys. Rev. E* 68, 011204. <https://doi.org/10.1103/PhysRevE.68.011204>
- Drozd-Rzoska, A., 2019. Activation volume in superpressed glass-formers. *Sci Rep* 9, 13787. <https://doi.org/10.1038/s41598-019-49848-w>
- Dudowicz, J., Freed, K.F., Douglas, J.F., 2006. Entropy theory of polymer glass formation revisited. I. General formulation. *The Journal of Chemical Physics* 124, 064901. <https://doi.org/10.1063/1.2166391>
- Dudowicz, J., Freed, K.F., Douglas, J.F., 2005a. Fragility of Glass-Forming Polymer Liquids. *J. Phys. Chem. B* 109, 21350–21356. <https://doi.org/10.1021/jp053693k>
- Dudowicz, J., Freed, K.F., Douglas, J.F., 2005b. The Glass Transition Temperature of Polymer Melts. *J. Phys. Chem. B* 109, 21285–21292. <https://doi.org/10.1021/jp0523266>
- Dyre, J.C., 2014. Hidden Scale Invariance in Condensed Matter. *J. Phys. Chem. B* 118, 10007–10024. <https://doi.org/10.1021/jp501852b>
- Dyre, J.C., 2006. *Colloquium* : The glass transition and elastic models of glass-forming liquids. *Rev. Mod. Phys.* 78, 953–972. <https://doi.org/10.1103/RevModPhys.78.953>
- Dyre, J.C., Christensen, T., Olsen, N.B., 2006. Elastic models for the non-Arrhenius viscosity of glass-forming liquids. *Journal of non-crystalline solids* 352, 4635–4642.
- Ediger, M.D., 2017. Perspective: Highly stable vapor-deposited glasses. *The Journal of Chemical Physics* 147, 210901. <https://doi.org/10.1063/1.5006265>
- Ediger, M.D., 2000. Spatially Heterogeneous Dynamics in Supercooled Liquids. *Annu. Rev. Phys. Chem.* 51, 99–128. <https://doi.org/10.1146/annurev.physchem.51.1.99>
- Ediger, M.D., Angell, C.A., Nagel, S.R., 1996. Supercooled Liquids and Glasses. *J. Phys. Chem.* 100, 13200–13212. <https://doi.org/10.1021/jp953538d>
- El Masri, D., Berthier, L., Cipelletti, L., 2010. Subdiffusion and intermittent dynamic fluctuations in the aging regime of concentrated hard spheres. *Phys. Rev. E* 82, 031503. <https://doi.org/10.1103/PhysRevE.82.031503>
- Esposito, A., Delpouve, N., Causin, V., Dhotel, A., Delbreilh, L., Dargent, E., 2016. From a Three-Phase Model to a Continuous Description of Molecular Mobility in Semicrystalline

- Poly(hydroxybutyrate-*co*-hydroxyvalerate). *Macromolecules* 49, 4850–4861. <https://doi.org/10.1021/acs.macromol.6b00384>
- Evenson, Z., Koschine, T., Wei, S., Gross, O., Bednarcik, J., Gallino, I., Kruzic, J.J., Rätzke, K., Faupel, F., Busch, R., 2015. The effect of low-temperature structural relaxation on free volume and chemical short-range ordering in a Au₄₉Cu₂₆.₉Si₁₆.₃Ag₅.₅Pd₂.₃ bulk metallic glass. *Scripta Materialia* 103, 14–17.
- Everaers, R., Karimi-Varzaneh, H.A., Fleck, F., Hojdis, N., Svaneborg, C., 2020. Kremer–Grest Models for Commodity Polymer Melts: Linking Theory, Experiment, and Simulation at the Kuhn Scale. *Macromolecules* 53, 1901–1916. <https://doi.org/10.1021/acs.macromol.9b02428>
- Fetters, L.J., Lohse, D.J., Colby, R.H., 2007. Chain Dimensions and Entanglement Spacings, in: Mark, J.E. (Ed.), *Physical Properties of Polymers Handbook*. Springer New York, New York, NY, pp. 447–454. https://doi.org/10.1007/978-0-387-69002-5_25
- Floudas, G., 2004. Effects of pressure on systems with intrinsic orientational order. *Progress in Polymer Science* 29, 1143–1171. <https://doi.org/10.1016/j.progpolymsci.2004.08.004>
- Floudas, G., Gravalides, C., Reisinger, T., Wegner, G., 1999. Effect of pressure on the segmental and chain dynamics of polyisoprene. *Molecular weight dependence*. *The Journal of Chemical Physics* 111, 9847–9852. <https://doi.org/10.1063/1.480327>
- Floudas, G., Mpoukouvalas, K., Papadopoulos, P., 2006. The role of temperature and density on the glass-transition dynamics of glass formers. *The Journal of Chemical Physics* 124, 074905. <https://doi.org/10.1063/1.2170074>
- Floudas, G., Paluch, M., Grzybowski, A., Ngai, K., 2011. *Molecular Dynamics of Glass-Forming Systems, Advances in Dielectrics*. Springer Berlin Heidelberg, Berlin, Heidelberg. <https://doi.org/10.1007/978-3-642-04902-6>
- Fosse, C., Esposito, A., Thiyagarajan, S., Soccio, M., Lotti, N., Dargent, E., Delbreilh, L., 2022. Cooperativity and fragility in furan-based polyesters with different glycolic subunits as compared to their terephthalic counterparts. *Journal of Non-Crystalline Solids* 597, 121907.
- Fox, T.G., Flory, P.J., 1954. The glass temperature and related properties of polystyrene. Influence of molecular weight. *J. Polym. Sci.* 14, 315–319. <https://doi.org/10.1002/pol.1954.120147514>
- Fragiadakis, D., Casalini, R., Bogoslovov, R.B., Robertson, C.G., Roland, C.M., 2011a. Dynamic Heterogeneity and Density Scaling in 1,4-Polyisoprene. *Macromolecules* 44, 1149–1155. <https://doi.org/10.1021/ma102795w>
- Fragiadakis, D., Casalini, R., Roland, C.M., 2011b. Comparing dynamic correlation lengths from an approximation to the four-point dynamic susceptibility and from the picosecond vibrational dynamics. *Phys. Rev. E* 84, 042501. <https://doi.org/10.1103/PhysRevE.84.042501>
- Fredrickson, G.H., Andersen, H.C., 1985. Facilitated kinetic Ising models and the glass transition. *The Journal of Chemical Physics* 83, 5822–5831. <https://doi.org/10.1063/1.449662>
- Frick, B., Alba-Simionesco, C., 1999. Comparison of the pressure and temperature dependence of the elastic incoherent scattering for the polymers polybutadiene and polyisobutylene. *Physica B: Condensed Matter* 266, 13–19.
- Fröhlich, H., 1986. *Theory of dielectrics: dielectrics constant and dielectric loss*, 2nd ed. ed, Monographs on the physics and chemistry of materials. Clarendon Press, Oxford.
- Fulcher, G.S., 1925. Analysis of recent measurements of the viscosity of glasses. *J American Ceramic Society* 8, 339–355. <https://doi.org/10.1111/j.1151-2916.1925.tb16731.x>
- Fytas, G., Patkowski, A., Meier, G., Dorfmueller, T., 1982. Pressure- and temperature-dependent photon correlation study of bulk poly(ethyl acrylate) above the glass transition temperature. *Macromolecules* 15, 870–874. <https://doi.org/10.1021/ma00231a034>
- Garrahan, J.P., Sollich, P., Toninelli, C., 2011. Kinetically constrained models. *Dynamical heterogeneities in glasses, colloids, and granular media* 150, 111–137.

- Genix, A.-C., Lauprêtre, F., 2005. Subglass and Glass Transitions of Poly(di-n-alkylitaconate)s with Various Side-Chain Lengths: Dielectric Relaxation Investigation. *Macromolecules* 38, 2786–2794. <https://doi.org/10.1021/ma047600t>
- Gibbs, J.H., DiMarzio, E.A., 1958. Nature of the Glass Transition and the Glassy State. *The Journal of Chemical Physics* 28, 373–383. <https://doi.org/10.1063/1.1744141>
- Gitsas, A., Floudas, G., Wegner, G., 2004. Effects of temperature and pressure on the stability and mobility of phases in rigid rod poly (p -phenylenes). *Phys. Rev. E* 69, 041802. <https://doi.org/10.1103/PhysRevE.69.041802>
- Goldbart, P., Goldenfeld, N., 1989. Microscopic theory for cross-linked macromolecules. I. Broken symmetry, rigidity, and topology. *Phys. Rev. A* 39, 1402–1411. <https://doi.org/10.1103/PhysRevA.39.1402>
- Goldenfeld, N., 1999. Lectures on phase transitions and the renormalization group, 12.[pr.]. ed, *Frontiers in physics*. Perseus Books, Reading, Mass.
- Goldstein, M., 1975. Validity of the Ehrenfest equation for a system with more than one ordering parameter: Critique of a paper by DiMarzio. *Journal of Applied Physics* 46, 4153–4156. <https://doi.org/10.1063/1.321441>
- Goldstein, M., 1973. Viscous liquids and the glass transition. IV. Thermodynamic equations and the transition. *J. Phys. Chem.* 77, 667–673. <https://doi.org/10.1021/j100624a022>
- Goldstein, M., 1972. Glass and other relaxations in liquids. *Faraday Symp. Chem. Soc.* 6, 7. <https://doi.org/10.1039/fs9720600007>
- Goldstein, M., 1969. Viscous Liquids and the Glass Transition: A Potential Energy Barrier Picture. *The Journal of Chemical Physics* 51, 3728–3739. <https://doi.org/10.1063/1.1672587>
- Gomez Ribelles, J.L., Monleon Pradas, M., Vidaurre Garayo, A., Romero Colomer, F., Mas Estelles, J., Meseguer Duenas, J.M., 1995. Structural Relaxation of Glass-Forming Polymers Based on an Equation for Configurational Entropy. 2. Structural Relaxation in Polymethacrylates. *Macromolecules* 28, 5878–5885. <https://doi.org/10.1021/ma00121a026>
- Götze, W., 2008. *Complex Dynamics of Glass-Forming Liquids*. Oxford University Press. <https://doi.org/10.1093/acprof:oso/9780199235346.001.0001>
- Götze, W., Sjögren, L., 1996. Comments on the mode coupling theory for structural relaxation. *Chemical physics* 212, 47–59.
- Götze, W., Sjögren, L., 1995. The mode coupling theory of structural relaxations. *Transport Theory and Statistical Physics* 24, 801–853. <https://doi.org/10.1080/00411459508203936>
- Götze, W., Sjögren, L., 1992. Relaxation processes in supercooled liquids. *Reports on progress in Physics* 55, 241.
- Grigoras, C.V., Grigoras, A.G., 2011. Nanoscale cooperativity on a series of statistical methacrylates copolymers with electron donor–acceptor pendant groups. *J Therm Anal Calorim* 103, 661–668. <https://doi.org/10.1007/s10973-010-1019-y>
- Grzybowska, K., Adrjanowicz, K., Paluch, M., 2016. Application of Broadband Dielectric Spectroscopy to Study Molecular Mobility in Pharmaceutical Systems, in: Descamps, M. (Ed.), *Disordered Pharmaceutical Materials*. Wiley, pp. 301–360. <https://doi.org/10.1002/9783527652693.ch11>
- Grzybowska, K., Grzybowski, A., Wojnarowska, Z., Knapik, J., Paluch, M., 2015. Ionic liquids and their bases: Striking differences in the dynamic heterogeneity near the glass transition. *Sci Rep* 5, 16876. <https://doi.org/10.1038/srep16876>
- Grzybowska, K., Pawlus, S., Mierzwa, M., Paluch, M., Ngai, K.L., 2006. Changes of relaxation dynamics of a hydrogen-bonded glass former after removal of the hydrogen bonds. *The Journal of Chemical Physics* 125, 144507. <https://doi.org/10.1063/1.2354492>
- Grzybowski, A., Kolodziejczyk, K., Koperwas, K., Grzybowska, K., Paluch, M., 2012. Effects of lowering temperature and raising pressure on the spatially heterogeneous dynamics of glass-forming van der Waals liquids. *Phys. Rev. B* 85, 220201. <https://doi.org/10.1103/PhysRevB.85.220201>

- Grzybowski, A., Koperwas, K., Swiety-Pospiech, A., Grzybowska, K., Paluch, M., 2013. Activation volume in the density scaling regime: Equation of state and its test by using experimental and simulation data. *Phys. Rev. B* 87, 054105. <https://doi.org/10.1103/PhysRevB.87.054105>
- Grzybowski, A., Urban, S., Mroz, S., Paluch, M., 2017. Activation volume of selected liquid crystals in the density scaling regime. *Sci Rep* 7, 42174. <https://doi.org/10.1038/srep42174>
- Guggenheim, E.A., 1937. Thermodynamics of an activated complex. *Trans. Faraday Soc.* 33, 607. <https://doi.org/10.1039/tf9373300607>
- Guiselin, B., Scalliet, C., Berthier, L., 2022. Microscopic origin of excess wings in relaxation spectra of supercooled liquids. *Nat. Phys.* 18, 468–472. <https://doi.org/10.1038/s41567-022-01508-z>
- Hamonic, F., Prevosto, D., Dargent, E., Saiter, A., 2014. Contribution of chain alignment and crystallization in the evolution of cooperativity in drawn polymers. *Polymer* 55, 2882–2889. <https://doi.org/10.1016/j.polymer.2014.04.030>
- Havriliak, S., Negami, S., 1967. A complex plane representation of dielectric and mechanical relaxation processes in some polymers. *Polymer* 8, 161–210. [https://doi.org/10.1016/0032-3861\(67\)90021-3](https://doi.org/10.1016/0032-3861(67)90021-3)
- Hecksher, T., Nielsen, A.I., Olsen, N.B., Dyre, J.C., 2008. Little evidence for dynamic divergences in ultraviscous molecular liquids. *Nature Phys* 4, 737–741. <https://doi.org/10.1038/nphys1033>
- Heczko, D., Grelska, J., Jurkiewicz, K., Szychalska, P., Kasprzycka, A., Kamiński, K., Paluch, M., Kamińska, E., 2021. Anomalous narrowing of the shape of the structural process in derivatives of trehalose at high pressure. The role of the internal structure. *Journal of Molecular Liquids* 336, 116321. <https://doi.org/10.1016/j.molliq.2021.116321>
- Hempel, E., Hempel, G., Hensel, A., Schick, C., Donth, E., 2000. Characteristic Length of Dynamic Glass Transition near T_g for a Wide Assortment of Glass-Forming Substances. *J. Phys. Chem. B* 104, 2460–2466. <https://doi.org/10.1021/jp991153f>
- Hensel-Bielowka, S., Pawlus, S., Roland, C.M., Ziolo, J., Paluch, M., 2004. Effect of large hydrostatic pressure on the dielectric loss spectrum of type-A glass formers. *Phys. Rev. E* 69, 050501. <https://doi.org/10.1103/PhysRevE.69.050501>
- Hodge, I.M., 1995. Physical Aging in Polymer Glasses. *Science* 267, 1945–1947. <https://doi.org/10.1126/science.267.5206.1945>
- Hollander, A.G.S., Prins, K.O., 2001. Atactic polypropylene at high pressure. I. Deuteron-NMR determination of the glass-transition temperature. *Journal of non-crystalline solids* 286, 1–11.
- Holt, A.P., Fragiadakis, D., Roland, C.M., 2019. Pressure densified 1,3,5-tri(1-naphthyl)benzene glass. I. Volume recovery and physical aging. *The Journal of Chemical Physics* 151, 184502. <https://doi.org/10.1063/1.5122765>
- Hong, L., Begen, B., Kisliuk, A., Alba-Simionesco, C., Novikov, V.N., Sokolov, A.P., 2008. Pressure and density dependence of the boson peak in polymers. *Phys. Rev. B* 78, 134201. <https://doi.org/10.1103/PhysRevB.78.134201>
- Hong, L., Gujrati, P.D., Novikov, V.N., Sokolov, A.P., 2009. Molecular cooperativity in the dynamics of glass-forming systems: A new insight. *J. Chem. Phys.* 131, 194511. <https://doi.org/10.1063/1.3266508>
- Hong, L., Novikov, V.N., Sokolov, A.P., 2011a. Is there a connection between fragility of glass forming systems and dynamic heterogeneity/cooperativity? *Journal of Non-Crystalline Solids* 357, 351–356. <https://doi.org/10.1016/j.jnoncrysol.2010.06.071>
- Hong, L., Novikov, V.N., Sokolov, A.P., 2011b. Dynamic heterogeneities, boson peak, and activation volume in glass-forming liquids. *Phys. Rev. E* 83, 061508. <https://doi.org/10.1103/PhysRevE.83.061508>
- Hu, W., 2013. *Polymer physics: a molecular approach*. Springer, Vienna ; New York.

- Hu, Y.-C., Guan, P.-F., Wang, Q., Yang, Y., Bai, H.-Y., Wang, W.-H., 2017. Pressure effects on structure and dynamics of metallic glass-forming liquid. *The Journal of Chemical Physics* 146, 024507. <https://doi.org/10.1063/1.4973919>
- Huang, D., Colucci, D.M., McKenna, G.B., 2002. Dynamic fragility in polymers: A comparison in isobaric and isochoric conditions. *The Journal of Chemical Physics* 116, 3925–3934. <https://doi.org/10.1063/1.1448287>
- Huang, T., Miura, M., Nobukawa, S., Yamaguchi, M., 2015. Chain Packing and Its Anomalous Effect on Mechanical Toughness for Poly(lactic acid). *Biomacromolecules* 16, 1660–1666. <https://doi.org/10.1021/acs.biomac.5b00293>
- Hurley, M.M., Harrowell, P., 1995. Kinetic structure of a two-dimensional liquid. *Phys. Rev. E* 52, 1694–1698. <https://doi.org/10.1103/PhysRevE.52.1694>
- Hutchinson, J.M., 1995. Physical aging of polymers. *Progress in Polymer Science* 20, 703–760. [https://doi.org/10.1016/0079-6700\(94\)00001-I](https://doi.org/10.1016/0079-6700(94)00001-I)
- Hutchinson, J.M., Montserrat, S., Calventus, Y., Cortés, P., 2000. Application of the Adam–Gibbs Equation to the Non-Equilibrium Glassy State. *Macromolecules* 33, 5252–5262. <https://doi.org/10.1021/ma992015r>
- Ito, K., Moynihan, C.T., Angell, C.A., 1999. Thermodynamic determination of fragility in liquids and a fragile-to-strong liquid transition in water. *Nature* 398, 492–495.
- Jain, R.K., Simha, R., 1989. Theoretical equation of state: thermal expansivity, compressibility, and the Tait relation. *Macromolecules* 22, 464–468. <https://doi.org/10.1021/ma00191a084>
- Johari, G.P., 1973. Intrinsic mobility of molecular glasses. *The Journal of Chemical Physics* 58, 1766–1770. <https://doi.org/10.1063/1.1679421>
- Johari, G.P., Goldstein, M., 1970. Viscous Liquids and the Glass Transition. II. Secondary Relaxations in Glasses of Rigid Molecules. *The Journal of Chemical Physics* 53, 2372–2388. <https://doi.org/10.1063/1.1674335>
- Jung, G., Biroli, G., Berthier, L., 2024. Dynamic heterogeneity at the experimental glass transition predicted by transferable machine learning. *Phys. Rev. B* 109, 064205. <https://doi.org/10.1103/PhysRevB.109.064205>
- Kahouli, A., 2016. Spectroscopie diélectrique appliquée aux polymères. *Techniques de l'ingénieur, Conversion de l'énergie électrique* 1–13.
- Kaminski, K., Pawlus, S., Adrjanowicz, K., Wojnarowska, Z., Włodarczyk, P., Paluch, M., 2012. The importance of the activation volume for the description of the molecular dynamics of glass-forming liquids. *J. Phys.: Condens. Matter* 24, 065105. <https://doi.org/10.1088/0953-8984/24/6/065105>
- Kauzmann, Walter., 1948. The Nature of the Glassy State and the Behavior of Liquids at Low Temperatures. *Chem. Rev.* 43, 219–256. <https://doi.org/10.1021/cr60135a002>
- Ketkaew, J., Yamada, R., Wang, H., Kuldinow, D., Schroers, B.S., Dmowski, W., Egami, T., Schroers, J., 2020. The effect of thermal cycling on the fracture toughness of metallic glasses. *Acta Materialia* 184, 100–108. <https://doi.org/10.1016/j.actamat.2019.11.046>
- Ketov, S.V., Sun, Y.H., Nachum, S., Lu, Z., Checchi, A., Beraldin, A.R., Bai, H.Y., Wang, W.H., Louzguine-Luzgin, D.V., Carpenter, M.A., Greer, A.L., 2015. Rejuvenation of metallic glasses by non-affine thermal strain. *Nature* 524, 200–203. <https://doi.org/10.1038/nature14674>
- King Jr, H.E., Herbolzheimer, E., Cook, R.L., 1992. The diamond-anvil cell as a high-pressure viscometer. *Journal of applied physics* 71, 2071–2081.
- Kirkpatrick, T.R., Thirumalai, D., 1987. Dynamics of the Structural Glass Transition and the p -Spin—Interaction Spin-Glass Model. *Phys. Rev. Lett.* 58, 2091–2094. <https://doi.org/10.1103/PhysRevLett.58.2091>

- Kirkpatrick, T.R., Thirumalai, D., Wolynes, P.G., 1989. Scaling concepts for the dynamics of viscous liquids near an ideal glassy state. *Phys. Rev. A* 40, 1045–1054. <https://doi.org/10.1103/PhysRevA.40.1045>
- Kirkwood, J.G., 1940. THE LOCAL FIELD IN DIELECTRICS. *Annals of the New York Academy of Sciences* 40, 315–320. <https://doi.org/10.1111/j.1749-6632.1940.tb19543.x>
- Kivelson, D., Kivelson, S.A., Zhao, X., Nussinov, Z., Tarjus, G., 1995. A thermodynamic theory of supercooled liquids. *Physica A: Statistical Mechanics and its Applications* 219, 27–38. [https://doi.org/10.1016/0378-4371\(95\)00140-3](https://doi.org/10.1016/0378-4371(95)00140-3)
- Kob, W., Andersen, H.C., 1995. Testing mode-coupling theory for a supercooled binary Lennard-Jones mixture I: The van Hove correlation function. *Phys. Rev. E* 51, 4626–4641. <https://doi.org/10.1103/PhysRevE.51.4626>
- Kob, W., Andersen, H.C., 1994. Scaling Behavior in the β -Relaxation Regime of a Supercooled Lennard-Jones Mixture. *Phys. Rev. Lett.* 73, 1376–1379. <https://doi.org/10.1103/PhysRevLett.73.1376>
- Kob, W., Andersen, H.C., 1993. Kinetic lattice-gas model of cage effects in high-density liquids and a test of mode-coupling theory of the ideal-glass transition. *Phys. Rev. E* 48, 4364–4377. <https://doi.org/10.1103/PhysRevE.48.4364>
- Kohlrausch, F., 1863. Ueber die elastische Nachwirkung bei der Torsion. *Ann. Phys. Chem.* 195, 337–368. <https://doi.org/10.1002/andp.18631950702>
- Koran, F., Dealy, J.M., 1999. A high pressure sliding plate rheometer for polymer melts. *Journal of Rheology* 43, 1279–1290.
- Kremer, F., Schönhals, A. (Eds.), 2003. *Broadband Dielectric Spectroscopy*. Springer Berlin Heidelberg, Berlin, Heidelberg. <https://doi.org/10.1007/978-3-642-56120-7>
- Kummali, M.M., Alegría, A., Miccio, L.A., Colmenero, J., 2013. Study of the Dynamic Heterogeneity in Poly(ethylene-*ran*-vinyl acetate) Copolymer by Using Broadband Dielectric Spectroscopy and Electrostatic Force Microscopy. *Macromolecules* 46, 7502–7512. <https://doi.org/10.1021/ma4012522>
- Kunal, K., Robertson, C.G., Pawlus, S., Hahn, S.F., Sokolov, A.P., 2008. Role of Chemical Structure in Fragility of Polymers: A Qualitative Picture. *Macromolecules* 41, 7232–7238. <https://doi.org/10.1021/ma801155c>
- Lei, M., Reid, C.G., Zoller, P., 1988. Stresses and volume changes in a polymer loaded axially in a rigid die. *Polymer* 29, 1784–1788.
- Leutheusser, E., 1984. Dynamical model of the liquid-glass transition. *Phys. Rev. A* 29, 2765–2773. <https://doi.org/10.1103/PhysRevA.29.2765>
- Lixon, C., Delpouve, N., Saiter, A., Dargent, E., Grohens, Y., 2008. Evidence of Cooperative Rearranging Region size anisotropy for drawn PET. *European Polymer Journal* 44, 3377–3384. <https://doi.org/10.1016/j.eurpolymj.2008.08.001>
- Ma, P., Hristova-Bogaerds, D.G., Goossens, J.G.P., Spoelstra, A.B., Zhang, Y., Lemstra, P.J., 2012. Toughening of poly(lactic acid) by ethylene-*co*-vinyl acetate copolymer with different vinyl acetate contents. *European Polymer Journal* 48, 146–154. <https://doi.org/10.1016/j.eurpolymj.2011.10.015>
- Malinovsky, V.K., Sokolov, A.P., 1986. The nature of boson peak in Raman scattering in glasses. *Solid State Communications* 57, 757–761. [https://doi.org/10.1016/0038-1098\(86\)90854-9](https://doi.org/10.1016/0038-1098(86)90854-9)
- Mapesa, E.U., Street, D.P., Heres, M.F., Kilbey, S.M.I., Sangoro, J., 2020. Wetting and Chain Packing across Interfacial Zones Affect Distribution of Relaxations in Polymer and Polymer-Grafted Nanocomposites. *Macromolecules* 53, 5315–5325. <https://doi.org/10.1021/acs.macromol.0c00399>

- Mark, H.F., Bikales, N.M., Overberger, C.G., Menges, G., Kroschwitz, J.I. (Eds.), 1986. Encyclopedia of Polymer Science and Engineering: Volume 5, Dielectric Heating to Embedding, Volume 5 edition. ed. Wiley-Interscience, New York.
- Mattsson, J., Wyss, H.M., Fernandez-Nieves, A., Miyazaki, K., Hu, Z., Reichman, D.R., Weitz, D.A., 2009. Soft colloids make strong glasses. *Nature* 462, 83–86. <https://doi.org/10.1038/nature08457>
- Mauro, J.C., Tandia, A., Vargheese, K.D., Mauro, Y.Z., Smedskjaer, M.M., 2016. Accelerating the Design of Functional Glasses through Modeling. *Chem. Mater.* 28, 4267–4277. <https://doi.org/10.1021/acs.chemmater.6b01054>
- McKinney, J.E., Simha, R., 1974. Configurational Thermodynamic Properties of Polymer Liquids and Glasses. I. Poly(vinyl acetate). *Macromolecules* 7, 894–901. <https://doi.org/10.1021/ma60042a037>
- Mejres, M., Hallavant, K., Guidotti, G., Soccio, M., Lotti, N., Esposito, A., Saiter-Fourcin, A., 2024. Physical aging of a biodegradable alicyclic polymer: poly (pentamethylene *trans*-1,4-cyclohexanedicarboxylate). *Journal of Non-Crystalline Solids* 629, 122874. <https://doi.org/10.1016/j.jnoncrysol.2024.122874>
- Micoulaut, M., 2016. Relaxation and physical aging in network glasses: a review. *Rep. Prog. Phys.* 79, 066504. <https://doi.org/10.1088/0034-4885/79/6/066504>
- Monnier, X., Delpouve, N., Basson, N., Guinault, A., Domenek, S., Saiter, A., Mallon, P.E., Dargent, E., 2015. Molecular dynamics in electrospun amorphous plasticized polylactide fibers. *Polymer* 73, 68–78. <https://doi.org/10.1016/j.polymer.2015.07.047>
- Montanari, A., Semerjian, G., 2006. Rigorous Inequalities between Length and Time Scales in Glassy Systems. *J Stat Phys* 125, 23–54. <https://doi.org/10.1007/s10955-006-9175-y>
- Morvan, A., Calvez, L., Vella, A., Saiter-Fourcin, A., 2022. Physical aging of the 62.5GeS₂-12.5Sb₂S₃-25CsCl chalcogenide glass: Assessing the mechanisms of equilibration and crystallization. *Journal of Non-Crystalline Solids* 598, 121955. <https://doi.org/10.1016/j.jnoncrysol.2022.121955>
- Morvan, A., Delpouve, N., Vella, A., Saiter-Fourcin, A., 2021. Physical aging of selenium glass: Assessing the double mechanism of equilibration and the crystallization process. *Journal of Non-Crystalline Solids* 570, 121013. <https://doi.org/10.1016/j.jnoncrysol.2021.121013>
- Moynihan, C.T., Macedo, P.B., Montrose, C.J., Montrose, C.J., Gupta, P.K., DeBolt, M.A., Dill, J.F., Dom, B.E., Drake, P.W., Eastal, A.J., Elterman, P.B., Moeller, R.P., Sasabe, H., Wilder, J.A., 1976. STRUCTURAL RELAXATION IN VITREOUS MATERIALS. *Ann NY Acad Sci* 279, 15–35. <https://doi.org/10.1111/j.1749-6632.1976.tb39688.x>
- Mpoukouvalas, K., Floudas, G., Williams, G., 2009. Origin of the α , β , ($\beta\alpha$), and “Slow” Dielectric Processes in Poly(ethyl methacrylate). *Macromolecules* 42, 4690–4700. <https://doi.org/10.1021/ma900644t>
- Munro, R.G., Piermarini, G.J., Block, S., 1979. Wall effects in a diamond-anvil pressure-cell falling-sphere viscometer. *Journal of Applied Physics* 50, 3180–3184.
- Nakanishi, M., Nozaki, R., 2011. Model of the cooperative rearranging region for polyhydric alcohols. *Phys. Rev. E* 84, 011503. <https://doi.org/10.1103/PhysRevE.84.011503>
- Narayanaswamy, O.S., 1971. A Model of Structural Relaxation in Glass. *J American Ceramic Society* 54, 491–498. <https://doi.org/10.1111/j.1151-2916.1971.tb12186.x>
- Ngai, K.L., 2023. Universal properties of relaxation and diffusion in complex materials: Originating from fundamental physics with rich applications. *Progress in Materials Science* 139, 101130. <https://doi.org/10.1016/j.pmatsci.2023.101130>
- Ngai, K.L., 2011. *Relaxation and Diffusion in Complex Systems, Partially Ordered Systems*. Springer New York, New York, NY. <https://doi.org/10.1007/978-1-4419-7649-9>
- Ngai, K.L., 2007. Why the glass transition problem remains unsolved? *Journal of non-crystalline solids* 353, 709–718.

- Ngai, K.L., 2000. Dynamic and thermodynamic properties of glass-forming substances. *Journal of Non-Crystalline Solids* 275, 7–51. [https://doi.org/10.1016/S0022-3093\(00\)00238-6](https://doi.org/10.1016/S0022-3093(00)00238-6)
- Ngai, K.L., Casalini, R., Capaccioli, S., Paluch, M., Roland, C.M., 2005. Do Theories of the Glass Transition, in which the Structural Relaxation Time Does Not Define the Dispersion of the Structural Relaxation, Need Revision? *J. Phys. Chem. B* 109, 17356–17360. <https://doi.org/10.1021/jp053439s>
- Ngai, K.L., Paluch, M., 2004. Classification of secondary relaxation in glass-formers based on dynamic properties. *The Journal of Chemical Physics* 120, 857–873. <https://doi.org/10.1063/1.1630295>
- Ngai, K.L., Roland, C.M., 1993a. Chemical structure and intermolecular cooperativity: dielectric relaxation results. *Macromolecules* 26, 6824–6830. <https://doi.org/10.1021/ma00077a019>
- Ngai, K.L., Roland, C.M., 1993b. Intermolecular cooperativity and the temperature dependence of segmental relaxation in semicrystalline polymers. *Macromolecules* 26, 2688–2690. <https://doi.org/10.1021/ma00063a008>
- Niss, K., Alba-Simionesco, C., 2006. Effects of density and temperature on correlations between fragility and glassy properties. *Phys. Rev. B* 74, 024205. <https://doi.org/10.1103/PhysRevB.74.024205>
- Niss, K., Dalle-Ferrier, C., Tarjus, G., Alba-Simionesco, C., 2007. On the correlation between fragility and stretching in glass-forming liquids. *J. Phys.: Condens. Matter* 19, 076102. <https://doi.org/10.1088/0953-8984/19/7/076102>
- Niss, K., Hecksher, T., 2018. Perspective: Searching for simplicity rather than universality in glass-forming liquids. *The Journal of Chemical Physics* 149, 230901. <https://doi.org/10.1063/1.5048093>
- Novikov, V.N., Sokolov, A.P., 2004. Poisson's ratio and the fragility of glass-forming liquids. *Nature* 431, 961–963.
- Novocontrol Technologies, 2017. WinDETA 6.02 Program's Manual.
- Nozaki, R., Mashimo, S., 1987. Dielectric relaxation measurements of poly(vinyl acetate) in glassy state in the frequency range 10^{-6} – 10^6 Hz. *The Journal of Chemical Physics* 87, 2271–2277. <https://doi.org/10.1063/1.453156>
- Oliver, W., Herbst, C., Lindsay, S., Wolf, G., 1991. High-pressure viscoelastic properties and equation of state of liquids derived from Brillouin data. *Phys. Rev. Lett.* 67, 2795–2798. <https://doi.org/10.1103/PhysRevLett.67.2795>
- Onsager, L., 1936. Electric Moments of Molecules in Liquids. *J. Am. Chem. Soc.* 58, 1486–1493. <https://doi.org/10.1021/ja01299a050>
- O'Reilly, J.M., 1977. Conformational specific heat of polymers. *Journal of Applied Physics* 48, 4043–4048.
- Orwoll, R.A., 2007. Densities, Coefficients of Thermal Expansion, and Compressibilities of Amorphous Polymers, in: Mark, J.E. (Ed.), *Physical Properties of Polymers Handbook*. Springer New York, New York, NY, pp. 93–101. https://doi.org/10.1007/978-0-387-69002-5_7
- Paluch, M., Gapinski, J., Patkowski, A., Fischer, E.W., 2001. Does fragility depend on pressure? A dynamic light scattering study of a fragile glass-former. *The Journal of Chemical Physics* 114, 8048–8055. <https://doi.org/10.1063/1.1362293>
- Paluch, M., Grzybowska, K., Grzybowski, A., 2007. Effect of high pressure on the relaxation dynamics of glass-forming liquids. *Journal of Physics: Condensed Matter* 19, 205117. <https://doi.org/10.1088/0953-8984/19/20/205117>
- Paluch, M., Hensel-Bielowka, S., Psurek, T., 2000. Analysis of “equation of state” for supercooled liquid. *The Journal of Chemical Physics* 113, 4374–4378.
- Paluch, M., Hensel-Bielowka, S., Ziolo, J., 1999. Effect of pressure on fragility and glass transition temperature in fragile glass-former. *The Journal of Chemical Physics* 110, 10978–10981. <https://doi.org/10.1063/1.479035>

- Paluch, M., Knapik, J., Wojnarowska, Z., Grzybowski, A., Ngai, K.L., 2016. Universal Behavior of Dielectric Responses of Glass Formers: Role of Dipole-Dipole Interactions. *Phys. Rev. Lett.* 116, 025702. <https://doi.org/10.1103/PhysRevLett.116.025702>
- Paluch, M., Pawlus, S., Roland, C.M., 2002a. Pressure and Temperature Dependence of the α -Relaxation in Poly(methyltolylsiloxane). *Macromolecules* 35, 7338–7342. <https://doi.org/10.1021/ma020587x>
- Paluch, M., Roland, C.M., 2003. The Avramov model of structural relaxation. *Journal of non-crystalline solids* 316, 413–417.
- Paluch, M., Roland, C.M., Gapinski, J., Patkowski, A., 2003. Pressure and temperature dependence of structural relaxation in diglycidylether of bisphenol A. *The Journal of Chemical Physics* 118, 3177–3186. <https://doi.org/10.1063/1.1538597>
- Paluch, M., Roland, C.M., Pawlus, S., 2002b. Temperature and pressure dependence of the α -relaxation in polymethylphenylsiloxane. *The Journal of Chemical Physics* 116, 10932–10937. <https://doi.org/10.1063/1.1478767>
- Paluch, M., Rzoska, S.J., Habdas, P., Ziolo, J., 1998. On the isothermal pressure behaviour of the relaxation times for supercooled glass-forming liquids. *J. Phys.: Condens. Matter* 10, 4131–4138. <https://doi.org/10.1088/0953-8984/10/19/001>
- Paluch, M., Rzoska, S.J., Habdas, P., Ziolo, J., 1996. Isothermal and high-pressure studies of dielectric relaxation in supercooled glycerol. *J. Phys.: Condens. Matter* 8, 10885–10890. <https://doi.org/10.1088/0953-8984/8/50/014>
- Pan, P., Zhu, B., Inoue, Y., 2007. Enthalpy Relaxation and Embrittlement of Poly(L-lactide) during Physical Aging. *Macromolecules* 40, 9664–9671. <https://doi.org/10.1021/ma071737c>
- Pawlus, S., Paluch, M., Ziolo, J., Roland, C.M., 2009. On the pressure dependence of the fragility of glycerol. *J. Phys.: Condens. Matter* 21, 332101. <https://doi.org/10.1088/0953-8984/21/33/332101>
- Peng, X., McKenna, G.B., 2016. Physical aging and structural recovery in a colloidal glass subjected to volume-fraction jump conditions. *Phys. Rev. E* 93, 042603. <https://doi.org/10.1103/PhysRevE.93.042603>
- Phan, A.D., Koperwas, K., Paluch, M., Wakabayashi, K., 2020. Coupling between structural relaxation and diffusion in glass-forming liquids under pressure variation. *Phys. Chem. Chem. Phys.* 22, 24365–24371. <https://doi.org/10.1039/D0CP02761H>
- Prigogine, I., Defay, R., 1986. *Chemical thermodynamics*. University Microfilms International, Ann Arbor, MI.
- Puente, J.A.S., Rijal, B., Delbreilh, L., Fatyeyeva, K., Saiter, A., Dargent, E., 2015. Segmental mobility and glass transition of poly(ethylene-vinyl acetate) copolymers: Is there a continuum in the dynamic glass transitions from PVAc to PE? *Polymer* 76, 213–219. <https://doi.org/10.1016/j.polymer.2015.09.007>
- Qin, Q., McKenna, G.B., 2006. Correlation between dynamic fragility and glass transition temperature for different classes of glass forming liquids. *Journal of Non-Crystalline Solids* 352, 2977–2985. <https://doi.org/10.1016/j.jnoncrysol.2006.04.014>
- Qiu, X.H., Ediger, M.D., 2003. Length Scale of Dynamic Heterogeneity in Supercooled D-Sorbitol: Comparison to Model Predictions. *J. Phys. Chem. B* 107, 459–464. <https://doi.org/10.1021/jp021888b>
- Rams-Baron, M., Blazytko, A., Casalini, R., Paluch, M., 2024. Insight into properties of sizable glass former from volumetric measurements. <https://doi.org/10.48550/ARXIV.2403.04367>
- Reading, M., Hahn, B.K., Crowe, B.S., 1993. Method and apparatus for modulated differential analysis.
- Reading, M., Hourston, D.J. (Eds.), 2006. *Modulated Temperature Differential Scanning Calorimetry, Hot Topics in Thermal Analysis and Calorimetry*. Springer Netherlands, Dordrecht. <https://doi.org/10.1007/1-4020-3750-3>

- Reiner, M., 1964. The Deborah Number. *Physics Today* 17, 62. <https://doi.org/10.1063/1.3051374>
- Reinsberg, S.A., Heuer, A., Doliwa, B., Zimmermann, H., Spiess, H.W., 2002. Comparative study of the NMR length scale of dynamic heterogeneities of three different glass formers. *Journal of Non-Crystalline Solids* 307–310, 208–214. [https://doi.org/10.1016/S0022-3093\(02\)01460-6](https://doi.org/10.1016/S0022-3093(02)01460-6)
- Reiser, A., Kasper, G., Hunklinger, S., 2004. Effect of Pressure on the Secondary Relaxation in a Simple Glass Former. *Phys. Rev. Lett.* 92, 125701. <https://doi.org/10.1103/PhysRevLett.92.125701>
- Richert, R., 2002. Heterogeneous dynamics in liquids: fluctuations in space and time. *J. Phys.: Condens. Matter* 14, R703–R738. <https://doi.org/10.1088/0953-8984/14/23/201>
- Richert, R., 1996. Geometrical confinement and cooperativity in supercooled liquids studied by solvation dynamics. *Phys. Rev. B* 54, 15762–15766. <https://doi.org/10.1103/PhysRevB.54.15762>
- Richert, R., Angell, C.A., 1998. Dynamics of glass-forming liquids. V. On the link between molecular dynamics and configurational entropy. *The Journal of Chemical Physics* 108, 9016–9026. <https://doi.org/10.1063/1.476348>
- Rijal, B., Delbreilh, L., Saiter, A., 2015. Dynamic Heterogeneity and Cooperative Length Scale at Dynamic Glass Transition in Glass Forming Liquids. *Macromolecules* 48, 8219–8231. <https://doi.org/10.1021/acs.macromol.5b01152>
- Rijal, B., Soto Puente, J.A., Atawa, B., Delbreilh, L., Fatyeyeva, K., Saiter, A., Dargent, E., 2016. Correlated and cooperative motions in segmental relaxation: Influence of constitutive unit weight and intermolecular interactions. *Phys. Rev. E* 94, 062502. <https://doi.org/10.1103/PhysRevE.94.062502>
- Roland, C.M., Bair, S., Casalini, R., 2006. Thermodynamic scaling of the viscosity of van der Waals, H-bonded, and ionic liquids. *The Journal of Chemical Physics* 125, 124508. <https://doi.org/10.1063/1.2346679>
- Roland, C.M., Casalini, R., 2005. Effect of chemical structure on the isobaric and isochoric fragility in polychlorinated biphenyls. *The Journal of Chemical Physics* 122, 134505. <https://doi.org/10.1063/1.1863173>
- Roland, C.M., Casalini, R., 2003a. Temperature and Volume Effects on Local Segmental Relaxation in Poly(vinyl acetate). *Macromolecules* 36, 1361–1367. <https://doi.org/10.1021/ma025791z>
- Roland, C.M., Casalini, R., 2003b. Temperature dependence of local segmental motion in polystyrene and its variation with molecular weight. *The Journal of Chemical Physics* 119, 1838–1842. <https://doi.org/10.1063/1.1581850>
- Roland, C.M., Casalini, R., Paluch, M., 2003. Isochronal temperature–pressure superpositioning of the α -relaxation in type-A glass formers. *Chemical Physics Letters* 367, 259–264. [https://doi.org/10.1016/S0009-2614\(02\)01655-X](https://doi.org/10.1016/S0009-2614(02)01655-X)
- Roland, C.M., Hensel-Bielowka, S., Paluch, M., Casalini, R., 2005. Supercooled dynamics of glass-forming liquids and polymers under hydrostatic pressure. *Rep. Prog. Phys.* 68, 1405–1478. <https://doi.org/10.1088/0034-4885/68/6/R03>
- Roland, C.M., Ngai, K.L., 1996. The anomalous Debye–Waller factor and the fragility of glasses. *The Journal of chemical physics* 104, 2967–2970.
- Romanini, M., Barrio, M., Macovez, R., Ruiz-Martin, M.D., Capaccioli, S., Tamarit, J.L., 2017. Thermodynamic Scaling of the Dynamics of a Strongly Hydrogen-Bonded Glass-Former. *Sci Rep* 7, 1346. <https://doi.org/10.1038/s41598-017-01464-2>
- Roseveare, W.E., Powell, R.E., Eyring, H., 1941. The structure and dynamics of liquids. *Journal of Applied Physics* 12, 669–679.
- Rouxel, T., Ji, H., Hammouda, T., Moréac, A., 2008. Poisson’s Ratio and the Densification of Glass under High Pressure. *Phys. Rev. Lett.* 100, 225501. <https://doi.org/10.1103/PhysRevLett.100.225501>
- Rubinstein, M., Colby, R.H., 2003. *Polymer physics*. Oxford University Press, Oxford ; New York.

- Saint-Exupéry, A. de, 1995. *Le petit prince*, Folio junior ed. speciale. ed, Collection folio junior. Gallimard, France.
- Saiter, A., Delbreilh, L., Couderc, H., Arabeche, K., Schönhals, A., Saiter, J.-M., 2010. Temperature dependence of the characteristic length scale for glassy dynamics: Combination of dielectric and specific heat spectroscopy. *Phys. Rev. E* 81, 041805. <https://doi.org/10.1103/PhysRevE.81.041805>
- Saiter, A., Prevosto, D., Passaglia, E., Couderc, H., Delbreilh, L., Saiter, J.M., 2013. Cooperativity length scale in nanocomposites: Interfacial and confinement effects. *Phys. Rev. E* 88, 042605. <https://doi.org/10.1103/PhysRevE.88.042605>
- Saiter, A., Saiter, J.-M., Golovchak, R., Shpotyuk, M., Shpotyuk, O., 2009. Cooperative rearranging region size and free volume in As–Se glasses. *J. Phys.: Condens. Matter* 21, 075105. <https://doi.org/10.1088/0953-8984/21/7/075105>
- Sandberg, O., Bäckström, G., 1980. Thermal conductivity and heat capacity of liquid and glassy poly(vinyl acetate) under pressure. *J. Polym. Sci. Polym. Phys. Ed.* 18, 2123–2133. <https://doi.org/10.1002/pol.1980.180181010>
- Santangelo, P.G., Roland, C.M., 1998. Molecular Weight Dependence of Fragility in Polystyrene. *Macromolecules* 31, 4581–4585. <https://doi.org/10.1021/ma971823k>
- Schammé, B., Couvrat, N., Malpeli, P., Dudognon, E., Delbreilh, L., Dupray, V., Dargent, É., Coquerel, G., 2016. Transformation of an active pharmaceutical ingredient upon high-energy milling: A process-induced disorder in Biclotymol. *International Journal of Pharmaceutics* 499, 67–73. <https://doi.org/10.1016/j.ijpharm.2015.12.032>
- Schick, C., 2009. Differential scanning calorimetry (DSC) of semicrystalline polymers. *Anal Bioanal Chem* 395, 1589–1611. <https://doi.org/10.1007/s00216-009-3169-y>
- Schmelzer, J., Schmelzer, J.W.P., Gutzow, I.S., Mazurin, O.V., 2011. *Glasses and the glass transition*. Wiley-VCH, Weinheim.
- Schmidt, M., Maurer, F.H.J., 2000. Isotropic Pressure-Densified Atactic Poly(methyl methacrylate) Glasses: Free-Volume Properties from Equation-of-State Data and Positron Annihilation Lifetime Spectroscopy. *Macromolecules* 33, 3879–3891. <https://doi.org/10.1021/ma991722h>
- Schmidt-Rohr, K., Spiess, H.W., 1991. Nature of nonexponential loss of correlation above the glass transition investigated by multidimensional NMR. *Phys. Rev. Lett.* 66, 3020–3023. <https://doi.org/10.1103/PhysRevLett.66.3020>
- Schneider, U., Brand, R., Lunkenheimer, P., Loidl, A., 2000. Excess Wing in the Dielectric Loss of Glass Formers: A Johari-Goldstein β Relaxation? *Phys. Rev. Lett.* 84, 5560–5563. <https://doi.org/10.1103/PhysRevLett.84.5560>
- Schönhals, A., 2001. Evidence for a universal crossover behaviour of the dynamic glass transition. *Europhys. Lett.* 56, 815–821. <https://doi.org/10.1209/epl/i2001-00115-8>
- Schröter, K., 2006. Characteristic length of glass transition heterogeneity from calorimetry. *Journal of Non-Crystalline Solids* 352, 3249–3254. <https://doi.org/10.1016/j.jnoncrysol.2006.05.024>
- Scopigno, T., Ruocco, G., Sette, F., Monaco, G., 2003. Is the Fragility of a Liquid Embedded in the Properties of Its Glass? *Science* 302, 849–852. <https://doi.org/10.1126/science.1089446>
- Sepúlveda, A., Leon-Gutierrez, E., Gonzalez-Silveira, M., Rodríguez-Tinoco, C., Clavaguera-Mora, M.T., Rodríguez-Viejo, J., 2011. Accelerated Aging in Ultrathin Films of a Molecular Glass Former. *Phys. Rev. Lett.* 107, 025901. <https://doi.org/10.1103/PhysRevLett.107.025901>
- Sokolov, A.P., Rössler, E., Kisliuk, A., Quitmann, D., 1993. Dynamics of strong and fragile glass formers: Differences and correlation with low-temperature properties. *Phys. Rev. Lett.* 71, 2062–2065. <https://doi.org/10.1103/PhysRevLett.71.2062>
- Sonaglioni, D., Tombari, E., Johari, G.P., 2023. Pressure Scanning Volumetry of Physically Aged Polymer Glasses, Fictive Pressure, and Memory Effect. *J. Phys. Chem. B* 127, 7070–7081. <https://doi.org/10.1021/acs.jpcc.3c03401>

- Sonaglioni, D., Tombari, E., Johari, G.P., 2022. Pressure scanning volumetry. *Thermochimica Acta* 717, 179319. <https://doi.org/10.1016/j.tca.2022.179319>
- Song, Z., Rodríguez-Tinoco, C., Mathew, A., Napolitano, S., 2022. Fast equilibration mechanisms in disordered materials mediated by slow liquid dynamics. *Sci. Adv.* 8, eabm7154. <https://doi.org/10.1126/sciadv.abm7154>
- Stillinger, F.H., Debenedetti, P.G., Truskett, T.M., 2001. The Kauzmann Paradox Revisited. *J. Phys. Chem. B* 105, 11809–11816. <https://doi.org/10.1021/jp011840i>
- Stukalin, E.B., Douglas, J.F., Freed, K.F., 2009. Application of the entropy theory of glass formation to poly(α -olefins). *The Journal of Chemical Physics* 131, 114905. <https://doi.org/10.1063/1.3216109>
- Swallen, S.F., Kearns, K.L., Mapes, M.K., Kim, Y.S., McMahan, R.J., Ediger, M.D., Wu, T., Yu, L., Satija, S., 2007. Organic Glasses with Exceptional Thermodynamic and Kinetic Stability. *Science* 315, 353–356. <https://doi.org/10.1126/science.1135795>
- Tammann, G., Hesse, W., 1926. Die Abhängigkeit der Viscosität von der Temperatur bei unterkühlten Flüssigkeiten. *Z. Anorg. Allg. Chem.* 156, 245–257. <https://doi.org/10.1002/zaac.19261560121>
- Tanaka, H., 2003. Relation between Thermodynamics and Kinetics of Glass-Forming Liquids. *Phys. Rev. Lett.* 90, 055701. <https://doi.org/10.1103/PhysRevLett.90.055701>
- Tarjus, G., Alba-Simionesco, C., Grousson, M., Viot, P., Kivelson, D., 2003. Locally preferred structure and frustration in glass-forming liquids: a clue to polyamorphism? *J. Phys.: Condens. Matter* 15, S1077. <https://doi.org/10.1088/0953-8984/15/11/329>
- Tarjus, G., Kivelson, S.A., Nussinov, Z., Viot, P., 2005. The frustration-based approach of supercooled liquids and the glass transition: a review and critical assessment. *J. Phys.: Condens. Matter* 17, R1143–R1182. <https://doi.org/10.1088/0953-8984/17/50/R01>
- Theobald, S., Pechhold, W., Stoll, B., 2001. The pressure and temperature dependence of the relaxation processes in poly(methylmethacrylate). *Polymer* 42, 289–295. [https://doi.org/10.1016/S0032-3861\(00\)00317-7](https://doi.org/10.1016/S0032-3861(00)00317-7)
- Tölle, A., 2001. Neutron scattering studies of the model glass former ortho-terphenyl. *Reports on Progress in Physics* 64, 1473–1532. <https://doi.org/10.1088/0034-4885/64/11/203>
- Tölle, A., Schober, H., Wuttke, J., Randl, O.G., Fujara, F., 1998. Fast Relaxation in a Fragile Liquid under Pressure. *Phys. Rev. Lett.* 80, 2374–2377. <https://doi.org/10.1103/PhysRevLett.80.2374>
- Toninelli, C., Wyart, M., Berthier, L., Biroli, G., Bouchaud, J.-P., 2005. Dynamical susceptibility of glass formers: Contrasting the predictions of theoretical scenarios. *Phys. Rev. E* 71, 041505. <https://doi.org/10.1103/PhysRevE.71.041505>
- Tool, A.Q., 1946. Relation Between Inelastic Deformability and Thermal Expansion of Glass in Its Annealing Range*. *Journal of the American Ceramic Society* 29, 240–253. <https://doi.org/10.1111/j.1151-2916.1946.tb11592.x>
- Tool, A.Q., Eichlin, C.G., 1925. VARIATIONS IN GLASS CAUSED BY HEAT TREATMENT. *J American Ceramic Society* 8, 1–17. <https://doi.org/10.1111/j.1151-2916.1925.tb16325.x>
- Tool, A.Q., Eicitlin, C.G., 1931. Variations Caused in the Heating Curves of Glass by Heat Treatment1. *Journal of the American Ceramic Society* 14, 276–308. <https://doi.org/10.1111/j.1151-2916.1931.tb16602.x>
- Tracht, U., Wilhelm, M., Heuer, A., Feng, H., Schmidt-Rohr, K., Spiess, H.W., 1998. Length Scale of Dynamic Heterogeneities at the Glass Transition Determined by Multidimensional Nuclear Magnetic Resonance. *Phys. Rev. Lett.* 81, 2727–2730. <https://doi.org/10.1103/PhysRevLett.81.2727>
- Turnbull, D., Cohen, M.H., 1961. Free-Volume Model of the Amorphous Phase: Glass Transition. *The Journal of Chemical Physics* 34, 120–125. <https://doi.org/10.1063/1.1731549>

- Urbanowicz, P., Rzoska, S.J., Paluch, M., Sawicki, B., Szulc, A., Ziolo, J., 1995. Influence of intermolecular interactions on the sign of dTC/dp in critical solutions. *Chemical Physics* 201, 575–582. [https://doi.org/10.1016/0301-0104\(95\)00302-9](https://doi.org/10.1016/0301-0104(95)00302-9)
- Varol, N., Monnier, X., Delbreilh, L., Saiter, A., Fatyeyeva, K., Dargent, E., 2020. Highlight of primary and secondary relaxations in amorphous stereocomplex polylactides. *Express Polym. Lett.* 14, 48–62. <https://doi.org/10.3144/expresspolymlett.2020.5>
- Vogel, Hans, 1921. Das Temperaturabhangigkeitsgesetz der Viskosität von Flüssigkeiten. *Physikalische Zeitschrift* 22.
- Vyazovkin, S., Dranca, I., 2007. Effect of Physical Aging on Nucleation of Amorphous Indomethacin. *J. Phys. Chem. B* 111, 7283–7287. <https://doi.org/10.1021/jp0700027>
- Weeks, E.R., Crocker, J.C., Levitt, A.C., Schofield, A., Weitz, D.A., 2000. Three-Dimensional Direct Imaging of Structural Relaxation Near the Colloidal Glass Transition. *Science* 287, 627–631. <https://doi.org/10.1126/science.287.5453.627>
- Weitz, A., Wunderlich, B., 1974. Thermal analysis and dilatometry of glasses formed under elevated pressure. *J. Polym. Sci. Polym. Phys. Ed.* 12, 2473–2491. <https://doi.org/10.1002/pol.1974.180121208>
- White, R.P., Lipson, J.E.G., 2017. How Free Volume Does Influence the Dynamics of Glass Forming Liquids. *ACS Macro Lett.* 6, 529–534. <https://doi.org/10.1021/acsmacrolett.7b00179>
- Williams, E., Angell, C.A., 1977. Pressure dependence of the glass transition temperature in ionic liquids and solutions. Evidence against free volume theories. *J. Phys. Chem.* 81, 232–237. <https://doi.org/10.1021/j100518a010>
- Williams, G., Watts, D.C., 1970. Non-symmetrical dielectric relaxation behaviour arising from a simple empirical decay function. *Trans. Faraday Soc.* 66, 80. <https://doi.org/10.1039/tf9706600080>
- Williams, M.L., Landel, R.F., Ferry, J.D., 1955. The Temperature Dependence of Relaxation Mechanisms in Amorphous Polymers and Other Glass-forming Liquids. *J. Am. Chem. Soc.* 77, 3701–3707. <https://doi.org/10.1021/ja01619a008>
- Wojnarowska, Z., Smolka, W., Zotova, J., Knapik-Kowalczyk, J., Sherif, A., Tajber, L., Paluch, M., 2018. The effect of electrostatic interactions on the formation of pharmaceutical eutectics. *Phys. Chem. Chem. Phys.* 20, 27361–27367. <https://doi.org/10.1039/C8CP05905E>
- Wuttke, J., Petry, W., Pouget, S., 1996. Structural relaxation in viscous glycerol: Coherent neutron scattering. *The Journal of Chemical Physics* 105, 5177–5182. <https://doi.org/10.1063/1.472336>
- Yin, H., Napolitano, S., Schönhals, A., 2012. Molecular Mobility and Glass Transition of Thin Films of Poly(bisphenol A carbonate). *Macromolecules* 45, 1652–1662. <https://doi.org/10.1021/ma202127p>
- Zhang, H., Douglas, J.F., 2013. Glassy interfacial dynamics of Ni nanoparticles: part I Colored noise, dynamic heterogeneity and collective atomic motion. *Soft Matter* 9, 1254–1265. <https://doi.org/10.1039/C2SM26789F>
- Zhang, J., Jia, D.-Z., Ma, G.-Q., Lin, H., Huang, H.-D., Zhong, G.-J., Li, Z.-M., 2024. Mechanically rejuvenated glassy polylactide with spatial heterogeneity and packing efficiency: Time dependence of deformation behavior. *Polymer* 298, 126876. <https://doi.org/10.1016/j.polymer.2024.126876>
- Zhang, Y., Fakhraai, Z., 2017. Invariant Fast Diffusion on the Surfaces of Ultrastable and Aged Molecular Glasses. *Phys. Rev. Lett.* 118, 066101. <https://doi.org/10.1103/PhysRevLett.118.066101>
- Zheng, Q., Mauro, J.C., 2017. Viscosity of glass-forming systems. *J. Am. Ceram. Soc.* 100, 6–25. <https://doi.org/10.1111/jace.14678>
- Zimny, S., Tarnacka, M., Wojnarowska, Z., Heczko, D., Maksym, P., Paluch, M., Kamiński, K., 2023. Impact of the graft' structure on the behavior of PMMS-based brushes. *High pressure studies. Polymer* 271, 125790. <https://doi.org/10.1016/j.polymer.2023.125790>

References

- Zoller, P., Bolli, P., Pahud, V., Ackermann, H., 1976. Apparatus for measuring pressure–volume–temperature relationships of polymers to 350 °C and 2200 kg/cm². *Review of Scientific Instruments* 47, 948–952. <https://doi.org/10.1063/1.1134779>
- Zoller, P., Walsh, D.J., 1995. *Standard pressure-volume-temperature data for polymers*. Technomic Pub. Co, Lancaster, PA.

Apport de la spectroscopie à relaxation diélectrique sous pression pour investiguer la mobilité moléculaire dans les polymères thermoplastiques amorphes

Mot clés : transition vitreuse, mobilité moléculaire, polymères, spectroscopie à relaxation diélectrique, pression, relaxation structurelle, coopérativité.

Résumé

La relation entre la température de transition vitreuse, la fragilité isobare et la taille caractéristique des régions de réarrangement coopératif (CRR) pour les liquides vitreux est clarifiée en tenant compte des contributions volumétriques et thermiques de la relaxation structurelle. Ces contributions sont habituellement estimées en considérant certaines hypothèses à la pression atmosphérique, alors qu'elles nécessitent de mesurer des variations de grandeurs physiques sous pression. L'utilisation de la spectroscopie à relaxation diélectrique sous pression offre une nouvelle perspective pour déterminer expérimentalement les contributions de la fragilité isobare.

D'une part, ces mesures sont effectuées pour trois polymères thermoplastiques amorphes : le polylactide (PLA), le polyéthylène glycol téréphtalate (PETg) et le polyvinyle acétate (PVAc). Ces polymères présentent une forte corrélation entre le volume d'activation, qui conduit à la contribution volumétrique de la fragilité isobare, et le volume CRR. La contribution thermique est déterminée par deux méthodes et évolue de manière opposée à la contribution volumétrique en fonction de la pression. Les contributions expliquent le comportement de fragilité isobare à la pression atmosphérique. D'autre part, la série de copolymères poly(éthylène-co-vinyle acétate) (EVA), présente un rapport différent de groupes latéraux polaires avec une chaîne principale inchangée, est analysée en termes d'interactions intermoléculaires à partir de la forme de relaxation diélectrique. Dans cette série, les groupes latéraux polaires jouent un rôle crucial dans les contributions volumétriques et thermiques de la fragilité isobare, qui sont également liées aux interactions inter et intramoléculaires.

En combinant ces différents résultats, il est possible d'établir une relation entre la structure chimique et l'influence de la pression/température sur la mobilité moléculaire. Les effets des paramètres structurels, tels que la rigidité de la chaîne principale et des groupes latéraux ou la packing efficiency, sont mis en évidence et expliquent comment ils affectent la fragilité isobare.

Application of broadband dielectric spectroscopy under pressure to the study of molecular mobility in amorphous thermoplastic polymers

Keywords : glass transition, molecular mobility, polymers, broadband dielectric spectroscopy, pressure, structural relaxation, cooperativity.

Abstract

The ambiguity surrounding the relationship between the glass transition temperature, isobaric fragility, and the characteristic size of the Cooperative Rearranging Regions (CRR) for glass-forming liquids has been resolved by considering the volumetric and thermal contributions of the structural relaxation. These contributions have traditionally been estimated by considering assumptions at atmospheric pressure, whereas they require pressure variations to be measured. The use of broadband dielectric spectroscopy under pressure offers a new perspective to experimentally determine the contributions of isobaric fragility.

On the one hand, the measurement is performed for three amorphous thermoplastic polymers: Poly(lactic acid) (PLA), poly(ethylene glycol terephthalate) (PETg) and poly(vinyl acetate) (PVAc). These polymers show a strong correlation between the activation volume, which leads to the volumetric contribution of isobaric fragility, and the CRR volume. The thermal contribution is determined by two methods and evolves in an opposite manner to the volumetric contribution as function of pressure. The contributions explain the isobaric fragility behavior at atmospheric pressure. On the other hand, the poly(ethylene-co-vinyl acetate) (EVA) copolymer series, which presents a different ratio of polar side groups with an unchanged backbone chain, is analyzed in terms of intermolecular interactions from the dielectric relaxation shape. In this series, the polar side groups play a crucial role in the volumetric and thermal contributions of the isobaric fragility, which are also related to inter and intramolecular interactions.

By combining these different results, a relationship between chemical structure and the influence of pressure/temperature on molecular mobility can be established. The effects of structural parameters, such as backbone and side group stiffness or packing efficiency, are highlighted and explain how isobaric fragility is affected.